Probing the Physiological Roles of *Saccharomyces cerevisiae* Cytochrome *c* Peroxidase Using Biochemical and Proteomics Approaches

Heng Jiang

A Thesis

in

The Department

of

Biology

Presented in Partial Fulfillment of the Requirements

for the Degree of Doctor of Philosophy at

Concordia University

Montreal, Quebec, Canada

May 2006

Your file Votre référence
ISBN: 978-0-494-23830-1
Our file Notre référence
ISBN: 978-0-494-23830-1

Abstract

Probing the Physiological Roles of *Saccharomyces cerevisiae* Cytochrome *c* Peroxidase Using Biochemical and Proteomics Approaches

Heng Jiang, Ph.D.

Concordia University, 2006

Yeast cytochrome *c* peroxidase (CCP) efficiently catalyzes the reduction of H_2O_2 to H_2O by ferrocytochrome *c* and is presumed to be a key component in cellular redox signaling. The CCP^{W191F} variant does not possess ferrocytochrome *c*-oxidizing activity but does signal oxidative stress. A biophysical study of the recombinant proteins showed that CCP exhibited greater spectral (absorption and near-UV circular dichroism) changes than CCP^{W191F} over 30 min following exposure to 10 molar equivalents of H_2O_2. The stable nitroxyl radical, 2,2,6,6-tetramethylpiperidinyl-1-oxy ($TEMPO^{\bullet}$), inhibited H_2O_2-induced protein crosslinking and accelerated the rate of oxyferryl (Fe^{IV}=O) heme reduction. Diethylenetriaminopentaacetic acid (DTPA) inhibited crosslinking of the mutant but not of wild-type CCP.

The mass spectral behavior of $TEMPO^{\bullet}$ in aqueous solutions was investigated prior to characterizing its reaction with the H_2O_2-oxidized peroxidases. The electrospray ionization mass spectrum showed that $TEMPO^{+}$, $TEMPOH^{\bullet+}$ and $TEMPOH_2^{+}$ ions were formed in the ionization source. $TEMPONa^{\bullet+}$ ions were dominant in the presence of sodium and fragmented by cleavage of the weak $TEMPO^{\bullet}$–Na^{+} bond. Quantum

chemistry calculations revealed that protonation unlike sodiation destabilized the electronic structure of TEMPO$^{\bullet}$, which complicated the mass spectra.

The function of CCP *in vivo* was systematically investigated. Cell survival, antioxidant activity and tolerance to heat and oxidants of wild-type, *ccp1Δ* (*CCP1*-null-mutant) and *ccp1Δ-ccp1*^{W191F} (*ccp1Δ* cells transformed with *ccp1*^{W191F}) *S. cerevisiae* strains were compared. The phenotypic differences provide strong evidence that yeast CCP has separate antioxidant and signaling functions in both exponential- and stationary-phase cells.

Mitochondria of wild-type and *ccp1Δ* strains of *S. cerevisiae* in the W303-1B genetic background were isolated for proteome analysis. Over 200 protein spots were detected for both strains on 7×10-cm two-dimensional (2D) gels over the pI range 3–10. Since 2DE image analysis was not reliable for proteins with less than three-fold changes in expression, a metabolic labeling approach for isotope-ratio quantitation of proteomes by mass spectrometry (MS) was developed. The W303-1B strain, a leucine auxotroph, was grown on synthetic complete medium containing natural abundance (H_{10}-Leu) or perdeuterated Leu (D_{10}-Leu), and the cultures were mixed prior to 2DE separation. The D_{10}-Leu label provided an internal mass calibrant for accurate quantitation of Leu-containing tryptic peptides by matrix-assisted laser desorption ionization time-of-flight MS. Using this methodology to measure the stress-response indices to H_2O_2 of six glycolytic enzymes revealed that glycolysis was initially inhibited but restored within about two hours after challenging exponentially growing yeast cells with 0.4 mM H_2O_2.

Acknowledgements

First of all, I would like to thank Dr. Ann English, my supervisor, for her guidance, support and research ideas during my Ph.D. During these years I have profited greatly from her critical thinking and from the introduction to the fantastic world of mass spectrometry at Concordia. I wish to thank the members of my committee, Drs. Paul Joyce and Reginald Storms, for their scientific support as well as Dr. Paul Albert, the former Graduate Program Director in the Department of Biology, for his warmhearted guidance. I thank Concordia University for an International Student Tuition Remission.

Thanks to Biao Shen, Mengwei Ye and Limei Tao for sharing their experience both in scientific research and in life in Montreal. Thank you Pascal Turcotte and Mihai Ciortea, my best Western friends, for discussions of my experiments and our mutual interests. A special thanks to David Yeung for his patience in correcting my written English. Thanks to Jean-Francois Roy for help with the SSQ ESI-MS and for rebooting my car. Many thanks to Ali, Andrea, Ernesto, Etienne, Farida, Georgia, Houston, Line, Jaffer, John, Julie, Michelle, Qadir, Steve, Tyrone and everyone who worked with me at Concordia.

I would also like to thank my wife, Li Zhang, for her countless support. Thanks to my cute Lucas for giving me the joys of fatherhood. Thanks to my parents and my in-laws for their support and for their help in taking care of Lucas.

Tables of Contents

List of Figures xi

List of Tables xiv

List of Appendices xvi

1 Introduction 1

1.1 Oxidative stress 1

1.1.1 Reactive oxygen species (ROS) and oxidative damage 1

1.1.2 Antioxidant defense systems 3

1.1.3 H_2O_2-induced signaling 7

1.2 Yeast mitochondria 10

1.3 Cytochrome *c* peroxidase (CCP) 13

1.3.1 CCP catalysis 14

1.3.2 Electron transfer between cytochrome *c* and CCP 16

1.3.3 Oxidation of CCP in the absence of ferrocytochrome *c* 17

1.4 Proteomics 19

1.4.1 Proteomics and genomics 19

1.4.2 Methodology in proteomics 20

1.5 Thesis outline and contributions of colleagues 23

2 Biophysical comparison of yeast CCP and its W191F mutant following H_2O_2-exposure 25

2.1 Abstract 25

2.2 Introduction 25

2.3 Materials and methods 29

2.3.1 Materials 29

2.3.2 Methods 29

2.4 Results 31

2.4.1 The W191F mutation does not cause a significant conformational change in CCP 31

2.4.2 Reaction with H_2O_2 causes more significant changes in CCP than in CCP^{W191F} 34
2.4.3 Radicals are formed during CCP oxidation 39
2.5 Discussion 44
2.6 Conclusions 48

3 Mass spectrometric and computational studies on the relative stabilities of TEMPO• ions formed in an electrospray ionization source in aqueous solution 49
3.1 Abstract 49
3.2 Introduction 50
3.3 Materials and methods 52
3.3.1 Mass spectrometric analysis 52
3.3.2 Quantum chemistry calculations 53
3.4 Results 53
3.4.1 ESI mass spectrum of $TEMPO^{\bullet}$ 53
3.4.2 MS/MS analysis of the $TEMPO^{+}$, $TEMPOH^{\bullet+}$ and $TEMPOH_2^{+}$ ions 54
3.4.3 Fractional abundances of the $TEMPO^{\bullet}$ ions 59
3.4.4 Relative stability of $TEMPOH^{\bullet+}$ *vs* $TEMPONa^{\bullet+}$ in the ESI source 60
3.4.5 DFT calculations to determine the protonation and sodiation sites in $TEMPO^{\bullet}$ and TEMPOH 61
3.5 Discussion 64
3.6 Conclusions 67
Appendix 3.1 MS/MS analysis and DFT calculation of $NAYAH^{+}$ and $NAYANa^{+}$ 68

4 Phenotypic analysis of the *ccp1Δ* and *ccp1Δ-ccp1*^{W191F} mutant strains of *Saccharomyces cerevisiae* indicates that cytochrome *c* peroxidase functions in oxidative-stress signaling 72
4.1 Abstract 72
4.2 Introduction 73

4.3 Materials and methods 75
4.3.1 Yeast strains and plasmids 75
4.3.2 Media and growth conditions 79
4.3.3 Cell viability and IRC 79
4.3.4 Enzyme assays 80
4.3.5 Cell survival after heat stress 80
4.3.6 Cell survival after exposure to H_2O_2 and paraquat 81
4.3.7 H_2O_2 agar diffusion assays 82
4.4 Results 82
4.4.1 *ccp1Δ* cells exhibit a shortened initial doubling time but comparable viability to *ccp1Δ-ccp1*^{W191F} cells 82
4.4.2 Absence of CCP activity does not result in decreased viability or mitochondrial function in unstressed cells 84
4.4.3 *CCP1* does not protect cells against heat stress 85
4.4.4 *CCP1* protects respiring mitochondria from H_2O_2 challenge 87
4.4.5 YCplac33-*CCP1* complements the H_2O_2-sensitive phenotype of *ccp1Δ* 90
4.4.6 Antioxidant enzyme activities are regulated differently in *ccp1Δ* and *ccp1Δ-ccp1*^{W191F} 91
4.5 Discussion 94
4.5.1 Control of initial doubling time 94
4.5.2 Index of respiratory competence 96
4.5.3 Sensitivity to H_2O_2 challenge 97
4.5.4 Antioxidant enzyme activities 97
4.5.5 Strain-specific stress responses 100
4.6 Conclusions 101
4.7 Acknowledgements 102
Appendix 4.1 DNA sequence of the YCplac33-*ccp1*^{W191F} insert and of *CCP1* Alleles 1 and 2 103
Appendix 4.2 Construction of the YCplac33-E and YCplac33-*CCP1* vectors 108
Appendix 4.3 YCplac33-*ccp1*^{W191F} plasmid loss from the *ccp1Δ-ccp1*^{W191F} strain 113
Appendix 4.4 Procedures for the enzymatic assays 114

5 Two-dimensional electrophoresis mapping of yeast mitochondrial proteomes from wild-type and *ccp1Δ* cells 117

5.1 Abstract 117

5.2 Introduction 117

5.3 Materials and methods 118

5.3.1 Mitochondria isolation 118

5.3.2 2DE separation 119

5.4 Results 120

5.5 Discussion 122

5.6 Conclusions 124

6 Quantitative analysis of the yeast proteome by incorporation of isotopically labeled leucine 125

6.1 Abstract 125

6.2 Introduction 125

6.3 Materials and methods 128

6.3.1 Materials 128

6.3.2 Media and growth conditions 128

6.3.3 Two-dimensional electrophoresis 129

6.3.4 Mass spectrometry 130

6.4 Results 131

6.4.1 Yeast growth 131

6.4.2 Protein identification and quantitative analysis 132

6.5 Discussion 136

6.6 Conclusions 140

6.7 Acknowledgement 141

Appendix 6.1. Preparation of yeast cell lysate for 2DE analysis 141

7 Evaluation of D_{10}-Leu metabolic labeling coupled with MALDI-MS analysis in studying the response of the yeast proteome to H_2O_2 challenge 142

7.1 Abstract 142

7.2 Introduction 142
7.3 Materials and methods 144
7.3.1 Materials 144
7.3.2 Cell growth and protein separation by 2DE 144
7.3.3 In-gel digestion and MALDI-ToF MS analysis 145
7.4 Results 146
7.4.1 Yeast growth 146
7.4.2 Protein separation and identification 148
7.4.3 Isotope-ratio quantitation by MALDI-ToF MS 149
7.4.4 Effects of H_2O_2 challenge on glycolytic enzyme expression 152
7.4.5 Relative protein accumulation in unstressed cells 154
7.5 Discussion 156
7.5.1 Use of stable *vs* radioisotopes in investigating a proteome's response to stress 156
7.5.2 Metabolic *vs* chemical labeling of proteomes 159
7.5.3 Further optimization of D_{10}-Leu metabolic labeling for isotope-ratio quantitation 160
7.5.4 H_2O_2-induced inhibition of cell growth as viewed from a proteomics perspective 162
7.6 Conclusions 163
7.7 Supporting Information 163

8 Conclusions and suggestions for future work 166
8.1 Chapter 2 166
8.2 Chapter 3 166
8.3 Chapter 4 167
8.4 Chapters 5, 6 and 7 167
8.5 Suggestions for further work 168

9 References 170

List of Figures

Figure 1.1	Reactive oxygen species (ROS) and its defense system.	2
Figure 1.2	Electron transport chain and electron leakage in yeast mitochondria.	12
Figure 1.3	Structure of yeast CCP active site.	15
Figure 1.4	3D structure of the yeast CCP/yeast cytochrome *c* complex.	16
Figure 1.5	Absorption spectrum of native and oxidized recombinant yeast CCP.	18
Figure 1.6	Example of a peptide mass fingerprint generated by MALDI-ToF MS of a tryptic digest of a protein spot.	21
Figure 2.1	Deconvolved ESI mass spectra of (A) yeast CCP(MI) and (B) its W191F mutant.	32
Figure 2.2	Far-UV CD spectra of ferric yeast CCP and its W191F mutant.	32
Figure 2.3	Heme CD spectra of ferric yeast CCP, CCP^{W191F} and their ferricytochrome *c* complexes.	33
Figure 2.4	Absorption spectra of ferric yeast CCP and its W191F mutant.	35
Figure 2.5	Absorption spectra of H_2O_2-oxidized yeast CCP and its W191F mutant.	37
Figure 2.6	Relative absorption at 424 nm *vs* time of H_2O_2-oxidized yeast CCP and its W191F mutant.	38
Figure 2.7	Effects of 10× H_2O_2 on the near-UV CD spectra of yeast CCP and its W191F mutant.	39
Figure 2.8	Effects of 10× H_2O_2 on the heme CD spectra of yeast CCP and its W191F mutant.	40
Figure 2.9	SDS-PAGE analysis of the effects of $TEMPO^{\bullet}$ on H_2O_2-oxidized CCP and its W191F mutant.	41
Figure 2.10	Effects of $TEMPO^{\bullet}$ on the absorption spectra of H_2O_2-oxidized yeast CCP and its W191F mutant.	43
Figure 2.11	Effects of $TEMPO^{\bullet}$ on the relative absorption at 424 nm *vs* time of H_2O_2-oxidized yeast CCP and its W191F mutant.	44
Figure 2.12	Effects of DTPA on H_2O_2-induced crosslinking of CCP and its W191F mutant.	47

Figure 3.1	Postulated mechanism for the CuCl/TEMPO$^{\bullet}$-catalyzed aerobic oxidation of alcohols.	50
Figure 3.2	ESI mass spectrum of TEMPO$^{\bullet}$ in water.	53
Figure 3.3	MS/MS spectrum *vs* collision voltage of the TEMPO^{+} ion at m/z 156.	55
Figure 3.4	Proposed fragmentation pathways of the TEMPO^{+} ion at m/z 156.	56
Figure 3.5	MS/MS spectrum *vs* collision voltage of the TEMPOH$^{\bullet+}$ ion at m/z 157.	57
Figure 3.6	Proposed fragmentation pathways of the TEMPOH$^{\bullet+}$ ion at m/z 157.	57
Figure 3.7	MS/MS spectrum *vs* collision voltage of the $TEMPOH_2^{+}$ ion at m/z 158.	58
Figure 3.8	Proposed fragmentation pathways of the $TEMPOH_2^{+}$ ion at m/z 158.	58
Figure 3.9	ESI mass spectrum of TEMPO$^{\bullet}$ in sodium phosphate buffer.	59
Figure 3.10	TICs *vs* collision voltage in the MS/MS product-ion spectra of TEMPOH$^{\bullet+}$ (m/z 157) *vs* TEMPONa$^{\bullet+}$ (m/z 179).	61
Figure 3.11	Calculated structure of $TEMPOH_2^{+}$.	62
Figure 3.12	Calculated structures of protonated TEMPO$^{\bullet}$.	62
Figure 3.13	Calculated structure of TEMPONa$^{\bullet+}$.	63
Figure A3.14	TICs in the MS/MS product-ion spectra of NAYAH^{+} (m/z 223) *vs* NAYANa^{+} (m/z 245) ions.	69
Figure A3.15	Proposed fragmentation pathways of the NAYAH^{+} ion at m/z 223.	69
Figure A3.16	Calculated structures of NAYAH^{+}.	70
Figure A3.17	Calculated structures of NAYANa^{+}.	71
Figure 4.1	Growth curves of wild-type, *ccp1Δ* and *ccp1Δ-ccp1*^{W191F} *S. cerevisiae* cells on different carbon sources over 3 days.	83
Figure 4.2	Percent growth relative to wild-type of *ccp1Δ* and *ccp1Δ-ccp1*^{W191F} *S. cerevisiae* cells.	83
Figure 4.3	Index of respiratory competence (IRC) of wild-type, *ccp1Δ* and *ccp1Δ-ccp1*^{W191F} *S. cerevisiae* cells.	84

Figure 4.4 Percent survival *vs* age of wild-type, *ccp1Δ* and *ccp1Δ-ccp1*^{W191F} *S. cerevisiae* cells following incubation at 48°C for 60 min under anaerobic conditions. 85

Figure 4.5 Percent survival and IRC of 3-day wild-type, *ccp1Δ* and *ccp1Δ-ccp1*^{W191F} *S. cerevisiae* cells *vs* exposure time to anaerobic heat stress at 48°C. 86

Figure 4.6 H_2O_2 and paraquat tolerance of late-exponential-phase wild-type, *ccp1Δ* and *ccp1Δ-ccp1*^{W191F} *S. cerevisiae* cells. 87

Figure 4.7 Effects of 0.4 mM H_2O_2 exposure on the incremental growth over2 h of early-exponential-phase wild-type, *ccp1Δ* and *ccp1Δ-ccp1*^{W191F} *S. cerevisiae* cells in SCD and SCE. 88

Figure 4.8 Percent survival and IRC of 1-, 3- and 7-day wild-type, *ccp1Δ* and *ccp1Δ-ccp1*^{W191F} *S. cerevisiae* cells after 1-h exposure to 60 mM H_2O_2. 90

Figure 4.9 H_2O_2 agar diffusion assays. 91

Figure A4.10 Restriction endonuclease analysis of the YCplac33-*ccp1*^{W191F} vector. 104

Figure A4.11 *Sma*I analysis of *CCP1* from wild-type W303-1B yeast. 108

Figure A4.12 Plasmid map of the YCplac33-E vector. 110

Figure A4.13 Construction and restriction endonuclease analysis of the YCplac33-E vector. 110

Figure A4.14 Construction of the YCplac33-*CCP1* vector. 112

Figure A4.15 Construction and restriction endonuclease analysis of the YCplac33-*CCP1* vector. 113

Figure 5.1 Mitochondrial proteomes analyzed by 2DE of wild-type (left) and *ccp1Δ* (right) *S. cerevisiae* from 48-h YPD cultures. 121

Figure 5.2 Reproducibility of 2DE gels of the *S. cerevisiae* mitochondrial proteome. 121

Figure 5.3 Reproducibility of 2DE analysis of the mitochondrial proteome from wild-type. 123

Figure 6.1 Growth curves of wild-type (W303-1B) and *ccp1Δ* strains of *S. cerevisiae*. 131

Figure 6.2 2D separation of the proteomes from *S. cerevisiae* cultures grown on SCM with 80 mg/L H_{10}- and 80 mg/L D_{10}-Leu. 132
Figure 6.3 MALDI-ToF mass spectra of tryptic peptides from spot TPI1 in Figure 6.2. 134
Figure 6.4 MALDI-ToF mass spectra of tryptic peptides from spots (A) TPI1, (B) HS26 and (C) ENO1 in Figure 6.2. 135
Figure 7.1 Workflow to quantify proteome response to H_2O_2. 146
Figure 7.2 Effects of challenge with 0.4 mM H_2O_2 on cell growth. 147
Figure 7.3 2DE gels showing protein expression at t = 180 min after *S. cerevisiae* cells were switched to D_{10}-SCD (A) without and (B) with exposure to 0.4 mM H_2O_2. 148
Figure 7.4 MALDI-ToF peptide mass maps of protein TPI1. 150
Figure 7.5 Glycolysis in yeast. 154
Figure 7.6 MALDI-ToF peptide mass maps of protein ASC1. 155
Figure 7.7 Relative protein accumulation in unstressed exponentially growing *S. cerevisiae* following medium change. 156

List of Tables

Table 1.1 Peroxidases and catalases of *S. cerevisiae* 7
Table 2.1 Comparison of physical and catalytic properties of oxidized CCP and its W191F mutant 28
Table 3.1 Fractional abundances corrected for isotopic contributions of ions in the ESI mass spectrum of $TEMPO^{\bullet}$ at low collision voltage 60
Table 3.2 DFT calculated gas-phase proton affinities (PA) and sodium affinities (SA) of $TEMPO^{\bullet}$, TEMPOH and H_2O 63
Table 3.3 DFT optimized bond lengths (Å) calculated for $TEMPO^{+}$, $TEMPO^{\bullet}$, $TEMPOH^{\bullet+}$, $TEMPONa^{\bullet+}$, TEMPOH and $TEMPOH_2^{+}$ in the gas phase 64
Table 3.4 Relative abundances (%) of ions in the ESI mass spectrum of $TEMPO^{\bullet}$ reported in literature 65

Table A3.5	DFT calculated gas-phase proton affinities (PA) and sodium affinities (SA) of NAYA	71
Table 4.1	*S. cerevisiae* strains, plasmids and primers used in this study	76
Table 4.2	CCP, catalase, SOD and GLR activities at 25°C of wild-type, *ccp1Δ* and *ccp1Δ-ccp1*^{W191F} *S. cerevisiae* cells in the absence and presence of exogenous H_2O_2	92
Table A4.3	DNA sequence of the YCplac33-*ccp1*^{W191F} insert and *CCP1* alleles 1 and 2	105
Table A4.4	Amino acid sequence encoded by the pYCplac33-*ccp1*^{W191F} insert and those of *CCP1* alleles 1 and 2	107
Table A4.5	YCplac33-*ccp1*^{W191F} plasmid loss from *ccp1Δ-ccp1*^{W191F} yeast during growth on YPD medium	114
Table 6.1	Mass shifts (ΔM_r) and relative intensities of tryptic peptides from *S. cerevisiae* proteins expressed in media containing H_{10}- and D_{10}-Leu	138
Table 6.2	Relative expression levels (REL) of *S. cerevisiae* proteins grown on H_{10}- and D_{10}-Leu	139
Table 7.1	Proteins selected from the 2DE gels for analysis	149
Table 7.2	Average %R values of six glycolytic enzymes and the ribosomal protein ASC1 at 45–225 min following challenge of *S. cerevisiae* with H_2O_2	151
Table 7.3	$SRIH_2O_2$ values of six glycolytic enzymes and the ribosomal protein ASC1 at 30–225 min following challenge of *S. cerevisiae* with H_2O_2	152
Table S7.4A	Tryptic peptides chosen for quantitation	164
Table S7.4B	%R values of six glycolytic enzymes and the ribosomal protein ASC1 at 45–225 min following challenge of *S. cerevisiae* with H_2O_2	165

List of Abbreviations

2DE, two-dimensional gel electrophoresis; ABTS, 2,2'-azino-bis(3-ethylbenzthiazoline-6-sulfonic acid); ACN, acetonitrile; AIM, atoms in-molecules; AMP, ampicillin; C^{2+}, ferrocytochrome *c*; C^{3+}, ferricytochrome *c*; CCP, cytochrome *c* peroxidase; *CCP1*, the gene encoding CCP; *ccp1Δ*, *CCP1* null-mutant *S. cerevisiae*; CCP-I, CCP compound I; CCP-II, CCP compound II; CCP^{W191F}, a Trp191-to-Phe point mutant of CCP; CD, circular dichroism; CFU, colony forming unit; CTA, catalase A; CTT, catalase T; *CYC1*, the gene encoding cytochrome *c* isoform 1; *CYC7*, the gene encoding cytochrome *c* isoform 2; CYGD, comprehensive yeast genome database; D_{10}-Leu, perdeuterated leucine; DFT, density functional theory; DIGE, differential in-gel electrophoresis; DTPA, diethylenetriamino-pentaacetic acid; DTT, dithiothreitol; ESI, electrospray ionization; ER, endoplasmic reticulum; FA, formic acid; FTICR, fourier transform ion cyclotron resonance; G418, geneticin; GFP, green fluorescence protein; GLR, glutathione reductase; GPX, glutathione peroxidase; GSH, glutathione; GSSG, oxidized glutathione; H_{10}-Leu, natural isotopic abundance leucine; h_D, peak-centroid-height of deuterated peptide; h_H, peak-centroid-height of natural isotopic abundance peptide; HRP, horseradish peroxidase; ICAT, isotope-coded affinity tag; IEF, isoelectric focusing; IRC, index of respiratory competence; KAN, kanamycin; LC, liquid chromatography; MALDI-ToF, matrix-assisted laser desorption ionization time-of-flight; MCS, multiple cloning site; M_r, theoretical average mass; ΔM_r, mass increase due to labeling; MS, mass spectrometry; MS/MS, tandem mass spectrometry; mtDNA, mitochondrial DNA; *n*, the number of Leu residues; NAYA, *N*-acteyl-*L*-tyrosinamide; NHE, normal hydrogen electrode; O_2^-, superoxide anion; $^{\bullet}OH$, hydroxyl radical; ORF, open reading frame; PA,

proton affinity; paraquat, 1,1'-dimethyl-4,4'-bipyridinium dichloride; PBS, phosphate buffered saline; PHGPX, phospholipid hydroperoxide glutathione peroxidase; PMF, peptide mass fingerprinting; Q-ToF, quadrupole-time of flight; R, h_D/h_H ratio; RC, respiratory competent; RD, respiratory deficient; RE, restriction endonucleases; REL, relative expression level; *rho*$^+$, cells with normal mtDNA; *rho*$^-$, cells with mutations in mtDNA; *rho*^{0}, cells without mtDNA; ROS, reactive oxygen species; SA, sodium affinity; SC medium, synthetic complete medium; SCD, SCE, SCG and SCL, SC medium supplemented with glucose (D), ethanol (E), glycerol (G), lactate (L); SDS-PAGE, polyacrylamide gel electrophoresis; SOD, superoxide dismutases; $SRI_{H_2O_2}$, stress-response index to H_2O_2; TAP protein, tandem-affinity purification tagged protein; *t*-BHP, *tert*-butyl hydroperoxide; TEMPO$^\bullet$, 2,2,6,6-tetramethylpiperidinyl-1-oxy; TEMPO$^+$, oxidized form of TEMPO$^\bullet$, *N*-oxoammonium cation; TEMPOH, reduced form of TEMPO$^\bullet$, hydroxylamine; TIC, total ion count; TRR, thioredoxin reductase; TRX, thioredoxin; TSA, thioredoxin peroxidase; UV-Vis, ultraviolet-visible; YP medium, 1% yeast extract and 2% peptone containing-medium.

`1 Introduction

1.1 Oxidative stress

Yeast cells have evolved a wide range of responses to many different types of stress, including osmotic, heat, oxidative, starvation, low-pH and exposure to organic solvents [1]. The cell's defenses are intrinsic or inducible, and the acquisition of inducible resistance to one form of stress can lead to cross-resistance to others. For instance, cells pre-exposed to a mild osmotic or ethanol stress are more resistant than unexposed cells to heat shock [2-4]. However, pre-exposure to H_2O_2 does not elicit resistance to the superoxide-generating drug menadione, indicating the existence of stress-specific response mechanisms within yeast [5, 6]. Furthermore, oxidative stress plays an important role in heat-induced cell death in yeast. For example, anaerobic conditions caused a 500- to 20000-fold increase in cell viability of *Saccharomyces cerevisiae* exposed to lethal heat shock, and this thermotolerance was completely and immediately removed upon oxygen exposure [7].

1.1.1 Reactive oxygen species (ROS) and oxidative damage

ROS, which are associated with the energy-generation process of aerobic respiration, can react with and damage most constituents in the cell including nucleic acids, proteins and lipids [8]. Oxidative stress is the result of an imbalance that occurs when cells are unable to adequately deal with the reactive ROS including the superoxide anion (O_2^-), H_2O_2 and the hydroxyl radical ($^{\bullet}OH$). O_2^- is primarily formed by the one-electron reduction of O_2 during respiration in the mitochondria. H_2O_2 is formed in the cell *via* the disproportionation of O_2^-, which is catalyzed by superoxide dismutases (SOD). Both O_2^- and H_2O_2 are relatively unreactive, the main toxic effects resulting from their

conversion to the extremely reactive •OH species [1]. These conversions are metal catalyzed *via* the Haber-Weiss reaction, which using O_2^- as a reductant to produce the reduced forms of metal ions such as Fe^{II} or Cu^{I}. These are available for the Fenton reaction with H_2O_2 (Figure 1.1).

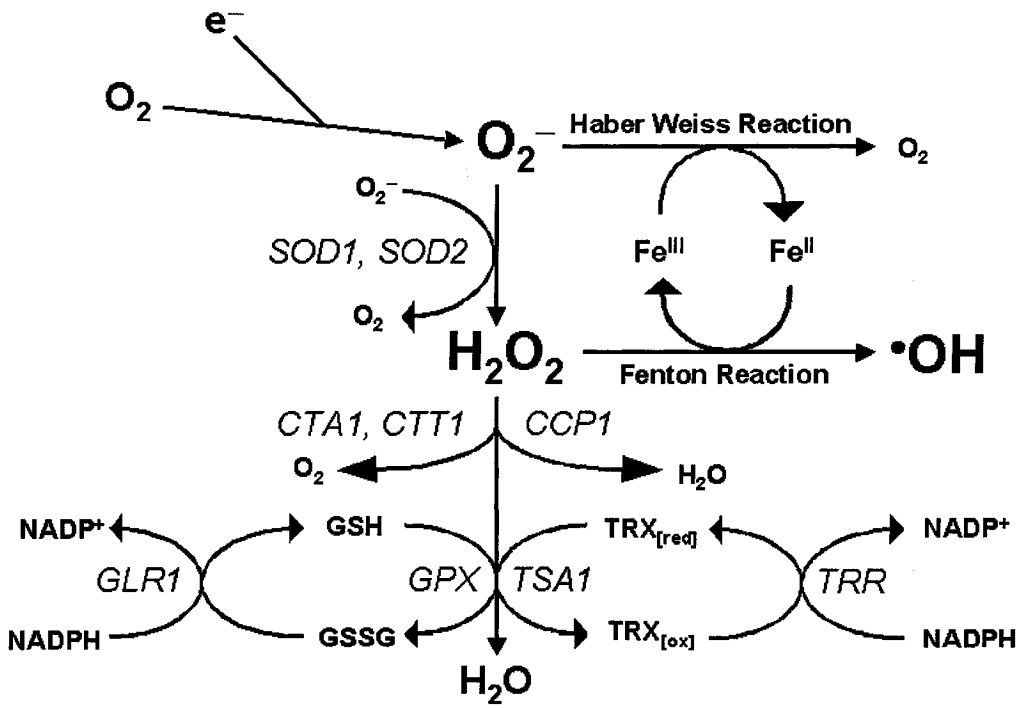

Figure 1.1. Reactive oxygen species (ROS) and its defense system. The main ROS are printed in large type, and include the superoxide anion (O_2^-), hydrogen peroxide (H_2O_2) and the hydroxyl radical (•OH). The yeast genes that encode the antioxidant enzymes are indicated in *italics*. The involvement of metal ions is shown using Fe^{III} ions in examples of the Fenton and Haber-Weiss reactions. Figure is modified from Ref [1].

Unsaturated lipid is a major target of attack by ROS, leading to the process of autocatalytic lipid peroxidation [9]. This results in significant membrane damage in cells and causes the rancidity of foods. ROS can damage DNA by initiating double- and single-stranded breaks, sugar damage and DNA-protein crosslinking [1]. ROS alter

protein structure and function by modifying critical amino acid residues, inducing protein dimerization, and interacting with Fe-S moieties or other metal complexes [10].

1.1.2 Antioxidant defense systems

Cells possess both enzymatic and non-enzymatic defense systems to protect their cellular constituents and maintain a certain cellular redox state. Non-enzymatic defense systems typically consist of small molecules, which are soluble in either an aqueous or a lipid environment. In general, they act as radical scavengers, being oxidized by ROS and thereby removing oxidants from the organism [11]. The best-known example of a non-enzymatic defense system is glutathione (GSH), a tripeptide, γ-glutamyl-cystinyl-glycine. GSH acts as a radical scavenger with its redox-active sulphydryl group reacting with oxidants to produce oxidized glutathione (GSSG). GSH is possibly the most abundant redox-scavenging molecule in cells. The genes involved in GSH biosynthesis, *GSH1* and *GSH2* (encoding γ-glutamyl-cysteine synthase and glutathione synthase, respectively), have been identified in *S. cerevisiae*. Yeast *GSH1*- (*gsh1Δ*) and *GSH2*-null-mutants (*gsh2Δ*) are still viable, although they have a slower growth rate and a longer lag phase than wild-type cells [12, 13]. *gsh1Δ* cells are absolutely dependent upon exogenous GSH for growth in minimal media, while the *gsh2Δ* strains can grow in unsupplemented minimal media, albeit less well than their wild-type counterparts [14]. In addition, *gsh1Δ* displays a petite phenotype, being unable to grow on non-fermentable carbon sources such as glycerol [12]. The wild-type *GSH1* gene was used to rescue a mutant of *PET5155TS*, which encodes a mitochondrial protein, suggesting that GSH plays an important role in protecting the mitochondrion from oxidants produced during respiration [15]. Despite being hypersensitive to oxidants, GSH-deficient mutants are still able to

mount an adaptive stress response to both H_2O_2 and menadione, suggesting that GSH is not important as a sensor molecule in response to these stressors [16].

Thioredoxin is a small, sulphydryl rich protein that acts as a reductant of thioredoxin peroxidase (TSA) and ribonucleotide reductase. *S. cerevisiae* possesses two genes encoding thioredoxin proteins, *TRX1* and *TRX2*, and deletion of both genes results in an extension of the S-phase of the cell cycle, a marked increase in the level of GSSG and activation of the transcription factor Yap1 [17, 18]. The antioxidant activity of thioredoxin is required for the protection against oxidative stress during stationary-phase growth, and correlates with increased expression of both *TRX1* and *TRX2* [19].

Cellular antioxidant defenses also include several enzymes that are capable of removing O_2^- and H_2O_2. The hemoprotein catalase catalyzes the breakdown of H_2O_2 to O_2 and H_2O. *S. cerevisiae* has two such enzymes, catalase A and catalase T, encoded by the *CTA1* and *CTT1* genes, respectively (Figure 1.1). Catalase A is located in the peroxisome and the main physiological role of this enzyme appears to be the removal of H_2O_2 produced by fatty acid oxidation. Recently, catalase A was also found to be present in the mitochondrial matrix of *S. cerevisiae* [20]. Catalase T is thought to play a more general role in the yeast defense system since its expression is regulated by various stress conditions including H_2O_2, heat, osmotic and starvation stress [21, 22]. In addition, copper was found to specifically induce transcription of *CTT1* but not *CTA1* [23]. Yeast strains deficient in both *CTA1* and *CTT1* are hypersensitive to H_2O_2 in stationary phase, and both single and double catalase mutants are unable to mount an adaptive stress response to H_2O_2 [24]. Thus, although the catalase genes are only moderately inducible by H_2O_2, both catalases are clearly important for resistance to H_2O_2.

Yeast cells, in common with other eukaryotes, possess two intracellular superoxide dismutases (SOD), the mitochondrially located MnSOD (encoded by the *SOD2* gene) and the cytoplasmically located CuZnSOD (encoded by the *SOD1* gene). SOD catalyzes O_2^- disproportionation to H_2O_2 and O_2 (Figure 1.1). CuZnSOD appears to be the major enzyme involved in removing O_2^- from the cytoplasm and possibly also the peroxisome [25, 26]. CuZnSOD is also located in the intermembrane space of yeast mitochondria to play a role in protecting against mitochondrial oxidative damage [27]. The physiological role of MnSOD appears to be to protect mitochondria from O_2^- generated during respiration and exposure to ethanol, but it seems not to counter the toxicity of O_2^- generated by exogenously added redox cycling compounds, such as menadione and plumbagin, during fermentative growth [26, 28, 29]. In contrast to the yeast *SOD2*-null mutant (*sod2Δ*), growth of the *SOD1*-null mutant (*sod1Δ*) is significantly inhibited by these two compounds [30]. Both *sod1Δ* and *sod2Δ* are hypersensitive to oxygen. When cells were incubated in a non-fermentable carbon source at low aeration rates both single- and double-mutant strains can grow. However, under high aeration, growth of the single mutants is much reduced while the double mutant fails to grow [1].

Three molecular variants of enzyme glutathione peroxidase (GPX), encoded by nuclear genes, *GPX1, GPX2* and *GPX3*, catalyze the reduction of hydroperoxides using GSH as a reductant. A triple-deletion mutant lacking all three genes was hypersensitive to H_2O_2 and *tert*-butyl hydroperoxide (*t*-BHP) [31], which is a larger hydroperoxide that can be reduced by GPX but not by yeast catalases [1]. A study showed that yeast GPXs in fact exhibit greater similarity to phospholipid hydroperoxide glutathione peroxidases

(PHGPXs) than to GPXs, and that these enzymes are required for cellular protection against lipid peroxidation [32]. Cytoplasm-located GPX3 [33] has been renamed as HYR1 because besides its peroxidase activity, it also serves as a H_2O_2 receptor and transduces the redox-signal to transcription factor Yap1 [34]. The GPX of the yeast *Hansenula mrakii* was found mainly in mitochondrial and cytoplasmic membranes [35]. *S. cerevisiae* GPX2 was found in both the cytoplasm and nucleus, but the location of GPX1 has not been identified in *S. cerevisiae* [33].

Glutathione reductase (GLR) is primarily responsible for the reduction of oxidized glutathione and the maintenance of the GSH/GSSG ratio in cells (Figure 1.1). The nuclear gene encoding GLR is *GLR1* in *S. cerevisiae,* and the *GLR1*-null mutant, although viable, accumulates excess GSSG and is hypersensitive to oxidants [17, 36, 37].

Yeast cytosolic thioredoxin peroxidase, encoded by *TSA1*, contains two cysteine residues presumably essential for its peroxidase activity [38]. TSA reduces H_2O_2 using reducing equivalents provided by the NADPH-dependent thioredoxin system, which includes thioredoxin, thioredoxin reductase (TRR) and NADPH (Figure 1.1) [38, 39]. TSA prevented cell damage induced by metal-catalyzed oxidation systems comprised of Fe^{3+}, O_2, and thiol (such as DTT), but not when the thiol was replaced by ascorbate. Thus, this enzyme was also called thiol-dependent protector protein and thiol-specific antioxidant protein [40]. The *TSA1*-null mutant (*tsa1Δ*) exhibits no change in phenotype under anaerobic conditions but grows slowly under aerobic conditions in the presence of H_2O_2 [41]. Also, *tsa1Δ* cells exhibit much lower survival to heat-shock than wild-type strains [42] as well as an elevated total glutathione level and enhanced GLR and GPX activities [31].

Cytochrome *c* peroxidase (CCP) is found in the inter-membrane space of mitochondria [43] and appears to protect cells against H_2O_2 but so far its exact physiological function is not known. An extensive study on the role of yeast CCP in cell growth, tolerance to heat shock and oxidants is presented in Chapter 4. Table 1.1 summarizes the peroxidases and catalases characterized in *S. cerevisiae*.

Table 1.1. Peroxidases and catalases of *S. cerevisiae*

Protein	Gene	Localization	Reaction
Catalase	*CTA1*	Peroxisomal matrix and mitochondrial matrix	$2\ H_2O_2 \rightarrow 2\ H_2O + O_2$
	CTT1	Cytoplasm	
CCP	*CCP1*	Mitochondrial intermembrane space	$2\ C^{II} + H_2O_2 + 2\ H^+ \rightarrow 2\ C^{III} + 2\ H_2O$[a]
GPX (PHGPX)	*GPX1*	Unknown	ROOH + 2 GSH → 2 ROH + GSSG[b]
	GPX2	Cytoplasm and nucleus	
TSA	*TSA1*	Cytoplasm	$H_2O_2 + TRX_{[RED]} \rightarrow 2\ H_2O + TRX_{[OX]}$

[a] C^{II} represents ferrocytochrome *c* and C^{III} ferricytochrome *c*.

[b] ROOH includes H_2O_2 and larger hydroperoxides such as *tert*-butyl hydroperoxide and phospholipid hydroperoxide.

1.1.3 H_2O_2-induced signaling

The regulation of the response of *S. cerevisiae* to oxidants is not well understood. The Ras/PKA signal transduction pathway, which is responsible for regulating intracellular cAMP levels (PKA is a cAMP-dependent protein kinase), is clearly important [44]. Many stress-inducible genes, including some that are regulated by oxidants, are responsive to decreased cAMP or PKA levels [45]. In yeast and mammalian

cells, heme synthesis directly correlates with oxygen tension and thus heme serves as a secondary signal for oxygen [46]. When cells are grown aerobically, heme is synthesized in mitochondria [47] and then utilized to form hemoproteins. Heme can be transported into the nucleus to activate transcriptional factor Hap1 to regulate genes required for oxygen utilization and oxidative stress defense, such as *CYC1* [48], *CYC7* [49] and *CTT1* [50]. Hap1 also activates the aerobic repressor Rox1, which specifically represses the genes required for anaerobic growth [51].

H_2O_2 is continuously produced *in vivo* and gradients are established since membranes separate H_2O_2 production and consumption sites [52]. Recently, H_2O_2 was found not to freely diffuse across biomembranes in *E. coli*, *S. cerevisiae* and mammalian cells [53-55]. For example, yeast cells in stationary phase exhibit a low plasma membrane permeability to H_2O_2, which results in an enhanced tolerance to exogenous H_2O_2 compared to exponential-phase cells [56]. H_2O_2 has been implicated in the redox regulation of several physiological processes including signal transduction, response to oxidative stress, development, cell proliferation and apoptosis in mammals [57]. For example, H_2O_2 has the same stimulatory effect as insulin on glucose transport and lipid synthesis in adipocytes, activation of transcription factors such as NF-κB and Ap1[58], stimulation of protein phosphorylation and Ca^{2+} release [59]. It is noteworthy that calcium is a ubiquitous intracellular signal, participating a wide array of cellular processes including secretion, cell proliferation and cellular metabolism [60, 61].

In prokaryotes, the *E. coli* transcription factor OxyR is directly activated by H_2O_2 through formation of a disulfide bond between two reactive cysteine residues (C) and is deactivated by glutaredoxins [62]. It is believed that the yeast transcription factor Yap1

and OxyR are functionally homologous. Yap1 becomes oxidized upon exposure to H_2O_2 and activates genes required for the response to oxidative stress [18, 63]. Formation of two intramolecular disulfide bonds (C303-C598 and C310-C629) in oxidized Yap1 [64, 65] inhibits nuclear export in response to peroxide stress [66], and the resultant enhancement of the nuclear localization of Yap1 induces gene expression. Hyr1, a H_2O_2 sensor and redox-transducer, is essential for Yap1 oxidation by H_2O_2 [34]. Hyr1 C36 is first oxidized by H_2O_2 and then forms an intermolecular disulfide bond with Yap1 C598. Yap1 becomes activated once Yap1 forms an intramolecular disulfide bond (C303-C598) instead of the HYR1-Yap1 disulfide linkage. Unlike OxyR, Yap1 is inactivated by thioredoxin which restores its free cysteine residues.

Besides Yap1, the transcription factor Skn7 (also known as Pos9, a Skn7 mutant with an increased sensitivity to H_2O_2 [67]) was also implicated in a cellular pathway that controls the oxidative-stress response [63]. Yap1 controls a large regulon of at least 32 proteins, 15 of which (e.g., *CCP1, CTT1, SOD1, SOD2, TRR1, TRR2,* and *TSA1*) require the additional presence of Skn7 for their induction by H_2O_2 [63]. The binding sites of Yap1 and Skn7 in the *CCP1* promoter have been identified and they also exist in the promoter regions of many other oxidative-stress response genes [68].

Fap7, located in the yeast nucleus, is essential for activation of Pos9-dependent target gene transcription upon oxidative stress [69]. Fap7 is suggested to stabilize the interaction of active Pos9 and DNA, but so far the mechanism of Pos9/Skn7 activation by H_2O_2 has not been revealed. Yeast CCP was found to mediate Pos9 transcriptional activation in cells exposed to oxidative stress [70], thus further study of the relationship between CCP and Skn7/Pos9 is of interest.

Apoptosis is an active form of cell death crucial for the development and homeostasis of multicellular organisms [71]. In mammals, apoptosis can be induced by various intra- or extra-cellular stimuli and *via* several signaling pathways. ROS were the first regulators of apoptosis found to be shared between yeast and higher animals. ROS accumulate in aging yeast cells and are necessary and sufficient to induce an apoptotic phenotype in yeast [71]. Death of exponentially growing yeast cells triggered by low H_2O_2 concentrations (3–15 mM) is not caused by cell damage but involves the active cooperation of the cell [71]. At higher concentration of H_2O_2 (180 mM), most intracellular structures are destroyed, indicating necrotic cell death [71].

There is increasing evidence that mitochondrial inter-membrane proteins, such as cytochrome *c*, play a key role in the control of apoptosis triggered by various stimuli [72]. Apoptosis of mouse fibrosarcoid L929 cells was induced by microinjection of cytochrome *c*, or by exposure to H_2O_2, which altered the permeability of the mitochondrial membrane resulting in cytochrome *c* release to the cytosol [72]. Cytochrome *c* translocation from the mitochondria to the cytosol in *S. cerevisiae* has been found in apoptotic cells induced by acetic acid [73] or amiodarone [74] but has not been reported for H_2O_2-treated cells.

1.2 Yeast mitochondria

The main function of mitochondria is the production of energy in the form of ATP. Mitochondria are also involved in a number of other functions such as regulation of cellular redox status, cell signaling, apoptosis, and the synthesis of lipids and heme [75, 76]. All mitochondria consist of a double membrane structure, which forms two compartments, the matrix enclosed by the inner membrane and the inter-membrane space

between the inner and outer membranes. Both membranes, the matrix and the inter-membrane space can all be thought of as individual compartments since each is associated with a set of enzymes that performs specific metabolic processes [77]. For example, the outer membrane is very similar to the endoplasmic reticulum (ER) in terms of composition but possesses additional receptors for the import of mitochondrial proteins synthesized on cytoplasmic ribosome. Cytochrome *c*, located in the inter-membrane space, can donate electrons to CCP to reduce H_2O_2 or transfer them to complex IV that uses four electrons and four protons to reduce O_2 to two H_2O molecules (Figure 1.2). Complex IV and the other components of the respiratory chain form an integral part of the inner membrane, which is impermeable to ions, and the pH gradient that forms across this membrane is essential for ATP generation. The mitochondrial matrix is a soluble fraction containing the enzymes of the citric acid cycle and for the oxidation of fatty acids.

The mitochondrion, in addition to the nucleus, contains DNA. The matrix contains mitochondrial ribosomes for the translation of mRNA transcribed from mitochondrial DNA (mtDNA) [78]. A normal *S. cerevisiae* yeast cell contains ~20–35 copies of mtDNA [79] with a size of 78–85kb [80], depending on the strain and the growth conditions. Yeast mtDNA encodes several subunits of critical enzymes, such as ubiquinol cytochrome *c* reductase (complex III), cytochrome *c* oxidase (complex IV) and ATP synthase (complex V), all of which are members of the electron-transfer chain [81]. Yeast mtDNA lacks introns and histones, as well as a complete proofreading mechanism, which results in mtDNA being especially susceptible to ROS induced damage [8]. *S. cerevisiae* is a facultative aerobe that has the ability to survive mutations to mtDNA (*rho*$^-$

mutants) or even its complete loss (*rho*^{0} mutants), events that would be fatal to obligate aerobic species [78].

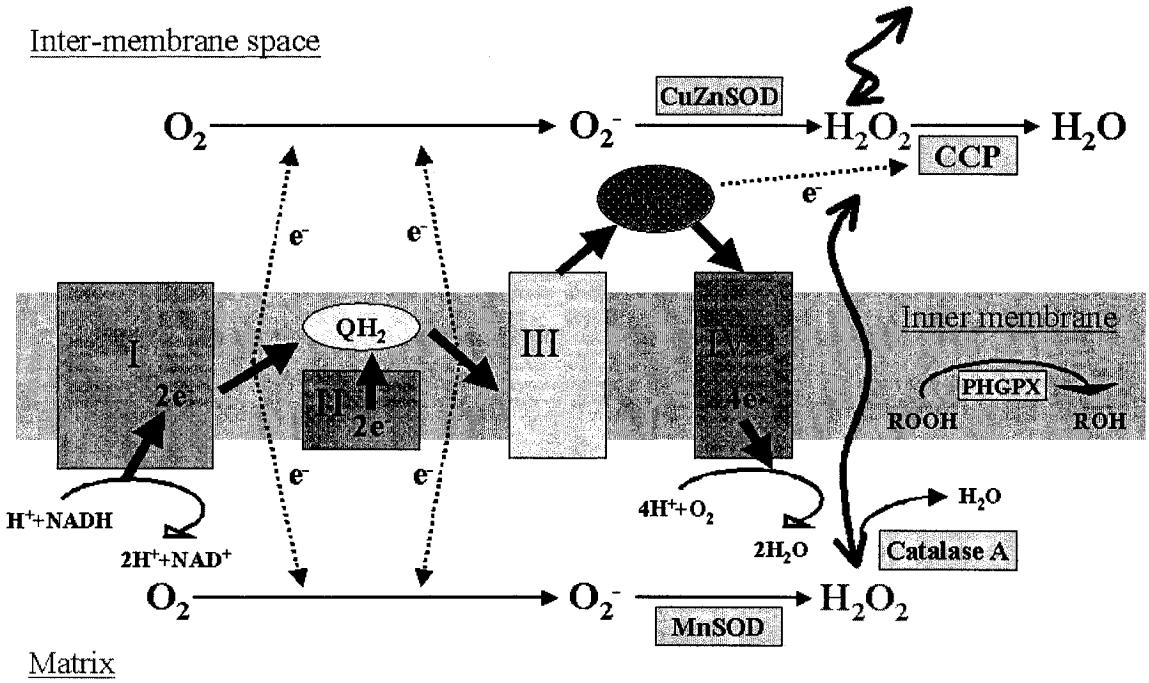

Figure 1.2. Electron transport chain and electron leakage in yeast mitochondria. The main electron flux is shown by the large arrows. About 1–2% of the electrons leak from the chain (dotted arrows) and generate superoxide anions (O_2^-). All known and proposed enzymic defenses to ROS in yeast mitochondria are indicated here. This figure is based on Refs [20, 27, 32, 52, 82-85].

The primary source of intracellular O_2^-, which is formed by the one-electron reduction of O_2, is the leakage of electrons from complex I (NADH:ubiquinone) and complex III (QH_2:cytochrome *c*) during respiration in the mitochondria [52, 83]. Approximately 80% of mitochondrial O_2^- production occurs at complex III (Figure 1.2). A recent study suggests that O_2^-, produced in the mammalian mitochondrial respiratory chain, is released from the inner membrane into both the matrix and inter-membrane space [84], instead of solely to the matrix [86]. Under normal physiological conditions,

MnSOD is the primary defence against O_2^- generated in the mitochondria [87]. When MnSOD activity is disrupted, O_2^- mediates iron release from mitochondrial iron-sulfur clusters, leading first to loss of mitochondrial function and then to death, independently of mtDNA damage. Figure 1.2 summarizes the generation of ROS in yeast mitochondria and its probable defense system.

1.3 Cytochrome *c* peroxidase

CCP (ferrocytochome-*c*:hydrogen-peroxide oxidoreductase, EC 1.11.1.5) is found in the mitochondria of aerobically grown yeast, the periplasmic space of some bacteria and in the trematodes, *Fasciola hepatica* and *Schistosoma mansoni* [88]. *S. cerevisiae* CCP was first discovered in 1940 [89] and alleles 1 and 2 were found in strains D273-10B in 1982 [90, 91] and FY1679 in 1994 [92, 93], respectively. *CCP1* is a nuclear gene and codes for CCP translated in the cytosol. CCP contains a 68 amino-acid leader sequence to target the apo-enzyme to the intermembrane space of mitochondria [90]. The leader sequence is cleaved upon importation giving rise to the mature protein containing 294 amino-acid residues with a molecular weight of ~34 kDa, including a single non-covalently bound heme group. Unlike other heme proteins such as catalase and cytochrome *c*, oxygen induces the interconversion between apo- and holo-CCP *in vivo* by heme insertion and removal [94-96], suggesting a role for the interaction between apoCCP and heme in response to oxidative stress.

So far, CCP does not have a well-defined role *in vivo*. A study has shown that *Fasciola hepatica* CCP protects against oxidative damage to deoxyribose *in vitro* by preventing $^{\bullet}OH$ formation from H_2O_2 by the Fenton reaction [88]. *Cryptococcus neoformans* CCP was found to increase the survival of cells exposed to exogenous H_2O_2

[97]. In *S. cerevisiae*, CCP behaves as an antioxidant enzyme because it detoxifies over 50% of the H_2O_2 formed in mitochondria during aerobic metabolism [85]. Using a Pos9-lacZ reporter system, CCP was also found to be important in mediating transcriptional activation of oxidative stress genes [70]. Thus, CCP is suggested to exhibit both antioxidant and signaling functions in *S. cerevisiae*.

The mechanism of yeast CCP catalysis *in vitro* is well understood as a result of extensive protein engineering [98]. CCP was the first heme enzyme to have its crystal structure determined and, as a consequence, has played a pivotal role in our understanding of the structural control of hemoprotein reactivity.

1.3.1 CCP catalysis

CCP catalyzes the reduction of H_2O_2 to H_2O, utilizing reducing equivalents from ferrocytochrome *c*:

$$2 \text{ ferrocytochrome } c + H_2O_2 + 2\ H^+ \rightarrow 2 \text{ ferricytochrome } c + 2\ H_2O \qquad (1.1)$$

The catalytic mechanism of CCP couples the one-electron oxidation of ferroytochrome *c* to the two-electron reduction of H_2O_2 to H_2O. Three redox states of CCP are involved (Eqs. (1.2)-(1.4)):

$$CCP + H_2O_2 \rightarrow CCP\text{-}I + H_2O \qquad (1.2)$$

$$CCP\text{-}I + \text{ferrocytochrome } c + H^+ \rightarrow CCP\text{-}II + \text{ferricytochrome } c \qquad (1.3)$$

$$CCP\text{-}II + \text{ferrocytochrome } c + H^+ \rightarrow CCP + \text{ferricytochrome } c + H_2O \qquad (1.4)$$

Here CCP represents the resting ferric (Fe^{III}) enzyme, and CCP compound I (CCP-I) and compound II (CCP-II) are intermediate oxidized forms of CCP. The oxidized sites in CCP-I are an oxyferryl (Fe^{IV}=O) and a radical localized on Trp191. CCP-II is the one-electron reduced product of CCP-I and contains an oxyferryl heme. Reactions (1.3) and

(1.4) involve electron transfer from ferrocytochrome *c* to the oxidized sites of CCP forming the products ferricytochrome *c* and H_2O.

Reaction (1.1) is rapid around neutral pH with a bimolecular rate constant of $4.5 \times 10^7 M^{-1} s^{-1}$ [99]. A proposed mechanism for the formation of CCP-I based on a model for the peroxy complex has been elaborated [100]. His175 coordinates to the heme iron and Asp235 is hydrogen bonded to the side chains of both Trp191 and His175 in the proximal heme pocket [101]. H_2O_2 diffuses into the distal heme pocket defined by Arg48, Trp51 and His52, binds to the heme iron and donates a proton to His52 in a concerted fashion. The positively charged His52 and Arg48 stabilize the transition state for heterolytic cleavage of the O–O bond of the bound peroxide to form an oxyferryl porphyrin π-cation radical species. This state is stabilized by hydrogen bonding between the iron-bound oxygen and Arg48 and Trp51. Finally, Trp191 donates an electron to the porphyrin π-cation radical giving the stable form of CCP-I. Figure 1.3 presents the active site of yeast CCP.

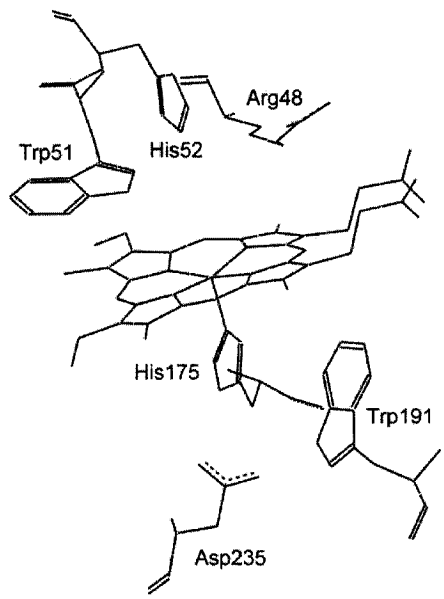

Figure 1.3. Structure of yeast CCP active site [101].

1.3.2 Electron transfer between cytochrome *c* and CCP

The refined high-resolution 3D-structures of yeast CCP (1.7 Å) [101] and the yeast CCP/yeast cytochrome *c* complex (2.3 Å, Figure 1.4) [102] were published in 1984 and 1992, respectively. The complex formed between CCP and cytochrome *c* has been investigated by almost all available physical techniques including absorption, fluorescence, circular dichroism, infrared and resonance Raman spectroscopy, nuclear magnetic resonance, affinity chromatography and titration calorimetry as reviewed in [98].

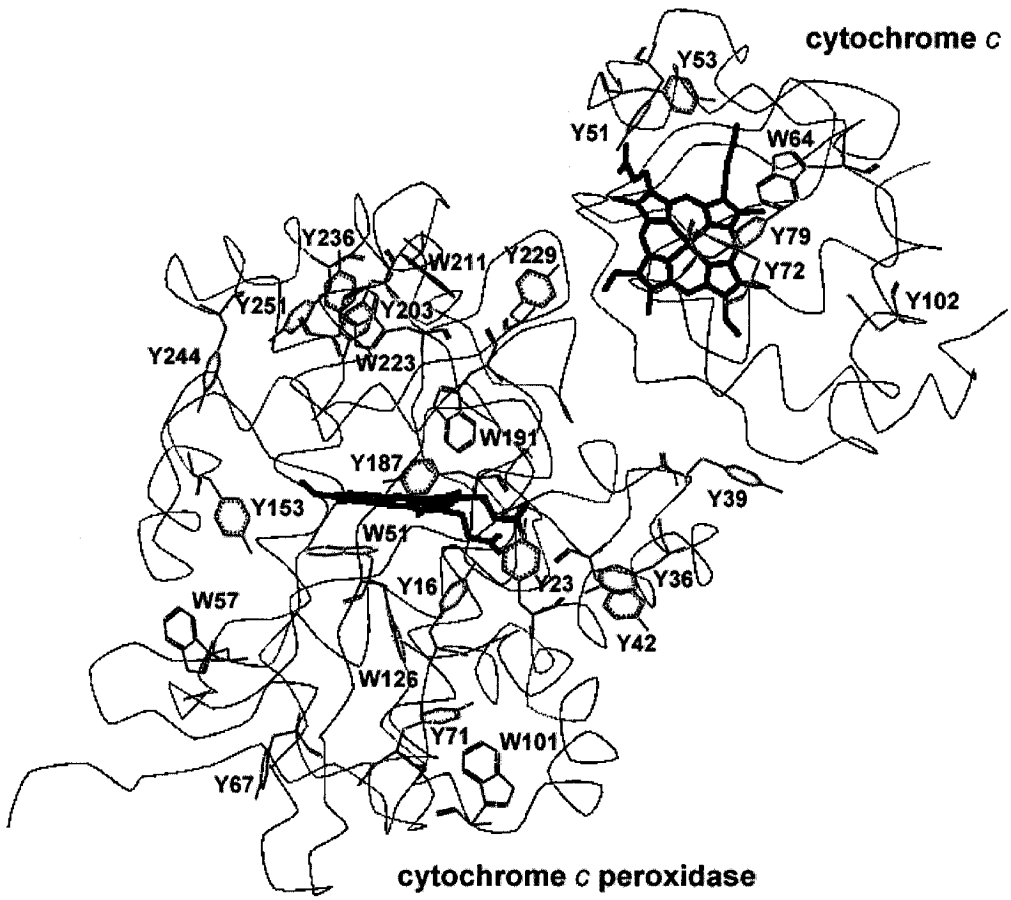

Figure 1.4. 3D structure of the yeast CCP/yeast cytochrome *c* complex [102]. The structure was downloaded from the NCBI database at http://www.ncbi.nlm.nih.gov. The protein backbone of the complex is shown with the tyrosine (Y) and tryptophan (W) side chains. Tyr39 and Tyr229 of CCP are located at the binding region of cytochrome *c*. The hemes are shown in bold in each protein.

Yeast CCP is an acidic protein, with a reported isoelectric point between 4.9–5.25 [103-105], while yeast cytochrome *c* is a basic protein with an isoelectric point of 10.05 [106]. There is universal agreement that CCP can bind both ferro- and ferri-cytochrome *c* to form 1:1 complexes with a K_{D1} that increases substantially with increasing ionic strength [98]. The affinity for a second cytochrome *c* molecule to form a 1:2 CCP/cytochrome *c* complex is much smaller (K_{D2} ~10^3K_{D1}–10^4K_{D1}). The detailed mechanism of electron transfer between cytochrome *c* and CCP has been reviewed in [98]. After ferrocytochrome *c* binds to the high-affinity binding site (Figure 1.4), intracomplex electron transfer reduces the Trp191 radical in CCP-I, producing CCP-II and ferricytochrome *c*. Ferricytochrome *c* dissociates from the high-affinity site at a rate that is determined by the nature of cytochrome *c* and the ionic strength of the solution. A second molecule of ferrocytochrome *c* binds at the high-affinity site and reduces the Fe^{IV}=O heme in CCP-II, producing a CCP/ferricytochrome *c* complex.

1.3.3 Oxidation of CCP in the absence of ferrocytochrome *c*

In the absence of cytochrome *c*, CCP can be oxidized by H_2O_2 in various ways [107]. The reaction between CCP and H_2O_2 depends on the molar ratio of the reagents. When a stoichiometric amount of H_2O_2 is reacted with CCP, CCP-I is rapidly formed within seconds, with changes in the enzyme's absorption spectrum (Figure 1.5). Heme oxidation causes a 10-nm red-shift of the Soret peak and a decrease in absorption at 380 nm. Two well-defined charge-transfer peaks appear at 530 and 560 nm, and a blue-shift from 282 to 276 nm indicates a change in protein conformation [108, 109]. The Fe^{IV}=O heme and the Trp191 radical in CCP-I decay with half-times of 6.6 h and 2.5 h,

respectively, to a ferric CCP product [110], which has lost the two oxidizing equivalents of CCP-I but retains ~75% peroxidase activity [111].

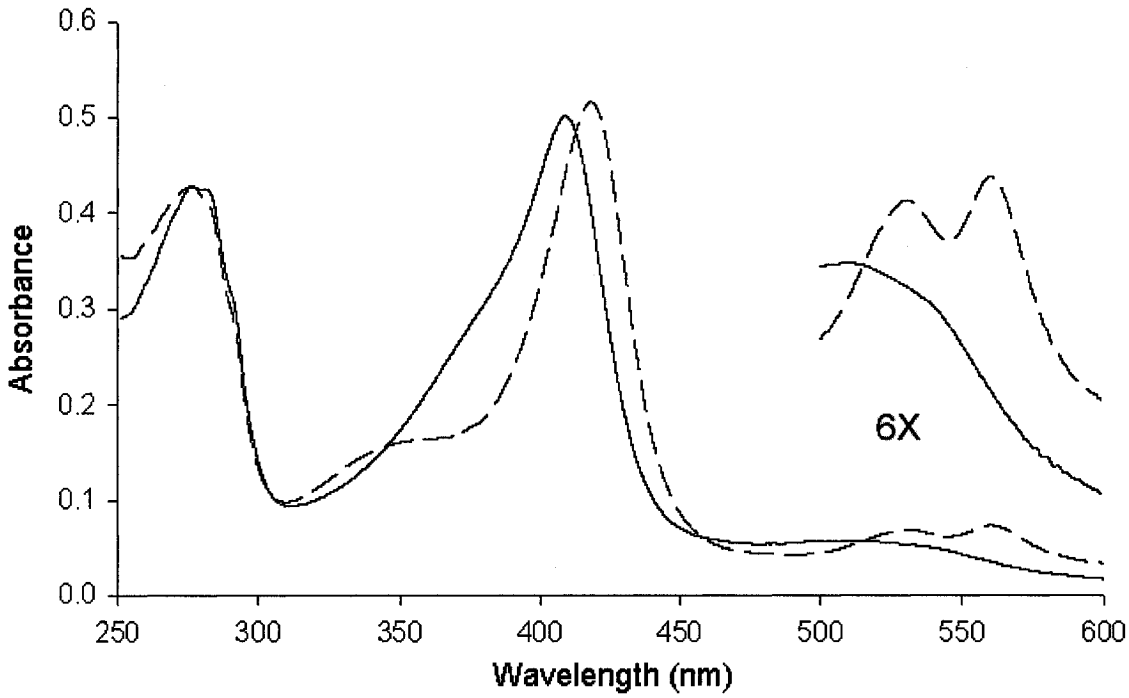

Figure 1.5. Absorption spectrum of native and oxidized recombinant yeast CCP. Solid line (——) is the spectrum of 5 μM of resting ferric CCP and dashed line (– – –) is the spectrum recorded 10 s after CCP was oxidized with 5 μM H_2O_2. Spectra of recombinant CCP(MI) [112] were recorded in 100 mM sodium phosphate buffer (pH 7.0) at 25°C in a 1-cm cuvette.

CCP can reduce 10 molar equivalents of H_2O_2 within 5 min by further oxidizing some of its 7 Trp and 14 Tyr residues (Figure 1.4). This occurs without detectable O_2 release [107, 113] and Tyr residues on the protein surface are considered to be endogenous electron donors. On reaction with 10 molar equivalents of H_2O_2 in the presence of the spin scavenging reagent, 2,2,6,6-tetramethylpiperidinyl-oxy (TEMPO$^\bullet$), yeast CCP was found to be labeled with nine TEMPO$^\bullet$ groups, indicating that nine possible tyrosyl radicals were scavenged in the protein [114]. In another study using the

spin-trap 2-methyl-2-nitrosopropane, Tyr39 and Tyr153 were identified as sites of radical formation [115] (Figure 1.4). H_2O_2 also promotes intermolecular crosslinking of CCP [111, 116], and the two crosslinked peptides identified contain Tyr36, Tyr39 and Tyr42, and Tyr229 and Tyr236 [116, 117] (Figure 1.4). It is noteworthy that Tyr39 and Tyr229 are located in the cytochrome *c* docking site (Figure 1.4) [102], suggesting a possible role for H_2O_2-induced tyrosyl radicals within the CCP/cytochrome *c* complex.

1.4 Proteomics

Proteomics is the term used for the global analysis of gene expression at the protein level in a cell, and was first defined in 1995 [118]. The goals of proteomics are to establish the biological functions of all proteins, and to develop networks and fluxes of all the proteins in an organism [119].

1.4.1 Proteomics and genomics

Gene expression can be detected quantitatively and reproducibly using DNA microarray techniques. Unique regions in each gene are chosen as probes, allowing for specific detection of individual gene transcripts, even among genes from the same family [120]. The complete DNA sequence of the *S. cerevisiae* genome was published in 1996 [121] and a global study on yeast genomic expression patterns during environmental changes such as progression into stationary phase, heat shock, osmotic shock or oxidative stress was reported in 2000 [22]. The online database at http://www-genome.stanford.edu /yeast_stress provides the experimental data for individual genes.

Although the genome provides an overview of the genes present, it is increasingly clear that this is only the very beginning of unraveling how cells function at the molecular level. Cellular proteins are not invariant products of genes, but are subject to a

high degree of interdependent processing that is critical in cellular function and regulation. Genomic methods are not adequate to define the forms, levels, and spatial distribution of proteins. In contrast to the static genome, where all information could in principle be obtained from the DNA of a single cell, the proteome is dynamic and highly dependent not only on cell type, but also on the state of the cell.

1.4.2 Methodology in proteomics

The power of proteomics resides in its ability to examine biological responses over thousands of proteins simultaneously and provide a relatively comprehensive view of cellular metabolism. For example, proteins tagged for tandem affinity purification (TAP) were first introduced to systematically investigate protein complexes in *S. cerevisiae* in 2002 [122]. The data, which are accessible at http://yeast.cellzome.com, reveal that no CCP protein complexes were detected in yeast growing exponentially in YPD. Global studies of protein localization and expression levels in *S. cerevisiae* expressing chromosomally tagged green fluorescence protein (GFP) and TAP tag fusion proteins were reported in 2003 [33, 123]. These data, available at http://yeastgfp.ucsf.edu, reveal that CCP is a low abundance (6730 molecules per cell) mitochondrially localized protein in budding yeast.

A popular method for the analysis of whole proteomes is two-dimensional gel electrophoresis (2DE) mapping that combines protein separation with mass spectrometric (MS) identification of selected protein spots. 2DE maps of total cellular proteins have been used to probe proteome alterations in *S. cerevisiae* during the dauxic-shift [124], H_2O_2 exposure [125] and metal challenge [126, 127], as well as proteome differences between strains [128]. The proteins from each culture are separated on a 2D gel, and the

gels are analyzed to identify proteins with altered expression in cultures grown under different conditions.

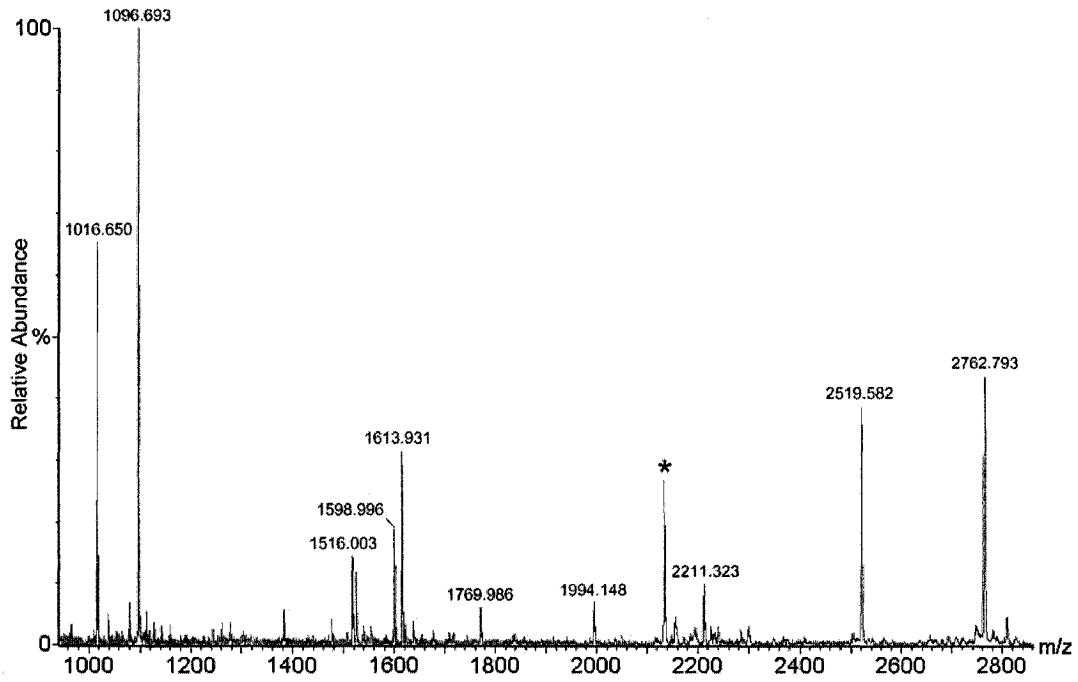

Figure 1.6. Example of a peptide mass fingerprint generated by MALDI-ToF MS of a tryptic digest of a protein spot. A spot was cut from a 2D gel of 3-day *S. cerevisiae* W303-1B cells and the protein was in-gel digested by trypsin. The protein was identified as TPI1 using the *S. cerevisiae* database of the National Center for Biotechnology Information (NCBI) with the Mascot search engine [129]. The peaks are labeled with the m/z of their MH^+ ions, and the asterisk (*) represents a peptide arising from trypsin autolysis.

2DE separates proteins by isoelectric focusing (IEF) in the first dimension and by molecular mass *via* polyacrylamide gel electrophoresis (SDS-PAGE) in the second dimension [130]. Mapping of the *S. cerevisiae* proteome has yielded 1000–1400 protein spots on 2D gels within a pI range of 4–8 and M_r of 15–150 kDa [131-133]. Matrix-assisted laser desorption ionization-time-of-flight (MALDI-ToF) MS is an essential tool for rapid protein identification. Masses of the peptides obtained by enzymatic protein

fragmentation are used to search gene sequence databases for proteins with peptide mass fingerprints (PMF) that match those obtained [134]. Figure 1.6 shows the PMF generated by MALDI-ToF MS of the tryptic digest of a protein identified as yeast TPI1 (triosephosphate isomerase) from a search of the *S. cerevisiae* database in NCBI using the Mascot search engine [129].

The protein constituents of subcellular complexes and organelles are also being examined at the proteomics level. This approach is used for identifying protein-protein interactions and it also provides crucial information about the spatial distribution of proteins in cells. Liquid chromatography-tandem MS (LC-MS/MS) is being widely employed to analyze proteomes of organelles and protein complexes. All the proteins in a complex are denatured, subjected to tryptic digestion, and desalted. The peptide mixture can then be analyzed by a biphasic microcapillary chromatographic system involving, for example, separation by stepwise-salt-gradient elution from a strong ion-exchange column followed by reversed-phase chromatography of the individual fractions from the ion-exchange column. MS/MS peptide fragmentation data can be obtained on-line, and a program such as SEQUEST can correlate the MS/MS spectra of fragmented peptides to proteins in the original protein complex based on data in nucleotide databases. Using this LC-MS/MS approach, 546 proteins from purified mitochondria [135] and 75 out of 78 proteins from the ribosome [136] have been identified in *S. cerevisiae*. A study of *E. coli* ribosomes provides a second example of the current possibilities. Using complete ribosomes (M_r ~2.3 MDa) as targets for MALDI-ToF MS, 55 of the 56 proteins in the ribosome were observed as intact proteins without fragmentation and a wide variety of post-translational modifications were detected [137].

Our focus here is on CCP which is targeted to mitochondria. Thus, a comparison of the mitochondrial proteomes of wild-type and *ccp1Δ* yeast cells under different growth conditions could help us understand the physiological roles of CCP. Over 700 proteins have been identified in the mitochondria of exponentially growing *S. cerevisiae* cells [138]. MitoP2, a database of mitochondria-related genes, proteins and diseases, currently (May, 2006) contains 523 entries on genes of known function in *S. cerevisiae* mitochondria [139]. There are 477 proteins conclusively located in yeast mitochondria, of which 469 are nuclear-encoded and eight are mitochondrial-encoded [138, 139].

1.5 Thesis outline and contributions of colleagues

Changes in absorption and circular dichroism spectra of yeast CCP and its W191F mutant on oxidation in the presence or absence of TEMPO$^{\bullet}$ (a radical scavenger) were compared *in vitro* and the results are presented in Chapter 2. Since mass spectrometry is extensively used to investigate radical trapping [115, 117] and radical scavenging [114], a systematic investigation of the mass spectral behavior of TEMPO$^{\bullet}$ and NAYA (a low-mass model of tyrosine residues in proteins) in a Z-spray electrospray ionization source in aqueous solutions is discussed in Chapter 3. The physiological roles of CCP in *S. cerevisiae* cell growth and survival under heat-shock and oxidative stress were monitored by studying wild-type, *ccp1Δ* and *ccp1Δ-CCP*^{W191F} strains and the results are given in Chapter 4. To further probe the function of CCP, an effort to map the mitochondrial proteomes of wild-type and *ccp1Δ* yeast cells using 2DE is discussed in Chapter 5. An effective metabolic-labeling method using D_{10}-Leu for quantitatively comparing different yeast proteomes was developed and is described in Chapter 6. Using this isotope-ratio quantitation approach, a method for monitoring changes with time in the yeast proteome

following H_2O_2 challenge is introduced in Chapter 7. Finally, Chapter 8 provides a brief summary of the results as well as suggestions for future work.

Chapter 6 was published in the *Journal of Proteome Research* [Jiang H. and English A. M. (2002) J Proteome Res. 1, 345-350] and reproduced here with the permission of the journal (© 2002 American Chemical Society). I carried out all the work reported in this publication and prepared the manuscript. A. M. English provided intellectual support and edited the manuscript.

Chapter 4 is currently in press at the *Journal of Inorganic Biochemistry* and reproduced here with the permission of the journal. I carried out all the work reported in this publication and prepared the manuscript. A. M. English provided intellectual support and edited the manuscript.

Chapter 7 is currently in press at the *Journal of Proteome Research* and reproduced here with the permission of the journal (unpublished work © 2006 American Chemical Society). I carried out all the work reported in this publication and prepared the manuscript. A. M. English provided intellectual support and edited the manuscript.

All abbreviations, and citation, figure and table numbering systems in the published work were changed to the format of this thesis.

The DFT calculations described in Chapter 3 were carried out in collaboration with Etienne Paradis and Qadir Timerghazin. I carried out all MS experiments reported in this Chapter and have prepared a manuscript based on the results which will be submitted for publication. A. M. English provided intellectual support and is editing the manuscript.

2 Biophysical comparison of yeast CCP and its W191F mutant following H_2O_2-exposure

2.1 Abstract

Changes in the absorption and circular dichroism (CD) spectra of recombinant yeast cytochrome *c* peroxidase [CCP(MI)] and its W191F mutant (CCP^{W191F}) on oxidation by H_2O_2 were compared in 100 mM sodium phosphate buffer (pH 7.0). The W191F mutation resulted in little detectable alteration of the protein's secondary or tertiary structure or in its complex with ferricytochrome *c*. CCP^{W191F} exhibited fewer spectral changes than CCP from 10 s to 30 min following addition of 10 molar equivalents of H_2O_2. The radical scavenger, 2,2,6,6-tetramethylpiperidinyl-1-oxy (TEMPO$^{\bullet}$), efficiently inhibited H_2O_2-induced crosslinking of CCP and CCP^{W191F}, consistent with the formation of surface-exposed radicals on the oxidation. TEMPO$^{\bullet}$ accelerated the rate of oxyferryl heme reduction in the oxidized proteins. In addition, DTPA inhibited crosslinking of the W191F mutant but not wild-type CCP.

2.2 Introduction

Mature yeast CCP is located in the intermembrane space of mitochondria [90]. It contains a single non-covalently bound heme group and behaves as an antioxidant enzyme because it catalyzes the reduction of H_2O_2 to H_2O, utilizing reducing equivalents from ferrocytochrome *c* [98]:

$$2 \text{ ferrocytochrome } c + H_2O_2 + 2\ H^+ \rightarrow 2 \text{ ferricytochrome } c + 2\ H_2O \qquad (1.1)$$

The catalytic mechanism of CCP involves electron transfer from ferrocytochrome *c* to the oxidized sites of CCP forming the products ferricytochrome *c* and H_2O. Trp191 on the proximal side of the heme (Figure 1.3) accepts electrons donated from ferrocytochrome *c*

after CCP is two-electron oxidized by H_2O_2 in a heme-mediated process [100]. The CCP^{W191F} point mutant exhibits negligible ferrocytochrome *c*-oxidizing activity due to a 10^4-reduced rate of CCP-cytochrome *c* intracomplex electron transfer [140]. However, introduction of CCP^{W191F} into *ccp1Δ* yeast cells restored their ability to activate the transcription factor, Skn7/Pos9, in response to H_2O_2 stress [70]. Thus, in addition to its antioxidant properties, yeast CCP may play a role in transducing redox signals. Although the physiological roles of CCP are not well understood, the biophysical properties of yeast CCP and its W191F mutant have been extensively studied, and are summarized in Table 2.1.

Oxidation of CCP to form CCP compound I (CCP-I) is a rapid reaction ($k = 3.2 \times 10^7$ $M^{-1}s^{-1}$) [141] and H_2O_2 causes a significant change in the absorption spectrum within 1 s [109]. The oxidized sites in CCP-I are an oxyferryl (Fe^{IV}=O) heme and a radical localized at Trp191 ($P^{\bullet+}$):

$$PFe^{III} + H_2O_2 \rightarrow P^{\bullet+}Fe^{IV}=O + H_2O \qquad (2.1)$$

CCP^{W191F} reacts almost twice as fast with H_2O_2 as CCP, forming a transient ($t_{1/2}$ ~14 ms) oxyferryl porphyrin π-cation radical [110, 141, 142]. Both CCP and CCP^{W191F} can reduce up to 10 molar equivalents (10×) of H_2O_2 in the absence of an exogenous electron donor [113] by further oxidizing their aromatic residues ($P_x^{\bullet+}$ and $P_y^{\bullet+}$) [143]:

$$P^{\bullet+},P_x,P_yFe^{IV}=O + 2\ H^+ \rightarrow P,P_x^{\bullet+},P_y^{\bullet+}Fe^{III} + H_2O \qquad (2.2)$$

This process is mediated by the heme since heme-free apoCCP does not consume H_2O_2 [107]. The time for 10× H_2O_2 consumption by CCP^{W191F} (30 min) was 6-fold longer than for CCP (5 min) [113], revealing that the former has impaired endogenous reduction ability in addition to its inability to accept electrons from ferrocytochrome *c*. The number

of oxidized Trp residues in both CCP and CCP^{W191F} increased over 20 min following 10× H_2O_2 addition but was unchanged from 20 min to 24 h. CCP exhibited loss of two more Trp residues than CCP^{W191F} [113] but based on the number of Tyr residues reported 24 h after H_2O_2 addition [113], both oxidized proteins lost ~4 Tyr residues (Table 2.1).

Oxidation of CCP and CCP^{W191F} with H_2O_2 also resulted in protein crosslinking due to the formation of solvent-exposed tyrosyl radicals [111, 116, 117]. Up to nine carbon-centered radicals on surface Tyr residues were scavenged by 2,2,6,6-tetramethylpiperidinyl-1-oxy ($TEMPO^{\bullet}$) within 10 min exposure of CCP to 10× H_2O_2 [114]. H_2O_2-induced radical formation in heme proteins including CCP [70] has been suggested to be involved in cell signaling [117, 144]. The stimulation of most yeast stress genes upon exposure to exogenous H_2O_2 occurs within 5 min and returns to baseline within 60 min [125]. Since CCP^{W191F} generates a more persistent oxidative-stress signal than CCP *in vivo* [70], it is of interest to compare their oxidized forms. Thus, CCP and its W191F mutant were oxidized with 1× and 10× H_2O_2 and changes in their absorption and circular dichroism (CD) spectra from 10 s to 30 min were monitored. $TEMPO^{\bullet}$ was used to probe radical formation leading to protein crosslinking. The efficiency of $TEMPO^{\bullet}$ as a donor to the oxyferryl heme of CCP is also discussed.

Table 2.1. Comparison of physical and catalytic properties of oxidized CCP and its W191F mutant

Property		H_2O_2/CCP	CCP	CCP^{W191F}	References
k ($M^{-1}s^{-1}$) [a] $PFe^{III} + H_2O_2 \rightarrow P^{\bullet+}Fe^{IV}=O + H_2O$		1×	3.2×10^7	5.7×10^7	[141, 142]
$t_{1/2}$ of Trp191 radical[b]		1×	2.5 h	–	[110]
$t_{1/2}$ of porphyrin π-cation radical[b]		1×	ND	~14 ms	[142]
$t_{1/2}$ of $Fe^{IV}=O$ heme[b]		1×	6.6 h	4.9 h	[110, 112]
% monomer in H_2O_2-oxidized protein[c]		1×	100	65	[113]
		10×	67	65	
H_2O_2 turnover (min)[d]		3×	1	1	[113]
		10×	5	30	
H_2O_2-oxidized protein after 24 h[e]	CCP activity (%)[e,f]	1×	73	–	[113]
		10×	19	–	
	Trp loss[e,g]	1×	1.4	0.2	[113]
		10×	3.8	1.8	
	Tyr Loss[e,h]	1×	0.7	1.5	[113]
		10×	4.4	3.8	
Surface tyrosyl radical sites[i]			Y39, Y153 Y236		[115, 117]

[a] k values in 10 mM potassium phosphate (pH 6.0) with KNO_3 to adjust the ionic strength to 100 mM at 25 °C.

[b] The proteins (10 μM) were oxidized by equimolar H_2O_2 at pH 6 and radical decay rates were determined by EPR and absorption spectroscopy. The porphyrin π-cation radical in CCP is too short lived to be detected.

[c] Determined by SDS-PAGE following reaction of 5 μM protein with 5 μM or 50 μM H_2O_2 at pH 7 for 1 h.

[d] HRP-catalyzed oxidation of ABTS was used to monitor H_2O_2 turnover by 5 μM CCP in the absence of electron donors at pH 7.

[e] The proteins (5 μM) were reacted with 5 μM or 50 μM H_2O_2 at pH 7 and incubated at room temperature for 24 h.

[f] CCP^{W191F} exhibits negligible ferrocytochrome *c* oxidizing activity [140].

[g] Trp loss was estimated from loss of fluorescence in the decay products in 8 M urea at pH 1.5 following reaction with H_2O_2.

[h] Tyr loss was determined by amino acid analysis.

[i] Radical location was determined by mass spectrometric analysis of MNP (2-methyl-2-nitrosopropane)-labeled tryptic peptides from H_2O_2-oxidized CCP.

2.3 Materials and methods

2.3.1 Materials

Recombinant baker's yeast CCP(MI) and its W191F mutant (CCP^{W191F}), isolated as previously described [145], were kindly provided by Dr. Mark Miller (University of California, San Diego). DNA sequencing (Appendix 4.1) revealed that the gene encoding CCP(MI) was cloned from allele 1 of yeast *CCP1* [90]. Yeast cytochrome *c* was purchased from Sigma and used without further purification. The proteins were stored at –20°C and dissolved in 100 mM sodium phosphate (NaPi) buffer (pH 7.0) prior to use. Protein concentrations in buffer were determined spectrophotometrically using ε_{408} = 102, ε_{408} = 109 and ε_{410} = 106.1 $mM^{-1}cm^{-1}$ for CCP(MI) [145], CCP^{W191F} [112] and ferricytochrome *c* [146], respectively. The purity index (A_{408}/A_{280}) of CCP (1.02) and CCP^{W191F} (1.10) are close to the value of ~1.2 for the freshly purified proteins [112]. The A_{408}/A_{380} (1.6) and A_{620}/A_{647} (0.9) ratios of CCP are comparable to the reported values (1.5 and 0.8, respectively) [147], revealing that the heme of the wild-type protein was predominantly 5-coordinate, high-spin [148] in 100 mM NaPi (pH 7.0). The A_{408}/A_{380} and A_{620}/A_{647} ratios of CCP^{W191F} were 1.4 and 1.0, respectively, indicating an increased amount of 6-coordinate heme in the mutant [147, 148].

2.3.2 Methods

The commercial H_2O_2 stock solution (30%, Fisher) was diluted into 100 mM NaPi buffer (pH 7.0), and TEMPO$^{\bullet}$ (Sigma) was dissolved in the above buffer just prior to use. H_2O_2 and TEMPO$^{\bullet}$ concentrations were determined spectrophotometrically using ε_{240} = 43.6 $M^{-1}cm^{-1}$ [149] and ε_{445} = 11 $M^{-1}cm^{-1}$ [150], respectively.

The absorption spectra of 2.5 μM CCP and CCP^{W191F} were recorded using a Hewlet-Packard 8453 spectrophotometer. H_2O_2 was added to the protein solutions to give a final concentration of 2.5 or 25 μM and spectra were recorded at 10 s, 1, 3, 5, 10, 20 and 30 min in the presence or absence of 25 μM TEMPO•.

CD spectra were recorded on a JASCO J-710 spectropolarimeter. The far-UV (200–250 nm) CD spectra of 20 μM CCP and CCP^{W191F} were recorded in a 0.1-cm rectangular cell using a scan speed of 100 nm/min with a response time of 0.25 s. The near-UV (250–300 nm) and the heme (380–450 nm) spectra were recorded in a 0.5-cm rectangular cell at a protein concentration of 20 μM with or without 200 μM H_2O_2. The spectra were recorded 10 s, 10 min and 20 min after H_2O_2 addition at a scan speed of 20 nm/min and a response time of 2 s.

Both ferro- and ferricytochrome *c* bind CCP to form a 1:1 complex with a dissociation constant (K_{DI}) that increases substantially with increasing ionic strength [98]. To study the effects of W191F mutation on the CCP/cytochrome *c* interaction, the proteins were dissolved in 25 mM NaPi (51 mM ionic strength, pH 7.0) to promote complex formation. CCP or CCP^{W191F} was mixed with yeast ferricytochrome *c* to give a final concentration of 10 μM in each protein. Heme CD spectra were recorded and compared with the calculated spectra obtained by adding the spectra of free CCP and ferricytochrome *c*.

Crosslinking following addition of 5 μM or 50 μM H_2O_2 to 5 μM CCP and CCP^{W191F} in 100 mM NaPi buffer (pH 7.0) was studied using SDS-PAGE [113]. To investigate its effects on crosslinking, 50 μM TEMPO• was added to the reactions. A 10-μL aliquot was removed from each sample after 30 min, mixed with 40 μL of 10% (w/v)

SDS, incubated for 30 min at room temperature and heated for 5 min at 95°C. A 10-μL aliquot of each sample containing 0.34 μg of protein was loaded on a 10% SDS-PAGE gel and the proteins were separated at a constant current of 15 mA. Crosslinking was also investigated in 100 mM NaPi buffer (pH 7.0) with 100 μM DTPA to chelate free trace metal ions.

2.4 Results

2.4.1 The W191F mutation does not cause a significant conformational change in CCP

Mutation of W191F was confirmed by mass spectrometry. Due to the difference in mass of Trp and Phe residues (39.0 u), the theoretical average mass (M_r) of yeast CCP(MI) and its W191F mutant are 33599.6 and 33560.6 u based on their amino acid sequences minus the initial methionine (−131.2 u) [151]. The most abundant peaks in the deconvolved electrospray ionization quadrupole-time of flight (ESI-Q-ToF) mass spectra appear at 33598.4 and 33559.0 u (Figure 2.1) in agreement with the theoretical M_r values within the mass accuracy of the QToF2 (± 50 ppm or ± 1.7 u at 34000 u).

The far-UV CD spectra both show a minimum at 210 nm and a broad shoulder around 222 nm (Figure 2.2) consistent with ~20% α-helical secondary structure in CCP [101]. The similarity of the CCP and CCP^{W191F} spectra, which are identical to those previously reported [101], confirms that the W191F mutation causes negligible secondary structural changes [116].

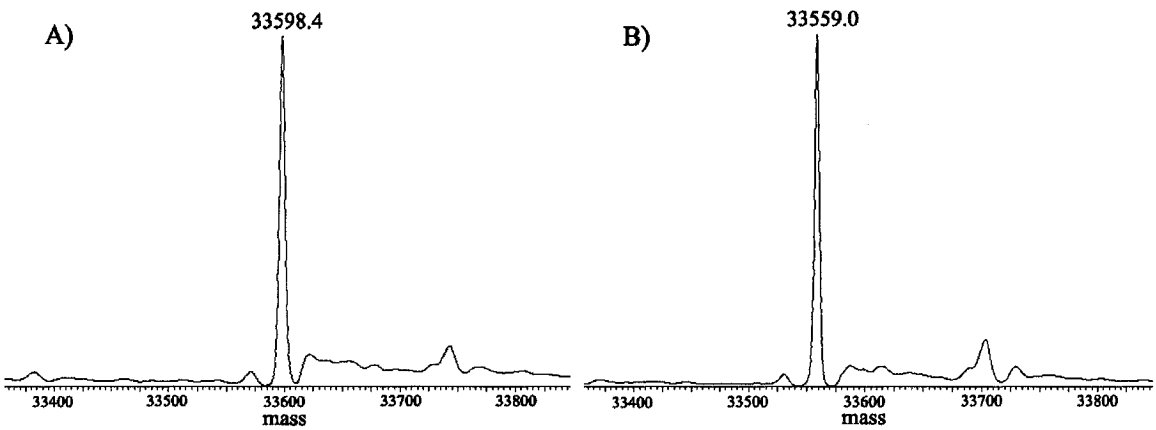

Figure 2.1. Deconvolved ESI mass spectra of (A) yeast CCP(MI) and (B) its W191F mutant. The proteins were diluted into 50% acetonitrile plus 0.05% TFA to a final concentration of 5 μM. Samples were directly infused into the Z-spray source of the QToF2 mass spectrometer (Waters Micromass) at a flow rate of 1 μL/min. The instrumental parameters were: capillary voltage 3.3 kV, cone voltage 45 V, multiplier 550 V, MCP 2100 V and ToF -9.1V.

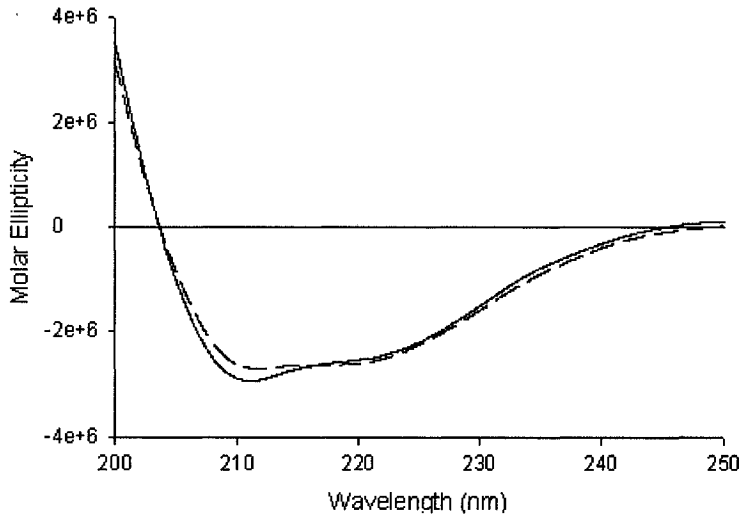

Figure 2.2. Far-UV CD spectra of ferric yeast CCP and its W191F mutant. The spectra are the average of five scans recorded for 20 μM CCP (——) and CCP^{W191F} (— — —) in 100 mM sodium phosphate buffer (pH 7.0) in a 0.1-cm rectangular cell at 0.2-nm resolution and a bandwidth of 1 nm at 25°C. The molar ellipticity ($[\theta]$, $M^{-1}cm^{-1}$) = $3298\Delta\varepsilon$, where $\Delta\varepsilon$ (molar CD, $M^{-1}cm^{-1}$) = $\Delta A/cl$. ΔA the difference between measured absorbance of left- and right-circularly polarized light, c the molar concentration and l the path length.

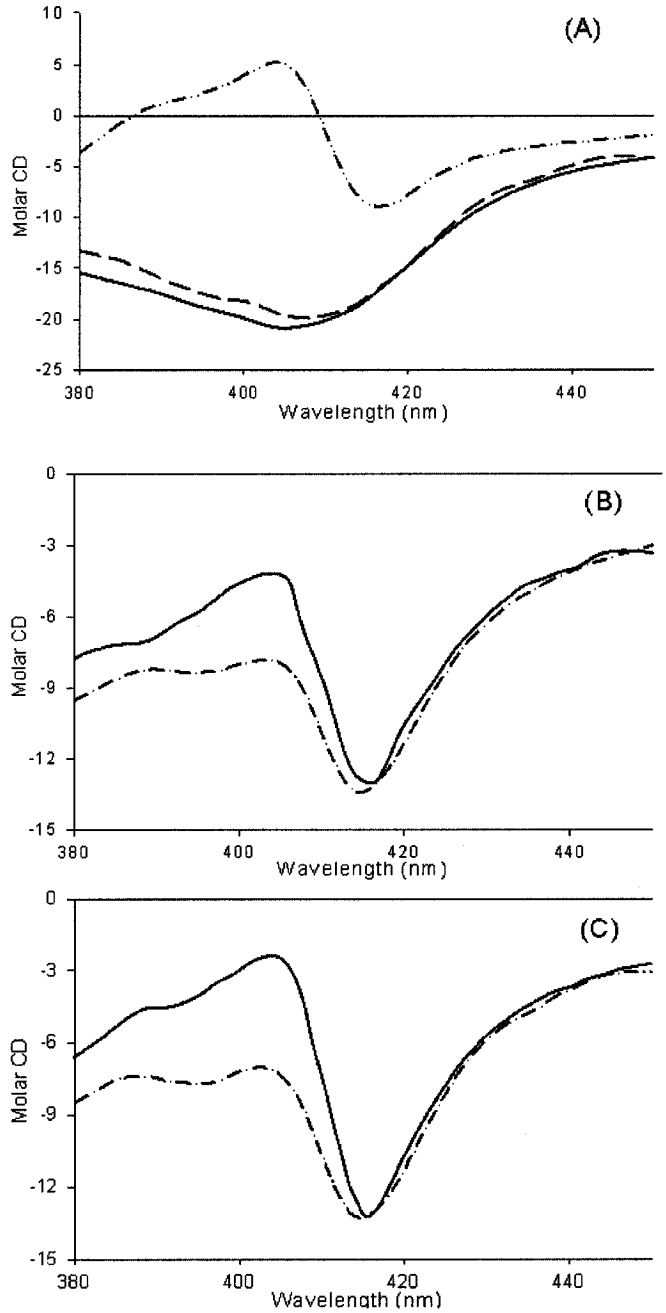

Figure 2.3. Heme CD spectra of ferric yeast CCP, CCP^{W191F} and their ferricytochrome *c* complexes. (A) CD spectra of 20 μM CCP (——), CCP^{W191F} (– – –) and yeast cytochrome *c* (–··–··) in 25 mM sodium phosphate buffer (pH 7.0). Spectra (B) and (C) are 1:1 mixtures of ferricytochrome *c* with CCP and CCP^{W191F}, respectively. The solid lines (——) are the experimental spectra and the dashed-dotted lines (–·–·–) are the calculated spectra obtained by adding the spectrum of CCP or CCP^{W191F} to that of cytochrome *c* using the JASCO CD software. The experimental spectra are the average of five scans recorded in a 0.5-cm rectangular cell at 0.2-nm resolution and a bandwidth of 1 nm at 25°C. The definition of molar CD is given in legend to Figure 2.2.

Free heme is a symmetrical molecule and therefore displays no CD spectrum [152]. Binding to a protein induces asymmetry in the electronic absorption of the heme, resulting in optical activity. The heme CD spectra of ferric CCP and ferricytochrome *c* (Figure 2.3A) reflect the different heme coordination and heme environment in the two proteins. However, the similarity of the spectra of CCP and its W191F mutant reveals that mutation at Trp191 causes little conformational change around the heme (Figure 2.3A).

The broad negative Cotton effect centred at ~400 nm (Figure 2.3A) of ferric CCP is consistent with a previous report for the wild-type protein [153]. The ferricytochrome *c* CD spectrum displays major positive and negative Cotton effects at 404 nm and 417 nm, respectively, which are independent of pH between 6.8–8.0 and of ionic strength between 10–150 mM [153]. Complexation with CCP elicits a strong positive change in the Cotton effect at 404 nm but no significant change at 417 nm [153]. Since Figures 2.3B and C display large increases in ellipticity at 404 nm, both CCP and CCP^{W191F} complex with ferricytochrome *c* in 25 mM NaPi (pH 7.0). CD absorption is clearly more sensitive than UV-Vis absorption in detecting the formation of a CCP/cytochrome *c* complex since binding of the proteins caused only slight changes in the latter [154]. Also, the greater positive change and the shoulder at ~390 nm in the heme CD spectra of CCP^{W191F} compared to CCP (Figures 2.3C *vs* B) indicate that the heme environments in the two complexes are not identical.

2.4.2 Reaction with H_2O_2 causes more significant changes in CCP than in CCP^{W191F}

The absorption spectra of ferric CCP and CCP^{W191F}, compared in Figure 2.4, show that the wild-type protein displays lower Soret absorption since its ε_{408} value (102 $mM^{-1}cm^{-1}$) is ~6% less than that of the mutant (109 $mM^{-1}cm^{-1}$) [112, 145]. CCP^{W191F} exhibits higher absorption around 300–380 nm than previously reported [112], suggesting that storage of the protein crystals at –20°C may alter its heme environment. Nonetheless, all the ferric heme appears to react with H_2O_2 as discussed next.

The spectral changes in CCP and CCP^{W191F} 10 s following H_2O_2 exposure are the same as those previously reported [108, 142]. These include a red-shift in the Soret maximum from 408 to 419 nm, decreased intensity of the shoulder at ~380 nm and the formation of charge-transfer bands at 530 and 560 nm [109].

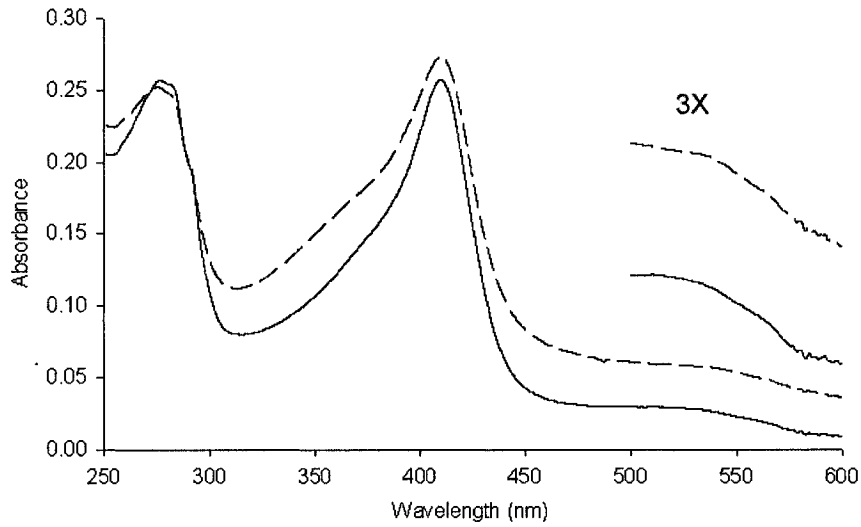

Figure 2.4. Absorption spectra of ferric yeast CCP and its W191F mutant. CCP (——) and CCP^{W191F} (— — —) were dissolved in 100 mM sodium phosphate buffer (pH 7.0) to a final concentration of 2.5 μM. Spectra were recorded in a 1-cm cuvette at 25°C.

Figure 2.5 shows that the ferric heme in both CCP and its W191F mutant was rapidly oxidized by 1× and 10× H_2O_2 to Fe^{IV}=O heme before the first measurements were

taken at 10 s. Once H_2O_2 is consumed by CCP, the Fe^{IV}=O heme begins to decay to Fe^{III} ($t_{1/2}$ = 6.6 h, [110]) by endogenous reduction [107]. The absorption maximum in the difference spectrum of Fe^{III} and Fe^{IV}=O CCP is at 424 nm [109, 110]. One molar equivalent of H_2O_2 is consumed by the wild-type CCP or its W191F mutant within 1 min [113] and oxidized CCP decays to a product with ~5% less absorption at 424 nm compared to the untreated enzyme [107]. Reaction of CCP with 10× H_2O_2 also causes a decrease in absorption at 424 nm [107].

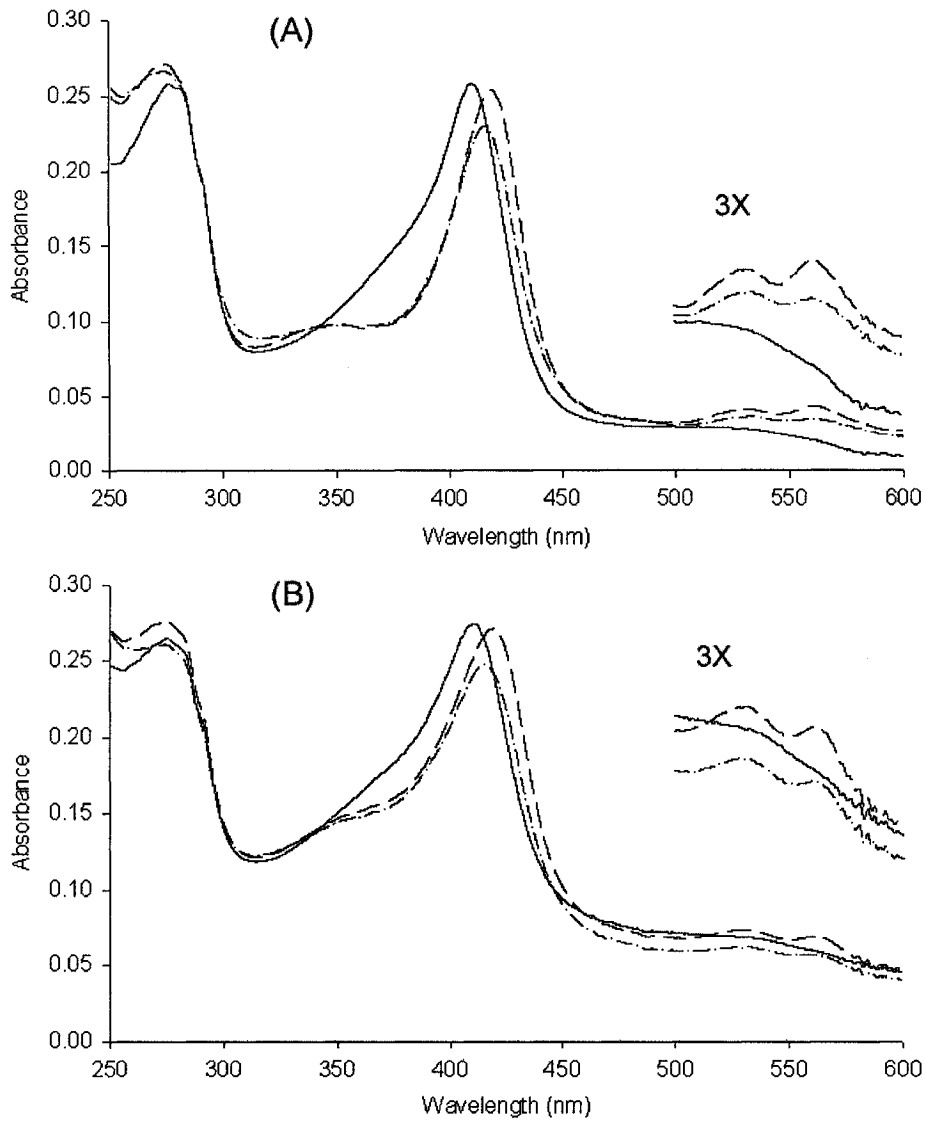

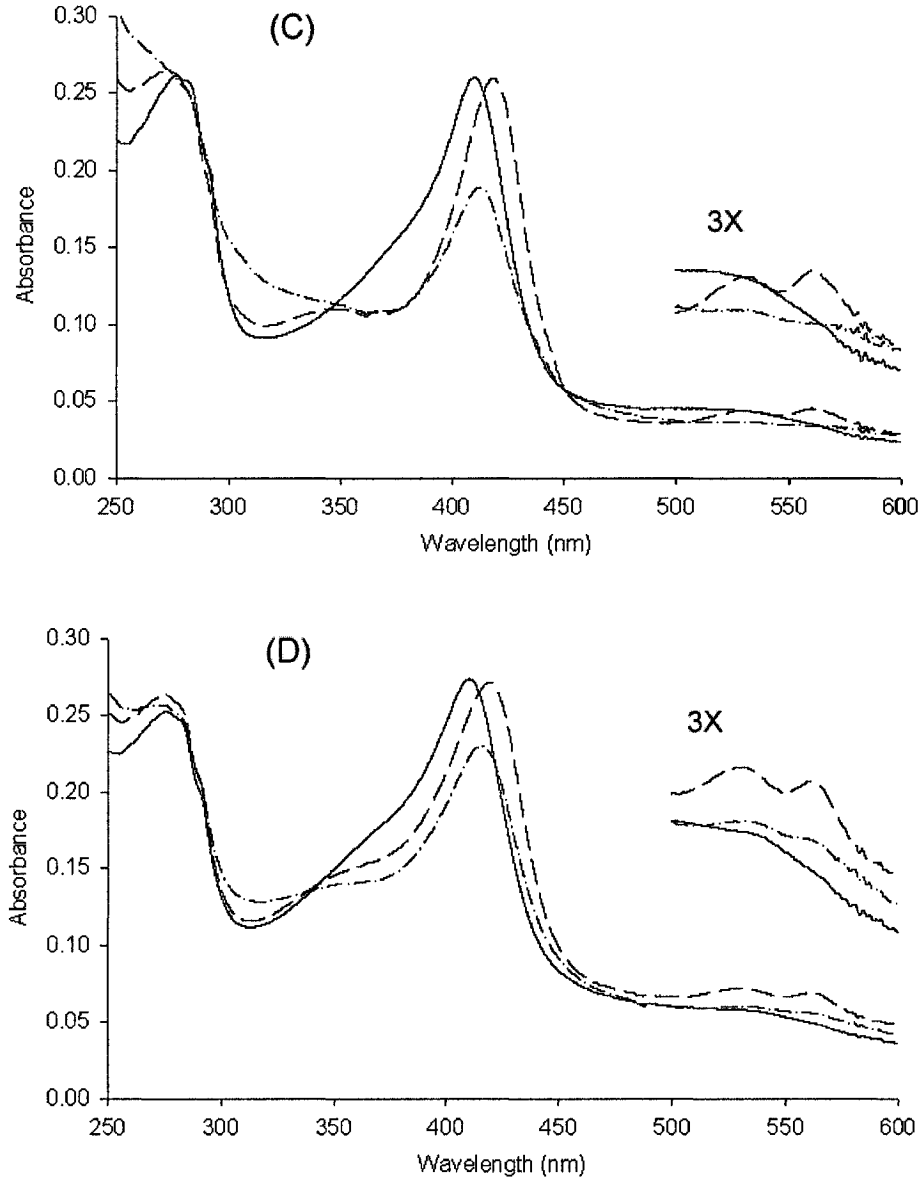

Figure 2.5. Absorption spectra of H_2O_2-oxidized yeast CCP and its W191F mutant. CCP (2.5 μM) was oxidized by (A) 2.5 μM H_2O_2 and (C) 25 μM H_2O_2. CCP^{W191F} (2.5 μM) was oxidized by (B) 2.5 μM H_2O_2 and (D) 25 μM H_2O_2. Spectra were recorded in a 1-cm cuvette at 25°C before (——), 10 s (— — —) and 30 min (—·—·—) after the addition of H_2O_2 to the proteins in 100 mM sodium phosphate buffer (pH 7.0).

Figure 2.6 displays the time course of 424-nm absorption following H_2O_2 addition. The absorption decays by ~20% over 30 min following CCP or CCP^{W191F} oxidation with 1× H_2O_2 (Figure 2.6). A significantly larger decay (~ 50%) is observed for

CCP after addition of 10× H_2O_2 but not for CCP^{W191F} (Figure 2.6), revealing that the mutant may possess impaired ability for endogenous Fe^{IV}=O heme reduction. Consistent with this hypothesis, greater changes were observed in the aromatic region (250–280 nm) [109] of the CCP (Figure 2.5C) *vs* the CCP^{W191F} spectrum (Figure 2.5D). Also, the slower consumption of 10× H_2O_2 by the mutant (30 min) compared to wild-type CCP (5 min) [113] indicates that the transfer of reducing equivalents from aromatic residues to H_2O_2 *via* the heme occurred more efficiently in CCP than that in CCP^{W191F}.

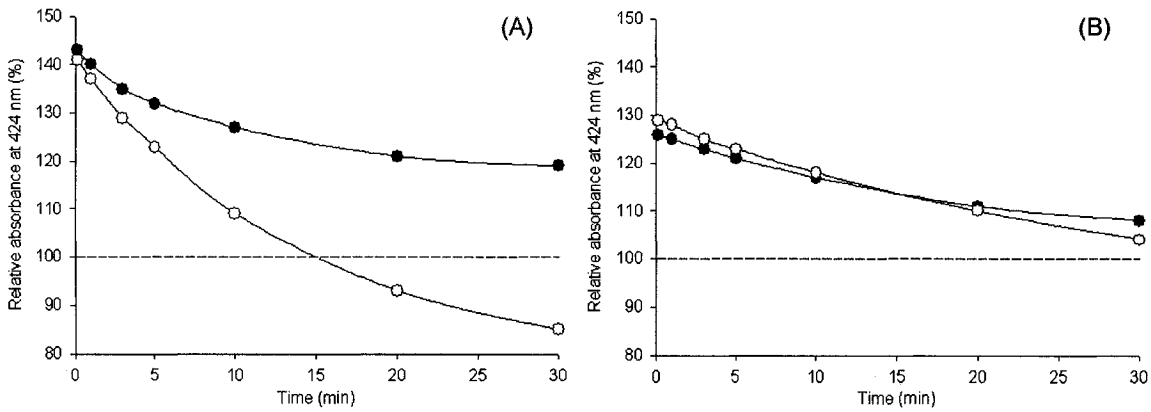

Figure 2.6. Relative absorption at 424 nm *vs* time of H_2O_2-oxidized yeast CCP and its W191F mutant. The absorption of the ferric proteins (dashed line) before H_2O_2 addition is taken as 100%. (A) CCP; (B) CCP^{W191F}. The proteins (2.5 μM) were oxidized by 2.5 μM (closed circles) or 25 μM H_2O_2 (open circles) in 100 mM sodium phosphate buffer (pH 7.0) at 25°C.

CCP exhibits an enhanced signal in its near-UV CD spectra due to the presence in its polypeptide of 7 *vs* 6 Trp residues in the W191F mutant (Figure 2.7, spectrum 1 *vs* 2). Only protein exposed to 10× H_2O_2 was investigated by CD since there is less change in the absorption spectra following reaction with 1× H_2O_2 (Figure 2.5). Figure 2.7 shows that oxidative modification of the proteins caused loss of aromatic residues [143] and possibly changes in their environment. Consistent with the results in Figure 2.5, CCP

exhibits more dramatic changes than CCP^{W191F} in the ~30-min interval following H_2O_2 exposure.

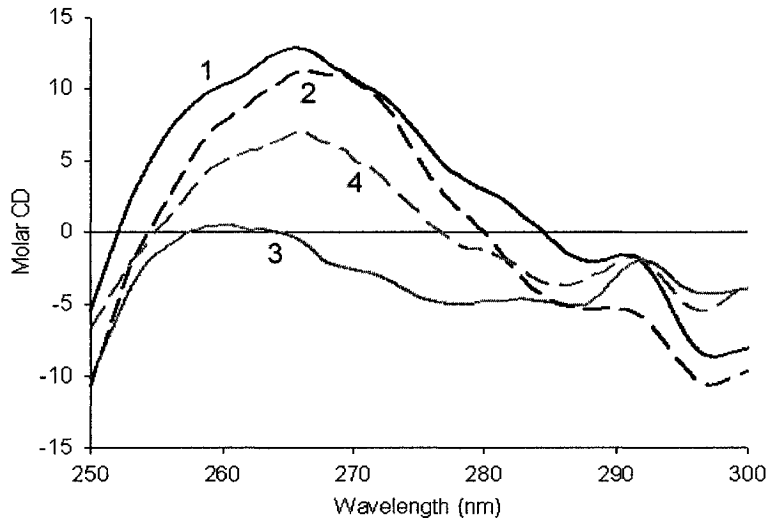

Figure 2.7. Effects of 10× H_2O_2 on the near-UV CD spectra of yeast CCP and its W191F mutant. CD spectra of 20 μM ferric yeast (1) CCP and (2) CCP^{W191F} in 100 mM sodium phosphate buffer (pH 7.0). CD spectra 20 min after the addition of 200 μM H_2O_2 to (3) 20 μM CCP and (4) 20 μM CCP^{W191F}. The spectra are the average of two scans recorded in 5 min in a 0.5-cm rectangular cell at 0.2-nm resolution and a bandwidth of 1 nm at 25°C. The definition of molar CD is given in the legend to Figure 2.2.

The heme CD spectra show that H_2O_2 addition causes a shift in the trough from 408 to 420 nm in both CCP and CCP^{W191F} (Figure 2.8). The CCP heme appears to undergo faster endogenous reduction and/or environmental changes since its spectra change faster with time than those of the CCP^{W191F} heme.

2.4.3 Radicals are formed during CCP oxidation

TEMPO$^{\bullet}$ has been shown to scavenge protein tyrosyl radicals [114]. Some of these residues form intermolecular crosslinks between CCP molecules when the enzyme reacts with H_2O_2 in the absence of donor substrates [115, 117]. Most intermolecular crosslinking occurs within 10 min because longer incubation times (up to 120 min) did not increase the amount of high-molecular-weight species observed [140]. SDS-PAGE

analysis of CCP and CCP^{W191F} 30 min after exposure to 1× or 10× H_2O_2 in the absence or presence of 10× TEMPO• is shown in Figure 2.9. In the absence of TEMPO•, crosslinked species are detected except for CCP oxidized with 1× H_2O_2. Addition of TEMPO• results in fewer dimerized species and less diffuse monomer bands, clearly indicating that TEMPO• inhibits H_2O_2-induced intermolecular and intramolecular crosslinking of CCP.

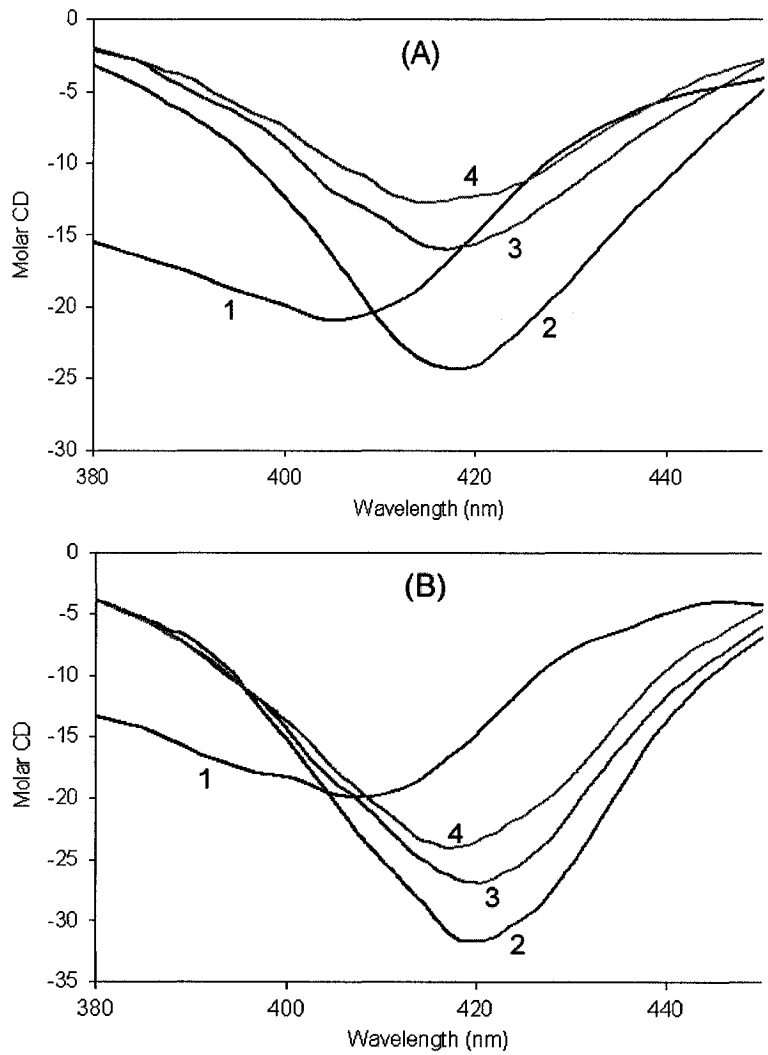

Figure 2.8. Effects of 10× H_2O_2 on the heme CD spectra of yeast CCP and its W191F mutant. CD spectra of 20 μM (A) CCP and (B) CCP^{W191F} in 100 mM NaPi buffer (pH 7.0) at 25°C. Spectra were recorded (1) before and (2) 10 s, (3) 10 min and (4) 20 min after the addition of 200 μM H_2O_2 to the proteins. The spectra are the average of two scans recorded in 7 min. Sample preparation and instrument setting are given in the legend to Figure 2.7.

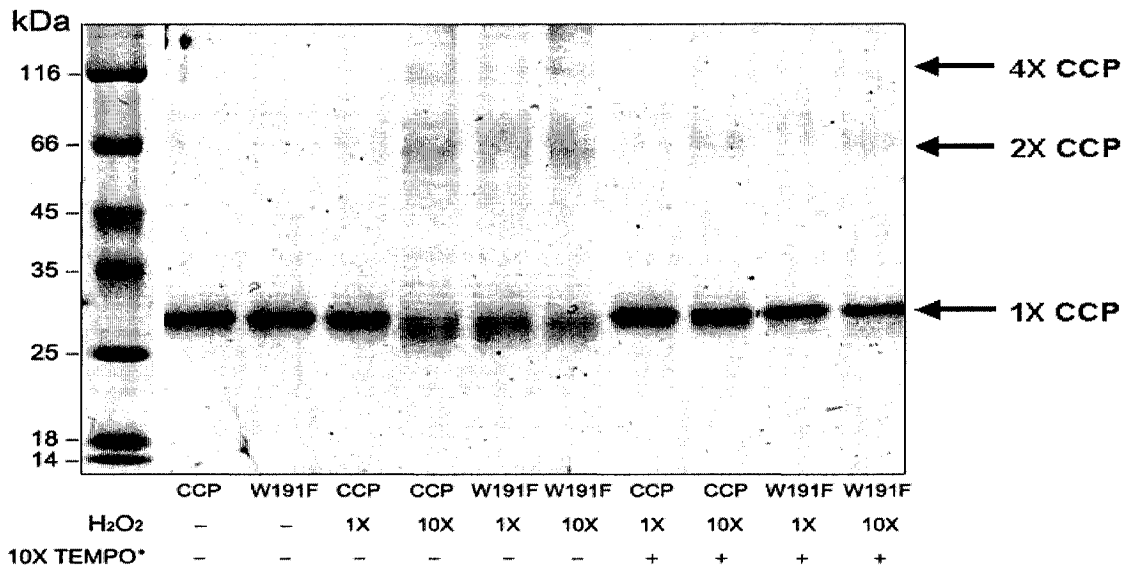

Figure 2.9. SDS-PAGE analysis of the effects of TEMPO• on H_2O_2-oxidized CCP and its W191F mutant. Proteins (5 μM) in 100 mM sodium phosphate buffer (pH 7.0) at room temperature were reacted with 5 μM (1×) or 50 μM (10×) H_2O_2 and 50 μM TEMPO• where indicated. A 10-μL aliquot of each sample was removed 30 min after H_2O_2 and TEMPO• addition, mixed with 40 μL of 10% (w/v) SDS, incubated for 30 min at room temperature, and heated for 5 min at 95°C before loading on the gel.

Addition of TEMPO• decreased the changes in the aromatic absorption (250–280 nm) over 30 min following H_2O_2-addition to the proteins (Figures 2.10 *vs* 2.5). Thus, TEMPO• may scavenge protein tyrosyl radicals or act as an electron donor [114].

Both CCP and CCP^{W191F} are rapidly oxidized by 1× and 10× H_2O_2 to a CCP-I-type species in the presence of 10× TEMPO• (Figure 2.10). The 424-nm absorption decreases faster following protein oxidation by 1× H_2O_2 in the presence (Figure 2.11) than in the absence of TEMPO• (Figure 2.6). Thus, the nitroxyl acts as an electron donor to CCP-I but since small molecules are generally poor donor substrates for CCP [98], the oxyferryl heme has a $t_{1/2}$ = ~3 min in the presence 25 μM TEMPO•. The absorption changes at 424 nm following exposure to 10× H_2O_2 (Figures 2.11 *vs* 2.6) are consistent with TEMPO• acting as a more efficient electron donor than the aromatic residues. In

addition, the accelerated reduction by TEMPO• of the CCP oxyferryl heme is evidenced by the blue-shift in the Soret maximum from 419 to 411 nm over 30 min following 1× H_2O_2-exposure (Figure 2.10A) compared to the shift to 415 nm in the absence of TEMPO• (Figure 2.5A). The CCP^{W191F} oxyferryl heme reacts more slowly with TEMPO• since less absorption decay at 424 nm is observed for CCP^{W191F} 30 min after addition of H_2O_2 (Figure 2.11B).

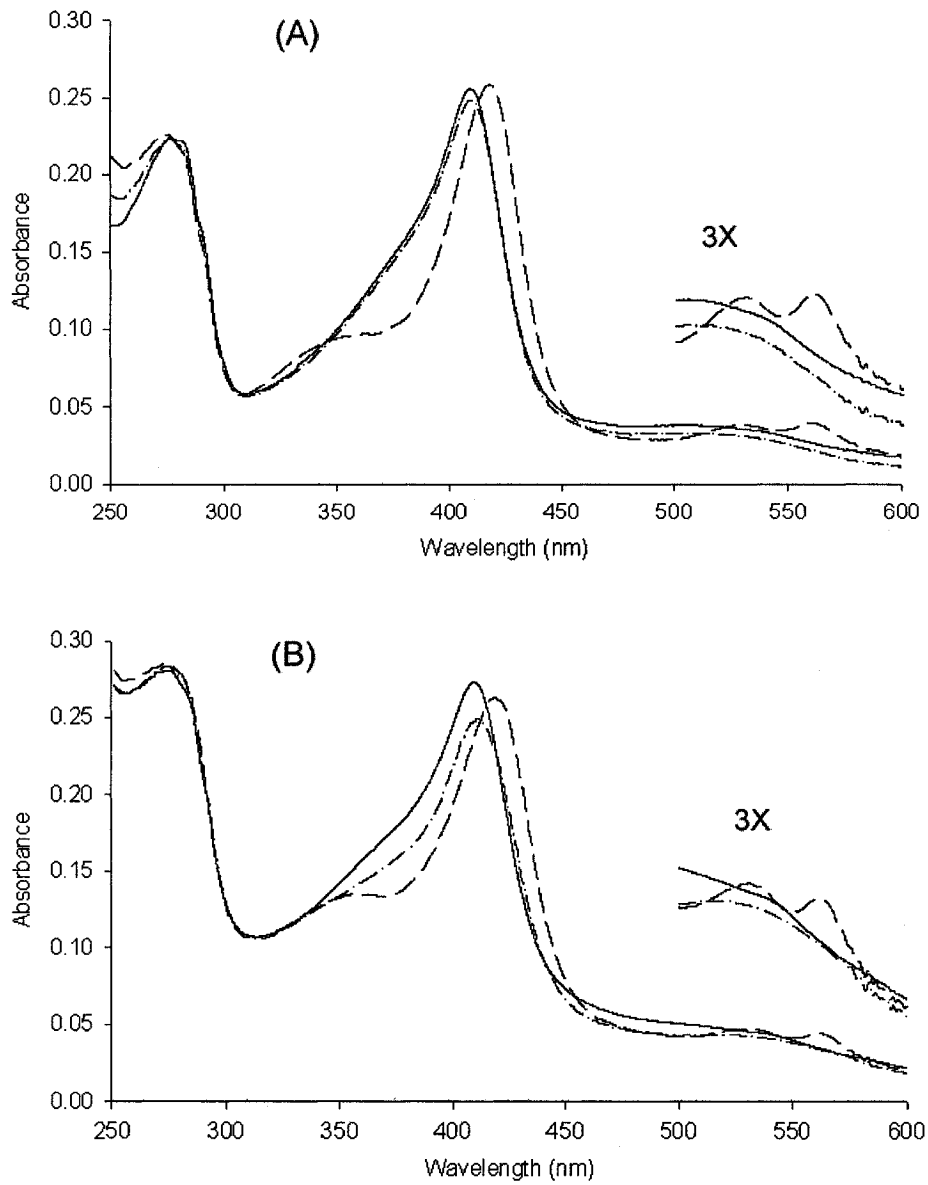

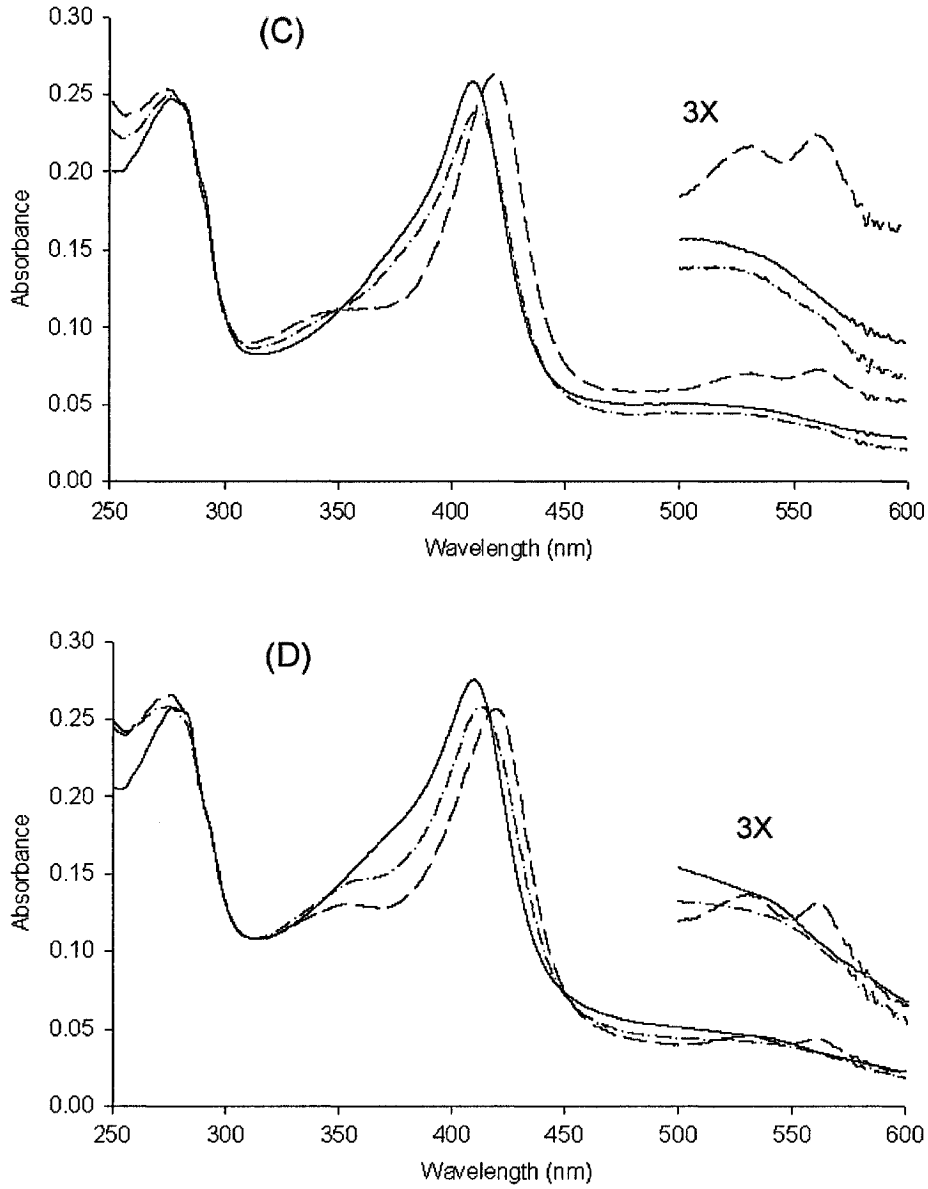

Figure 2.10. Effects of TEMPO• on the absorption spectra of H_2O_2-oxidized yeast CCP and its W191F mutant. CCP (2.5 μM) was oxidized by (A) 2.5 μM H_2O_2 and (C) 25 μM H_2O_2. CCP^{W191F} (2.5 μM) was oxidized by (B) 2.5 μM H_2O_2 and (D) 25 μM H_2O_2. Spectra were recorded in a 1-cm cuvette at 25°C before (——), 10 s (— — —) and 30 min (—·—·—) after the addition of H_2O_2 to the proteins in 100 mM sodium phosphate buffer (pH 7.0) containing 25 μM TEMPO•.

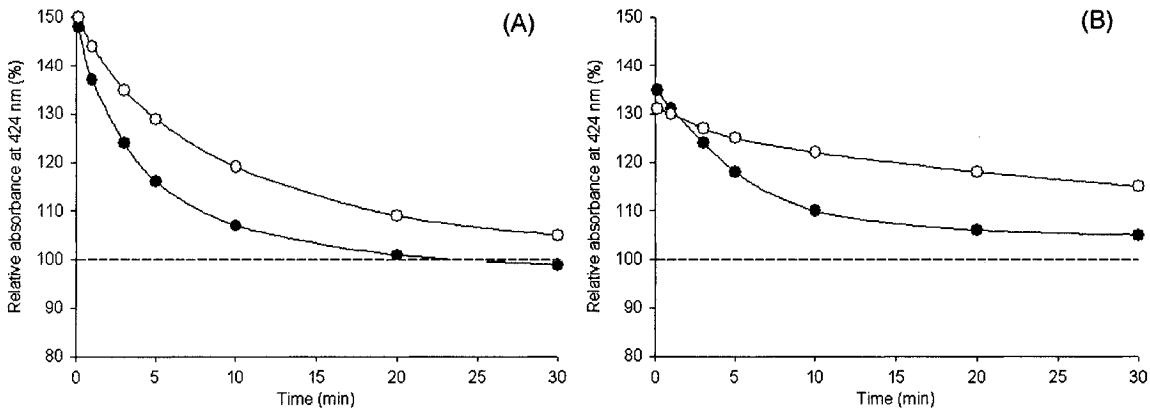

Figure 2.11. Effects of TEMPO• on the relative absorption at 424 nm *vs* time of H_2O_2-oxidized yeast CCP and its W191F mutant. The absorption of the ferric proteins (dashed line) before H_2O_2 addition is taken as 100%. (A) CCP; (B) CCP^{W191F}. The proteins (2.5 μM) were oxidized by 2.5 μM (closed circles) or 25 μM H_2O_2 (open circles) in 100 mM sodium phosphate buffer (pH 7.0) containing 25 μM TEMPO• at 25°C.

2.5 Discussion

CCP is believed to function as an antioxidant enzyme and a signaling molecule in yeast (Chapter 4). Ferrocytochrome *c* is its putative physiological redox partner such that the ferrocytochrome *c*-oxidizing activity of CCP in mitochondria removes H_2O_2 and prevents oxidation of the peroxidase. In the presence of excess H_2O_2, surface Tyr residues on CCP can be oxidized to form radicals that may transduce oxidative signals. CCP^{W191F} exhibits not only a greatly impaired ability to accept electrons from ferrocytochrome *c* [140] but also decreased endogenous reduction leading to slow consumption of H_2O_2 [113]. This could be a reason why CCP^{W191F} mediates a more persistent oxidative-stress signal than wild-type CCP to Skn7/Pos9 *in vivo* [70].

To better understand the signaling role of CCP, the spectral changes of CCP and its W191F mutant over 30 min following H_2O_2-exposure were compared here. The W191F mutation results in little detectable alteration of the protein's secondary or tertiary

structure or in its complex with cytochrome *c* (Figures 2.2–2.3, 2.7). However, the absorption and near-UV CD spectra spectral changes following addition of 10× H_2O_2 (Figures 2.5 and 2.7) suggest that aromatic residues in CCP are more readily oxidized than in CCP^{W191F} (Figures 2.5 and 2.7).

In agreement with previous work [113, 116, 117], SDS-PAGE analysis of the oxidized proteins (Figure 2.9) revealed that CCP^{W191F} but not CCP crosslinks on exposure to 1× H_2O_2 while both proteins undergo crosslinking on exposure to 10× H_2O_2. The oxidizing equivalent in the transient porphyrin π-cation radical ($t_{1/2}$ = 14 ms) in W191F must be efficiently transferred to surface tyrosine residues such as Tyr39 and Tyr229, which have been identified as likely crosslinking sites [115, 117].

Figure 2.9 shows that TEMPO$^\bullet$ effectively inhibited the H_2O_2-induced intramolecular and intermolecular crosslinking of CCP. MS analysis revealed that nine TEMPO$^\bullet$ adducts were formed 10 min following CCP exposure to 10× H_2O_2 [114] and peptide mapping indicated that peptides containing surface-exposed Tyr and Trp residues were TEMPO$^\bullet$-labeled. Thus, TEMPO$^\bullet$ could inhibit CCP crosslinking (Figure 2.9) by effectively scavenging H_2O_2-induced aromatic radicals (R$^\bullet$):

$$\text{TEMPO}^\bullet + \text{R}^\bullet \rightarrow \text{TEMPO–R} \qquad (2.3)$$

Scavenging could also explain the smaller aromatic absorption changes on CCP-oxidation in the presence of TEMPO$^\bullet$ (Figures 2.5 *vs* 2.10) since TEMPO–R formation should result in less conformational change than protein intermolecular and intramolecular crosslinking.

TEMPO$^\bullet$ catalyzes the oxidation of alcohols to carbonyls and thus has many applications in organic synthesis [155]. TEMPO$^\bullet$ together with its oxidized form

(TEMPO$^+$, N-oxoammonium cation) and its reduced form (TEMPOH, hydroxylamine) are involved in the catalytic cycle (Figure 3.1) as discussed in Chapter 3 of this thesis. Previously our lab reported [114] that TEMPO$^\bullet$ minimized the Soret shift in horseradish peroxidase upon oxidation of the enzyme by H_2O_2. Addition of TEMPO$^\bullet$ causes faster decay in absorption at 424 nm over 30 min following CCP oxidation by 1× H_2O_2 (Figures 2.11 *vs* 2.6), indicating that TEMPO$^\bullet$ reduces the oxyferryl heme in the oxidized peroxidases. The 10-nm blue-shift in the Soret maximum and the loss of the visible charge-transfer bands at 30 min following 1× H_2O_2-exposure (Figure 2.10) in the presence of TEMPO$^\bullet$ confirms that the nitroxyl radical acts as a reductant and accelerates the rate of Fe^{IV}=O heme reduction:

$$TEMPO^\bullet + PFe^{IV}{=}O + 2\,H^+ \rightarrow TEMPO^+ + PFe^{III} + H_2O \qquad (2.4)$$

The Fe^{IV}=O center generated on the reaction of heme proteins with H_2O_2 exhibits a higher reduction potential (E° Fe^{IV}=O/Fe^{III} ~1.0 V) [156] than that of TEMPO$^\bullet$ (E° TEMPO$^+$/TEMPO$^\bullet$ ~0.6 V) [157] such that oxidation of TEMPO$^\bullet$ by Fe^{IV}=O (Eq. 2.4) is thermodynamically favorable. Thus, TEMPO$^\bullet$ could compete with endogenous aromatic residues as a reductant of the Fe^{IV}=O heme resulting in less spectral change upon addition of 10× H_2O_2 when 10× TEMPO$^\bullet$ is present (Figures 2.10 *vs* 2.5 and Figures 2.11 *vs* 2.6).

H_2O_2-induced crosslinking of CCP and CCP^{W191F} was also examined in 100 mM NaPi buffer (pH 7.0) containing 100 μM DTPA, which is widely used in protein redox reactions to prevent interference from trace free metal ions [114, 117]. Interestingly, a ~100-kDa-species corresponding to a protein-trimer was detected by SDS-PAGE for untreated CCP or CCP^{W191F} in the presence of DTPA but not in its absence (Figures 2.12 *vs* 2.9). The trimer band disappeared when TEMPO$^\bullet$ was present and when 10× H_2O_2

was added to wild-type CCP (Figure 2.12). Surprisingly, DTPA suppressed H_2O_2-induced crosslinking of CCP^{W191F} but not of CCP on exposure to 10× H_2O_2 (Figure 2.12). Since the formation of surface-exposed tyrosyl radicals is mediated by the heme [107], DTPA might act as an electron donor to the oxyferryl heme of CCP^{W191F}. EDTA is a well-known electron donor [158, 159] and recently DTPA, which is structurally similar to EDTA, has also been shown to be an efficient donor in the photoreduction of flavin mononucleotide (FMN) to $FMNH_2$ [160]. In addition, $EDTA/Fe^{II}$ is a free-radical generating system that is used in biological radical oxidations [161-164]. The different behavior of CCP and its W191F mutant in H_2O_2/DTPA incubates is of interest and the effects of DTPA on heme-mediated H_2O_2-induced radical formation should be further probed.

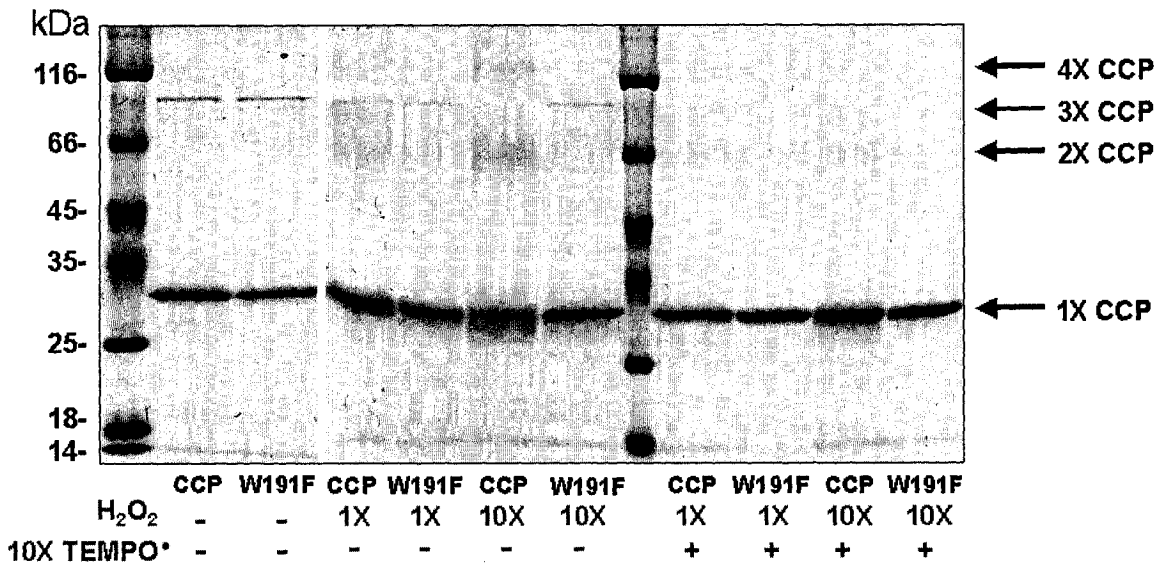

Figure 2.12. Effects of DTPA on H_2O_2-induced crosslinking of CCP and its W191F mutant. Proteins (5 μM) in 100 mM NaPi buffer (pH 7.0) containing 100 μM DTPA were reacted with H_2O_2 and TEMPO• at the molar equivalents indicated. Experimental procedures are given in the legend to Figure 2.9.

2.6 Conclusions

The spectroscopic studies reported here (Figures 2.5, 2.7 and 2.8) reveal that the different reactivities of CCP and its W191F mutant with 1× and 10× H_2O_2 in the absence of donors is due to differences in the extent of polypeptide oxidation. This heme-mediated process appears to be more efficient in the wild-type protein. The rapid crosslinking of CCP^{W191F} on 1× H_2O_2 addition indicates that oxidizing equivalents are translocated to protein surface (possibly Tyr39) resulting in dead end electron-transfer pathways. In a cellular environment such surface-exposed radicals may signal oxidative stress. Since CCP and its W191F mutant show remarkable differences in behavior upon H_2O_2 oxidation, yeast strains with the wild-type enzyme and its W191F mutant were systematically studied, and the results are presented in Chapter 4. $TEMPO^{\bullet}$ inhibited H_2O_2-induced CCP crosslinking most likely by acting as a donor to heme. To facilitate further studies on $TEMPO^{\bullet}$ as a donor to heme peroxidases, the mass spectral behavior of the nitroxyl in aqueous solutions was investigated as described in Chapter 3.

3 Mass spectrometric and computational studies on the relative stabilities of TEMPO$^{\bullet}$ ions formed in an electrospray ionization source in aqueous solution

3.1 Abstract

To develop the use of stable nitroxides in characterizing biological redox reactions by mass spectrometry (MS), a systematic investigation of the mass spectral behavior of 2,2,6,6-tetramethylpiperidinyl-1-oxy (TEMPO$^{\bullet}$) dissolved in 100% aqueous solutions was carried out in an electrospray ionization (ESI) source. The positive-ion ESI mass spectrum of TEMPO$^{\bullet}$ exhibits three peaks at m/z 156, 157 and 158 that are assigned to TEMPO^{+}, TEMPOH$^{\bullet+}$ and TEMPOH$_2^{+}$, and MS/MS analysis confirms that the three ions arise from electrochemical processes in the ESI source and are not derived from fragmentation. The odd-electron TEMPOH$^{\bullet+}$ ion, which readily loses $CH_3^{\bullet}$, is more abundant than its oxidized (TEMPO^{+}) or its reduced forms (TEMPOH$_2^{+}$). In the presence of sodium, TEMPONa$^{\bullet+}$ (m/z 179) becomes dominant, but its intensity decreases dramatically as the collision voltage is increased. Quantum chemistry calculations using density functional theory reveal that the sodium affinity (SA) of TEMPO$^{\bullet}$ is 5.7-fold less than its proton affinity but 1.8-fold higher than the SA of H_2O. Thus, sodiation of TEMPO$^{\bullet}$ is highly favorable in the ESI source, and loss of Na^{+} provides a low-energy fragmentation pathway for TEMPONa$^{\bullet+}$. Unlike sodiation, protonation significantly destabilizes the electronic structure of TEMPO$^{\bullet}$ by stretching the N–O bond. Consequently, sodiation should simplify the ESI MS analysis of solution-based TEMPO$^{\bullet}$ redox reactions by inhibiting the redox turnover of the nitroxyl in the source and by removing TEMPO$^{\bullet}$-derived fragments from the mass spectra.

3.2 Introduction

2,2,6,6-Tetramethylpiperidine-1-oxyl (TEMPO•), a stable nitroxide with four methyls surrounding the nitroxylamine group (Figure 3.1), has many applications in organic synthesis [165-167]. It effectively catalyzes the oxidation of primary and secondary alcohols to aldehydes or carboxylic acids and ketones. For example, in the CuCl/TEMPO•-catalyzed aerobic oxidation of alcohols, TEMPO• serves as an active and recyclable catalyst (Figure 3.1) [168]. TEMPO• first reacts with Cu^{I} to form a piperidinyloxyl-Cu^{II} complex. The latter oxidizes a molecule of alcohol (R^1R^2CHOH) to afford an alkoxy-Cu^{II} complex and TEMPOH. Next, a second molecule of TEMPO• reacts with the alkoxy-Cu^{II} complex to give the carbonyl compound, Cu^{I} and TEMPOH, which is reoxidized to TEMPO• by dioxygen. This is a representative reaction in "green chemistry" that employs clean oxidants (O_2) and a recyclable catalyst (CuCl/TEMPO•), maximizing reagent consumption and minimizing waste.

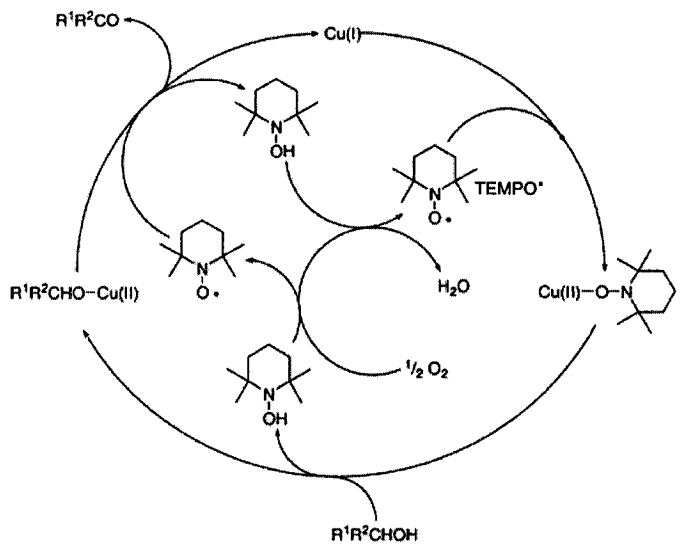

Figure 3.1. Postulated mechanism for the CuCl/TEMPO•-catalyzed aerobic oxidation of alcohols [168].

Nitroxides reportedly possess antioxidant activity *in vivo* and protect against a range of agents that impose oxidative stress. TEMPO$^{\bullet}$ administered to mice decreased obesity and incidences of age-related spontaneous tumor formation [169]. TEMPO$^{\bullet}$ rescues mammalian cells from H_2O_2-induced killing by penetrating cell membranes and lowering intracellular hydroxyl radical ($OH^{\bullet}$) levels [170]. It also protects against superoxide-induced DNA breakage [171]. In our lab, the use of TEMPO$^{\bullet}$ as a radical scavenger has been developed into a sensitive method for protein-based radical detection by mass spectrometry (MS) [114]. Oxidation of yeast cytochrome *c* peroxidase (CCP) with a 10-fold molar excess of H_2O_2 in the absence of an electron donor (such as ferrocytochrome *c*) results in the formation of tyrosyl radicals on the protein's surface [115, 117]. Use of matrix-assisted laser desorption ionization/time-of-flight (MALDI-ToF) MS to analyze its tryptic peptides revealed that CCP formed up to 9 TEMPO$^{\bullet}$ adducts *in vitro* within 10 min following exposure to 10× H_2O_2 and TEMPO$^{\bullet}$ [114].

Electrospray ionization (ESI) and MALDI are complementary ionization techniques. MALDI tends to ionize tryptic peptides ending in arginine while ESI favors peptides with a C-terminal lysine [172, 173]. Thus, a combination of both techniques can lead to the detection of more peptides [173, 174]. For example, liquid chromatography coupled to both MALDI and ESI sources and tandem MS detection (LC-MALDI-MS/MS and LC-ESI-MS/MS) improved peptide coverage and hence identification of bovine ribosomal proteins. A total of 51 proteins were identified, with 8 unique to ESI and 11 unique to MALDI [174]. Therefore, building on our MALDI data [114], ESI MS will be used to further investigate radical scavenging and detection with TEMPO$^{\bullet}$ in our lab. In

particular, TEMPO•-labeled peptides will be identified using a Waters Micromass ESI-QToF2 mass spectrometer to establish sites of radical formation.

It has been reported that the ESI mass spectrum of TEMPO• strongly depends on the MS solvent and source parameters such as capillary voltage [175-177]. Since H_2O_2-induced radicals in heme-proteins are suggested to be involved in cell signaling [117, 144], it is desirable to carry out MS analysis of TEMPO•-labeled peptides in water or sodium phosphate buffer at physiological pH. Also, since TEMPO• may act as an electron donor to oxyferryl heme (Eq. 2.4), it is necessary to know the extent of $TEMPO^+$ formation in solution *vs* in the ESI source. Here we describe a systematic investigation of the TEMPO•-derived ions formed in a Z-spray source using water as a solvent with and without formic acid (FA) and sodium. Quantum chemistry calculations using density functional theory (DFT) [178] were performed to probe the basis for the relative stabilities of the observed ions, and operating conditions were establish to minimize redox reactions involving TEMPO• in the ESI source.

3.3 Materials and methods

3.3.1 Mass spectrometric analysis

TEMPO• (Sigma) was dissolved in water or 0.5% FA (Fisher) to a concentration of 50 μM. For the sodiation studies, 50 μM TEMPO• was dissolved in 50 μM sodium phosphate buffer (NaPi, pH 7.0). ESI-MS and MS/MS analysis was performed on a QToF2 mass spectrometer (Waters Micromass) operating in the positive ion mode. Samples were directly infused into the Z-spray source at a flow rate of 1 μL/min. Mass calibration was carried out using human [Glu^1]-fibrinopeptide B, and the mass accuracy of the instrument was 60 ppm.

3.3.2 Quantum chemistry calculations

DFT calculations [178] were carried out by Etienne Paradis and Qadir Timerghazin using B3LYP/6-31+G* model chemistry in Gaussian 03 [179, 180]. All geometry optimizations were symmetry-unconstrained and energies were corrected for zero-point vibrational energy. Proton affinities (PA) and sodium affinities (SA) of TEMPO$^{\bullet}$ and TEMPOH (M) were computed from the following enthalpies:

$$PA = H°(MH^+) - H°(M) - H°(H^+) \qquad (3.1)$$

$$SA = H°(MNa^+) - H°(M) - H°(Na^+) \qquad (3.2)$$

3.4 Results

3.4.1 ESI mass spectrum of TEMPO$^{\bullet}$

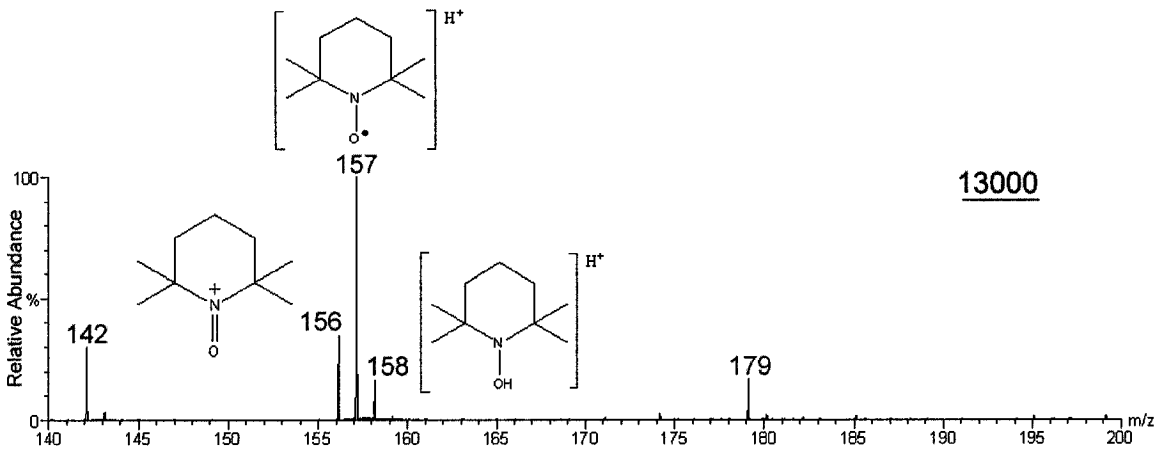

Figure 3.2. ESI mass spectrum of TEMPO$^{\bullet}$ in water. A solution of 50 μM TEMPO$^{\bullet}$ in water was directly infused into the Z-spray source of the QToF2 mass spectrometer at a flow rate of 1 μL/min. The instrumental parameters were as follows: capillary voltage 3.4 kV, cone voltage 20 V, collision voltage 5 V, multiplier 550 V, MCP 2200 V, ToF -9.1V and source block temperature 80°C. The number of total ion counts per 20 scans (TICs) is underlined.

As previously reported [175-177], the ESI mass spectrum of TEMPO$^{\bullet}$ in water exhibits three peaks at m/z 156, 157 and 158 that are assigned to TEMPO$^+$, TEMPOH$^{\bullet+}$

and $TEMPOH_2^+$, respectively (Figure 3.2). Since a glass capillary emitter in a nanoESI source was used here, the dominant ion is observed at m/z 157 (Figure 3.2) in agreement with a recent study [177]. In contrast, the base peak (100%) was at m/z 156 and the relative intensities of the m/z 157 and 158 peaks were 15% and 8%, respectively, in the $TEMPO^•$ spectrum recorded in acetonitrile on a Waters Micromass Quattro II triple-quadrupole mass spectrometer with a metal capillary emitter in a normal ESI source [181].

3.4.2 MS/MS analysis of the $TEMPO^+$, $TEMPOH^{•+}$ and $TEMPOH_2^+$ ions

To confirm that the ions observed at m/z 156 and 157 are not derived from the ion at m/z 158, MS/MS analysis of each ion was performed. $TEMPO^+$ (Figure 3.3) and $TEMPOH^{•+}$ (Figure 3.5) yield dominant fragment ions at m/z 123 and m/z 142, respectively. Since no fragment ions at m/z 123, 142, 156 or 157 are observed for $TEMPOH_2^+$ (Figure 3.7), the species at m/z 156 and 157 are not product ions of $TEMPOH_2^+$.

The proposed fragmentation pathways (Figures 3.4, 3.6 and 3.8) based on the observed MS/MS spectra are given in Figures 3.3, 3.5 and 3.7. Loss of hydroxylamine (NH_2OH, 33 u) from $TEMPO^+$ gives rise to the peak at m/z 123 as reported [181], and additional fragmentation pathways based on the observed peaks at m/z 69, 81 and 95 reveal that $TEMPO^+$ can be fragmented by loss of four RNO moieties (Figures 3.4 and 3.5). Previously, the peak at m/z 81 was assigned to a product ion of the species at m/z 123 [177], but we propose that the ion at m/z 81 arises directly from the parent ion (m/z 156) since the m/z 123 ion is stable based on DFT calculations (Q. Timerghazin, personal communication).

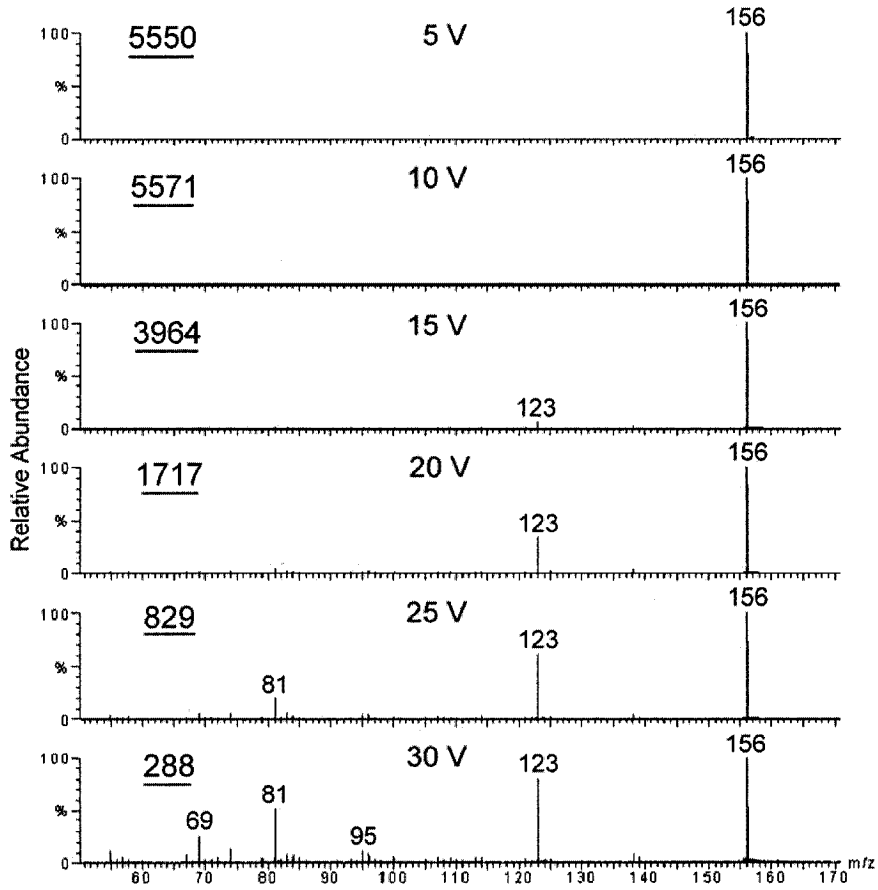

Figure 3.3. MS/MS spectrum *vs* collision voltage of the TEMPO$^+$ ion at m/z 156. To record the MS/MS spectra, a solution of 50 μM TEMPO$^\bullet$ in 0.5% formic acid was directly infused into the Z-spray source of the QToF2 mass spectrometer. The instrument was set in the ToF MS/MS mode with the selected parent ion at m/z 156 and a low mass/high mass (LM/HM) resolution of 12.0. Spectra were recorded at the collision voltages (V) indicated on the spectra and the other MS parameters are given in Figure 3.2. The total ion counts per 20 scans (TICs) are underlined.

The MS/MS spectrum of TEMPOH$^{\bullet+}$ has not been published. Loss of $CH_3^\bullet$ from TEMPOH$^{\bullet+}$ gives rise to a stable even-electron ion at m/z 142, which is the base peak in the MS/MS spectrum recorded at collision voltages ≥ 15 V (Figure 3.5). The weak peaks at m/z 109 and 69 are attributed to loss of hydroxylamine (NH_2OH, 33 u) and *N,N'*-ethylmethylhydroxylamine (C_3H_6NOH, 73 u), respectively, from the ion at m/z 142 (Figure 3.6).

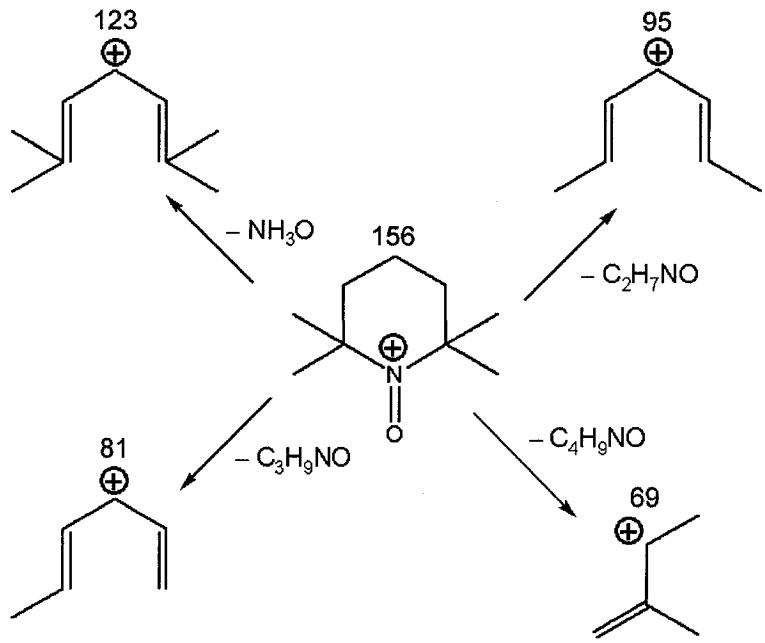

Figure 3.4. Proposed fragmentation pathways of the TEMPO$^+$ ion at m/z 156.

$TEMPOH_2^+$ (Figure 3.8) also loses hydroxylamine (NH_2OH, 33 u) to form an ion at m/z 125, which is further cleaved to produce ions at m/z 69 and 83 as previously reported [177]. We additionally detected the odd-electron $TEMPOH_2^+$–$CH_3^\bullet$ ion at m/z 143 due to loss of $CH_3^\bullet$ from the even-electron $TEMPOH_2^+$ ion. Loss of CH_4 gives rise to the low-abundant, even-electron ion at m/z 142 indicating that $CH_3^\bullet$ loss provides a lower-energy fragmentation pathway. Interestingly the ions at m/z 69 in the MS/MS spectra of all three parent ions (Figures 3.3, 3.5 and 3.7) are attributed to different precursor ions in each case (Figures 3.4, 3.6 and 3.8).

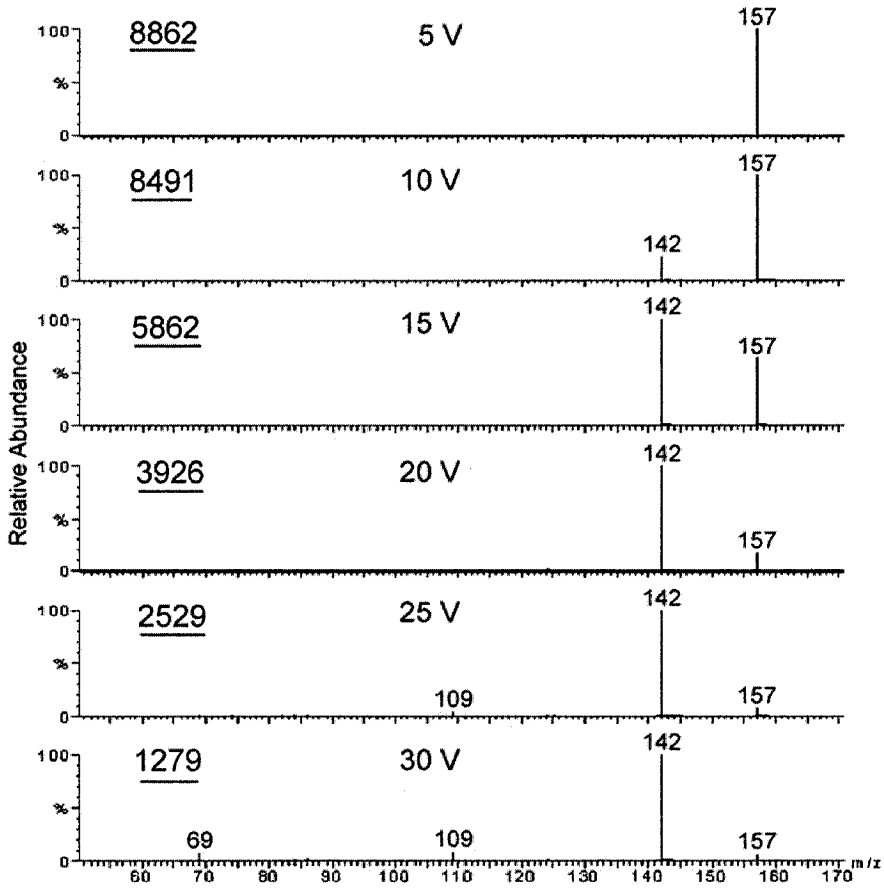

Figure 3.5. MS/MS spectrum *vs* collision voltage of the TEMPOH$^{\bullet+}$ ion at m/z 157. The sample preparation and MS procedures are given in Figure 3.3.

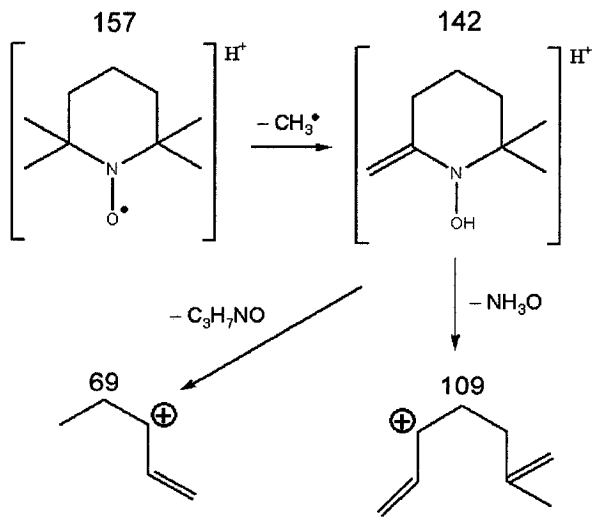

Figure 3.6. Proposed fragmentation pathways of the TEMPOH$^{\bullet+}$ ion at m/z 157.

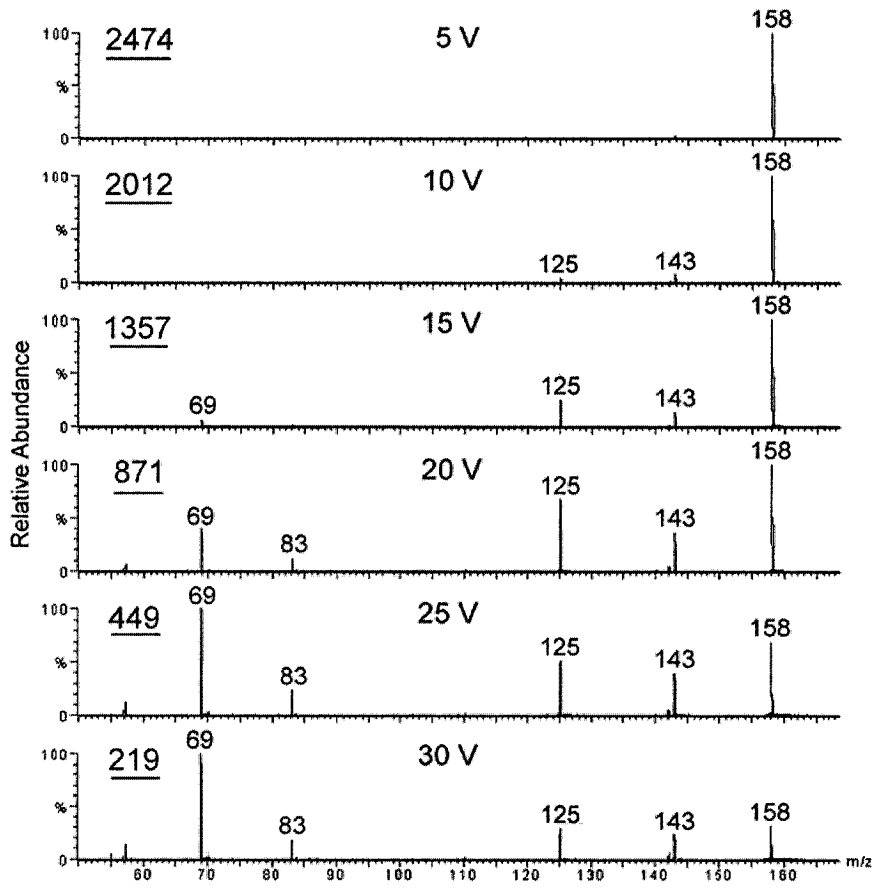

Figure 3.7. MS/MS spectrum *vs* collision voltage of the $TEMPOH_2^+$ ion at m/z 158. The sample preparation and MS procedures are given in Figure 3.3.

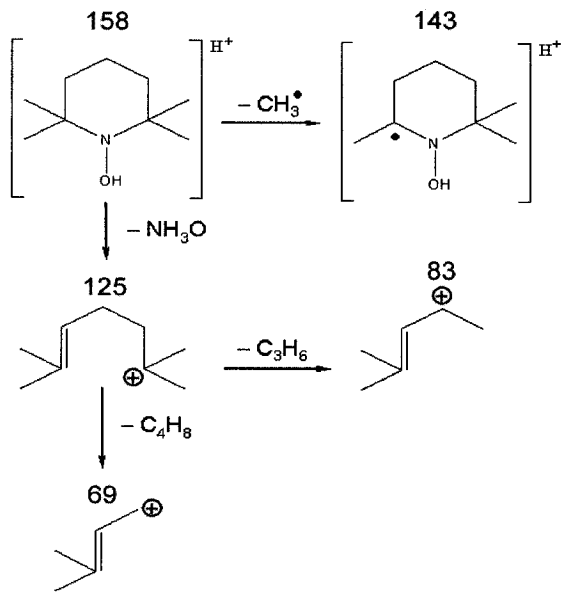

Figure 3.8. Proposed fragmentation pathways of the $TEMPOH_2^+$ ion at m/z 158.

3.4.3 Fractional abundances of the TEMPO• ions

Table 3.1 lists the fractional abundances of the ions observed in ESI mass spectrum of TEMPO• recorded in water, 0.5% FA and 50 μM NaPi. As seen in the MS/MS spectra (Figure 3.5), a methyl radical (CH_3•) is easily lost from $TEMPOH^{\bullet+}$ to give a fragment ion at m/z 142. In water (Figure 3.2), a low-intensity peak at m/z 179 corresponding to $TEMPONa^{\bullet+}$ is also present and the fractional abundance of the m/z 142, 157 and 179 ions derived directly from TEMPO• in the ion source is > 80% (Table 3.1). The addition of FA increases the fractional abundance of TEMPOH-derived ions (m/z 143 and 158) by 10-fold (Table 3.1) and that of $TEMPO^+$ also increases largely at the expense of the $TEMPOH^{\bullet+}$ ion. In 50 μM NaPi, $TEMPONa^{\bullet+}$ (m/z 179) is the base peak with a fractional abundance of 61% and a $(H_2O+TEMPONa)^{\bullet+}$ adduct (m/z 197) is also detected with a fractional abundance of 12% (Figure 3.9 and Table 3.1). No peaks above the noise due to $TEMPO^+$ or $TEMPOHNa^+$ (m/z 180) were detected in NaPi after correction for isotopic contributions (Figure 3.9), but the $TEMPOH_2^+$ ion (m/z 158) had a fractional abundance of 7.3%.

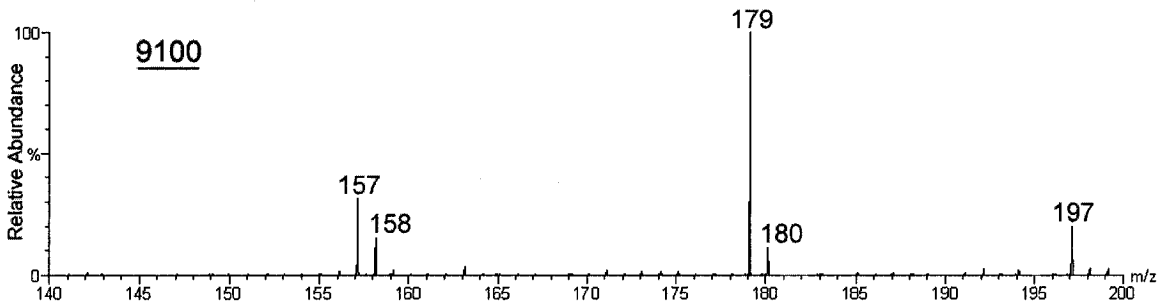

Figure 3.9. ESI mass spectrum of TEMPO• in sodium phosphate buffer. A solution of 50 μM TEMPO• in 50 μM sodium phosphate buffer (pH 7.0) was directly infused into the Z-spray source of the QToF2 mass spectrometer. The MS parameters are listed in Figure 3.2. Note that the peak at m/z 180 is due to isotopes of $TEMPONa^{\bullet+}$ and not $TEMPOHNa^+$ (see text). The number of total ion counts per 20 scans (TICs) is underlined.

Table 3.1. Fractional abundances corrected for isotopic contributions of ions in the ESI mass spectrum of TEMPO• at low collision voltage[a]

Ion	m/z	Fractional abundance (%)[b]		
		H_2O	0.5% FA	50 μM NaPi
$TEMPO^+$	156	18	30	0
$TEMPOH^{\bullet+}$-$CH_3^\bullet$	**142**	**14**	**17**	**0**
$TEMPOH^{\bullet+}$	**157**	**60**	**33**	**19**
$TEMPONa^{\bullet+}$	**179**	**6.4**	**< 1.0**	**61**
$(H_2O+TEMPONa)^{\bullet+}$	**197**	**0**	**0**	**12**
$TEMPOH_2^+$-$CH_3^\bullet$	143	0	< 1.0	0
$TEMPOH_2^+$	158	1.7	19	7.3
$TEMPOHNa^+$	180	0	0	0
TIC[c]	142–197	1.3×10^4	2.9×10^4	9.1×10^3

[a] Solutions of 50 μM TEMPO• in water, 0.5% formic acid and 50 μM sodium phosphate buffer (pH 7.0) were analyzed by ESI-MS. The collision voltage was 5 V and the other MS conditions are given in Figure 3.2. TEMPO•-derived ions are in bold font for clarity.

[b] The fractional abundance of each ion was calculated by the Masslynx software and corrected for isotopic contributions based on the theoretical isotopic distribution patterns determined using IsoPro 3.0 software (http://members.aol.com/msmssoft).

[c] TIC (total ion counts per 20 scans) in the ESI MS spectra.

3.4.4 Relative stability of $TEMPOH^{\bullet+}$ *vs* $TEMPONa^{\bullet+}$ in the ESI source

The MS/MS spectrum of $TEMPOH^{\bullet+}$ in 0.5% FA recorded at a collision voltage of 10 V (Figure 3.10A) clearly reveals a fragment ion at m/z 142 due to $CH_3^\bullet$ loss. At a collision voltage of 20 V, $CH_3^\bullet$ loss from $TEMPONa^{\bullet+}$ is observed (m/z 164; Figure 3.10D). Higher energy is required to fragment the organic moiety of the MNa^+ ion because a low-energy fragmentation pathway involving loss of Na^+ dominates, which is reflected in the total ion counts (TIC). The TIC of the sodiated ions is 2066 at 10 V and decreases to 34 (1.6%) at 20 V while the TIC of the protonated ions decreases by only

54% from 8491 to 3926 (Figures 3.10A and B). It is interesting that the $(H_2O+TEMPONa)^{\bullet+}$ adduct (m/z 197) is detected in the $TEMPONa^{\bullet+}$ product spectrum (Figures 3.10C and D). This adduct must form following mass selection of m/z 179 ions in the quadrupole, which reflects the relatively high SA of water (Table 3.2).

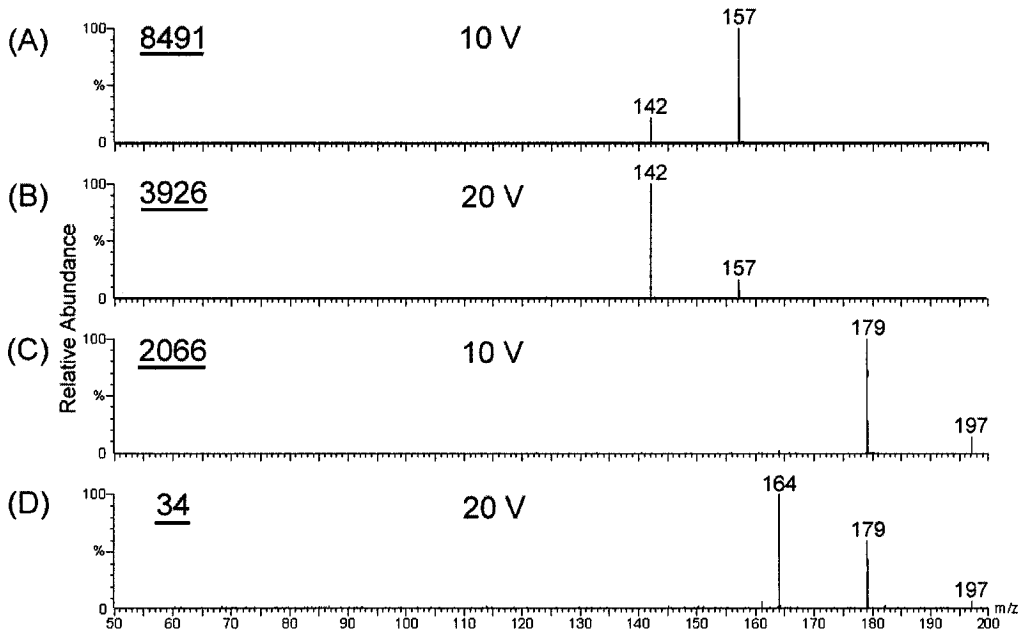

Figure 3.10. TICs *vs* collision voltage in the MS/MS product-ion spectra of $TEMPOH^{\bullet+}$ (m/z 157) *vs* $TEMPONa^{\bullet+}$ (m/z 179). Solutions of 50 μM $TEMPO^{\bullet}$ in (A and B) 0.5% formic acid and (C and D) 50 μM sodium phosphate buffer (pH 7.0) were directly infused into the Z-spray source of the QToF2 mass spectrometer and the MS/MS spectra recorded as in Figure 3.3. The total ion counts per 20 scans (TICs) at each collision voltage (V) are underlined.

3.4.5 DFT calculations to determine the protonation and sodiation sites in $TEMPO^{\bullet}$ and TEMPOH

The proton affinity (PA) of the nitrogen and oxygen atoms in TEMPOH and $TEMPO^{\bullet}$ were determined using DFT calculations (Figures 3.11 and 3.12). In the gas phase, the PA is defined as the negative of the protonation enthalpy ($M + H^+ \rightarrow MH^+$). The PA of the TEMPOH nitrogen atom was calculated to be 227.2 kcal/mol (Table 3.2).

No stable structure could be optimized with the proton on oxygen atom; thus, protonation is assumed to take place only at the nitrogen atom.

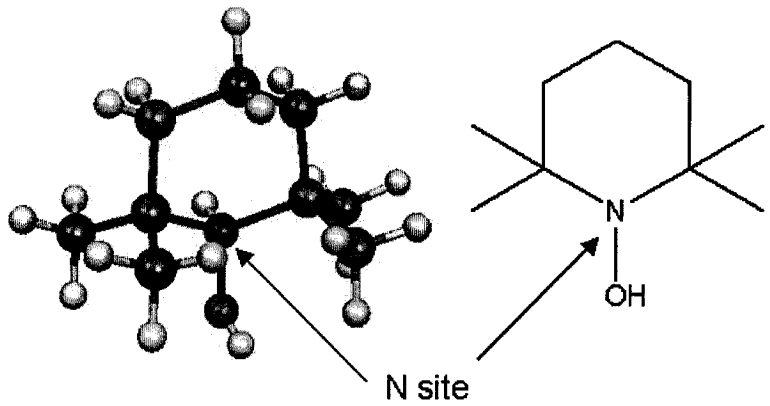

Figure 3.11. Calculated structure of $TEMPOH_2^+$.

The reported experimental PA of TEMPO$^\bullet$ determined by a kinetic method is 209.5 kcal/mol [182]. This value is 4 kcal/mol less than the calculated value of 213.5 kcal/mol for the oxygen atom but 16.5 kcal/mol higher than that of the nitrogen atom (Table 3.2), revealing that protonation takes place at oxygen in TEMPO$^\bullet$. Using Atoms In-Molecules (AIM) analysis, the Laplacian ($\nabla^2\rho$ = -1.8076 e/Å^5 < 0) of the O–H$^+$ bond is negative, which is typical for a covalent bond [183].

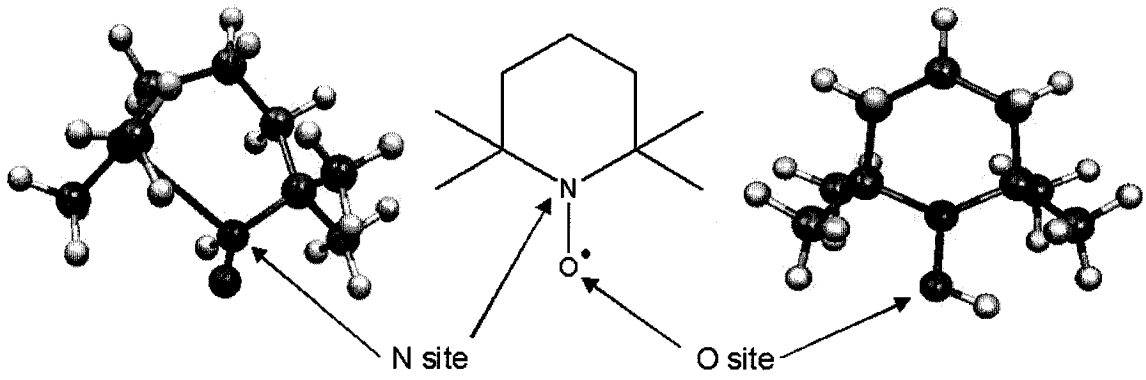

Figure 3.12. Calculated structures of protonated TEMPO$^\bullet$. The lowest-energy structure is achieved by protonating at the O site.

When Na^+ is present, $TEMPONa^{\bullet+}$ (m/z 179) becomes the base peak in the ESI mass spectrum (Figure 3.9). DFT calculations reveal that the interaction between Na^+ and oxygen in the lowest-energy conformer of $TEMPO^\bullet$ (Figure 3.13) yields a SA of 37.5 kcal/mol (Table 3.2), and AIM analysis indicated that the O–Na^+ bond is electrostatic in character (Laplacian $\nabla^2\rho = 0.2512$ e/Å$^5 > 0$) [183]. The calculated and experimental PA [184] and SA [185] for H_2O are included in Table 3.2 for comparison.

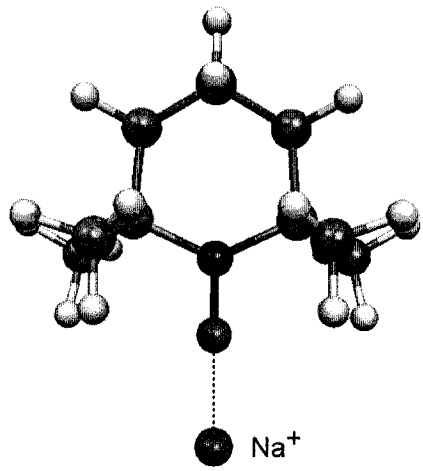

Figure 3.13. Calculated structure of $TEMPONa^{\bullet+}$.

Table 3.2. DFT calculated gas-phase proton affinities (PA) and sodium affinities (SA) of $TEMPO^\bullet$, TEMPOH and H_2O

Molecule	PA (kcal/mol)			SA (kcal/mol)	
	Nitrogen	Oxygen	Exp[a]	Oxygen	Exp[a]
$TEMPO^\bullet$	193.0	213.5	209.5	37.5	——
TEMPOH	227.2	0[b]	——	0[b]	——
H_2O	——	158.4	165.0	25.6	21.0

[a] Experimental values from Refs [182, 184, 185].

[b] Unstable structure.

Table 3.3. DFT optimized bond lengths (Å) calculated for $TEMPO^+$, $TEMPO^•$, $TEMPOH^{•+}$, $TEMPONa^{•+}$, TEMPOH and $TEMPOH_2^+$ in the gas phase

Molecule / Bond[a]	$TEMPO^+$	$TEMPO^•$		$TEMPOH^{•+}$		$TEMPONa^{•+}$	TEMPOH	$TEMPOH_2^+$
		Exp[b]		$N–H^{+c}$	$O–H^{+c}$	$O–Na^{+c}$		$N–H^{+c}$
N–O	1.186	1.296	1.281	1.260	1.335	1.286	1.449	1.417
N–C1	1.543	1.482	1.503	1.510	1.502	1.508	1.492	1.570
N–C2	1.543	1.482	1.503	2.457	1.506	1.508	1.492	1.570
C2–C3	1.527	1.533	1.541	1.475	1.545	1.541	1.538	1.528
C2–C4	1.547	1.529	1.534	1.480	1.538	1.534	1.544	1.531
C1–C5	1.527	1.533	1.541	1.526	1.546	1.541	1.538	1.528
C1–C6	1.547	1.529	1.534	1.541	1.536	1.534	1.544	1.531
O–H							0.961	0.968

[a] The carbon atom numbers are as follows:

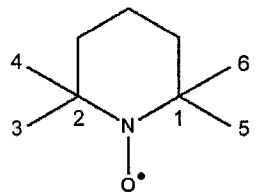

[b] Data from Ref [186]. Values were obtained from an EPR study of single crystals.

[c] $TEMPO^•$ was protonated at the nitrogen atom ($N–H^+$) or oxygen atom ($O–H^+$) and sodiated at the oxygen atom ($O–Na^+$). TEMPOH was protonated at the nitrogen atom ($N–H^+$).

3.5 Discussion

$TEMPO^•$ is frequently used to catalyze the oxidation of alcohols to carbonyls in organic synthesis [155]. This process involves redox cycling of $TEMPO^•$ between its oxidized ($TEMPO^+$, *N*-oxoammonium cation) and reduced forms (TEMPOH, hydroxylamine) (Figure 3.1) [168]. Redox cycling of $TEMPO^•$ in the ESI source also occurs since $TEMPO^+$ and $TEMPOH_2^+$ ions are observed in the ESI spectrum of $TEMPO^•$ in water (Figure 3.2). The oxidation of $TEMPO^•$ to $TEMPO^+$ ($E°$ $TEMPO^+/TEMPO^•$ = 0.64 V *vs* NHE) [157] should readily occur in the emitter under a

positive potential [176, 177, 181]. $TEMPO^+$ can oxidize the solvent depending on its nucleophilicity through an Anelli-type reaction to yield TEMPOH [187, 188] and hence the $TEMPOH_2^+$ ion in the ESI mass spectrum [176, 177, 181]. The formation of TEMPOH in the ESI source is inefficient in water (Table 3.1), but since the electrochemical reduction of $TEMPO^\bullet$ to TEMPOH is an irreversible process [189], $TEMPOH_2^+$ ions are observed in the ESI spectrum (Figure 3.2).

Due to the Anelli reaction, the ESI spectrum of $TEMPO^\bullet$ varies with the MS solvent. It is not surprising that the mass spectrum obtained here in water (Figure 3.2) differs from the previously reported $TEMPO^\bullet$ ESI spectra in organic solvents (Table 3.4).

Table 3.4. Relative abundances (%) of ions in the ESI mass spectrum of $TEMPO^\bullet$ reported in literature

MS solvent	$TEMPO^+$	$TEMPOH^{\bullet+}$	$TEMPOH_2^+$	References
100% water[a]	22	100	2.1	Table 3.1
50% water/methanol, 1% acetic acid[b,c]	44	100	72	[176]
100% acetonitrile[d,e]	100	15	8	[181]
50% dichloromethane/ acetonitrile, 1 mM lithium trifluoromethanesulfonate[b,e]	100	0	1	[176]

[a] Data for H_2O from Table 3.1. All ions derived from $TEMPO^\bullet$ without any redox processes are included under $TEMPOH^{\bullet+}$.

[b] Carried out on a Thermoquest-Finnigan LCQ quadrupole ion trap mass spectrometer.

[c] Normal ESI source equipped with a glass capillary emitter. Other $TEMPO^\bullet$-derived ions not reported.

[d] Carried out on a Waters Micromass Quattro II triple-quadrupole mass spectrometer.

[e] Normal ESI source equipped with a metal capillary emitter. Other $TEMPO^\bullet$-derived ions not reported.

Under MS conditions that minimize fragmentation (see legend of Figure 3.2), the ions derived directly from $TEMPO^{\bullet}$ without any redox processes (m/z 142, 157 and 179) made the dominant contribution to the TIC in water (80%) and in 0.5% FA (50%) (Table 3.1). However, acid appears to increase the conversion of $TEMPO^{\bullet}$ to $TEMPO^{+}$ and TEMPOH or to destabilize $TEMPOH^{\bullet+}$ in the ESI source although the latter is less likely since the TICs are similar in both solvents (Table 3.1). In the presence of sodium, $TEMPONa^{\bullet+}$ (m/z 179) becomes dominant (Figure 3.9 and Table 3.1) consistent with the high SA calculated for $TEMPO^{\bullet}$ (Table 3.2). In comparison, water has a SA of 21.0 kcal/mol [185] so that Na^{+} is donated from the solvent to form $TEMPONa^{\bullet+}$, which can be adducted by H_2O to give the ion at m/z 197 (Figure 3.9). Sodiated TEMPOH ($TEMPOHNa^{+}$, M_r = 180 u) was found by DFT calculations to be structurally unstable and was not detected in the mass spectra (Figure 3.9 and Table 3.1).

As the TIC values indicate, the number of ions detected in the m/z range 50–200 decreased with increasing collision voltage (Figure 3.10). Since the SA of $TEMPO^{\bullet}$ is ~6-fold less than its PA (Table 3.2), Na^{+} release to form the neutral $TEMPO^{\bullet}$ radical is facile as reflected in the drastic drop in the TIC of $TEMPONa^{\bullet+}$ on doubling the collision voltage (Figure 3.10D). On the other hand, charging $TEMPO^{\bullet}$ by protonation at the oxygen atom stretches the N–O bond by ~0.05 Å whereas electrostatic interaction between Na^{+} and $TEMPO^{\bullet}$ does not perturb the structure (Table 3.3). As a result, fragmentation of the organic moiety of $TEMPONa^{\bullet+}$ is observed at a higher collision voltage than observed for $TEMPOH^{\bullet+}$ (Figure 3.10). Thus, the presence of sodium ions should simplify the analysis by ESI MS of $TEMPO^{\bullet}$ scavenging and redox reactions.

3.6 Conclusions

The redox turnover of TEMPO$^{\bullet}$ in the ESI source depends on the MS solvent and source parameters. TEMPO$^{\bullet}$ may act as an electron donor to CCP/H_2O_2, so to quantify $TEMPO^+$ formed in solution it is necessary to prevent $TEMPO^+$ formation in the ESI source. Our data show that TEMPO$^{\bullet}$ in sodium phosphate buffer (pH 7.0) gives rise to > 90% of the total ion abundance without redox turnover in the ESI source (Table 3.1). Furthermore, MS analysis and quantum chemistry calculations reveal that protonation but not sodiation perturbs the structure of TEMPO$^{\bullet}$. Sodiation will, therefore, simplify the ESI MS analysis of solution-based TEMPO$^{\bullet}$ redox reactions by inhibiting redox turnover of the nitroxyl in the ESI source and by removing TEMPO$^{\bullet}$-derived fragments from the mass spectra.

Appendix 3.1. MS/MS analysis and DFT calculation of $NAYAH^+$ and $NAYANa^+$

The protonated and sodiated forms of *N*-acteyl-*L*-tyrosinamide (NAYA), a low-mass model of tyrosine residues in proteins [190], were also investigated. No $NAYANa^+$ (m/z 245) fragment ions were observed above m/z 50 while $NAYAH^+$ (m/z 223) underwent extensive fragmentation as the collision voltage was increased (Figure A3.14). In fact, at 15 V the $NAYAH^+$ ion was no longer detectable although $NAYANa^+$ was the only visible ion above m/z 50 at 30 V. The fragmentation pathway (Figure A3.15) based on its MS/MS spectra (Figure A3.14A) revealed that loss of NH_3 (17 u) from $NAYAH^+$ was facile in the ESI source. This was followed by loss of CO (28 u) at higher collision energies.

Possible protonation and sodiation sites in NAYA are summarized in Figures A3.16 and A3.17. Protonation of the amide NH_2 site increase the length of the N–C bond (labeled with an asterisk in Figure A3.16) by 0.25 Å from 1.37 to 1.62 Å. This is consistent with the appearance of the MH^+–NH_3 ion (m/z 206) at low collision energy (Figure A3.14A). As shown in Figure 3.17, the sodium ion could bind to NAYA *via* the primary amide carbonyl oxygen (A), the secondary amide carbonyl oxygen plus the aromatic π face (B), the two amide carbonyl oxygens (C) or *via* the aromatic π face only (D). The length of the N–C bond in the most stable $NAYANa^+$ structure (C, Table A3.5) is unchanged (1.36 Å), indicating that the electronic structure is not altered by sodiation.

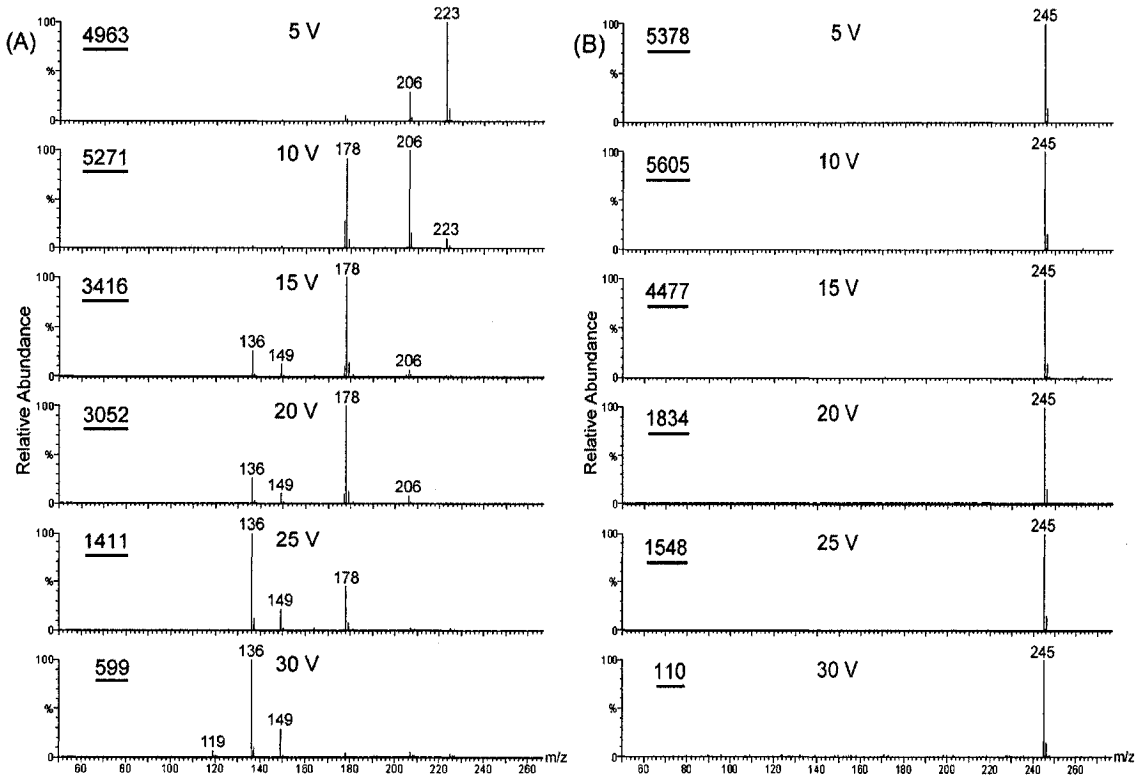

Figure A3.14. TICs in the MS/MS product-ion spectra of NAYAH$^+$ (m/z 223) *vs* NAYANa$^+$ (m/z 245) ions. A solution of 50 μM NAYA in (A) 0.5% formic acid and (B) 50 μM sodium phosphate buffer (pH 7.0) was directly infused into the Z-spray source of the QToF2 mass spectrometer and the MS/MS spectra recorded as in Figure 3.3. The total ion counts per 20 scans (TICs) at each collision voltage (V) are underlined on the spectra.

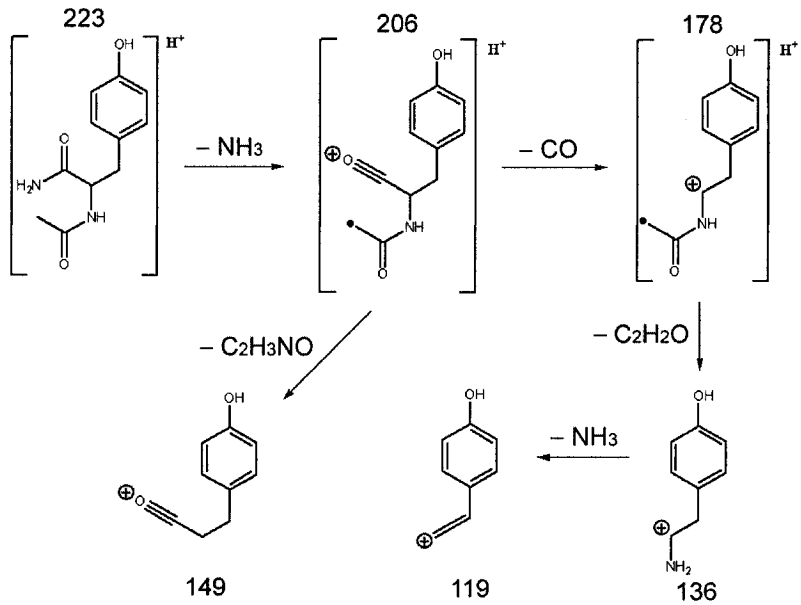

FigureA3.15. Proposed fragmentation pathways of the NAYAH$^+$ ion at m/z 223.

TIC values as a function of collision voltage are listed in Figure A3.14. As can be seen, doubling the collision voltage from 10 V to 20 V decreases the TIC of $NAYANa^+$ by 67% compared to the 98% drop observed for $TEMPONa^{\bullet+}$ (Figure 3.10). This is consistent with the higher SA of NAYA (54.0 kcal/mol, Table A3.5) *vs* $TEMPO^\bullet$ (37.5 kcal/mol, Table 3.2), which increases the stability of the $NAYANa^+$ ion.

In conclusion, fragmentation of the organic moiety is not observed for $NAYANa^+$ at a collision voltage of 30 V while $NAYAH^+$ fragments at 5V (Figure A3.14). The TIC of $NAYANa^+$ decreases more dramatically than that of the $NAYAH^+$-derived ions as the collision voltage is increased (Figure A3.14). DFT calculations reveal that the SA of NAYA is 3.9-fold less than its PA (Table A3.5). Thus, loss of Na^+ provides a low-energy fragmentation pathway for $NAYANa^+$. Consistent with the results for $TEMPO^\bullet$ (Table 3.3), protonation but not sodiation destabilizes the electronic structure of NAYA.

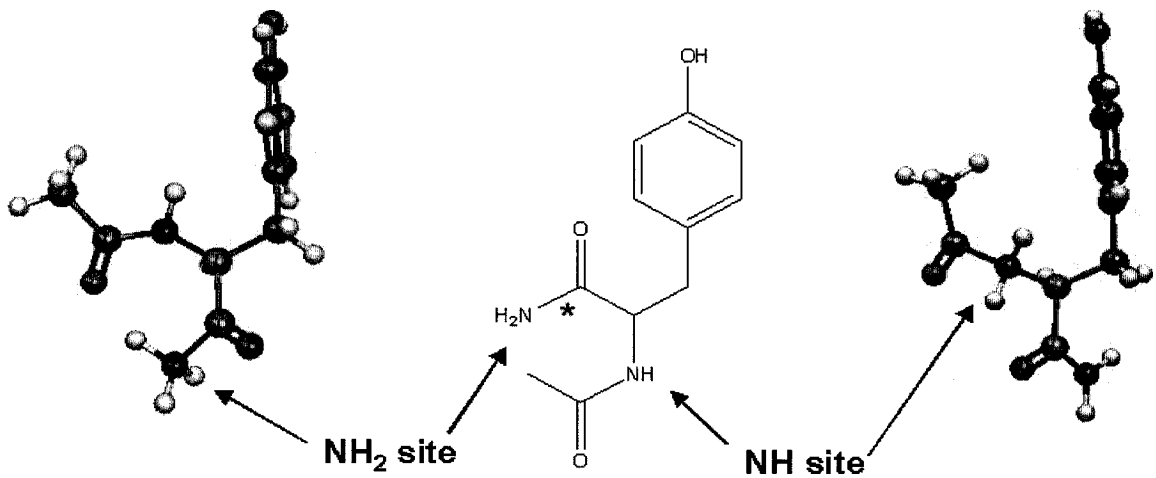

Figure A3.16. Calculated structures of $NAYAH^+$. The asterisk (*) represents the N–C bond that is cleaved to release NH_3 in the mass spectrometer.

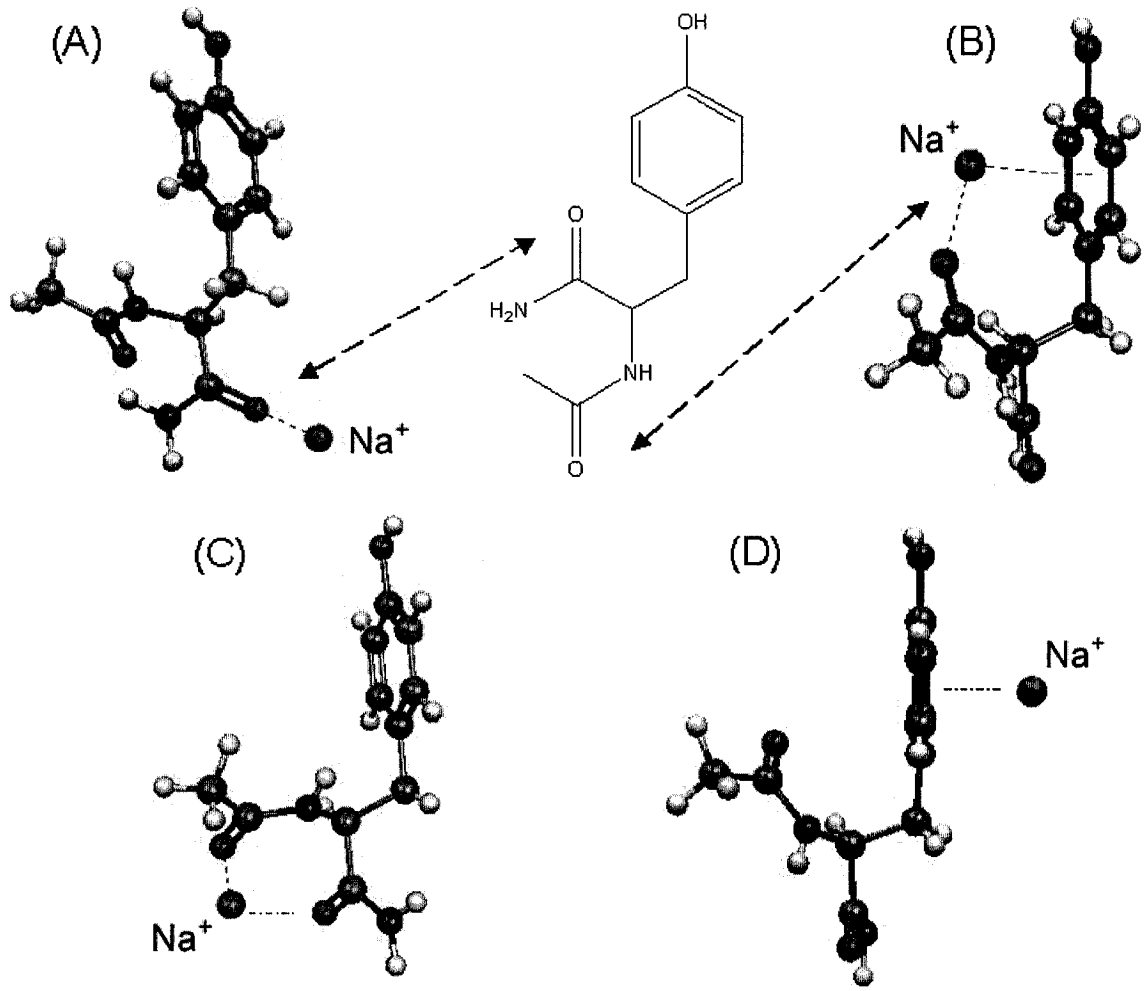

Figure A3.17. Calculated structures of NAYANa$^+$. Structures (B) and (D) involve interaction between Na^+ and the aromatic π face (see text).

Table A3.5. DFT calculated gas-phase proton affinities (PA) and sodium affinities (SA) of NAYA

PA (kcal/mol)[a]		SA (kcal/mol)[b]			
NH	NH_2	A	B	C	D
210.8	212.3	40.2	47.9	54.0	23.5

[a] Protonation sites are shown in Figure A3.16.

[b] Sodiation sites are shown in Figure A3.17.

4 Phenotypic analysis of the *ccp1Δ* and *ccp1Δ-ccp1*^{W191F} mutant strains of *Saccharomyces cerevisiae* indicates that cytochrome *c* peroxidase functions in oxidative-stress signaling

4.1 Abstract

Yeast cytochrome *c* peroxidase (CCP) efficiently catalyzes the reduction of H_2O_2 to H_2O by ferrocytochrome *c in vitro*. The physiological function of CCP, a heme peroxidase that is targeted to the mitochondrial intermembrane space of *S. cerevisiae*, is not known. *CCP1*-null-mutant cells in the W303-1B genetic background (*ccp1Δ*) grew as well as wild-type cells on glucose, ethanol, glycerol or lactate as carbon sources but with a shorter initial doubling time. Monitoring growth over ten days demonstrated that *CCP1* does not enhance mitochondrial function in unstressed cells. No role for *CCP1* was apparent in cells exposed to heat stress under aerobic or anaerobic conditions. However, the detoxification function of CCP protected respiring mitochondria when cells were challenged with H_2O_2. Transformation of *ccp1Δ* with *ccp1*^{W191F}, which encodes the CCP^{W191F} mutant enzyme lacking CCP activity, significantly increased the sensitivity to H_2O_2 of exponential-phase fermenting cells. In contrast, stationary-phase (7-day) *ccp1Δ-ccp1*^{W191F} exhibited wild-type tolerance to H_2O_2, which exceeded that of *ccp1Δ*. Challenge with H_2O_2 caused increased CCP, superoxide dismutase and catalase antioxidant enzyme activities (but not glutathione reductase activity) in exponentially growing cells and decreased antioxidant activities in stationary-phase cells. Although *unstressed* stationary-phase *ccp1Δ* exhibited the highest catalase and glutathione reductase activities, a greater loss of these antioxidant activities was observed on H_2O_2 exposure in *ccp1Δ* than in *ccp1Δ-ccp1*^{W191F} and wild-type cells. The phenotypic

differences reported here between the *ccp1Δ* and *ccp1Δ-ccp1*^{W191F} strains lacking CCP activity provide strong evidence that CCP has separate antioxidant and signaling functions in yeast.

4.2 Introduction

Yeast cells have evolved a range of responses to different environmental stresses including exposure to organic solvents and low pH, heat shock, osmotic shock, starvation and oxidative stress [1]. Oxidative stress arises when cells are unable to adequately deal with reactive oxygen species (ROS) such as the superoxide anion (O_2^-), H_2O_2 and the hydroxyl radical ($^{\bullet}OH$). Mitochondria in aerobes produce energy in the form of ATP and are the major intracellular source of ROS [52, 191] that damage cells if uncontrolled [8]. Since *S. cerevisiae* is a facultative aerobe, cells can survive with non-functioning mitochondria, which would be fatal for obligate aerobes [192]. Mitochondrial damage can convert respiratory-competent (RC) yeast cells into respiratory-deficient (RD) cells, and both RC and RD yeast can multiply on glucose and other fermentable carbon sources. When the glucose supply is exhausted, only RC cells multiply using the ethanol produced during fermentation as a carbon source [192]. RD cells cease growth in media containing only non-fermentable carbon sources such as ethanol, glycerol or lactate.

Both enzymatic and non-enzymatic defense systems against ROS are present in cells [1]. Cytochrome *c* peroxidase (CCP), which is nuclear encoded and targeted to the mitochondrial intermembrane space [90], reportedly functions as an antioxidant enzyme in yeast by detoxifying ~55% of the H_2O_2 formed in mitochondria during aerobic metabolism [85]. It is classified as a peroxidase based on its efficient catalysis *in vitro* ($k_{cat} = 4.5\times10^7\ M^{-1}s^{-1}$, pH 7) [99] of H_2O_2 reduction to H_2O by ferrocytochrome *c* [98]:

$$2 \text{ ferrocytochrome } c + H_2O_2 + 2\ H^+ \rightarrow 2 \text{ ferricytochrome } c + 2\ H_2O \qquad (1.1)$$

The mechanism of peroxidase catalysis by yeast CCP has been extensively examined *in vitro* over the last 50 years using both biochemical and genetic methods as reviewed in [98]. The catalytic cycle is given by [98]:

$$CCP + H_2O_2 \rightarrow CCP\text{-}I + H_2O \qquad (1.2)$$

$$CCP\text{-}I + \text{ferrocytochrome } c + H^+ \rightarrow CCP\text{-}II + \text{ferricytochrome } c \qquad (1.3)$$

$$CCP\text{-}II + \text{ferrocytochrome } c + H^+ \rightarrow CCP + \text{ferricytochrome } c + H_2O \qquad (1.4)$$

On H_2O_2 binding to the ferric heme, compound I (CCP-I) is formed (Eq. 1.2). This intermediate is two oxidizing equivalents above the ferric state with one equivalent residing on the heme as an oxyferryl (Fe^{IV}=O) species and the second on Trp191 as a tryptophanyl cation radical [98]. CCP compound II (CCP-II) is the one-electron reduced product of CCP-I and contains an oxyferryl heme. Trp191 at ~10 Å from the CCP heme [101] is an essential amino-acid residue since CCP^{W191F} with a Trp-to-Phe point mutation at residue 191 exhibits negligible ferrocytochrome *c*-peroxidizing activity due to a 10^4-reduced rate of CCP-cytochrome *c* intracomplex electron transfer (Eqs. 1.3, 1.4) [140]. CCP^{W191F} also differs from the wild-type enzyme in that dimerization occurs on reaction with one molar equivalent of H_2O_2 *in vitro* [117]. Dimerization involves dityrosine crosslinking [116, 193], which is considered a marker of oxidative stress in cells [194]. In contrast, wild-type CCP can reduce up to 10 molar equivalents of H_2O_2 in the absence of ferrocytochrome *c* before dimerization become significant [117].

In addition to its antioxidant function, CCP reportedly conveys an oxidative-stress signal to the transcription factor Skn7/Pos9 [70]. Skn7 is also known as Pos9 since a Skn7 mutant with increased sensitivity to H_2O_2 has been isolated [67]. Skn7/Pos9

cooperates with the yeast transcription factor Yap1 in controlling the H_2O_2-induced stress response, which involves upregulation of ROS scavenging genes including *CCP1*, *CTT1*, *SOD1* and *SOD2* [63]. The catalytically inactive CCP^{W191F} mutant also conveys an oxidative-stress signal to Skn7/Pos9 [70], so it was proposed that the signaling and antioxidant activity of CCP are independent [85].

Despite extensive *in-vitro* characterization of CCP [98], no systematic study of its physiological role in yeast has been reported to date. Considering that CCP and CCP^{W191F} exhibit very different properties *in vitro* [113, 116, 117, 141, 142], phenotypic comparison of *ccp1Δ* and *ccp1Δ-ccp1*^{W191F} yeast is of much interest. Here we compare the growth and survival of unstressed and H_2O_2-challenged *ccp1Δ*, *ccp1Δ-ccp1*^{W191F} and wild-type *S. cerevisiae* cells in the W303-1B genetic background. The thermotolerance of the three strains was also compared since heat induces oxidative stress and deletion of antioxidant enzymes decreases thermoresistance [42]. The index of respiratory competence (IRC) [195] of the cells was monitored to establish the effects of H_2O_2 challenge on mitochondrial function. This index corresponds to the fraction of RC cells in a culture and provides a quantitative measure of mitochondrial health of yeast cells. Variations in activities of key antioxidant enzymes under both Yap1 and Skn7/Pos9 control, CCP, catalase and superoxide dismutase (SOD), are reported for exponential- and stationary-phase cells. Activities of glutathione reductase (GLR), which is controlled by Yap1 but not Skn7/Pos9 [63], are also reported.

4.3 Materials and methods

4.3.1 Yeast strains and plasmids

Table 4.1. *S. cerevisiae* strains, plasmids and primers used in this study

Strain, plasmid or primer[a]	Description	Reference
wild-type	W303-1B cells; *MATα ade2-1 his3-11,15 leu2-3,112 ura3-1 trp1-1 can1-100*	[87]
ccp1Δ	W303-1B cells with *ccp1::KAN*	this work
ccp1Δ-ccp1^{W191F}	*ccp1Δ* with YCplac33-*ccp1*^{W191F}	this work
ccp1Δ-E	*ccp1Δ* with YCplac33-*E*	this work
ccp1Δ-CCP1	*ccp1Δ* with YCplac33-*CCP1*	this work
pFA6-kanMX4	pFA6 plasmid encoding *KAN* which replaces *CCP1* (ORF YKR066C) in the *ccp1Δ* genome	[196]
pYCplac33-*ccp1*^{W191F}	YCplac33 plasmid encoding the W191F point mutant of CCP	[70]
pYCplac33-*E*	YCplac33-*ccp1*^{W191F} minus bp 1–1697 of *CCP1*. This plasmid encodes the C-terminal residues 265–294 of CCP	this work
pYCplac33-*CCP1*	YCplac33 plasmid encoding wild-type CCP isoform 1	this work
primer 1*f*[b]	5′-ATTTCGCATTCATGCAGACGCAAAC ACACACGTATATCTACAATTCAGCTGA AGCTTCGTACGC-3′	this work
primer 2*r*[b]	5′-AATAATACGAAATATAACCAATAAA TAATATCTTTCCTCAGTGACTAGGCCA CTAGTGGATCTG-3′	this work
primer 3*f*	5′-TTCTCCCGCAGCTAGATCTC-3′	this work
primer 4*r*	5′-TCTGCAGCGAGGAGCCGTAAT-3′	this work
primer 5*r*	5′-TAAGGTTGTAGCAGTCGAGC-3′	this work
primer 6*f*	5′-TGATTTTGATGACGAGCGTAAT-3′	this work

[a] Forward and reverse primers are denoted by *f* and *r*, respectively.

[b] Underlined sequences contain 19 bases identical to the MCS of pFA6-kanMX4.

The yeast strains, vectors and primers used in this work are listed in Table 4.1. The *CCP1* gene-null-mutant of *S. cerevisiae* strain W303-1B *(ccp1Δ)* was created by a PCR-based gene-disruption method using the pFA6-kanMX4 plasmid containing the *kanMX* selection module for G418-resistance in yeast [196]. A 1632-bp PCR fragment was generated using pFA6-kanMX4 as a template, and primer set *1f/2r* containing 19 bases identical to the pFA6-kanMX4 multiple cloning site (MCS) (underlined sequences, Table 4.1). Additionally, primers *1f* and *2r* possess 45 bases identical to sequences immediately upstream of the start codon and immediately downstream of stop codon of *CCP1* (ORF YKR066C) in the yeast genome [41]. PCR reactions (50 μL) contained 2.5 units Taq DNA polymerase (Roche Applied Science) in its buffer with $MgCl_2$, 1 μM primers (Biocorp, Montreal), 200 μM dNTPs (Roche), 100 μg template DNA and water treated with DEPC (Sigma). The template was amplified (5 min at 94°C; 26 cycles of 45 s at 94°C, 45 s at 55°C, 60 s at 72°C; 1 cycle of 10 min at 70°C), and the expected 1632-bp PCR product was observed on a 1% agarose (Bioshop) gel (data not shown). Yeast cells were transformed using the lithium acetate method [197] with 10–25 μL of the PCR product. After 4 h of non-selective growth in liquid YPD and 48 h of selective growth on YPD plates containing 0.03% geneticin (G418, Gibco BRL), $G418^r$ transformants were obtained.

Deletion of the *CCP1* gene and correct targeting of the *kanMX4* module were verified by PCR with genomic DNA from $G418^r$ transformants as a template. To extract genomic DNA, a colony (~1 mm^3) of cells was resuspended in 100 μL of 10 mM Tris (Fisher) buffer (pH 8.0) with 1% Triton X-100 (Sigma), 50 mM NaCl (Bioshop) and 1 mM EDTA (BDH, Toronto). Acid-washed glass beads (0.1 g) and 50 μL phenol

(Sigma)/chloroform (Fisher) (1:1) were added and cells vortexed for 4×30 s. The cell lysate was centrifuged at 12000×g at 4°C for 15 min, 20 μL of the supernatant was transferred into a sterile tube, 5 μL of the aqueous phase was subjected to PCR (5 min at 94°C; 26 cycles of 1 min at 94°C, 1 min at 55°C, 2 min at 72°C; 1 cycle of 10 min at 70°C), and the PCR products were analyzed on a 1% agarose gel. Two PCR reactions with *ccp1Δ* genomic DNA as a template confirmed that *CCP1* was correctly deleted by the *kanMX* module. Primers 3*f* and 5*r* (Table 4.1) were designed to bind 317 bases upstream of the *CCP1* start codon and 316 bases downstream of the *CCP1* stop codon. Primers 4*r* and 6*f* (Table 4.1) bind 274 bases downstream of the *KAN* start codon and 611 bases upstream of the *KAN* stop codon. The expected 591-bp and 927-bp PCR products were synthesized by primer sets 3*f*/4*r* and 5*r*/6*f*, respectively (data not shown). The PCR product (1719 bp) corresponding to the *CCP1* gene was synthesized by primer set 3*f*/5*r* when genomic DNA from wild-type cells was used as a template (data not shown).

YCplac33 is a low-copy vector that carries the yeast *URA3* gene as a selectable marker [198]. *ccp1Δ* was transformed with YCplac33-$ccp1^{W191F}$ [70] (Table 4.1) by the lithium acetate method [197], and *ccp1Δ*-$ccp1^{W191F}$ transformants that express CCP^{W191F} protein were obtained after 2 days at 30°C on synthetic complete (SC) medium (Sigma) without uracil. DNA sequencing (data not shown) confirmed that YCplac33-$ccp1^{W191F}$ [70] contains $ccp1^{W191F}$ (and bp 1–619 of ORF YKR065C).

ccp1Δ cells were transformed with YCplac33-*CCP1* to restore the wild-type phenotype, and with YCplac33-*E* as a control. To remove bp 1–1697 (which encode the N-terminal mitochondrial targeting presequence and residues 1–264 of the mature protein), YCplac33-$ccp1^{W191F}$ was digested with *Hin*dIII (Fermentas), and the digested

vector was self-ligated with T4 ligase (Fermentas) to yield YCplac33-*E* (6266 bp). The *CCP1* gene (1719 bp) was amplified by PCR using primer set *3f/5r* (Table 4.1) and genomic DNA from wild-type W303-1B cells as a template. Both the PCR product and YCplac33-*ccp1*^{W191F} were digested with *Fse* I (New England BioLabs) and *Bam*HI (Fermentas), and ligated using T4 ligase to yield YCplac33-*CCP1* (7992 bp). The *ccp1Δ* strain was transformed by the lithium acetate method [197] with YCplac33-*E* and YCplac33-*CCP1* to give the *ccp1Δ-E* and *ccp1Δ-CCP1* strains, respectively (Table 4.1).

4.3.2 Media and growth conditions

SC medium was supplemented with a carbon source to give SCD (2% glucose, BDH), SCE (3% ethanol, Commercial Alcohol, Montreal), SCG (3% glycerol, Fisher), SCL (2% lactate, Sigma) and SCEG (2% ethanol and 2% glycerol). Since ~20% of the *ccp1Δ-ccp1*^{W191F} cells lost the YCplac33-*ccp1*^{W191F} plasmid after 1 day in YPD (Table 4.3), the *ccp1Δ-ccp1*^{W191F} cultures were grown in SC medium without uracil to avoid plasmid loss. YP media [1% yeast extract (Bioshop) and 2% peptone (Bioshop)] supplemented with 2% glucose (YPD) or 2% ethanol plus 2% glycerol (YPEG) were also used where indicated. For normoxic conditions (high aeration), cultures were incubated with shaking at 225 rpm at a flask-to-medium volume ratio of ≥ 5. Anaerobic cultures were incubated without shaking at a flask-to-medium volume ratio of ~1.

4.3.3 Cell viability and IRC

To compare long-term survival of the strains, cells were grown in SCD at 30°C under high aeration. After 3 days, the spent media was removed by washing the cells twice with 0.85% sterile saline, and incubation at 30°C in the same volume of saline was continued with shaking at 225 rpm. After 4 days (*i.e.,* day 7 of cell growth), the saline

was changed and incubation was continued until day 10. This treatment increases the survival time of wild-type yeast strains [87]. Cell viabilities were determined by counting the number of living and dead cells at 400× magnification using an optical microscope (Model M11, Wild, Switzerland) and 0.01% methylene blue (Sigma) as a vital stain [199]. Mitochondrial function of each strain was evaluated by measuring its IRC, which is the ratio of the number of colony forming units (CFU) on solid SCEG and SCD [195].

4.3.4 Enzyme assays

Cells growing exponentially at 30°C in SCD under high aeration were harvested at OD_{600} 0.15 (~8 h) and 0.5 (~12 h). One-, 3- and 7-day cells were grown and harvested as described in the previous section (*Cell viability and IRC*). The cells were vortexed with glass beads in 100 mM potassium phosphate buffer (pH 7.4) containing a protease inhibitor cocktail (Roche), the resultant lysates were centrifuged at 13000×*g* at 4°C for 10 min, and the total protein in the supernatants was determined using the Bio-Rad *DC* protein assay. CCP activity was assayed by monitoring the oxidation of ferrocytochrome *c* at 550 nm ($\Delta\varepsilon_{550}$ = 19.6 $mM^{-1}cm^{-1}$) [108]. Catalase activity was established by following the disappearance of H_2O_2 at 240 nm (ε_{240} = 43.6 $M^{-1}cm^{-1}$) [149], and the xanthine oxidase/cytochrome *c* method was used to measure SOD activity [200]. GLR activity was assayed by monitoring NADPH oxidation at 340 nm (ε_{340} = 6.3 mM^{-1} cm^{-1}) [201]. Activity units are defined in the footnotes to Table 4.2 and the experimental details are provided in Appendix 4.4.

4.3.5 Cell survival after heat stress

Cells grown for 0.5 to 10 days as described under *Cell viability and IRC* were diluted to 3×10^3 cells per 1 mL with PBS (pH 7.4, Sigma). The cells were exposed to

anaerobic heat stress at 48°C [450 μL of culture in 450-μL PCR tubes (Costar, England), no shaking] and plated on solid SCD and SCEG. Percent survival was calculated from the ratio of the CFUs of heat-stressed and control cultures (grown at 30°C) ×100. Aerobic heat stress was examined by plating late-exponential-phase (~16 h) cultures on solid YPD and YPEG, and monitoring growth for 3 (YPD) or 5 days (YPEG) at 30, 37 and 41°C.

4.3.6 Cell survival after exposure to H_2O_2 and paraquat

Cultures grown under high aeration to OD_{600} ~2.0 were serially diluted into sterile PBS. To screen for oxidant sensitivity, aliquots were spotted on YPD and YPEG plates containing H_2O_2 (Fisher) or the superoxide-generating compound paraquat (Sigma) [202], and incubated at 30°C for 3–5 days.

The sensitivity to H_2O_2 of exponential-phase cells was further examined in liquid SCD and SCE media. Cells grown under high aeration to OD_{600} 0.5 were divided into equal portions. H_2O_2 was added to one portion to a final concentration of 0.4 mM and an equivalent volume of 0.85% sterile saline was added to the control. The cells were incubated at 30°C with high aeration, enzyme activities were measured after 60 min as described under *Enzyme assays,* and the ΔOD_{600} values of the cultures recorded after 2 h.

Because of the decreased sensitivity of stationary-phase cells to oxidative stress [203], high levels of exogenous H_2O_2 were required to alter survival rates. Cells grown for 1–7 days as described under *Cell viability and IRC* were diluted to 3×10^3 cells per 1 mL with PBS, and 45 mL of culture in 50-mL centrifuge tubes was exposed to 60 mM H_2O_2 for 60 min at 30°C. The percent survival and IRC of each strain was calculated and enzyme activities were measured as described under *Enzyme assays*.

4.3.7 H_2O_2 agar diffusion assays

To establish their relative H_2O_2-tolerance, wild-type, *ccp1Δ*, *ccp1Δ-ccp1*^{W191F}, *ccp1Δ-E* and *ccp1Δ-CCP1* cells grown in SCD under high aeration (OD_{600} ~2.0) were diluted ~30-fold into sterile PBS (pH 7.4). Aliquots (15 μL, ~10^4 cells) were streaked onto solid YPD and YPEG plates prepared using 15 mL of media. After spotting 6 μL of 30% H_2O_2 in the centre, the plates were incubated at 30°C for 3–5 days.

4.4 Results

4.4.1 *ccp1Δ* cells exhibit a shortened initial doubling time but comparable viability to *ccp1Δ-ccp1*^{W191F} cells

The three strains exhibit similar growth curves over 3 days except in SCE (Figure 4.1). Cells grew fastest in SCD and ceased growth after ~1 day. Growth was 3–5-fold slower and cells continued to multiply up to ~2–3 days in the non-fermentable carbon sources, SCE, SCG and SCL (Figure 4.1). Despite similar growth curves, bar graphs of percent growth relative to wild-type cells highlight significant and reproducible differences between the strains (Figure 4.2). For example, *ccp1Δ* grew significantly faster than wild-type or *ccp1Δ-ccp1*^{W191F} cells over 0–12 h in SCD (Figure 4.2) revealing a shortened initial doubling time in the absence of CCP or CCP^{W191F}. The *ccp1Δ* cells also exhibited the highest growth over 24 h on the non-fermentable carbon sources (Figure 4.2, SCE, SCG and SCL) with the threefold higher OD_{600} in SCE of the *ccp1Δ vs* the *ccp1Δ-ccp1*^{W191F} culture (Figure 4.2) being particularly remarkable. However, the OD_{600} of the latter culture is higher by day 3 (Figure 4.1B).

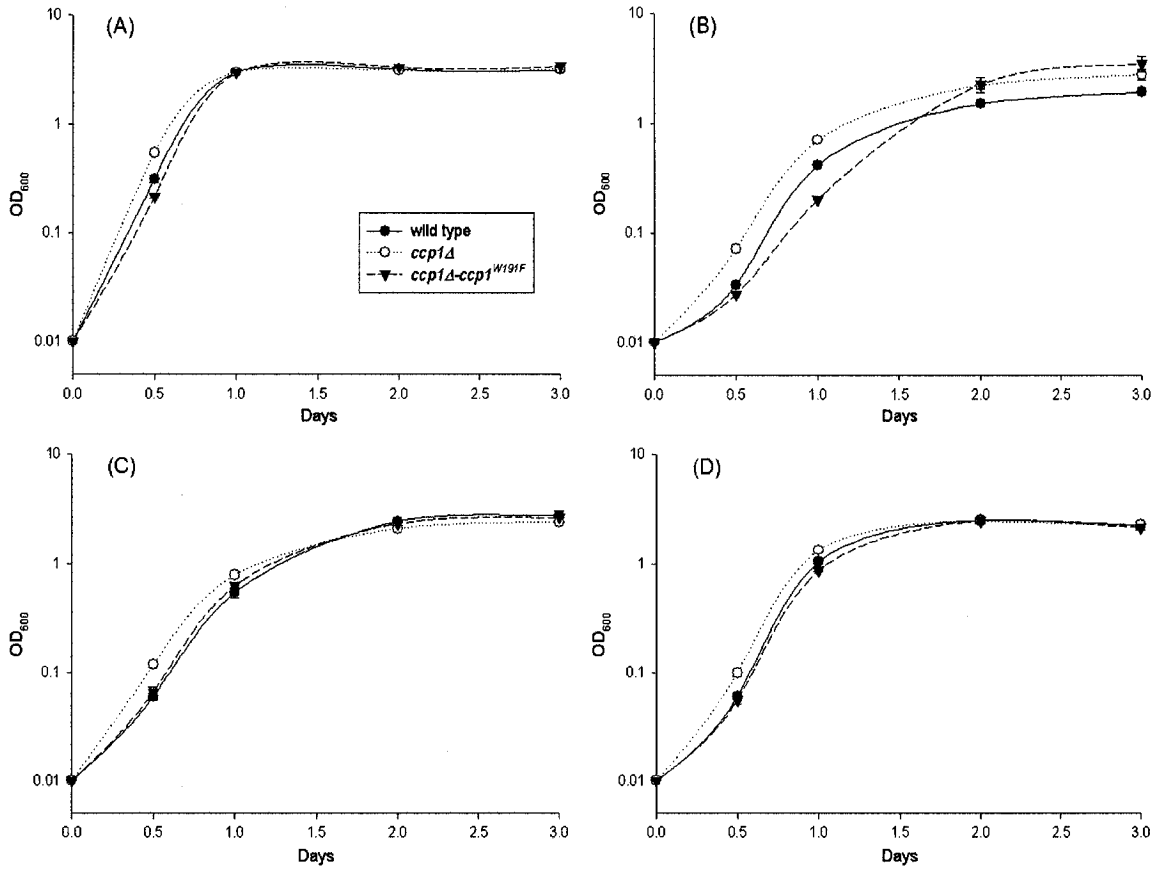

Figure 4.1. Growth curves of wild-type, *ccp1Δ* and *ccp1Δ-ccp1*^{W191F} *S. cerevisiae* cells on different carbon sources over 3 days. Late-exponential-phase cells (16 h, OD_{600} ~2.0) were inoculated at an initial OD_{600} of 0.01 and grown at 30°C in SC medium with (A) glucose (SCD), (B) ethanol (SCE), (C) glycerol (SCG), and (D) lactate (SCL) under high aeration (6 mL of media in 50-mL centrifuge tubes with shaking at 225 rpm). Data points are the OD_{600} values of the cultures at the times indicated (n=3).

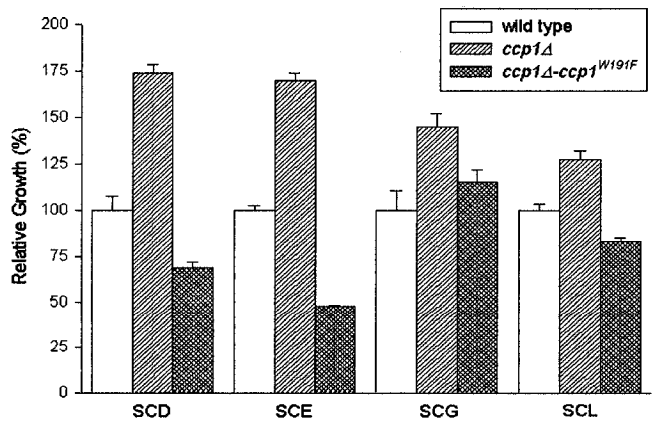

Figure 4.2. Percent growth relative to wild-type of *ccp1Δ* and *ccp1Δ-ccp1*^{W191F} *S. cerevisiae* cells. Cells were grown in SCD for 12 h and SCE, SCG and SCL for 24 h as described in the legend of Figure 4.1. The % Growth is the ratio of the OD_{600} of the mutant and wild-type strains ×100 (n=3).

4.4.2 Absence of CCP activity does not result in decreased viability or mitochondrial function in unstressed cells

Methylene blue was used to establish the number of viable cells in each culture. This vital stain is absorbed by the membranes of living cells but it penetrates into dead cells [199]. Following staining, examination under 400× magnification of 300 cells per culture revealed that 95% of cells grown under high aeration in liquid SCD, SCE or SCG and ~85% of the cells in SCL were viable after 3 days (data not shown). Thus, *CCP1* deletion and transformation with *CCP1*^{W191F} have no negative effects on the viability of unstressed cells grown on fermentable or non-fermentable carbon sources.

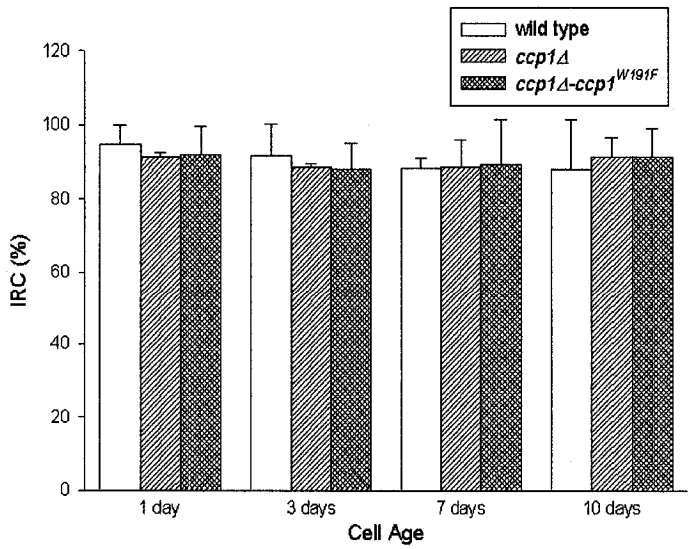

Figure 4.3. Index of respiratory competence (IRC) of wild-type, *ccp1Δ* and *ccp1Δ-ccp1*^{W191F} *S. cerevisiae* cells. Late-exponential-phase cells (16 h, OD_{600} ~2.0) were inoculated at an initial OD_{600} of 0.01 and grown in SCD at 30°C with high aeration (50 mL of media in 250-mL flasks with shaking at 225 rpm). After 3 days, the cells were washed twice and resuspended in 50 mL of 0.85% sterile saline. Incubation at 30°C under high aeration was continued until day 10, with a change of saline on day 7. Equal numbers of 1-, 3-, 7- and 10-day cells were plated onto solid SCD and SCEG and incubated at 30°C for 3 days. The % IRC of each strain is the ratio of the number of colony forming units (CFU) on solid SCEG and SCD ×100 (n=3).

IRC values of 90 ± 2% were found for 1–10-day unstressed cells from the three strains grown under high aeration (Figure 4.3). Thus, variation in mitochondrial function is unlikely the cause of the differential growth of the mutant strains seen in Figure 4.2.

4.4.3 *CCP1* does not protect cells against heat stress

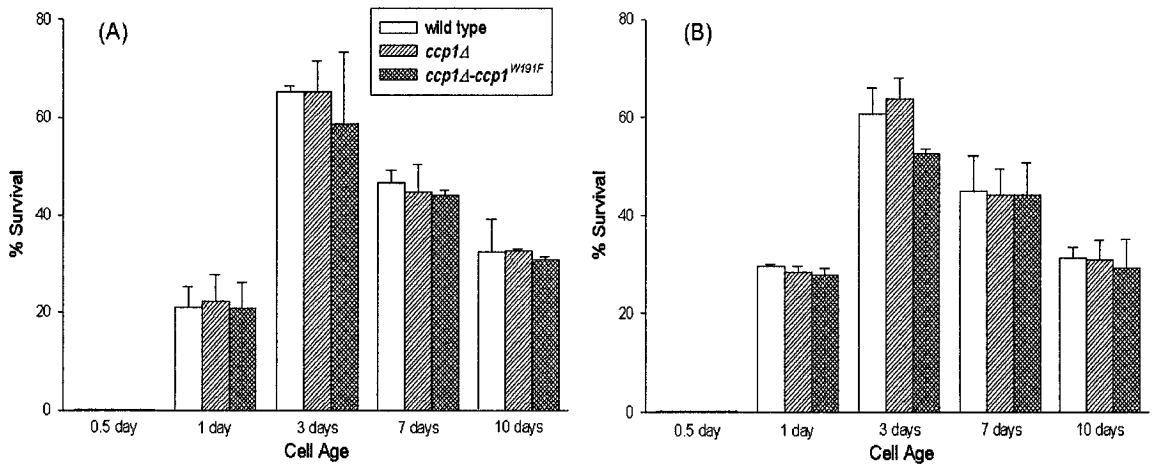

Figure 4.4. Percent survival *vs* age of wild-type, *ccp1Δ* and *ccp1Δ-ccp1*^{W191F} *S. cerevisiae* cells following incubation at 48°C for 60 min under anaerobic conditions. Cultures (grown as described in the legend of Figure 4.3) were diluted to 300 cells per 100 µL with sterile PBS (pH 7.4). The cells were incubated for 60 min at 48°C (or 30°C, control) under anaerobic conditions (full 0.45-mL tubes, no shaking) and plated (100 µL) onto solid (A) SCD and (B) SCEG. The % Survival is the ratio of the CFUs of the heat-stressed and control cells from the same culture ×100 (n=3).

Anaerobic heat stress (60 min at 48°C) is lethal to the 0.5-day cultures (Figure 4.4). Older (1–10-day) heat-stressed cells did not exhibit differential survival following plating on either SCD or SCEG (Figure 4.4). Being the most thermotolerant, the 3-day cells were additionally exposed to 48°C for 30 and 120 min. Survival rates dropped by half (~80–40%) over this 90-min period (Figure 4.5A and B), but remained the same within experimental error for the three strains. The IRCs (~80%) reveal little loss of mitochondrial function with the possible exception of *ccp1Δ-ccp1*^{W191F} heat stressed for

120 min (IRC = 55 ± 22%; Figure 4.5C). Any drop in IRC of this mutant strain cannot be attributed to the loss of CCP antioxidant activity since *ccp1Δ* and wild-type cells exhibited similar high IRC values (Figure 4.5C).

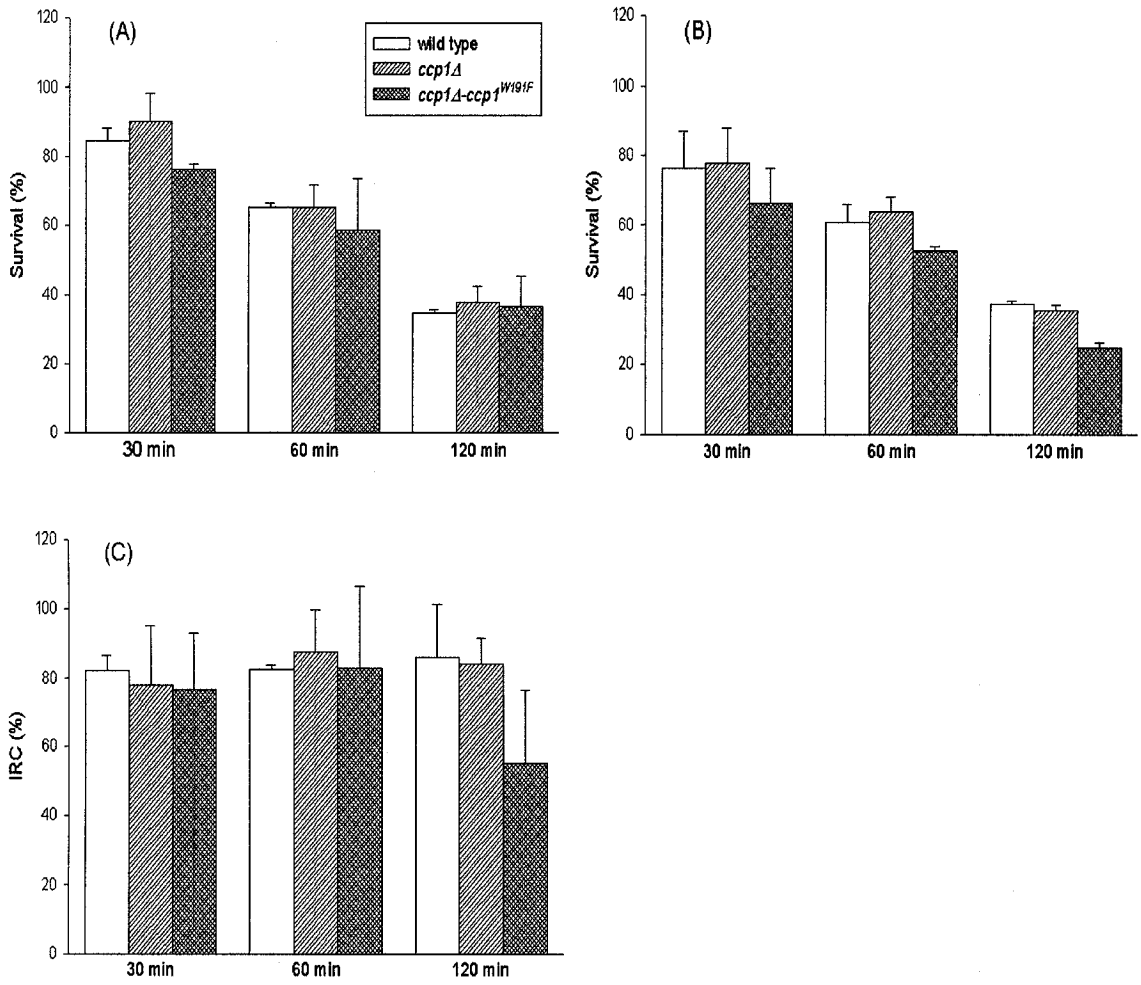

Figure 4.5. Percent survival and IRC of 3-day wild-type, *ccp1Δ* and *ccp1Δ-ccp1*^{W191F} *S. cerevisiae* cells *vs* exposure time to anaerobic heat stress at 48°C. The experimental conditions and definition of % Survival are given in the legend of Figure 4.4. Cells were plated on (A) SCD and (B) SCEG and values are the average of three independent experiments. The % IRC of each culture, which is the ratio of CFUs of the heat-stressed cells on SCEG and SCD ×100, is plotted in (C). The higher standard deviations in the IRC measurements in (C) may reflect minor variations in the media prepared on different days whereas the control and heat-stressed cells were grown on the same media in (A) and (B).

To probe for aerobic heat stress, late-exponential-phase (~16 h) cells were seeded on YPD and YPEG plates and incubated for 3 (YPD) or 5 (YPEG) days at 30, 37 and 41°C. The three strains exhibited 100% survival at 37°C (ratio of CFUs at 37°C and 30°C ×100%) and 0% survival at 41°C on both solid media (data not shown). Thus, *CCP1* offered no detectable protection to cells under the conditions of anaerobic or aerobic heat stress examined here.

4.4.4 *CCP1* protects respiring mitochondria from H_2O_2 challenge

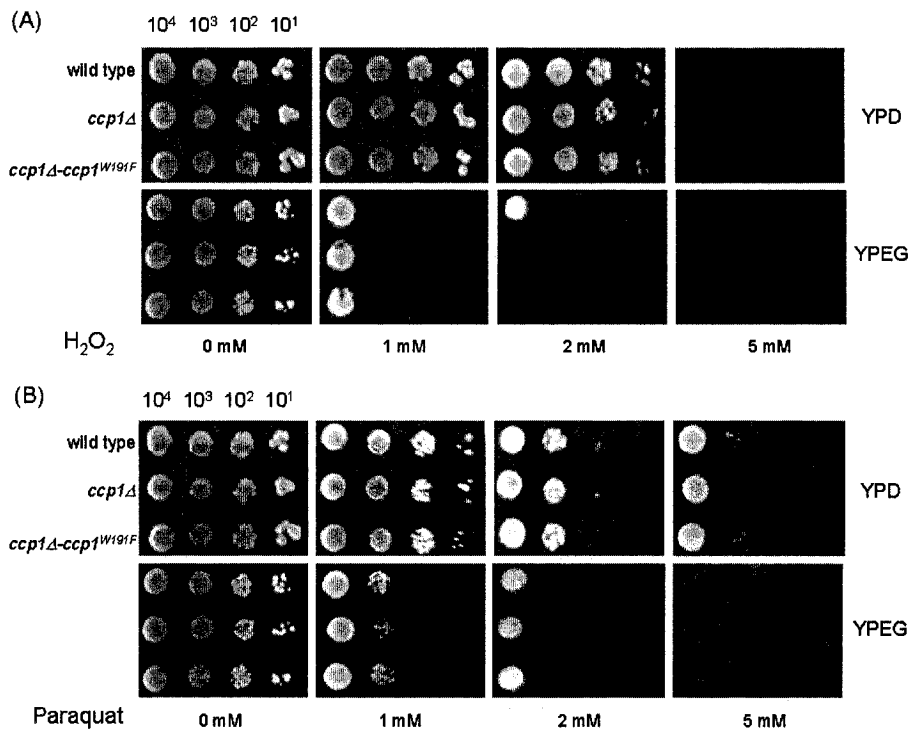

Figure 4.6. H_2O_2 and paraquat tolerance of late-exponential-phase wild-type, *ccp1Δ* and *ccp1Δ-ccp1^{W191F}* *S. cerevisiae* cells. To screen for oxidant tolerance, cells were grown at 30°C in SCD to late-exponential-phase (OD_{600} 2.0, ~16 h) under high aeration (50 mL of media in 250-mL flasks with shaking at 225 rpm), and serially diluted into sterile PBS (pH 7.4). Aliquots (2.5-μL) containing 10^4, 10^3, 10^2 or 10 cells were spotted on solid YPD and YPEG containing (A) H_2O_2 and (B) paraquat at the concentrations indicated. The photographs show cell growth following incubation for 3 (YPD plates) or 5 (YPEG plates) days at 30°C.

Figure 4.6 reveals that all three strains are sensitive to H_2O_2 or paraquat present in solid media. The absence of growth on YPEG plates containing 1–5 mM oxidant indicates that cells became RD. Only wild-type cells were RC on YPEG containing 2 mM H_2O_2 (Figure 4.6A) revealing that CCP is critical for mitochondrial function when cells are challenged with H_2O_2 above a threshold level. Since differential sensitivity to paraquat was not observed (Figure 4.6B), only the effects of H_2O_2-exposure were further probed.

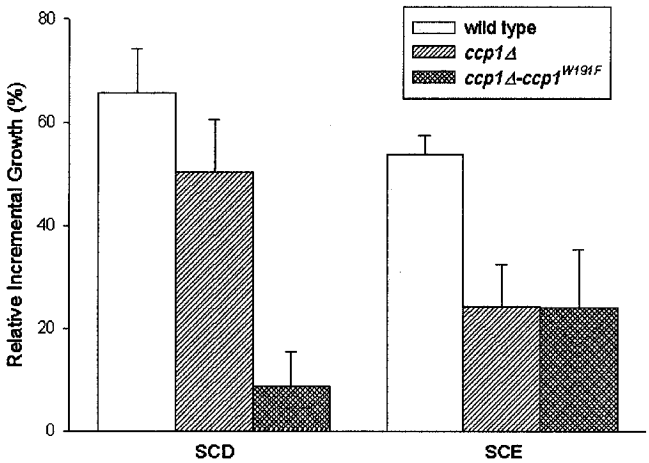

Figure 4.7. Effects of 0.4 mM H_2O_2 exposure on the incremental growth over 2 h of early-exponential-phase wild-type, *ccp1Δ* and *ccp1Δ-ccp1^{W191F}* *S. cerevisiae* cells in SCD and SCE. Cells were grown to early-exponential-phase at 30°C in SCD (OD_{600} 0.5, ~12 h) and SCE (OD_{600} 0.5, ~24 h) under high aeration (50 mL of media in 250-mL flasks with shaking at 225 rpm), and divided into two 25-mL portions. H_2O_2 (in 100 µL of 0.85% sterile saline) was added to one portion to a final concentration of 0.4 mM, and 100 µL of saline only was added to the control. Growth was continued under the same conditions, and the Relative Growth Rate is the ratio of the 2-h ΔOD_{600} values of the H_2O_2-exposed and control cultures ×100 (n=3).

The H_2O_2-sensitivity of exponentially growing (OD_{600} ~0.5) cells was examined in liquid SCD after 12 h when glucose is still present for glycolysis [204]. Surprisingly, the incremental growth over 2 h following 0.4 mM H_2O_2 addition to fermenting *ccp1Δ*-

ccp1^{W191F} (9 ± 7% *vs* the control without H_2O_2) was significantly lower than that of *ccp1Δ* (50 ± 10%) or wild-type cells (67 ± 9%) (Figure 4.7, SCD). This significant differential response to H_2O_2 challenge of the *ccp1Δ-ccp1*^{W191F} and *ccp1Δ* mutant strains devoid of CCP activity suggests a signaling as well as a detoxification function for the protein. H_2O_2-challenged *respiring ccp1Δ-ccp1*^{W191F} (24 ± 11%) and *ccp1Δ* (24 ± 8%) exhibited the same 2-h incremental growth that was around half that of respiring wild-type cells (54 ± 4%) (Figure 4.7, SCE).

Cells are more resistant to stress in the stationary phase [203], so higher levels of H_2O_2 are required to influence survival. As seen in Figure 4.8, significant differential tolerance to 60 mM H_2O_2 becomes apparent as cells age. Most notable is the low survival on SCEG after H_2O_2 challenge of 7-day *ccp1Δ* (10%) compared to *ccp1Δ-ccp1*^{W191F} (49%) (Figure 4.8B).

The IRC values (Figure 4.8C) indicate the fraction of RC cells remaining after H_2O_2 challenge. Compared to control cells (no H_2O_2 exposure; IRCs = 90 ± 2%, Figure 4.3), the mitochondria of the three strains are damaged on exposure to high H_2O_2 levels (Figure 4.8C). H_2O_2-stressed *ccp1Δ-ccp1*^{W191F} exhibit a constant IRC (54 ± 2%) over 1–7 days while the IRC of *ccp1Δ* drops 4-fold (82 to 19%) *vs* 1.4-fold (86 to 61%) for wild-type cells (Figure 4.8C) revealing that the development of the RD phenotype with age is strain dependent. It has been reported that H_2O_2-permeability determines the survival of yeast when challenged with this oxidant [56]. Thus, CCP signaling might regulate H_2O_2 diffusion in and out of the mitochondria.

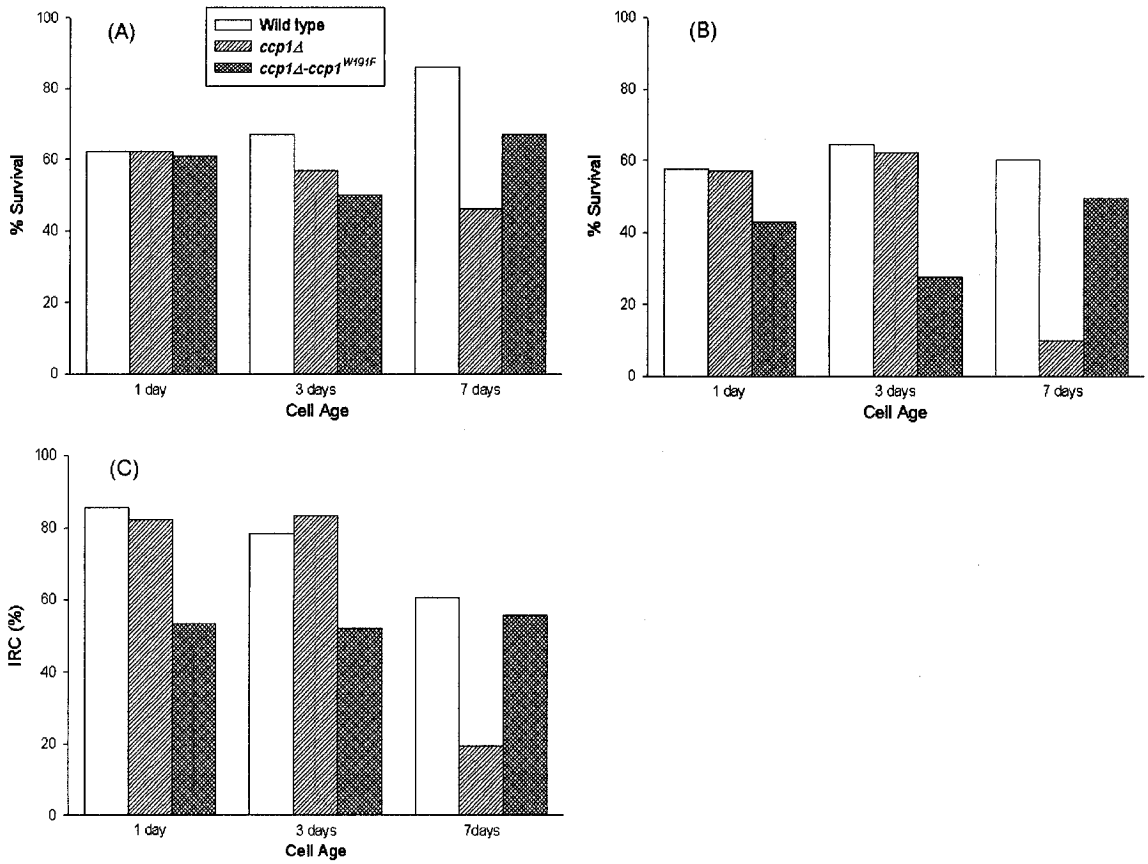

Figure 4.8. Percent survival and IRC of 1-, 3- and 7-day wild-type, *ccp1Δ* and *ccp1Δ-ccp1*^{W191F} *S. cerevisiae* cells after 1-h exposure to 60 mM H_2O_2. Cells grown as described in the legend of Figure 4.3 were diluted to 300 cells per 100 μL with sterile PBS (pH 7.4) with and without 60 mM H_2O_2 (control). The cells were incubated at 30°C under anaerobic conditions (45 mL of culture in 50-mL tubes, no shaking) for 60 min and plated onto solid (A) SCD or (B) SCEG. The % Survival is the ratio of the CFUs of the H_2O_2-exposed and control cells ×100. (C) The %IRC is the ratio of the CFUs of the H_2O_2-exposed cells on SCEG and SCD ×100. The experiment was repeated twice, and the results shown are representative.

4.4.5 YCplac33-*CCP1* complements the H_2O_2-sensitive phenotype of *ccp1Δ*

CCP was reintroduced into *ccp1Δ* cells to rescue the H_2O_2-sensitive phenotype. Aliquots (6 μL) of 30% H_2O_2 spotted onto the center of plates containing 15 mL of solid media effectively inhibited cell growth on both YPD and YPEG (Figure 4.9). All 5 strains grew more poorly on YPEG than YPD, and differential growth is observed in YPEG only (Figure 4.9B). As expected, the H_2O_2-sensitive phenotype of respiring *ccp1Δ*

was complemented by transformation with YCplac33-*CCP1* (Figure 4.9B) but not with YCplac33-*ccp1*^{W191F} or YCplac33-*E* encoding only residues 265–294 of CCP (Table 4.1).

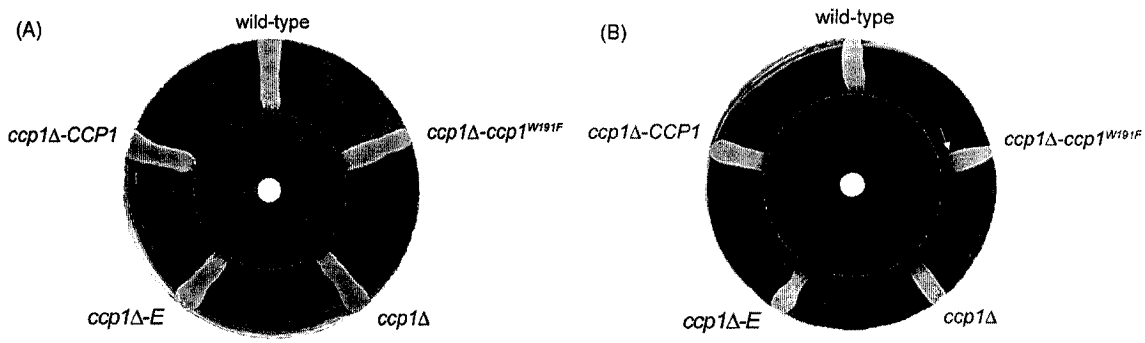

Figure 4.9. H_2O_2 agar diffusion assays. Wild-type and *ccp1Δ S. cerevisiae* cells (W303-1B) were grown at 30°C in SCD+uracil while *ccp1Δ-ccp1*^{W191F}, *ccp1Δ-E* and *ccp1Δ-CCP1* cells were grown in SCD–uracil to late-exponential-phase (OD_{600} 2.0, ~16 h) under high aeration (50 mL of media in 250-mL flasks with shaking at 225 rpm), and diluted into sterile PBS (pH 7.4). Aliquots (15 μL) containing 10^4 cells were streaked on solid (A) YPD and (B) YPEG plates following spotting of 6 μL of 30% H_2O_2 in the centre of the plates. The photographs show cell growth following incubation at 30°C for 3 days (YPD plates) or 5 days (YPEG plates). The arrow in (B) indicates the level of growth of the *ccp1Δ-ccp1*^{W191F} cells, which is obscured by the label in the Petri dish (Fisher).

4.4.6 Antioxidant enzyme activities are regulated differently in *ccp1Δ* and *ccp1Δ-ccp1*^{W191F}

Antioxidant enzyme activities in *S. cerevisiae* have been reported for YP [7, 24, 42, 203, 205] but not for SC cultures. As Table 4.2 reveals, only minor differences were observed for the activities measured here in YPD and SCD cultures. For example, the CCP activity of unstressed wild-type cells was lower and the SOD activity of the three strains was higher in the 3-day YPD *vs* SCD cultures (Table 4.2). The higher cell densities after 3 days in YPD ($OD_{600} > 11$; data not shown) compared to SCD ($OD_{600} < 4$; Figure 4.1A) may contribute to the observed activity differences.

Table 4.2. CCP, catalase, SOD and GLR activities at 25°C of wild-type, *ccp1Δ* and *ccp1Δ-ccp1*^{W191F} *S. cerevisiae* cells in the absence and presence of exogenous H_2O_2[a]

Cell age	OD_{600} 0.15	OD_{600} 0.5	1 day	3 days	7 days
Strain	CCP activity (m-units/mg of protein) [±10%][c,d,e]				
wild-type	2.4 (2.5)[b]	3.3	7.7	11 (5.9)[b]	8.3
+H_2O_2	4.7	6.3	3.8	5.6	2.7
	Catalase activity (units/mg of protein) [±8%][c,f]				
wild-type	1.6 (1.2)[b]	3.0	19	34 (34)[b]	33
+H_2O_2	3.5	5.5	14	25	29
ccp1Δ	2.3 (1.2)[b]	3.5	23	39 (39)[b]	45
+H_2O_2	8.1	10	9.4	17	21
ccp1Δ-ccp1^{W191F}	1.4 (1.4)[b]	2.7	25	34 (34)[b]	30
+H_2O_2	2.8	5.5	17	20	26
	SOD activity (units/mg of protein) [±19%][c,g]				
wild-type	16 (13)[b]	13	3.8	4.7 (6.5)[b]	9.6
+H_2O_2	20	17	ND	ND	ND
ccp1Δ	15 (14)[b]	14	4.0	2.6 (5.7)[b]	8.2
+H_2O_2	20	19	ND	ND	ND
ccp1Δ-ccp1^{W191F}	16 (13)[b]	14	5.1	2.5 (6.2)[b]	5.4
+H_2O_2	19	18	0.9	ND	ND
	GLR activity (units/mg of protein) [±8%][c,h]				
wild-type	19 (16)[b]	32	46	53 (47)[b]	70
+H_2O_2	26	46	32	42	53
ccp1Δ	20 (15)[b]	34	52	49 (50)[b]	90
+H_2O_2	20	32	22	32	53
ccp1Δ-ccp1^{W191F}	17 (15)[b]	30	49	51 (51)[b]	63
+H_2O_2	25	43	42	37	49

[a] SCD cultures were grown at 30°C under high aeration (50 mL of medium in 250-mL flasks with shaking at 225 rpm) in liquid SCD and harvested at OD_{600} values of 0.15 and 0.5 (exponential-phase), as well as at 1, 3 and 7 days as described in the legend of Figure 4.3. Where indicated (+H_2O_2), exponentially growing cells were exposed to 0.4 mM H_2O_2 and 1–7-day cells were exposed to 60 mM H_2O_2 for 1 h as described in the legends of Figures 4.7 and 4.8.

[b] Enzyme activities in YPD cultures are given in the parentheses. YPD cultures were grown in the same way as the SCD cultures and cells were harvested at OD_{600} 0.15 (exponential-phase, ~5 h) and 3 days (stationary-phase, OD_{600} ~11).

[c] The assay methods are described in the *Experimental section* and in Appendix 4.4. Unit (or m-unit) activities are reported per mg of total protein in the lysate supernatants at 25°C. Activities were measured in triplicate and the average errors are given in square parentheses. ND, not detected.

[d] One unit of CCP activity catalyzes the oxidation by H_2O_2 of 1 μmol of ferrocytochrome *c* per min [206].

[e] No CCP activity was detected in the *ccp1Δ* and *ccp1Δ-ccp1*^{W191F} cells.

[f] One unit of catalase activity catalyzes the degradation of 1 μmol of H_2O_2 per min [149].

[g] One unit of SOD activity inhibits by 50% the rate of ferricytochrome *c* reduction by superoxide [200].

[h] One unit of GLR activity catalyzes the oxidation of 1 nmol of NADPH per min by oxidized glutathione (GSSG) [201].

As expected, no CCP activity was detected in strains *ccp1Δ* and *ccp1Δ-ccp1*^{W191F} (data not shown). The CCP activity of wild-type cells in SCD increased 4.6-fold over 3 days and then decreased 1.3-fold between day 3 and day 7 (Table 4.2). After the H_2O_2 challenge, CCP activity essentially doubled in exponentially growing cells but decreased by ~50–70% in the 1–7-day cells (Table 4.2).

Catalase and GLR activities increased ~20-fold and ~3-fold in the three strains over 3 days (Table 4.2), consistent with the reported upregulation of antioxidant enzymes as cells progress through the diauxic shift [124] to stationary phase [24, 203]. After exposure to 0.4 mM H_2O_2 for 1 h, these activities increased ~1.5–2-fold in exponentially growing wild-type and *ccp1Δ-ccp1*^{W191F} cells (Table 4.2, OD_{600} 0.15 and 0.5) whereas catalase activity was induced ~3-fold but GLR activity was unchanged in the corresponding *ccp1Δ* cells. However, after 7 days the latter exhibited impaired stress adaptation on H_2O_2 challenge since their catalase and GLR activities were inhibited by ~50% compared to only 24% average inhibition in *ccp1Δ-ccp1*^{W191F} and wild-type cells. This is consistent with the low survival of 7-day stressed *ccp1Δ* (Figure 4.8) despite the fact that unstressed *ccp1Δ* exhibited 28–50% higher catalase and GLR activities compared to wild-type and *ccp1Δ-ccp1*^{W191F} cells after 7 days (Table 4.2).

Surprisingly, the SOD activity of all unstressed 1-day cells was 4-fold lower on average than the initial values (OD_{600} 0.15) although this was partially restored after 7 days (Table 4.2). Exposure to H_2O_2 resulted in a ~1.3-fold increased in SOD activity in exponentially growing cells but essentially no SOD activity was detected in the 1–7-day cells, which may be partially due to CuZnSOD inactivation by H_2O_2 [207].

4.5 Discussion

Despite the intense interest in CCP catalysis *in vitro* [98], the physiological role of the enzyme remains poorly characterized. *S. cerevisiae* deleted for *CCP1* has been investigated in W303-1A, CEN.PK2, S178-6B and JM749 genotypes [7, 70, 208, 209]. Consistent with the present results, *CCP1* was found not to affect the viability of unstressed [208, 209] or anaerobically heat-stressed cells [7], but did protect cells against H_2O_2-challenge [70, 208]. The oxidative-stress-sensitive phenotype of CEN.PK2-derived *ccp1Δ* was complemented by transformation with YCplac33-*CCP1* but not with YCplac33-*ccp1*^{W191F} or the empty YCplac33 vector [70]. Similarly, we found here that CCP expressed from YCplac33-*CCP1* complemented W303-1B-derived *ccp1Δ* whereas *ccp1Δ-E* exhibited the same H_2O_2-sensitivity as *ccp1Δ* cells (Figure 4.9B). However, the five W303-1B-derived strains in the present study exhibited similar growth in solid YPD containing oxidants (Figures 4.6 and 4.9A) whereas CEN.PK2-derived *ccp1Δ* exhibited lower H_2O_2 tolerance than wild-type in solid YPD [70]. This may reflect strain differences or some unidentified differences in growth conditions.

4.5.1 Control of initial doubling time

CCP1 was not among the hundreds of genes reportedly induced or repressed in genomic and proteomic investigations of the lag phase of *S. cerevisiae* [210, 211]. Nonetheless, during numerous cell-growth experiments, we consistently observed a shorter initial doubling time for *ccp1Δ* compared to *ccp1Δ-ccp1*^{W191F} or wild-type cells (Figure 4.2). Since the stress response pauses the cell cycle while cells repair any induced damage [1], the significantly lower growth of wild-type and *ccp1Δ-ccp1*^{W191F} after 12 h in liquid SCD (or 1 day in SCE) relative to *ccp1Δ* (Figure 4.2) suggests that CCP or

CCP^{W191F} is critical in the stress response that controls the transcription of genes required for proliferation. Delayed growth of *ccp1Δ-ccp1*^{W191F} was also observed on solid SCD and SCEG since this mutant strain formed smaller colonies than *ccp1Δ* and wild-type cells after incubation for 2 days at 30°C (data not shown).

Increased H_2O_2 stimulates Ca^{2+} release from mitochondria [59, 212] which shortens the lag phase of *S. cerevisiae* [213]. Thus, elevated mitochondrial H_2O_2 could shorten the initial doubling time of *ccp1Δ* compared to wild-type cells but not compared to *ccp1Δ-ccp1*^{W191F} since both lack CCP activity. However, an oxidative-stress signal from CCP^{W191F} could delay the cell cycle [1] of *ccp1Δ-ccp1*^{W191F} and account for the differential initial growth of the mutants. Since *ccp1Δ-ccp1*^{W191F} also exhibited delayed growth relative to wild-type cells (Figure 4.2, SCD and SCE), the CCP^{W191F} mutant protein may generate a more persistent stress signal than CCP under certain conditions. Consistent with this proposal, signal transduction *via* CCP^{W191F} led to a more persistent increase in *TPX1* (which encodes thioredoxin peroxidase and is induced by oxidative stress under Skn7/Pos9 control) than signal transduction *via* CCP [70].

CCP may convey an oxidative-stress signal to Skn7/Pos9 since H_2O_2 induced a Gal4-Skn7/Pos9 test system in wild-type and *ccp1Δ-ccp1*^{W191F} [70]. It is intriguing to consider possible molecular determinants of Skn7/Pos9 activation by CCP. Oxidation by H_2O_2 of CCP *in vitro* in the absence of its donor substrate, ferrocytochrome *c* (Eqs. 4.2 and 4.4), resulted in the formation of protein-based radicals and protein dimerization [111, 116, 117]. Surface residues, including Y39, Y153 and Y236, have been identified as sites of radical formation and CCP intermolecular crosslinking [115, 117]. Thus, it is possible that one or more of these surface radicals transduce an oxidative-stress response

in vivo [117, 144]. The heightened stress response of *ccp1Δ-ccp1*^{W191F} supports this hypothesis since H_2O_2-oxidized CCP^{W191F} is highly reactive towards dimerization [117, 140].

4.5.2 Index of respiratory competence

Respiring mitochondria are the primary source of intracellular ROS [52, 191, 214]. Recent studies suggest that both CuZnSOD [27] and catalase A [20] are present together with MnSOD (gene product of *SOD2*) and CCP in yeast mitochondria. Thus, yeast mitochondria may have a complete set of enzymes [CCP, catalase [24], GLR [37], SOD [87]] known to metabolize ROS. The high and constant IRC values of the three strains examined here (90 ± 2%, Figure 4.3) reveal that the mitochondria of unstressed cells lacking CCP activity are as healthy as those of wild-type cells after 10 days growth. In contrast, the IRC of an EG103 strain deleted for *SOD2* was only ~50% that of wild-type EG103 after 7 days under the same growth conditions [195]. Since MnSOD catalyzes the formation of H_2O_2 from superoxide, other antioxidant enzymes must compensate for the loss of *CCP1*.

We previously observed that 95% of both *ccp1Δ* and wild-type cells survived after 7 days in liquid YPD without washing and exhibited the same IRCs. However, the deletion mutant consumed 50% less oxygen than the wild-type cells [215], which is attributed to the fractional lost of respiratory capacity in each *ccp1Δ* cell rather than to a fraction of cells becoming RD. This same explanation was offered for the more rapid decrease in oxygen consumption *vs* viability as *sod2Δ* cells aged [195]. But unlike *sod2Δ* [195], the IRC of unstressed *ccp1Δ* remained constant over 10 days (Figure 4.3). Thus, only repairable mitochondrial damage must occur in *ccp1Δ*, while aconitase, succinate

dehydrogenase and NADH oxidase were inactivated by excess superoxide in *sod2Δ* mitochondria [195].

4.5.3 Sensitivity to H_2O_2 challenge

Stress-specific response mechanisms have been reported for *S. cerevisiae* [5, 6]. Our results show that the thermotolerance of the three strains are similar (Figures 4.4 and 4.5) but cells lacking CCP activity are more sensitive to H_2O_2 in solid YPEG (Figures 4.6 and 4.9) and liquid SCE (Figure 4.7). In addition, *ccp1Δ-ccp1*^{W191F} cells are particularly sensitive to H_2O_2 challenge after 12 h growth in liquid SCD (Figure 4.7). If, as suggested above, CCP^{W191F} is critical in the stress response that controls proliferation, challenging the cells with H_2O_2 should further delay proliferation. The apparent lower H_2O_2-sensitivity of *ccp1Δ-ccp1*^{W191F} in SCE (Figure 4.7) may be a reflection of the low growth after 1 day of unstressed cells in this medium (Figures 4.1 and 4.2).

When energy metabolism is shifted to respiration, the absence of both the detoxifying and signaling functions of CCP results in the decreased H_2O_2 tolerance with age of *ccp1Δ* (Figure 4.8B). In contrast, the constant IRC value (~55%) reveals that *ccp1Δ-ccp1*^{W191F} mitochondria function equally well on day 1 and 7, suggesting that the lack of CCP activity is offset by the enhanced oxidative-stress signaling of CCP^{W191F} in these cells. Hence, both the sensor and antioxidant activities of CCP provide protection against H_2O_2, particularly as cells age.

4.5.4 Antioxidant enzyme activities

Recently, using DNA microarrays *CCP1* expression in *S. cerevisiae* was found to increase ~2-fold over 12 h of exponential growth on YPD followed by a further ~3-fold increase over 3 days [22]. In contrast, proteomics analysis revealed that CCP protein

levels were similar in 16-h and 2-day YPD cultures [124], while we observed that the CCP activity of wild-type cells in SCD increased ~5-fold over 3 days followed by a 1.3-fold drop between days 3 and 7 (Table 4.2).

CCP1 expression was the same in cells grown on fermentable (glucose, galactose, fructose or sucrose) and non-fermentable carbon sources (raffinose or ethanol) [22]. It was also unaffected by mild heat stress (33°C for 30 min), hyperosmotic stress or amino acid starvation [22]. However, consistent with our observation that H_2O_2 challenge resulted in a doubling of CCP activity in exponential-phase cells (Table 4.2), *CCP1* was induced 11-fold [22] and the rate of CCP protein synthesis increased 6-fold [125] on exposure of liquid YPD cultures (OD_{600} 0.2–0.4) to 0.3–0.4 mM H_2O_2 for 20 min. These responses are indicative of a H_2O_2-detoxifying role for CCP.

It was previously found [24] that 3-day YPD cultures of a YPH250 strain deleted for *CTA1* and/or *CTT1* exhibited wild-type CCP activity. Table 4.2 reveals that unstressed exponentially growing cells all possessed similar catalase activity but H_2O_2-induced a 3-fold increase in this activity in *ccp1Δ* compared to a 2-fold increase in wild-type and *ccp1Δ-ccp1*^{W191F}. The drop in total SOD activity observed here between 12 h and 24 h (Table 4.2) is surprising but consistent with the report [22] that *SOD1* expression decreased in liquid YPD cultures over 5 days whereas *SOD2* expression increased [22]. Since CuZnSOD (gene product of *SOD1*) exhibits ~30-fold higher SOD activity than MnSOD (gene product of *SOD2*) in both exponential- and stationary-phase cells [216], a drop in total SOD activity is expected as cells age.

Unlike the CCP, catalase and SOD activities, a H_2O_2-induced increase in the GLR activity of exponentially growing cells was not observed (Table 4.2). Only a 2-fold

increase in the rate of GLR protein synthesis was reported on exposure of liquid YPD cultures (OD_{600} 0.3) to 0.2–0.8 mM H_2O_2 for 20 min compared to 15-, 6-, 6- and 4-fold increase in catalase T, MnSOD, CCP, CuZnSOD synthesis, respectively [125]. The latter antioxidant enzymes are under both Yap1 and Skn7/Pos9 control but GLR is controlled by Yap1 but not Skn7/Pos9 [63]. Although exponentially growing *ccp1Δ-ccp1*^{W191F} exhibited the same levels of induction of catalase, GLR and SOD activities as wild-type, the relative growth of these fermenting cells was low following H_2O_2 exposure (Figure 4.7, SCD). This may be due to persistent signaling from CCP^{W191F} which, as suggested above, may be critical in the stress response that controls the transcription of genes required for proliferation.

Seven-day unstressed *ccp1Δ* exhibited 28–50% higher catalase and GLR activities compared to wild-type and *ccp1Δ-ccp1*^{W191F} cells (Table 4.2), suggesting that signal transducion *via* CCP or CCP^{W191F} attenuates the induction of stress genes as cells age. However, the deletion mutant was less H_2O_2 resistant as reflected in its lower survival rates (Figure 4.8) and the ~50% inhibition (compared to ~25% in wild-type and *ccp1Δ-ccp1*^{W191F} cells) of its catalase and GLR activities (Table 4.2) following H_2O_2 exposure. It is noteworthy that antioxidant enzyme activities generally increased following H_2O_2 challenge of exponential-phase cells but decreased in the older cells (Table 4.2). Since older cells are more resistant to stress [203], high levels of H_2O_2 are required to influence their survival. Thus, the large decreases in antioxidant enzyme activities observed in the 1–7 day cells stressed with 60 mM H_2O_2 (Table 4.2) are likely oxidant-mediated rather than growth-phase-mediated. For instance, CuZnSOD inactivation by H_2O_2 *in vitro* has been reported [207], and since *SOD1* and *SOD2* are

crucial for stationary-phase survival [87, 195], the absence of SOD activity in the older cells following H_2O_2 exposure (Table 4.2) cannot be growth-phase mediated.

4.5.5 Strain-specific stress responses

The DNA sequence of yeast *CCP1* was first reported in 1982 in the D273-10B strain [90, 91], and a second *CCP1* allele was found in the FY1679 strain in 1994 [41, 92]. Ten and nine consecutive GCT codons (encoding for alanine) are present in alleles 1 and 2, respectively. These alanine residues are located in a ~23-residue apolar sequence that likely forms a transmembrane helix during CCP localization to the mitochondria [90]. Other DNA mismatches result in amino acid substitutions in the presequences (H *vs* Q and P *vs* A) and mature proteins (I53 *vs* T53 and G152 *vs* D152) of CCP isoforms 1 and 2, respectively. The G152 to D152 substitution in CCP isoforms 1 and 2 is of interest in the context of radical signaling (see above) given that surface residue Y153 has been identified as a radical-formation site [115]. The CCP^{W191F} sequence in YCplac33-$ccp1^{W191F}$ (data not shown) matches that of allele 1 except for A *vs* P in its presequence and a I53T substitution. Since a *Sma*I site (CCCGGG) is present in the presequence of allele 2 only, digestion of PCR-amplified *CCP1* and YCplac33-*CCP1* with *Sma*I (data not shown) revealed that W303-1B contains allele 1, which was confirmed by sequencing of *CCP1* in YCplac33-*CCP1* (data not shown).

Since two *CCP1* alleles have been identified [90, 92], phenotypic analyses of *CCP1* deletion and mutation strains in other genetic backgrounds are of interest. For example, W303 strains containing *CCP1* allele 1 were found to be more sensitive to the superoxide generator menadione than the FY1679 strains containing *CCP1* allele 2 used in deletion analysis by the European Functional Analysis Network (EUROFAN) [217].

W303, FY1679 and CEN.PK2 strains also exhibited 40–70 different protein spots on two-dimensional gels in a proteomics study [128].

4.6 Conclusions

The extensive phenotypic comparison presented here of two genotypes lacking CCP activity, *ccp1Δ* and *ccp1Δ-ccp1*^{W191F}, is the first systematic study to probe the separate antioxidant and signaling functions proposed for CCP in yeast [70]. Several lines of evidence support a dual role for CCP *in vivo:* (1) the considerably shorter initial doubling time of fermenting or respiring *ccp1Δ* compared to *ccp1Δ-ccp1*^{W191F} (Figure 4.2), (2) the dramatically increased H_2O_2-sensitivity of fermenting exponential-phase *ccp1Δ-ccp1*^{W191F} compared to *ccp1Δ* or wild-type cells (Figure 4.7), (3) the opposing trends in survival with age of H_2O_2-stressed respiring *ccp1Δ-ccp1*^{W191F} and *ccp1Δ* (Figure 4.8B), (4) the different IRC values of H_2O_2-stressed *ccp1Δ-ccp1*^{W191F} and *ccp1Δ* (Figure 4.8C), (5) the greater H_2O_2-induction of catalase activity in fermenting exponential-phase *ccp1Δ* compared to *ccp1Δ-ccp1*^{W191F} (Table 4.2), (6) the higher antioxidant enzyme activities and (7) the greater enzyme inactivation on H_2O_2 challenge in 7-day *ccp1Δ* compared to 7-day *ccp1Δ-ccp1*^{W191F} (Table 4.2); and (8) the higher H_2O_2-tolerance of respiring wild-type compared to *ccp1Δ* and *ccp1Δ-ccp1*^{W191F} (Figures 4.6 and 4.9). Although the phenotypic differences are subtle, in the aggregate they support a sensor function independent of antioxidant function for CCP and its CCP^{W191F} mutant lacking cytochrome *c* peroxidase activity in the redox-stress response of both exponential- and stationary-phase cells [70].

Seven-day yeast cells examined here in 0.85% saline can be considered a suitable model for higher eukaryotic cells since they generate energy *via* respiration, are not

undergoing cell division, and have survived for a prolonged period [218]. In addition to different H_2O_2-tolerance and antioxidant enzyme activity compared to 7-day wild-type cells, 7-day *ccp1Δ* exhibit the mitochondrial morphology of 1-day cells (L. Zhang, personal communication). Our particular interest is how signals generated in CCP are involved in the oxidative-stress response as well as cell aging. To shed light on this process, a quantitative comparison of the mitochondrial proteomes of 7-day old wild-type, *ccp1Δ* and *ccp1Δ-ccp1*^{W191F} *S. cerevisiae* will be performed using the stable-isotope labeling method developed in our laboratory [219]. Such studies should further clarify the physiological roles of CCP *in vivo* and provide insight into the aging process.

4.7 Acknowledgements

We thank Tyrone Shepard, Steeve Veronneau and Marcy Wright for preparing the *ccp1Δ* cells, and Drs P. J. Hannic-Joyce (Concordia University), H. Bussey (McGill University) and K. D. Entian (Johann Wolfgang Goethe-Universität Frankfurt) for kindly providing the W303-1B cells, pFA6-kanMX4 and pYCplac33-*ccp1*^{W191F}, respectively. This research was funded by a grant from the Natural Sciences and Engineering Research Council (NSERC) of Canada to A. M. E.

Appendix 4.1. DNA sequence of the YCplac33-*ccp1*^{W191F} insert and of *CCP1* alleles 1 and 2

E. coli DH5α strain transformed with pYCplac33-*ccp1*^{W191F} (from Dr. K. D. Entian, Johann Wolfgang Goethe-Universität Frankfurt) and the *S. cerevisiae* strain transformed with pYCplac33-*ccp1*^{W191F} in our lab (*ccp1Δ-ccp1*^{W191F} in the W303-1B genetic background, Table 4.1) were sent to Bio. S&T Inc., Montreal to confirm the sequence of the YCplac33-*ccp1*^{W191F} insert (Figure A4.10A). The sequencing results revealed that the inserts from both strains were identical. As expected, CCATGG of *CCP1* was substituted by CCCTTT in *ccp1*^{W191F} (bases 1470–1475, Table A4.3) to mutate $P^{190}W^{191}$ to $P^{190}F^{191}$ in the mutant protein (Table A4.4).

Restriction endonuclease (RE) analysis of the YCplac33-*ccp1*^{W191F} vector isolated from the DH5α cells was carried out prior to sequencing of its insert. Digestions were performed with *Bam*HI (in buffer *Bam*HI, Fermentas), *Fse* I (in buffer 4, New England), *Apa* I (in Buffer A, Promega) and *Hin*dIII (in buffer R, Fermentas) at 37°C for 1.5 h as well as with *Sma*I (in Buffer Tango™, Fermentas) at 30°C for 3 h. Figure A4.10B shows that the bands obtained from digestions of the vector are consistent with the plasmid map given in Figure A4.10A. For example, one *Bam*HI and one *Fse* I site together with three *Apa* I and three *Hin*dIII sites were found in the YCplac33-*ccp1*^{W191F} vector as expected.

The DNA sequence of the insert is compared with those of the two yeast *CCP1* alleles in Table A4.3. Sequence (1) is that of the YCplac33-*ccp1*^{W191F} insert; Sequence (2) is that of *CCP1* allele 1 found in yeast strain D273-10B [90, 91], and sequence (3) is that of *CCP1* allele 2 found in yeast strain FY1679 [92, 93]. The reported sequence of *CCP1* allele 1 did not include bases 1–396 of the *CCP1* promoter region [90].

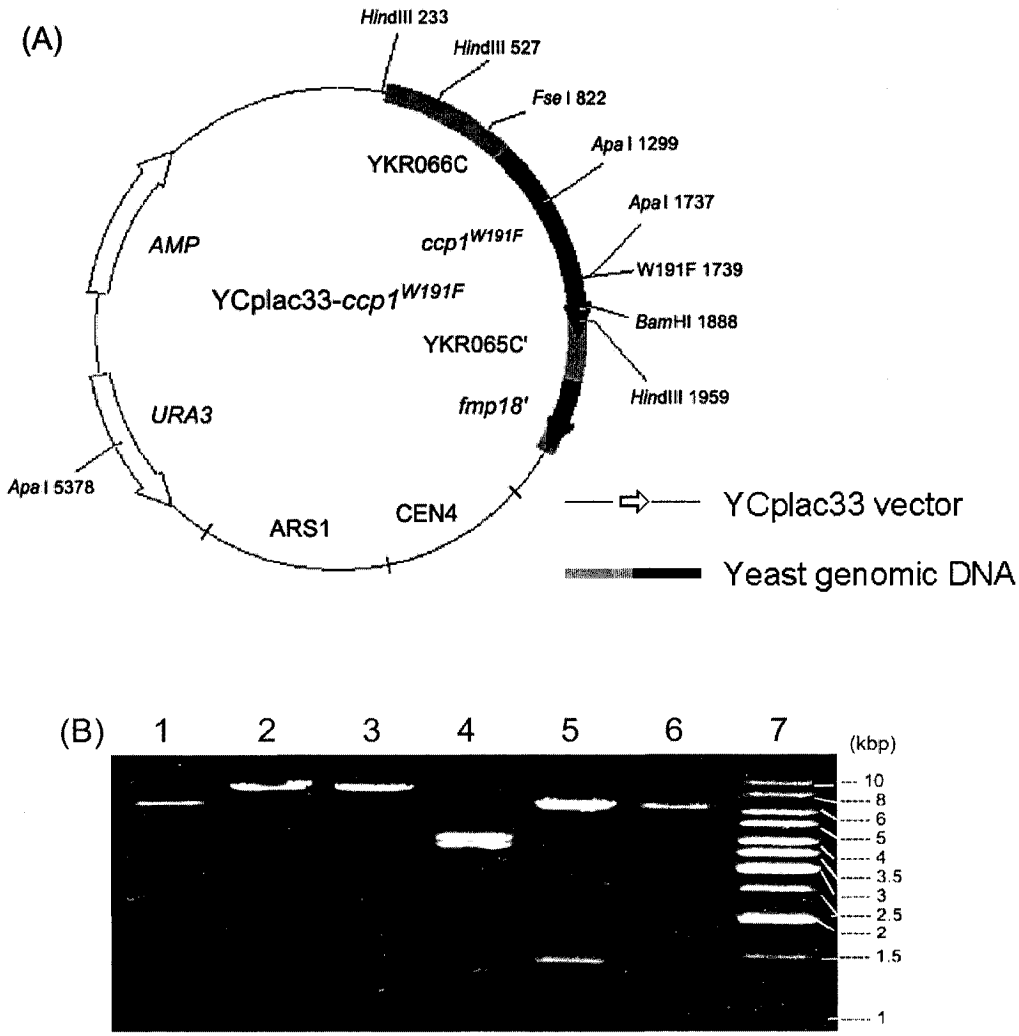

Figure A4.10. Restriction endonuclease analysis of the YCplac33-*ccp1*^{W191F} vector. (A) Plasmid map of pYCplac33-*ccp1*^{W191F}. (B) Restriction endonuclease analysis: Lane 1, undigested plasmid (7992 bp); Lane 2, *Bam*HI digest (7992 bp); Lane 3, *Fse* I digest (7992 bp); Lane 4, *Apa* I digest (3913, 3641 and 438 bp; the 438-bp band is not visible in the photo); lane 5, *Hin*dIII digest (6266, 1432 and 294 bp; the 294-bp band is not visible in the photo); Lane 6, *Sma*I digest (7992 bp); Lane 7, Fermentas GeneRuler^{TM} 1 kb DNA Ladder. The fragments were separated on a 0.7% agarose gel.

Table A4.3. DNA sequence of the YCplac33-*ccp1*^{W191F} insert and *CCP1* alleles 1 and 2[a,b]

MCS of YCplac33 vector

	*Hin*dIII	1	CACACAGGAA	ACAGCTATGA	CCATGATTAC	GCCAAGCTTG	CATGCCTGCA
		51	GGTCGACTCT	AGAG			

***CCP1* promoter region**[c]

(1) (3)		1	GATCGATTAA	TCGGCTTTAT	TAGATGTGAA	AGTAGAATTT	TGCTCTAGCG
(1) (3)		51	ACGAAGCACG	AAAAGACACT	ATCTTATACT	CAAGCTGCCA	CTTCTTCAGG
(1) (3)		101	GTCTCTCCTC	TTTTCTCTCC	CCTCTTTATT	ACTCCTCTCA	ACCTTACAAT
(1) (3)		151	CAAAGTGAGC	CATTTACTTC	GAAAATGCGG	AGCAACGGCG	GGTTACTGGT
(1) (3)		201	GTTCCAGCAA	GAGCTGTAAT	AATTCAATAT	AACTAGTAAG	AATAGCCAAG
(1)	*Hin*dIII	251	AAAGCCAAAA	GACAAGCTTG	GATCGATGCG	AAAATGTGGT	CGCTCCACCC
(3)				G			A
(1)		301	CAATTACTTG	TTATCATTTA	GCGCTGCCGT	GTGGCGACTA	CACTTCAGCG
(3)			A				
(1)		351	ACCTATGTAG	CTTACATAAT	ATCGGGATGA	TTTCTCCCGC	AGCTAGATCT
(3)					G		
(1) (2) (3)		401	CGCCAATGGA	AATTCCAAAG	CCAAAGAATA	TCCTGCTTTG	TCAGGAATTT
(1) (2) (3)		451	CGTAAACCAT	GGTCAGGCCC	AGATTTGTAG	TTTTCTTTAC	CAACGACAGC
(1) (2) (3)		501	GATGAGTTAT	TTGGTCCTGA	GTACTGAGTA	ATATGACTCT	CTTGGCATCC
(1) (2) (3)	*Fse* I	551	AGGGGCCGGC	CCAAGCCGGC	TGTTACCAAT	TTAGGAAAGG	ACCCTGGAGC
(1) (2)		601	GAAAAGTACT	TAAGCAGAGG	CTATTGTACA	CGCTCGCTAA	CTCAAGAACA
(3)				A			
(1) (2) (3)		651	TGAATTTCGC	ATTCATGCAG	ACGCAAACAC	ACACGTATAT	CTACAATT

Mitochondrial targeting presequence

(1)		699	ATGACTACTG	CTGTTAGGTT	TTTACCTTCA	CTGGGCAGAA	CCGCCCATAA
(2) (3)				C			
(1) (2)		749	GAGGTCTCTC	TACCTGTTCT	CCGCTGCTGC	TGCTGCTGCT	GCTGCTGCTG
(3)						Missing one GCT	
(1) (2)		799	CAACTTTTGC	TTACTCGCAA	TCCCACAAGA	GATCATCGTC	TTCTCCTGGG
(3)	*Sma*I				A		CCCGGG
(1) (3)		849	GGTGGTAGTA	ACCACGGATG	GAACAACTGG	GGGAAGGCAG	CTGCTTTGGC
(2)						C	
(1) (2) (3)		899	TTCC				

Mature CCP

(1) (2) (3)		903	ACTACACCGC	TCGTTCATGT	CGCCTCTGTC	GAAAAAGGGA	GGTCATACGA
(1) (2) (3)		953	GGACTTCCAA	AAGGTGTACA	ATGCGATTGC	ACTCAAGCTG	AGGGAAGATG
(1) (2) (3)		1003	ACGAATATGA	CAACTATATA	GGCTATGGGC	CCGTATTAGT	CCGTCTTGCT
(1) (3)		1053	TGGCACACTT	CAGGGACCTG	GGACAAGCAC	GACAATACAG	GCGGGTCATA
(2)			T				
(1) (2) (3)		1103	CGGTGGTACA	TACAGATTCA	AAAAGGAGTT	TAACGATCCA	TCCAATGCGG
(1) (2)		1153	GCTTGCAGAA	TGGCTTTAAG	TTCCTGGAGC	CCATTCACAA	AGAGTTTCCC
(3)				C			
(1) (2)		1203	TGGATCTCCT	CGGGTGATCT	GTTCAGTCTA	GGGGGTGTCA	CTGCTGTGCA
(3)							C

(1) (2) (3)		1253	GGAAATGCAG	GGTCCCAAGA	TTCCATGGAG	ATGTGGTAGA	GTCGACACGC
(1) (2)		1303	CAGAGGATAC	TACCCCTGAC	AACGGGAGAC	TGCCTGACGC	TGATAAGGAC
(3)							A
(1) (2)		1353	GCTGGCTATG	TCAGAACGTT	TTTTCAAAGA	CTTAATATGA	ATGACAGAGA
(3)			A	A			
(1) (2) (3)		1403	AGTAGTTGCT	CTTATGGGGG	CTCACGCTCT	GGGCAAGACC	CACTTGAAGA
(1)	W191F	1453	ACTCTGGATA	CGAAGGGCCC	TTTGGAGCCG	CTAACAACGT	CTTTACCAAT
(2) (3)				CCA	TGG		
(1) (2)		1503	GAGTTTTACT	TGAACTTGTT	GAATGAAGAC	TGGAAATTGG	AAAAGAACGA
(3)				C			
(1) (2) (3)		1553	CGCGAACAAC	GAACAGTGGG	ACTCTAAGAG	CGGCTACATG	ATGCTGCCCA
(1) (2) (3)	*Bam*HI	1603	CTGATTATTC	TTTGATTCAG	GATCCCAAGT	ACTTAAGCAT	TGTGAAAGAA
(1) (2) (3)	*Hin*dIII	1653	TACGCTAATG	ACCAGGACAA	GTTCTTCAAG	GATTTTTCCA	AAGCTTTTGA
(1) (2)		1703	AAAACTGTTG	GAAAACGGTA	TCACTTTCCC	TAAAGACGCG	CCCAGTCCAT
(3)				G			
(1) (2) (3)		1753	TTATTTTCAA	GACTTTAGAG	GAACAAGGTT	TATAG	

DNA after the *CCP1* stop-codon in YCplac33-*ccp1*^{W191F} [d]

(1) (2)		1803	GTCACTGAGG	AAGATAGTAT	TTATTGATTA	TATTTCGTAT	TATTTATCTA
(3)					G		
(1) (2)		1853	TTTATTATAT	TTATTATCAT	TTAGGCTTAT	GCTTTTTTCT	GAATATCATC
(3)				T			
(1) (2) (3)		1903	TAATACGTTT	GTACGGTACG	TCTATGAAAA	ATGGAAAGCC	ATACAATGGT
(1) (3)		1953	ATATCATAAG	GGAAACTATG	TTCAAAGAAG	TGTTAAAAAC	ATTCAGAAAA
(2)					G		
(1) (3)		2003	CATTGTCCGC	CTCTTCCAA			
(2)				G			

Bases 221–619 of *FMP18*[d]

(1)	1	ATGTTTACCA	GTGCCATTAG	ATTGTCATCG	CAAAGACTGT	TCGCTAGTCA
(1)	51	ACCTTCTGTC	ACCGCTGCGG	CATTGCGCTC	GACTGCTACA	ACCTTACCCT
(1)	101	TAAGATCATA	TTCTCAGCCC	GCATCCCTTC	AAGACTCCAG	TATCTTGACA
(1)	151	TGGTCTGATT	TTTTCAAATT	GAGGAAACAG	CAGCGTAGAA	TCAATGTTGG
(1)	201	T TCTTCGCTG	TTTACTGCTC	TTTTGGGCTG	TAACGTTTCA	TGGGCTTACC
(1)	251	TTTCCACAAT	GGAAATAGAC	CCGACTCAAA	TGCTATTCGG	ATTCGACCCA
(1)	301	T TAACTGTAA	TTTCAGCTGG	GATAATAGCC	TCTGGTGCAC	TAGGCTACTT
(1)	351	GTTGGGTCCG	ATAGTTGGTT	CGCAAGTTTT	CAAACTTTCC	CATAACCAAC

MCS of YCplac33 vector

1	AATTCACTGG	CCGTCGTTTT	ACAACGTCGT	GACTGGGAAA	ACCC

---

[a] (1) DNA sequencing results for the insert in YCplac33-*ccp1*^{W191F}; (2) yeast *CCP1* allele 1 (bases 397–2022) from Ref. [90, 91]; (3) yeast *CCP1* allele 2 from Ref. [92, 93]. Only variations in the two alleles are indicated.

[b] Restriction endonuclease sites are doubly underlined. Codon of F191 is bordered.

[c] The reported DNA sequence of *CCP1* allele 1 did not include bases 1–396 of the *CCP1* promoter region.

[d] Extra bases in YCplac33-*ccp1*^{W191F} after the *CCP1* stop codon including the promoter region of *FMP18* (ORF YKR065C) and bases 1-399 of its coding region.

Table A4.4. Amino acid sequence encoded by the pYCplac33-*ccp1*^{W191F} insert and those of *CCP1* alleles 1 and 2[a]

		Mitochondrial targeting presequence				
(1) (2)	1	MTTAVRLLPS	LGRTAHKRSL	YLFSAAAAAA	AAAATFAYSQ	SHKRSSSSPG
(3)				Missing one A		Q
(1) (3)	51	GGSNHGWNNW	GKAAALAS			
(2)			P			
		Mature CCP				
(1) (2) (3)	1	TTPLVHVASV	EKGRSYEDFQ	KVYNAIALKL	REDDEYDNYI	GYGPVLVRLA
(1) (3)	51	WHTSGTWDKH	DNTGGSYGGT	YRFKKEFNDP	SNAGLQNGFK	FLEPIHKEFP
(2)		I				
(1) (2) (3)	101	WISSGDLFSL	GGVTAVQEMQ	GPKIPWRCGR	VDTPEDTTPD	NGRLPDADKD
(1)	151	AGYVRTFFQR	LNMNDREVVA	LMGAHALGKT	HLKNSGYEGP	FGAANNVFT
(2)		G				W
(3)		D				W
(1) (2) (3)	201	NEFYLNLLNED	WKLEKNDANN	EQWDSKSGYM	MLPTDYSLIQ	DPKYLSIVKE
(1) (2) (3)	251	YANDQDKFFK	DFSKAFEKLL	ENGITFPKDA	PSPFIFKTLE	EQGL

[a] Based on the DNA sequences of the mitochondrial targeting presequence and mature CCP given in Table 4.3. (1) The YCplac33-*ccp1*^{W191F} insert, (2) allele 1 and (3) allele 2. Only variations in the alleles are indicated and F191 is underlined.

A *Sma*I site (CCCGGG) is located in the mitochondrial targeting presequence at bases 843–848 (between *Fse* I and *Bam*HI sites, Table A4.3) of *CCP1* allele 2 but not of allele 1. Thus, *Sma*I was used here to determine the *CCP1* allele in the W303-1B strain. The GEX-2T vector (Amersham Pharmacia Biotech) was used as a positive control for *Sma*I digestion because there is a *Sma*I as well as a *Bam*HI site in its multiple cloning site (MCS). The GEX-2T, YCplac33-*ccp1*^{W191F}, YCplac33-*CCP1* vectors and the PCR-amplified *CCP1* gene from W303-1B were digested with *Sma*I at 30°C for 3 h. Figure A4.11 shows that *Sma*I cuts pGEX-2T but not pYCplac33-*CCP1*, pYCplac33-*ccp1*^{W191F} or the PCR-amplified *CCP1* gene, suggesting that *CCP1* in W303-1B strain is allele 1. This was confirmed by sequencing bases 560–1621 (between *Fse* I and *Bam*HI sites) of the *CCP1* gene from W303-1B (sequence 2, Table A4.3) that was cloned into

pYCplac33-*CCP1* (Table 4.1). Sequencing (Bio. S&T) also revealed that *CCP1* allele 2 (sequence 3, Table A4.3) is present in strain BY4742.

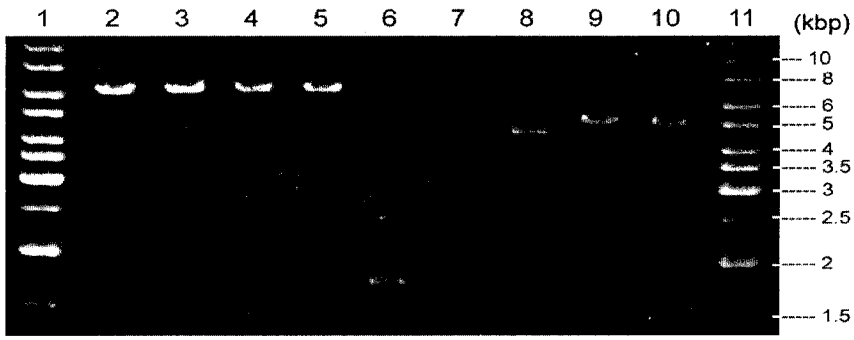

Figure A4.11. *Sma*I analysis of *CCP1* from wild-type W303-1B yeast. Lanes 1 and 11, Fermentas GeneRuler™ 1 kb DNA Ladder; Lane 2, undigested pYCplac33-*ccp1*^{W191F} (7992 bp); Lane 3, *Sma*I digest of pYCplac33-*ccp1*^{W191F} (7992 bp); Lane 4, undigested pYCplac33-*CCP1* (7992 bp); Lane 5, *Sma*I digest of pYCplac33-*CCP1* (7992 bp); Lane 6, undigested PCR-amplified *CCP1* from wild-type W303-1B yeast (1719 bp); Lane 7, *Sma*I digest of PCR product (1719 bp); Lane 8, undigested pGEX-2T (4948 bp); Lane 9, *Sma*I digest of pGEX-2T (4948 bp), Lane 10, *Bam*HI digest of pGEX-2T (4948 bp). The fragments were separated on a 0.7% agarose gel.

Appendix 4.2. Construction of the YCplac33-E and YCplac33-*CCP1* vectors

The YCplac33-*ccp1*^{W191F} plasmid extracted from DH5α cells (from Dr. K. D. Entian, Johann Wolfgang Goethe-Universität Frankfurt) was transformed using standard methods [220] into *E. coli* strain XL1-Blue (Novagen), which is a better host strain for cloning experiments because it is a *lac*Iq strain [221]. The XL1-blue cells in LB medium (1% Bacto-tryptone, 0.5% yeast extract and 1% NaCl, pH 7.5) with 100 mg/L ampicillin (AMP, Bioshop) were grown overnight at 37°C to OD_{600} ~3. The YCplac33-*ccp1*^{W191F} vector was isolated from the XL1-Blue cells using the QIAprep Spin Miniprep Kit (QIAGEN) as per the manufacturer's instructions.

Transformation of the XL1-Blue cells was carried out using standard procedures [220]. To prepare competent cells, a single colony selected from a LB plate incubated at 37°C overnight was used to inoculate 3 mL of LB medium in a 50-mL centrifugation tube. After overnight growth at 37°C with shaking at 250 rpm, 100 μL of culture was transferred to 50 mL of LB medium in a 250-mL flask and incubated at 37°C, 250 rpm until the OD_{600} reached 0.5. The cells were harvested by centrifugation at 7000×g for 10 min at 4°C, resuspended with gentle tapping in 50 mL of ice-cold 0.1 M $CaCl_2$ (ACP, Montreal) and incubated on ice for 30 min. The cells were pelleted, again resuspended in 20 mL of ice-cold 0.1 M $CaCl_2$, mixed with an equal volume of 30% glycerol and stored at −80°C until use.

The competent XL1-Blue cells (100 μL) were transformed with ~50 ng of pYCplac33-*ccp1*^{W191F} dissolved in 10 μL of water. After addition of the foreign DNA, the cells were incubated on ice for 2 min, heat-shocked at 42°C for 90 s, incubated on ice for 2 min and directly plated on a LB-AMP plate pre-heated to 37°C. AMP-resistant colonies were selected after overnight incubation at 37°C.

To construct the YCplac33-E vector, 100 ng of purified YCplac33-*ccp1*^{W191F} was digested with *Hin*dIII at 37°C for 1 h to remove bases 1–1697 (Table A4.3) of *CCP1* (ORF YKR066C) as well as 29 bases of MCS in pYCplac33 (Figures A4.10A and A4.12). The DNA fragments were separated on a 0.7% agarose gel (Figure A4.13) and the 6266-bp plasmid band was purified using the QIAquick Gel Extraction Kit (QIAGEN) as per the manufacturer's instructions. To construct the YCplac33-E vector, ~50 ng of the purified 6266-bp band was ligated with 0.5 μL of T4 ligase in the ligase buffer (Fermentas) at 22°C for 2 h. Competent XL1-Blue cells were transformed with the

ligation mixture and formation of YCplac33-E vector was verified by digestion with *Hin*dIII and *Apa* I at 37°C for 1 h (Figure A4.13). As expected, only one band at 6266 bp was observed for both digestions.

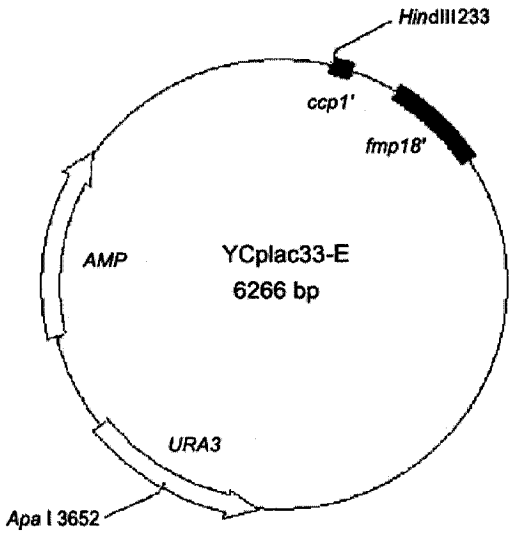

Figure A4.12. Plasmid map of the YCplac33-E vector.

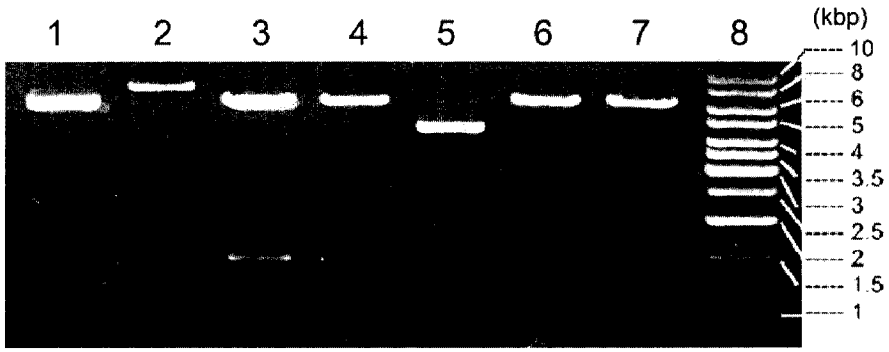

Figure A4.13. Construction and restriction endonuclease analysis of the YCplac33-E vector. Lane 1, undigested pYCplac33-*ccp1*^{W191F} (7992 bp); Lane 2, *Bam*HI digest of pYCplac33-*ccp1*^{W191F} (7992 bp); lane 3, *Hin*dIII digest of pYCplac33-*ccp1*^{W191F} (6266, 1432 and 294 bp; the 294-bp band is not visible in the photo); Lane 4, purified 6266-bp *Hin*dIII fragment; Lane 5, undigested pYCplac33-E (6266 bp); Lane 6, *Hin*dIII digest of pYCplac33-E (6266 bp); Lane 7, *Apa* I digest of pYCplac33-E (6266 bp); Lane 8, Fermentas GeneRuler^{TM} 1 kb DNA Ladder. The fragments were separated on a 0.7% agarose gel.

To construct YCplac33-*CCP1*, the *CCP1* gene from the genome of wild-type W303-1B yeast was used to replace *ccp1*^{W191F} in YCplac33-*ccp1*^{W191F} (Figure A4.14). Extraction of genomic DNA from wild-type cells and the PCR procedure using primers 3*f* and 5*r* (Table 4.1) were described in Section 4.3. *Fse* I and *Bam*HI cut sites are located up- and down-stream, respectively, of the W191F codon in *CCP*1 (bases 1473–1475, Table A4.3). The YCplac33-*ccp1*^{W191F} vector (7992 bp) and PCR-amplified *CCP1* (1719 bp) were first digested with *Fse* I at 37°C for 3 h, the DNA was cleaned using the QIAquick PCR Purification Kit (QIAGEN) as per the manufacturer's instructions, and digested with *Bam*HI at 37°C for 1 h. The DNA fragments were separated on a 0.7% agarose gel and the digested PCR product (1061 bp) and vector (6931 bp) were purified using the QIAquick Gel Extraction Kit (Figure A4.15A). A 1:3 molar ratio of vector (~50 ng) and insert (~20 ng) were ligated using T4 ligase at 22°C for 2 h and immediately used to transform competent XL1-Blue cells. The YCplac33-*CCP1* vector was isolated and its identity verified by digestion with *Bam*HI, *Fse* I, *Apa* I, *Hin*dIII and *Sma*I (Figure A4.15B). Sequencing (Bio. S&T) confirmed that the insert was *CCP1* allele 1 (sequence 2, Table A4.3).

ccp1Δ cells in the W303-1B genetic background (Table 4.1) were transformed with the YCplac33-E and YCplac33-*CCP1* vectors [222]. To prepare competent cells, a single *ccp1Δ* colony selected from a YPD plate incubated at 30°C for 2 d was used to inoculate 50 mL of YPD medium containing 0.03% geneticin G418 (Gibco BRL) in a 250-mL flask. The culture was incubated at 30°C and 225 rpm for 20 h and was used to inoculate 50 mL of YPD medium in a 250-mL flask to give an initial OD_{600} of 0.5. Incubation at 30°C, 225 rpm was continued for ~4 h until the OD_{600} reached 2.0. Cells

were collected by centrifugation at 3000×g for 5 min, washed once with sterile ultrapure H_2O, resuspended in 1 M LiAC (Sigma) and incubated at room temperature for 15 min. After centrifugation, sterile ultrapure H_2O was added to the cell pellet to a final volume of 1 mL, and 100 µL of cells were thoroughly mixed with 360 µL of transformation solution [240 µL of 50% PEG3500 (Sigma), 50 µL 1 M LiAC, 36 µL of 2 µg/µL carrier DNA (DNA sodium salt Type III from salmon testes, Sigma)] and 34 µL of purified YCplac33-E or YCplac33-*CCP1* plasmid (containing ~10 µg DNA). The mixture was incubated at 42°C for 40 min, diluted 100× with sterile H_2O, and 100 µL was plated onto SCD plates without uracil. The plates were incubated at 30°C for 3 days and transformants were selected.

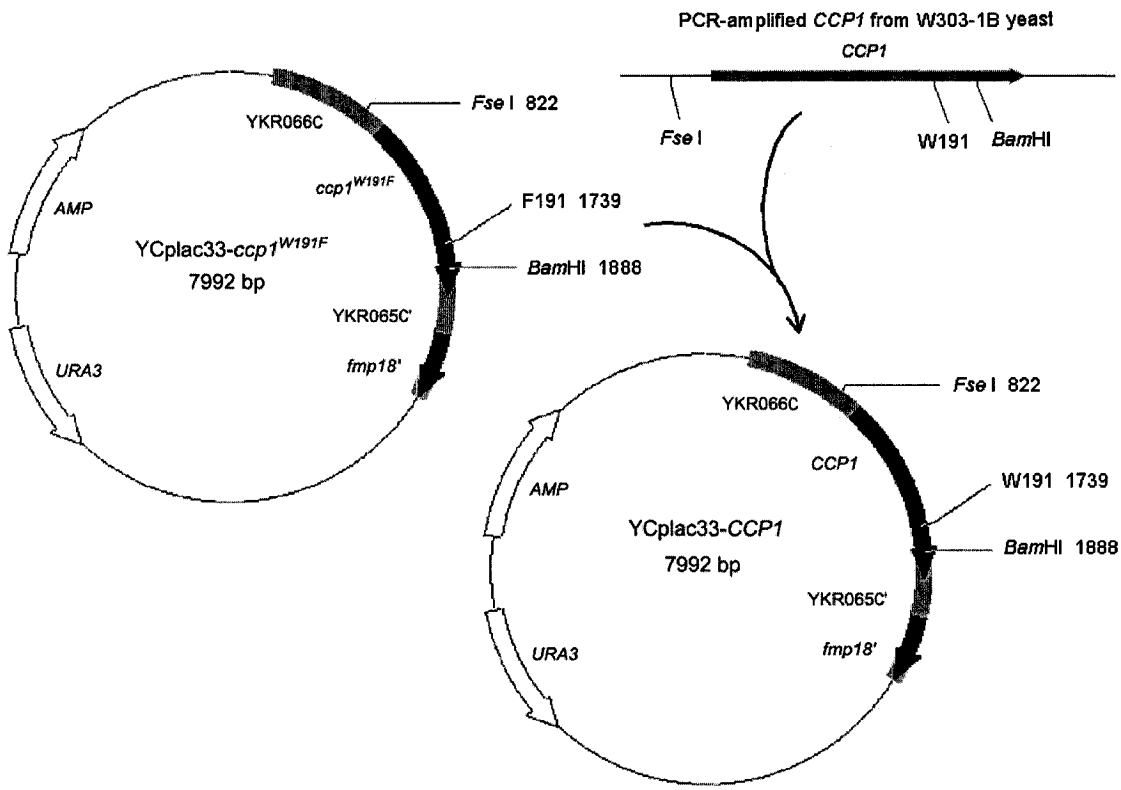

Figure A4.14. Construction of the YCplac33-*CCP1* vector.

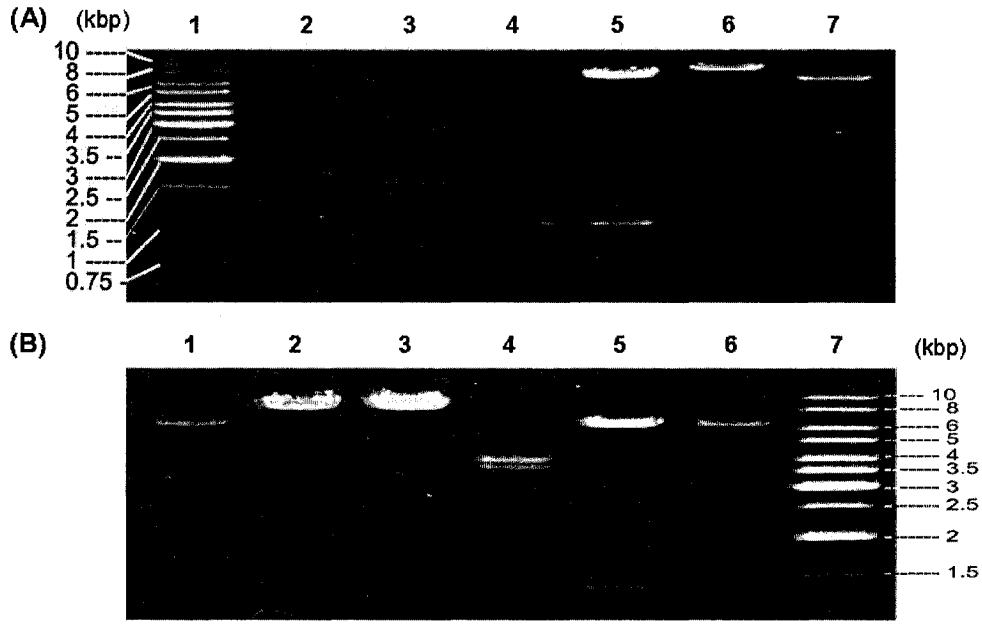

Figure A4.15. Construction and restriction endonuclease analysis of the YCplac33-*CCP1* vector. (A) Plasmid construction: Lane 1, Fermentas GeneRuler™ 1 kb DNA Ladder; Lane 2, PCR-amplified *CCP1* from W303-1B yeast (1719 bp); Lane 3, *Fse* I digest of PCR product from Lane 2 (1543 bp); Lane 4, *Bam*HI digest of fragment from Lane 3 (1061 bp); Lane 5, *Bam*HI digest of fragments from Lane 6 (6931 and 1061 bp); Lane 6, *Fse* I digest of pYCplac33-*ccp1*^{W191F} (7992 bp); Lane 7, undigested pYCplac33-*ccp1*^{W191F} (7992 bp). (B) Restriction endonuclease analysis of pYCplac33-*CCP1*: Lane 1, undigested (7992 bp); Lane 2, *Bam*HI digest (7992 bp); Lane 3, *Fse* I digest (7992 bp); Lane 4, *Apa* I digest (3913, 3641 and 438bp, the 438-bp band is not visible in the photo); Lane 5, *Hin*dIII digest (6266, 1432 and 294 bp, the 294-bp band is not visible in the photo); Lane 6, *Sma*I digest (7992 bp); Lane 7, Fermentas GeneRuler™ 1 kb DNA Ladder. The fragments were separated on a 0.7% agarose gel.

Appendix 4.3. YCplac33-*ccp1*^{W191F} plasmid loss from *ccp1Δ-ccp1*^{W191F} yeast

To determine if the *ccp1Δ-ccp1*^{W191F} cells used in Chapter 4 lost the YCplac33-*ccp1*^{W191F} vector, YPD cultures were plated in SCD with and without uracil. Cells were first grown for 24 h in YPD at 30°C under high aeration (shaking at 225 rpm), diluted to ~300 cells per 100 μL with 0.85% sterile saline, plated (100 μL) on SCD with or without 76 mg/L uracil and incubated at 30°C for 3 days.

As expected, both wild-type and *ccp1Δ* YPD cultures grew only on SCD+uracil (Table A4.5) because they do not contain the *URA3* gene (Table 4.1). Since 83±6% of *ccp1Δ-ccp1*^{W191F} cells survived in SCD–uracil, 11–23% of the cells lost the YCplac33-*ccp1*^{W191F} vector during 24 h growth in liquid YPD media. Thus, in Chapter 4, SC+uracil media were used for growth of wild-type and *ccp1Δ* cells, and SC–uracil media for growth of *ccp1Δ-ccp1*^{W191F} cells.

Table A4.5. YCplac33-*ccp1*^{W191F} plasmid loss from *ccp1Δ-ccp1*^{W191F} yeast during growth on YPD medium[a]

Medium	CFUs[b]			
	wild-type	*ccp1Δ*	*ccp1Δ-ccp1*^{W191F}	Ratio[c]
SCD+uracil	288 ± 24	315 ± 17	296 ± 16	83 ± 6%
SCD–uracil	0	0	247 ± 13	

[a] Yeast W303-1B strains (Table 4.1) were first grown in YPD for 24 h at 30°C with shaking at 225 rpm and plated in SCD with and without uracil.

[b] The number of colony forming units (CFUs) after 3 days' growth at 30°C on SCD plates.

[c] Ratio of CFUs for the *ccp1Δ-ccp1*^{W191F} strain on SCD–uracil and SCD+uracil.

Appendix 4.4. Procedures for the enzymatic assays

The experimental details for the enzymatic assays used in Chapter 4 (Table 4.2) are provided here. Cells (~2×10^8) harvested at the times indicated in Table 4.2, were vortexed for 4×30 s with glass beads in 300 μL of lysis solution [100 mM potassium phosphate buffer (KPi, pH 7.4) containing a complete protease inhibitor cocktail (EDTA-free, Roche)]. The resultant lysates were centrifuged at 12000×g at 4°C for 10 min, and the total protein concentration in the supernatant was determined to be ~3 μg/μL using

the Bio-Rad *DC* protein assay. The enzyme activities of 7–33 μL of the supernatants from the cell lysates were recorded. Assay blanks were measured by substituting 7–33 μL of lysis solution for cell lysate in the assays.

CCP activity was assayed by monitoring the oxidation of ferrocytochrome *c* at 550 nm ($\Delta\varepsilon_{550}$ = 19.6 $mM^{-1}cm^{-1}$) [108]. The assay solution contained 10 mM EDTA and 0.18 mM H_2O_2 in 100 mM KPi buffer (pH 7.0). A ferricytochrome *c* solution with A_{550} ~0.4 (~50 μM) was prepared from horse ferricytochrome *c* (Sigma) in 100 mM KPi buffer (pH 7.0) with 10 mM EDTA, and the cytochrome *c* was ~95% reduced (A_{550} ~1.3) by adding a grain of solid sodium dithionite (Fisher). Lysate supernatant (~33 μL) containing 100 μg of total protein was added to 500 μL of assay solution in a 1.5-mL cuvette. Following rapid mixing with 500 μL of ferrocytochrome *c* solution, the absorbance decrease at 550 nm was determined at 10-s intervals using a Hewlet-Packard 8453 spectrophotometer. One unit of CCP activity catalyzed the oxidation by H_2O_2 of 1 μmol of ferrocytochrome *c* per min at 25°C [206]. Using the purified enzyme, it was established that 10 μL of 65 μM CCP contained 1 unit of activity [108] or 10 μL of 20 μM CCP gave rise to an absorbance change of 1.0 in 10 s [108].

Catalase activity was established by following the disappearance of H_2O_2 at 240 nm (ε_{240} = 43.6 $M^{-1}cm^{-1}$) [149]. Lysate supernatant (~7 μL) containing 20 μg of total protein was added to 1 mL of assay solution containing 13.3 mM H_2O_2 in 33.3 mM KPi buffer (pH 7.0). Following mixing, the absorbance decrease at 240 nm was measured at 10-s intervals using a Hewlet-Packard 8453 spectrophotometer. One unit of catalase activity catalyzed the degradation of 1 μmol of H_2O_2 per min at 25°C [149].

The xanthine oxidase/cytochrome *c* method, which is widely used for yeast extracts [7, 205], was used here to measure superoxide dismutase (SOD) activity [200]. The assay solution contained 500 μM xanthine (Sigma), 200 μM horse ferricytochrome *c* (Sigma), 100 μM EDTA in 50 mM NaPi buffer (pH 7.8). A xanthine oxidase solution containing 0.75 mg/mL of the oxidase (Sigma) was also prepared in 50 mM NaPi buffer (pH 7.8) with 100 μM EDTA. Lysate supernatant (~17 μL) containing 50 μg of total protein was added to 3 mL of assay solution. Following addition of 35 μL of xanthine oxidase solution, the absorbance increase at 550 nm was measured at 10-s intervals using a Hewlet-Packard 8453 spectrophotometer. One unit of SOD activity inhibited by 50% the rate of ferricytochrome *c* reduction by the superoxide anion at 25°C [200].

Glutathione reductase (GLR) activity was assayed by monitoring NADPH oxidation at 340 nm (ε_{340} = 6.3 $mM^{-1}cm^{-1}$) [201]. A 4 mg/mL (6.5 mM) NADPH (Roche) stock solution was prepared in 0.5% $NaHCO_3$. Lysate supernatant (~7 μL) containing 20 μg of total protein was added to 1 mL of assay solution containing 1 mM GSSG (Sigma), 0.1 mM NADPH and 1 mM EDTA in 100 mM KPi buffer (pH 7.4). Following mixing, the absorbance decrease at 340 nm was measured at 10-s intervals using a Hewlet-Packard 8453 spectrophotometer. One unit of GLR activity catalyzed the oxidation of 1 nmol of NADPH per min by oxidized glutathione (GSSG) at 25°C [201].

5 Two-dimensional electrophoresis mapping of yeast mitochondrial proteomes from wild-type and *ccp1Δ* cells

5.1 Abstract

To determine the effects of deletion of cytochrome *c* peroxidase (CCP) on yeast cells, mitochondrial proteomes of wild-type *S. cerevisiae* and its *ccp1Δ* mutant were investigated by two-dimensional electrophoresis (2DE). Over 200 spots were detected for both strains on 7×10-cm 2D gels with a pI range of 3–10. Although more than 100 spots were matched in all six gels of wild-type mitochondria, the intensities of individual spots varied from gel to gel. Since 2DE analysis of yeast mitochondria did not yield reproducible data for quantitation by image analysis, methodology for isotope-ratio quantitation of different proteomes is discussed in Chapter 6.

5.2 Introduction

The main function of mitochondria is the production of energy in the form of ATP. Mitochondria are also known to play essential roles in many physiological functions, including regulation of cellular redox status, cell signaling, apoptosis, and the synthesis of lipids and heme [75, 76]. Many studies focus on the human mitochondrial proteome because mitochondrial dysfunction is implicated in many human diseases [223-225]. In fact, 10% of the proteins identified with human disease are localized in mitochondria [139].

Since their structure and function are highly conserved in eukaryotic organisms [78], yeast mitochondria are considered as a good model for mammalian mitochondria. The first comprehensive study of the *S. cerevisiae* mitochondrial proteome was reported in 2003 [138]. Mitochondria were purified from exponentially growing (OD_{600} 1.5–2.0)

YPG cultures. Up to 109 proteins were separated by 2DE and identified by peptide mass fingerprinting using matrix-assisted laser desorption ionization time-of-flight (MALDI-ToF) mass spectrometry (MS) [138]. Over 600 proteins were fractionated by 1DE and identified by analysis of their tryptic peptides using liquid chromatography-tandem MS. Thus, from over 20 million MS spectra, a total of 750 different mitochondrial proteins were identified and functionally classified. The function of 25% of the proteins is still unknown while another 25% of proteins are known to be involved in maintaining and expressing the mitochondrial genome. Only 14% of mitochondrial proteins are directly involved in energy metabolism, while others take part in protein translocation (8%), amino-acid, iron and lipid metabolism (9%), cell signaling (4%), transport of metabolites (5%) and other known functions [138]. In a more recent study, the proteomic change in yeast mitochondria during the diauxic shift was investigated [226]. A total of 253 proteins were identified from 459 spots in 2D gels with a pI range of 3–10. CCP was detected but it was not in the list of 18 proteins that underwent significant changes in abundance during the diauxic shift [226].

A quantitative comparison of protein expression in mitochondria from wild-type and *ccp1Δ* yeast cells may provide insight into the functions of CCP. Thus, the mitochondrial proteomes of wild-type and *ccp1Δ* in the W303-1B genetic background (Table 4.1) were separated and evaluated by 2DE.

5.3 Materials and methods

5.3.1 Mitochondria isolation

Reagents were purchased from Sigma except where indicated. All reagents were used as supplied. Isolation of mitochondria from wild-type and *ccp1Δ S. cerevisiae*

(W303-1B strain) (Table 4.1) was performed by a three-step centrifugation approach [223-225]. Cells were grown in liquid YPD medium at 30°C with high aeration (shaking at 225 rpm), harvested from 100 mL of 48-h cultures by centrifugation at 3000×g for 5 min at 4°C, and resuspended in 5 mL of lysis buffer [0.6 M sorbitol (BDH) and 1 mM EDTA (BDH) in 10 mM Tris-HCl (pH 7.4) (Fisher)] plus 0.5 g of glass beads. The tubes were vortexed vigorously for 4×30 s, the cell debris was removed by centrifugation at 2500×g for 20 min at 4°C, and the supernatant was centrifuged at 15000×*g* for 10 min at 4°C to pellet the mitochondria. The pellet was washed once with lysis buffer prior to storage at –80°C.

5.3.2 2DE separation

Mini gels (7×10-cm) were used for 2DE analysis of the yeast mitochondrial proteome. Protein extracts were prepared by resuspending the mitochondrial pellet (~0.5 µL) in 150 µL of isoelectric focusing (IEF) sample buffer [7 M urea, 2 M thiourea, 4% CHAPS, 1% Triton X-100, 1% DTT and 2% IPG ampholines (pH 4–7, Amersham Biosciences, GE Healthcare)] and incubating for 2 h at 30°C. After centrifugation at 15000×*g* for 20 min, the supernatant (125 µL) was used to actively (*i.e,* under a constant applied voltage of 50 V) rehydrate the 7-cm IPG strips (pH 4–7, Amersham Biosciences, GE Healthcare) under mineral oil (Bio-Rad) overnight at 20°C using a Bio-Rad PROTEIN® IEF System. Following rehydration of the strip, IEF was performed at 250 V for 1 h, 500 V for 30 min, 1000 V for 30 min, 2000 V for 30 min and 4000 V to achieve 26 kVh. Experimental conditions for 18×20-cm gels are also listed here for reference. The 18-cm IPG strip was rehydrated with 350 µL of mitochondrial supernatant and IEF

was performed at 250V for 45 min, 500 V for 30 min, 2000 V for 30 min, 5000 V for 30 min and 10000 V to achieve 66 kVh. The focused strips were dipped in SDS equilibration buffer [6 M urea, 30% glycerol (Bioshop) and 2% SDS in 50 mM Tris-HCl (pH 8.8)] containing 1% DTT for 15 min and transferred to SDS equilibration buffer with 2.5% iodoacetamide for a further 15 min at 30°C.

After the equilibration step, the strip was placed on the top of a 1-mm thick 7×10-cm or 18×20-cm 10% polyacrylamide gel and sealed in place with sealing solution [0.5% agarose (Bioshop) in SDS-PAGE running buffer with 0.0002% bromophenol blue]. Electrophoresis was performed at 10 mA per gel for 15 min followed by 20 mA per gel until the blue dye migrated to the bottom. The gels were silver stained using PlusOne™ Protein Silver Staining Kit (Amersham Biosciences) as per the manufacturer's instructions, and protein spots were evaluated using the Image Master™ 2D Elite V3.10 software (Amersham Biosciences).

5.4 Results

Figure 5.1 shows 2D gels (pI 3–10) of the mitochondrial proteins from 48-h YPD cultures of wild-type and *ccp1Δ S. cerevisiae*. A total of 224 and 215 spots were detected, respectively, by silver staining the 2D gels, which represents ~30% of the 700 proteins located in yeast mitochondria [227]. The low detection can be attributed to the fact that a considerable number of mitochondrial proteins are small (M_r < 10 kDa) or highly basic (pI > 10) and ~18% are membrane bound [228]. A high proportion of membrane-associated proteins are hydrophobic and difficult to solubilize [223-225]. Since only ~50 μg of total protein was loaded on each gel in this study (Figure 5.1), the detection can be improved by separating an increased amount of protein in a 18×20-cm gel.

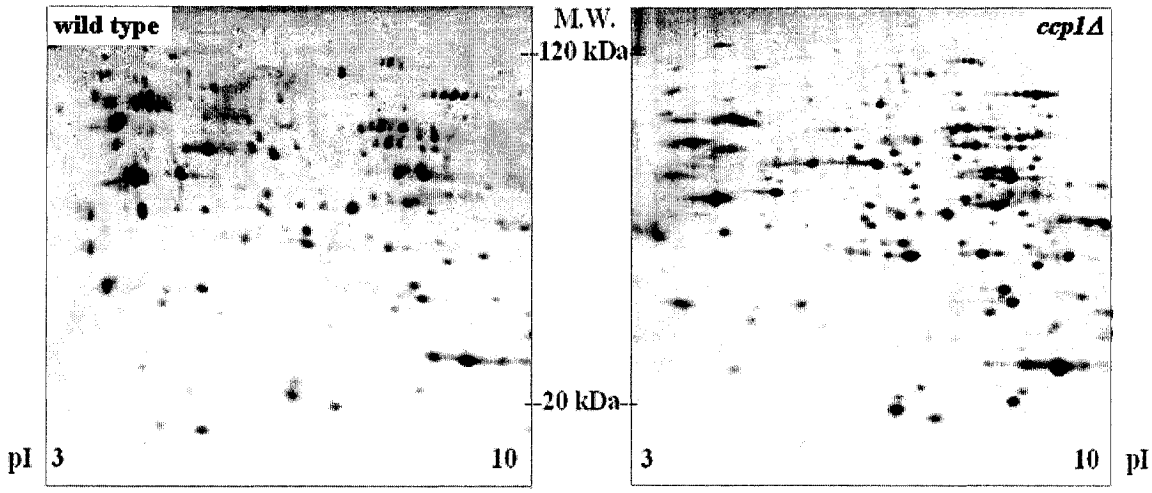

Figure 5.1. Mitochondrial proteomes analyzed by 2DE of wild-type (left) and *ccp1Δ* (right) *S. cerevisiae* from 48-h YPD cultures. Approximally 0.5 μL of mitochondrial pellet containing 50 μg total proteins was loaded on 7×10-cm gels. More than 200 proteins were detected by silver staining the 10% polyacrylamide gel over the pI range of 3–10.

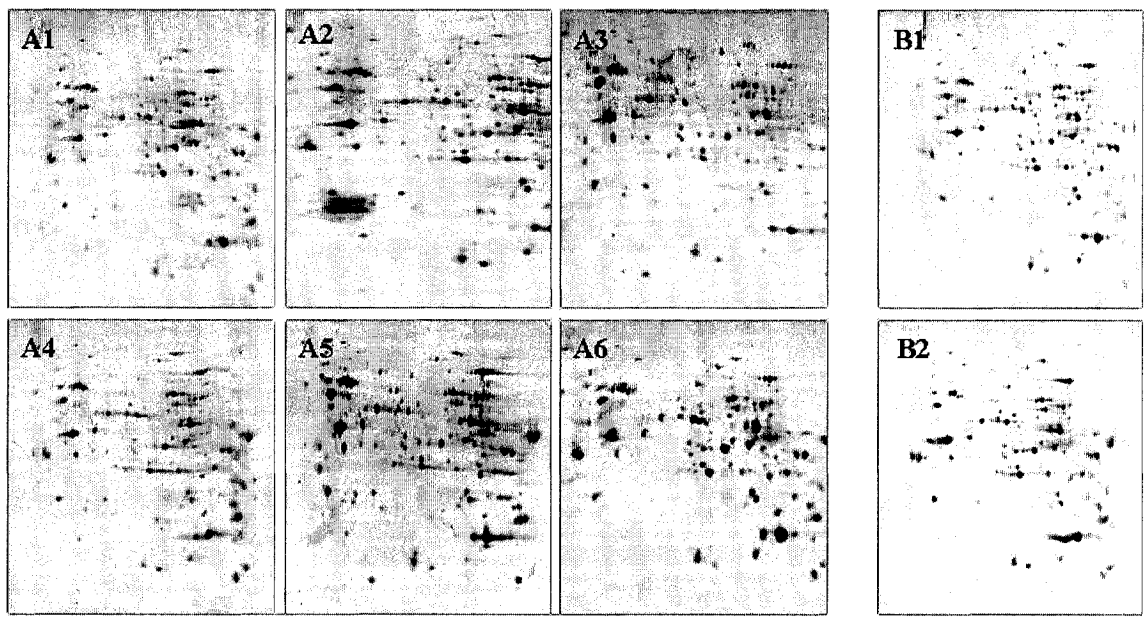

Figure 5.2. Reproducibility of 2DE gels of the *S. cerevisiae* mitochondrial proteome. Gels of proteins from (A) wild-type and (B) *ccp1Δ* yeast mitochondria. See Legend to Figure 5.1 for experimental details.

Figure 5.2 shows eight 2D gels of the mitochondrial proteomes of wild-type (A1–6) and *ccp1Δ* (B1–2) yeast from 48-h YPD cultures. Six gels prepared from the same mitochondrial pellet indicate the reproducibility of the analysis. The six wild-type gels were computationally processed using the Image Master™ 2D Elite V3.10 software to create two average gels, 1AV and 2AV, with spot intensities averaged over gels A1–3 and gels A4–6, respectively. Spot intensities are expressed as the volume of each spot relative to the total spot intensity in a gel [229]. Out of ~200 spots per gel, 111 spots were matched in gel 1AV and 2AV and their normalized volumes (%) are plotted in Figure 5.3. The correlation factor (m = 0.86) is less than the optimal value of 1.00 and up to 31% of the spots, particularly weak spots, differed in intensity by a factor of 2 or more. Thus, the reliability of image analysis is limited to proteins that undergo a 3-fold or greater change in expression. This is consistent with a previous study of yeast mitochondrial proteome alteration during the diauxic shift [226], where a protein expression change was considered significant only if its spot intensity differed reproducibly more than 3-fold.

5.5 Discussion

Efforts can be made to increase the number of protein spots detected by 2DE in the current study. More protein spots would be observed if 2DE were performed on a larger gel (18 × 20-cm *vs* 7 × 10-cm) and with narrow pI ranges (4–7, 6–9, 6–11, etc.) due to increased sample loading. Fractionation could also be used to reduce the complexity of the sample loaded and to increase the visibility of low abundance proteins. Several fractionation techniques are available including the use of sucrose gradients to separate mitochondrial complexes [225] and the sequential extraction of proteins in increasingly powerful solubilizing solutions [230].

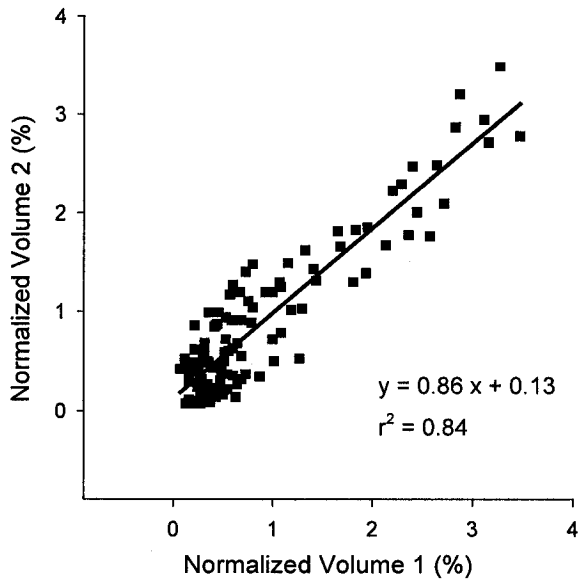

Figure 5.3. Reproducibility of 2DE analysis of the mitochondrial proteome from wild-type *S. cerevisiae*. The X- and Y-axis represent the normalized spot volume (%) of matched spots in average gel 1AV and gel 2AV. These averaged gels were obtained by averaging spot intensities in gels A1–3 and gels A4–6 in Figure 5.2 using the Image Master™ 2D Elite software (see text).

Non-mitochondrial proteins may also be present in the gel. Contamination from non-mitochondrial proteins can arise at four points in the isolation of mitochondria [223]: (1) carry over from the nuclear/debris pellet; (2) partial isolation of cytosolic or microsomal components; (3) isolation of fractions having similar sedimentation parameters under the conditions used, and (4) isolation of components of fractions that interact with mitochondria. Contaminations from the first 3 sources can be removed by washing the pelleted mitochondria or by Nycodenz density gradient centrifugation [231]. Proteins in close association with mitochondria, such as those located in the ER [232], are expected to be numerous based on entries in the CYGD database [41]. In fact, protein impurities can shed light on interactions between the mitochondrion and other organelles [223]. Hence, the three-step centrifugation method described here, which has been used

by numerous researchers studying isolated mitochondria [223-225], should be suitable for mitochondrial proteome analysis.

Our results reveal that 2D gels of wild-type yeast mitochondria are not very reproducible. The intensities of matched spots averaged over three gels varied ~0.2–3.5-fold from a second set of three gels (Figure 5.3) prepared from the same mitochondrial sample. Besides the variations accompanying 2DE separation, image analysis is error prone since it requires extensive manual input such as spot-boundary definition, which also lowers the reproducibility of the intensity measurements [233, 234]. The experimental errors inherent in 2DE image analysis are hard to eliminate [233, 234].

5.6 Conclusions

S. cerevisiae is relatively simple organism for exploring the molecular basis of human mitochondrial diseases caused by ROS [1]. Proteomics analyses of yeast mitochondria have the potential to demonstrate how mitochondrial ROS induce stress and apoptosis, which might provide some insight into human mitochondrial diseases. Our goal was to first compare mitochondrial proteomes of wild-type, *ccp1Δ* and *ccp1Δ-ccp1*^{W191F} cells under different growth conditions. Since our preliminary 2DE image-analysis approach revealed that changes in protein abundance are not reliable due to gel-to-gel variation, a MS approach using metabolic isotope labeling is discussed in Chapter 6.

6 Quantitative analysis of the yeast proteome by incorporation of isotopically labeled leucine

6.1 Abstract

Quantitative comparison of protein expression levels in 2D gels is complicated by the variables associated with protein separation and mass spectrometric responses. Metabolic-labeling allows cells from different experiments to be mixed prior to analysis. This approach has been reported for prokaryotic cells. Here we demonstrate that metabolic labeling can also be successfully applied to the eukaryote, *Saccharomyces cerevisiae*. Yeast leucine auxotrophs grown on synthetic complete media containing natural abundance Leu or D_{10}-Leu were mixed prior to 2D gel separation and MALDI analysis of the digested proteins. D_{10}-Leu labeling provided an effective internal calibrant for peptide MS analysis, and the number of Leu residues yielded an additional parameter for peptide identification at low mass resolution (1000). Metabolic incorporation of D_{10}-Leu into yeast proteins was found to be quantitative since the intensities of the peptide peaks corresponded to those expected based on the percent label in the media. Thus, D_{10}-Leu labeling should provide reliable data for comparing proteomes both quantitatively and qualitatively from wild-type and non-essential-gene-null-mutant strains of *S. cerevisiae*. Given the central role played by yeast in our understanding of eukaryotic gene and protein expression, it is anticipated that the quantitative expressional proteomic method outlined here will have widespread applications.

6.2 Introduction

Proteomics is the term used for the global analysis of gene expression at the protein level in a cell. The standard method for proteome analysis combines protein

separation by two-dimensional gel electrophoresis (2DE) with mass spectrometric (MS) identification of selected protein spots [235]. 2DE separates proteins by isoelectric focusing (IEF) in the first dimension and by molecular mass *via* polyacrylamide gel electrophoresis (SDS-PAGE) in the second dimension. The power of proteomics resides in its ability to examine biological responses over thousands of proteins simultaneously and provide a relatively comprehensive view of cellular metabolism [236]. Modern imaging techniques can extract quantitative information for each of the spots in a single 2D gel. However, quantitative comparisons of protein expression levels from two different gels are plagued by the difficulties in controlling the range of variables associated with cell lysis, sample handling, 2DE separation and sample recovery from the gel, as well as variations in the mass spectrometric response [237].

Since the yeast genome has been sequenced for some time [121], the interest has shifted to functional genomics. Up to the end of October 2001, of the ~6000 *S. cerevisiae* genes, 3158 were found to be non-essential for viability of the cell [41]. Quantitative comparison of protein expression levels in wild-type *S. cerevisiae* and each non-essential-gene-null mutant is now necessary to comprehensively analyse the function of the deleted gene. Our particular interest is in genes involved in peroxide metabolism such as cytochrome *c* peroxidase (CCP) [85]. Thus, we explored the use of different labeling methods for the analysis of yeast proteomes in whole-cell lysates both qualitatively and quantitatively by means of 2DE in combination with matrix-assisted laser desorption ionization-time-of-flight mass spectrometry (MALDI-ToF MS). In outline, the metabolic labeling approach involves growing cells separately on normal and stable-isotope-labeled media. The two isotopically distinct cell populations (wild-type and mutant) are mixed

prior to sample processing, eliminating the experimental variables mentioned above [237]. Since isotopic labeling provides an effective internal mass calibrant for protein and peptide MS analyses, the ratio of expression levels of a labeled and unlabeled protein should be precisely reflected in the intensities of the MS peaks. This approach also decreases by half the number of 2D gels required, which is an important factor in high throughput screening of proteomes.

Quantitative analysis of proteomes using metabolic labeling requires stoichiometric incorporation of the label into an organism's proteins without metabolic scrambling. The most widely used method to obtain stable-isotope-enriched proteins is to grow cells on minimal media containing ^{13}C enriched glucose or ^{15}N enriched salts. We found such approaches to be unsatisfactory with *S. cerevisiae* because of poor cell growth, and uniform labeling with ^{15}N yielded unpredicted mass shifts in the labeled proteins. Our most promising metabolic labeling method for *S. cerevisiae* provided high quantities of isotopically labeled proteins at low cost. In this approach, leucine auxotrophic stains were grown on synthetic complete media (SCM) with either natural abundance (H_{10}-Leu) or deuterated leucine (D_{10}-Leu). Tryptic peptides were used for protein identification and the ratios of H_{10}- to D_{10}- peptides in the mixtures indicate the relative protein expression levels in the two cultures. The number of Leu residues found in each peptide not only determines the mass difference between peptides from H_{10}- and D_{10}-cultures, but it also provides an additional parameter for protein identification [238].

In summary, this paper describes a new metabolic labeling methodology for yeast involving stoichiometric incorporation of D_{10}-Leu into the organism's proteins for quantitative proteome analysis by 2DE and MALDI-ToF-MS. Data presented here on

3:1, 1:1 and 1:3 mixtures of wild-type *S. cerevisiae* grown on SCM with H_{10}- and D_{10}-Leu establish the feasibility of the labeling method, and the ease of analysis of the data by low-resolution (R~1000) MALDI-ToF-MS. Metabolic labeling of *E. coli* proteins with D_{10}-Leu has been reported [238] but its use in quantifying expression of bacterial proteins has not been demonstrated.

6.3 Materials and methods

6.3.1 Materials

Reagents were purchased from Sigma except where indicated. All reagents were used as supplied.

6.3.2 Media and growth conditions

Wild-type *S. cerevisiae* strain W303-1B (*MATα ade2*-1 *his3*-11,15 *leu2*-3,112 *ura3*-1 *trp1*-1 *can1*-100, a gift from Dr. P. Joyce, Concordia University) and its CCP gene-null-mutant (*ccp1Δ*) were used in this study. Wild-type and *ccp1Δ* cells were grown on the following media to determine the optimal growth and labeling conditions: (A) YPD (2% glucose + 2% peptone + 1% yeast extract); (B) Bio-Express®-2000 (^{15}N-labeled rich media for eukaryotic protein expression, Cambridge Isotope Labs); (C) synthetic complete media (SCM, glucose + yeast nitrogen base without amino acids + yeast synthetic drop-out media) without Leu; (D) SCM with 380 mg/L H_{10}-*l*-Leu; (E) SCM with 80 mg/L H_{10}-*l*-Leu and (F) SCM with 80 mg/L D_{10}-*l*-Leu [99.4% $(CD_3)_2CDCD_2CD(NH_2)COOH$, CDN]. Wild-type or *ccp1Δ* yeast grown for 48 h in YPD culture (50 μL culture; 1×10^7cells) was inoculated into 20 mL of media A–F. The cells were grown at 30°C with continuous shaking (180 rpm) for 72 h. OD_{550} data for all cultures were recorded at the following time points (T_{hours}): T_0, T_6, T_{20}, T_{28}, T_{44}, T_{72} to

compare growth in different media. To establish the feasibility of our labeling methodology, 50 μL of wild-type yeast grown for 48 h in YPD was also inoculated into 50 mL of SCM with either 80 mg/L H_{10}-*l*-Leu or D_{10}-*l*-Leu (media E or F) and the cells grown at 30°C for 72 h.

6.3.3 Two-dimensional electrophoresis

The 72-h SCM cultures grown on either H_{10}- or D_{10}-Leu were mixed together prior to cell harvest. Cell concentrations were determined from the OD_{550} value. The isotopically distinct cultures were also harvested separately as controls. Cell lysis and protein extraction was performed according to the method of Schieltz [239] (see Appendix 6.1 for details). Cells were suspended in lysis solution, mixed with glass beads and vigorously vortexed. DNAse I and RNAse A (Roche) were used to degrade nucleic acids, and protein concentrations determined using the Bio-Rad *DC* protein assay. 2DE was performed essentially as recommended by Amersham Pharmacia [240]. Proteins were precipitated in acetone (Fisher) and dissolved in IEF sample buffer (Amersham Pharmacia). After the IPG strip (pH 4–7, 18 cm, Amersham Pharmacia) was rehydrated with IEF sample buffer overnight, isoelectric focusing was performed using a Bio-Rad PROTEAN® IEF Cell. Focused IPG strips were equilibrated in SDS equilibration solution before proteins were separated on a 12% polyacrylamide 18 × 20 cm gel using a Bio-Rad PROTEAN® II xi gel electrophoresis system. Gels were stained with Gel Code Blue (Pierce) and scanned using an UMAX PowerLook III scanner. A polyacrylamide protective cover was fashioned in-house to waterproof the scanner. Spots were evaluated using Image Master™ 2D Elite V3.10 software (Amersham Pharmacia). See Chapter 5 for details on the 2DE analysis.

6.3.4 Mass spectrometry

Desired spots were cut from the gels into 1 × 1 mm^2 pieces. The in-gel proteins were reduced for 30 min in 10 mM potassium carbonate + 10 mM DL-dithiothreitol, and alkylated for 30 min in 10 mM 4-vinyl pyridine + 10 mM Tris-HCl (Fisher) at pH 8.5. The gel pieces were then incubated in each of the following solutions for 15 min: (1) 50% acetonitrile (ACN, Fisher), (2) 50% ACN + 50 mM ammonium bicarbonate and (3) 50% ACN + 15 mM N-ethyl morpholine (NEM) + 5 mM acetic acid (Fisher), and dried in a Speed Vac (Savant) for 1 h. Modified trypsin (8.3 ng/μL, Roche), 15 mM NEM, 42 mM acetic acid and 2mM $CaCl_2$ were incubated with the gel pieces for 16 h at room temperature. The tryptic peptides were recovered from the gel by extracting three times with 60% ACN + 0.5% formic acid (Fisher), the recovered peptides dried in the Speed Vac, resuspended in 10 μL of 5% methanol (Fisher) + 0.1% trifluoroacetic acid (TFA) and desalted on C18 Zip Tips (Millipore). The desalted peptides were collected from the Zip Tips in 1.5 μL of 60% ACN + 0.1% TFA solution and mixed with 1.5 μL of MALDI matrix solution prepared by mixing 10 volumes of acetone saturated with α–cyano-4-hydroxycinnamic acid, 1 volume of nitrocellulose (20 mg/mL in acetone), 4 volumes of acetone and 5 volumes of 2-propanol (Fisher). Samples (1.5 μL) were spotted on the MALDI target plate (Applied Biosystems) and analyzed using a Voyager DE Linear MALDI-ToF mass spectrometer (Applied Biosystems) with a mass accuracy of ±0.1% using external calibration. The tryptic peptide with M_r 2163.3 was used as internal standard to calculate the masses of the sample peptides. Proteins in the selected spots were identified based on the masses of multiple peptides from the H_{10}-cultures using the Mascot search engine (Matrix Science).

6.4 Results

6.4.1 Yeast growth

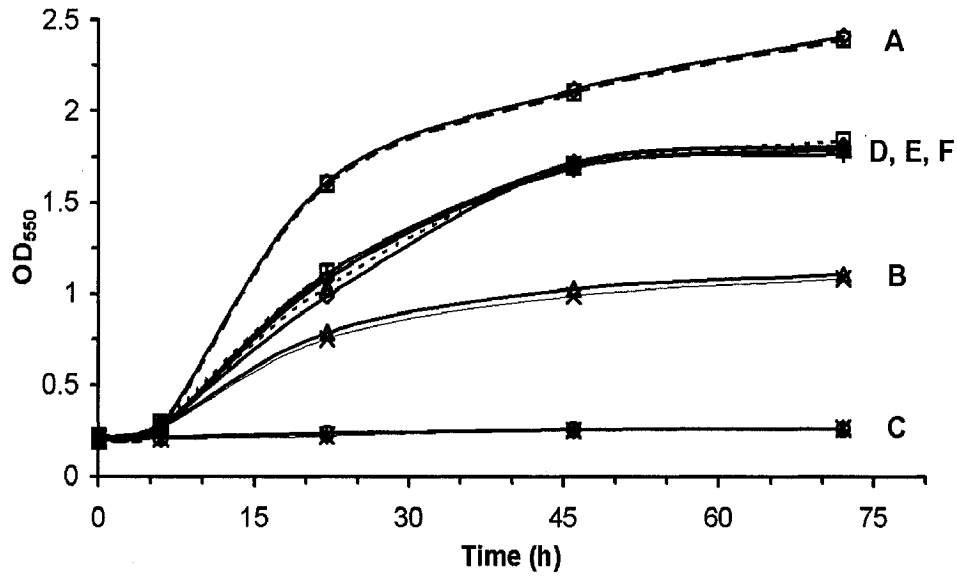

Figure 6.1. Growth curves of wild-type (W303-1B) and *ccp1Δ* strains of *S. cerevisiae*. Media A–F (20 mL) were inoculated with 50 µL of 48 h YPD cultures. The cells were grown at 30°C with continuous shaking (180 rpm) and OD_{550} values were recorded between 0 and 72 h at the times indicated. Media (A) YPD; (B) Bio-Express®-2000; (C) SCM without Leu; (D) SCM with 380 mg/L H_{10}-*l*-Leu; (E) SCM with 80 mg/L H_{10}-*l*-Leu and (F) SCM with 80 mg/L D_{10}-*l*-Leu.

Wild-type *S. cerevisiae* and its *ccp1Δ* mutant exhibit similar growth on all the media examined (Figure 6.1). Surprisingly, poor growth was observed on Bio-Express®-2000 (media B) which is recommended by the supplier for ^{15}N-labeling of eukaryotic proteins. The yeast strains used are multiple amino acid auxotrophs, but since leucine is the most common amino acid in proteins (9.1%) [241], it was the amino acid of choice for labeling. As expected, no cell growth was observed in SCM without Leu (media C). Cell growth on SCM in the presence of 80 or 380 mg/L Leu (media D–F) is essentially identical indicating that isotopically labeled Leu has no effect on the growth pattern of the strains even at low concentration, which makes it possible to compare proteomes

from the H_{10}- and D_{10}-cultures. To avoid transfer of label, only 21% (80 mg/L) of the recommended amount of Leu (380 mg/L) was provided in the media. Good cell growth (Figure 6.1E, F) as well as protein expression were observed under these minimal conditions. The mass spectrometry results discussed below reveal that all proteins examined were fully labeled with D_{10}-Leu, and no evidence for label transfer to other residues was found.

6.4.2 Protein identification and quantitative analysis

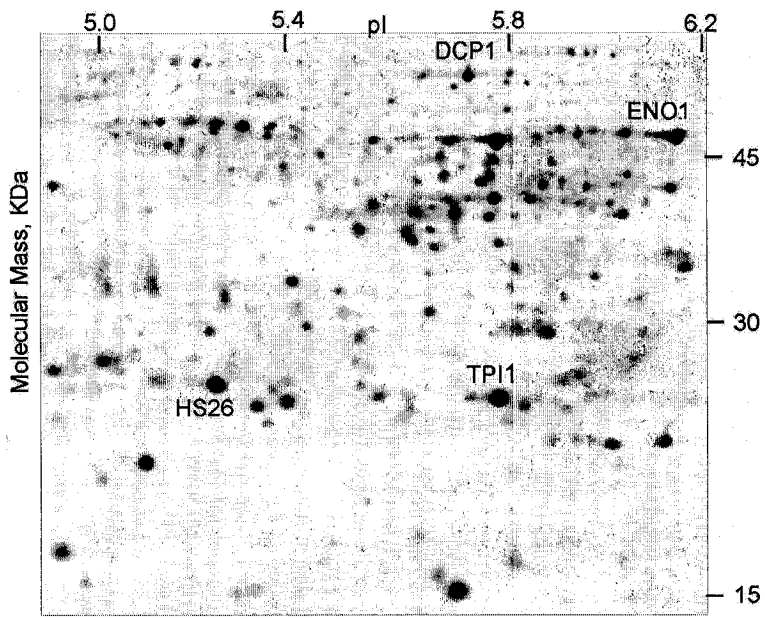

Figure 6.2. 2D separation of the proteomes from *S. cerevisiae* cultures grown on SCM with 80 mg/L H_{10}- and 80 mg/L D_{10}-Leu. Equal concentrations of cells were mixed prior to cell lysis and 2D analysis. The proteins were separated on a 12% polyacrylamide 18×20 cm gel in first (horizontal) dimension by IEF based on their pIs, and the second (vertical) dimension by SDS-PAGE based on their masses. The labels on the spots are the protein identifies from the Mascot search results.

Figure 6.2 shows the 2DE separation of a cell lysate from a 1:1 mixture of wild-type *S. cerevisiae* cultures grown on H_{10}- and D_{10}-Leu. Four spots that span the mass (15–70kDa) and pI range (5.0–6.2) of the 2D gel were selected and identified. The labels

on the spots are from the Mascot search results, and the proteins are the following: TPI1 (triosephosphate isomerase, M_r 27,006 Da and pI 5.74), HS26 (heat shock protein 26, M_r 23,880 Da and pI 5.31), ENO1 (enolase 1, M_r 46,921 Da and pI 6.16) and DCP1 (pyruvate decarboxylase isozyme 1, M_r 61,916 Da and pI 5.80).

The average mass (M_r) of each peptide was calculated using the average atomic weight, averaged over all isotopes, for each element. When D_{10}-Leu replaces H_{10}-Leu in the medium, the M_r of each Leu-containing peptide will change, depending on its number of Leu residues as well as the isotopic purity of D_{10}-Leu. Hence, the mass shift (ΔM_r) expected between labeled and unlabeled peptides is given by:

$$\Delta M_r = \Delta A_r \times n \times (a - b) \times 10 = n \times 10\text{Da} \qquad (6.1)$$

Here $\Delta A_r = A_r(D) - A_r(H) = 2.013999939 - 1.007825017$, n is the number of Leu residues in the peptide, a the isotopic purity of D_{10}-Leu (99.4%), and b the natural abundance of D (0.015%). For example, the calculated average masses (1096.3 and 1106.3 Da) of the TPI1_1 peptide WVILGHSER from the H_{10}- and D_{10}- cultures and the observed masses [1096.7 Da (Figure 6.3A) and 1105.6 Da (Figure 6.3B)] are in good agreement given the accuracy of the mass spectrometer used in this study (±0.1%).

Paired peaks with close to the predicted ΔM_r (Eq. 6.1) are observed in the mass spectra of tryptic digests of YEAST_TPI1 from the gels of the mixtures of H_{10}- and D_{10}- cultures (Figure 6.3C–E). Two peaks with 1:3 intensity and average masses of 1105.5 and 1096.2 Da are observed in the mass spectra of a 1:3 mixture of D_{10}- and H_{10}-Leu cultures (Figure 6.3C). Paired peaks with 1:1 and 3:1 intensities (Figures 6.3D and 6.3E) are also observed in the profiles of 1:1 and 3:1 mixtures. The observed ΔM_r of ~9 Da reveals that n = 1 consistent with the presence of one Leu residue in peptide

WVILGHSER. The peak at m/z 1017 Da is unpaired ($\Delta M_r = 0$) because of the absence of Leu in this peptide (TFFVGGNFK, theoretical M_r 1016.2 Da).

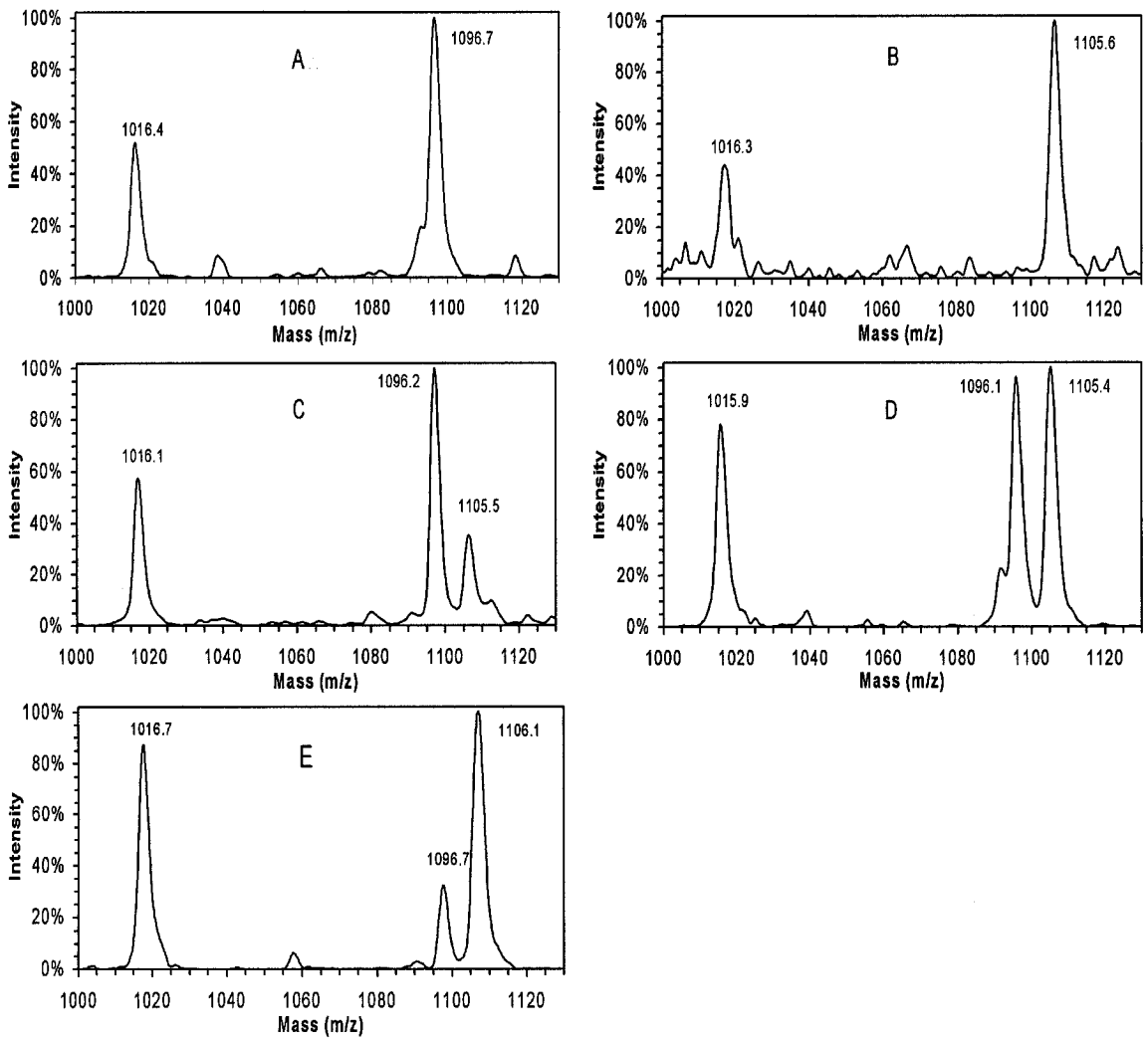

Figure 6.3. MALDI-ToF mass spectra of tryptic peptides from spot TPI1 in Figure 6.2. The sequence of the peptides, TFFVGGNFK (theoretical M_r 1016.2 Da) and WVILGHSER (theoretical M_r 1096.3 Da), were determined by searching the NCBI database using Mascot. Peaks from (A) H_{10}-culture, (B) D_{10}-culture, (C) 1:3, (D) 1:1 and (E) 3:1 D_{10}:H_{10} mixtures are shown. The mass spectrometer was operated in the linear, positive ion and delay mode with an accelerating voltage of +15 kV. Baseline correction and noise removal were performed using the default parameters (peakwidth 32, flexibility 0.5 and degree 0.1) based on the resolution (R~500) by the Data Explorer software on the Voyage DE mass spectrometer. The peaks are labeled with their average masses and the standard deviations are within ±0.1%.

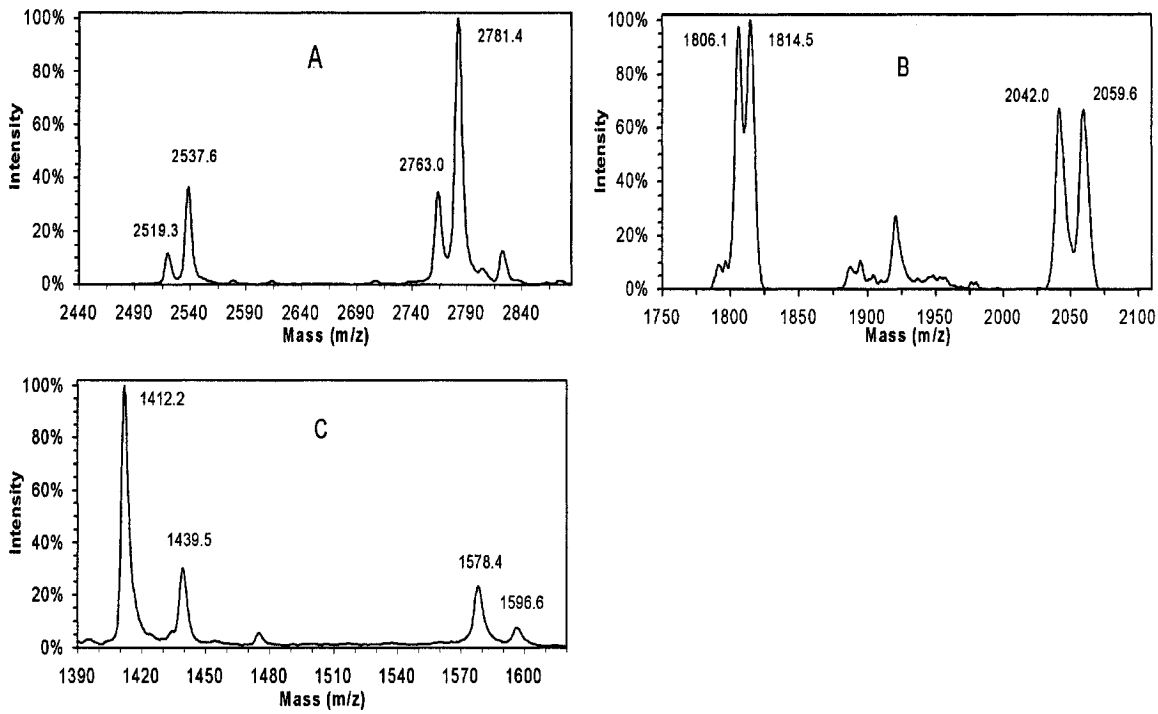

Figure 6.4. MALDI-ToF mass spectra of tryptic peptides from spots (A) TPI1, (B) HS26 and (C) ENO1 in Figure 6.2. (A) Peptides ADVDGFLVGGASLKPEFVDIINSR (theoretical M_r 2519.8 Da) and DKADVDGFLVGGASLKPEFVDIINSR (theoretical M_r 2763.1 Da) for a 3:1 D_{10}:H_{10} mixture. (B) Peptides EVARPNNYAGALYDPR (theoretical M_r 1806.0 Da) and SVAVPVDILDHDNNYELK (theoretical M_r 2041.3 Da) for a 1:1 D_{10}:H_{10} mixture. (C) Peptides LGANAILGVSLAASR (theoretical M_r 1412.7 Da) and AVDDFLISLDGTANK (theoretical M_r 1578.7 Da) for a 1:3 D_{10}:H_{10} mixture. The peaks are labeled with their average masses and the standard deviations are within ±0.1%. See Figure 6.3 for experimental conditions.

On repeated analysis, the same MS peaks were observed for a given protein digest. A limited number of peptides with M_r values in the range of 700 to 3000 Da (0~4 Leu residues) was detected from the > 50 possible peptides in the proteins examined. Since only 4 peptide masses with 10% sequence coverage are required to identify a protein with $p<0.05$ (p is probability that the observed match is a random event) [223], low peptide recovery from the MALDI source actually simplifies the analysis since fewer overlapping peaks are found in the isotopic mixtures. Based on the MS profiles and the known sequence of each protein, peptides with M_r values that did not overlap with other

peptides were selected for protein quantitation. The ratios of the peak-centroid-heights of the labeled and unlabeled peptides (H_D/H_H) were averaged over all the selected peptides of a given protein to obtain its relative expression levels (REL) in the mixtures of H_{10}- and D_{10}- cultures.

Figure 6.4A shows the MALDI profiles obtained for the high-mass peptides of YEAST_TPI1 from the 2D gel of a 3:1 D_{10}:H_{10} mixture. Two pairs of peaks with n~2 were detected. An average REL of 3.04 ± 0.13 was calculated for YEAST_TPI1 from the H_D/H_H ratios of the three pairs of peaks in Figures 6.3E and 6.4A. Figures 6.4B and 6.4C show the peptide peaks from YEAST_HS26 and YEAST_ENO1, and again paired peaks with n~1–3 and the expected intensity ratios are observed. This confirms that equal amounts of protein were synthesized in the normal and isotopically labeled media. On average, 4 suitable peptides were detected from each protein digest for quantitative analysis. Table 6.1 summarizes the mass spectral data obtained for the 4 protein spots marked in Figure 6.2, and Table 6.2 summarizes the average RELs observed for each protein.

6.5 Discussion

On average, proteins labeled with D_{10}-Leu will increase in mass by 0.762% as estimated from:

$$\Delta M_r = (M_r / 119.4) \times 9.1\% \times 10 \text{ Da} \qquad (6.2)$$

Here M_r is the average mass of the protein, *119.4* the average mass of an amino-acid residue, *9.1%* the frequency of Leu in proteins [241] and *10* the expected mass shift between H_{10}- and D_{10}-Leu. Thus, for example, the mass shift of a 60 kDa D_{10}-Leu labeled protein is expected to be ~450 Da, which will not be resolved from the unlabeled protein

in a standard 2D gel. In our experiments, very similar 2D gels were observed for all ratios of the H_{10}- and D_{10}-cultures indicating that metabolic labeling does not alter protein solubility and migration. This is not the case for chemically labeled proteins, which exhibit altered migration in gels and may thus elude detection [242]. Interestingly, the observed mass shift per Leu residue averaged over all measurements is 9.0 ± 0.5 Da (Table 6.1) and not 10 Da as expected based on the use of D_{10}-Leu with 99.4% isotopic purity. Since we confirmed the purity of the D_{10}-Leu by Electrospray Ionization MS (ESI-MS) in our laboratory, we assume that in the D_{10}-labeled peptides one deuteron is exchanged for hydrogen in the MALDI source as reported previously for D_{10}-Leu-labeled proteins [243].

Image-analysis software, such as ImageMaster used here, is a powerful tool for the quantitative analysis of proteomes separated on 2D gels. It can determine the percent volume of each spot in a whole proteome. Nonetheless, some inextricable problems limit the reliability of the analyses. For example, many staining techniques, such as silver staining, suffer from a limited dynamic range (4-60 ng) [244] so that the intensities of more abundant spots are not linearly correlated to those of less abundant spots [245]. Also, ionization efficiency is highly variable for peptides and the only suitable internal standard for a candidate peptide is that same peptide labeled with stable isotopes [246]. As the data in Table 6.2 demonstrate, the D_{10}-Leu internal standard provided by the present approach allows reliable quantitative information to be derived by MALDI-ToF-MS from a single 2D gel. Only one gel is needed to compare two different proteomes because analysis of separate H_{10}- and D_{10}- cultures is not necessary every time. In contrast to the excellent quantitative data obtained here (Table 6.2), it was previously reported that MALDI-ToF-MS does not yield accurate intensity ratios when comparing peptides [247].

Table 6.1. Mass shifts (ΔM_r) and relative intensities of tryptic peptides from *S. cerevisiae* proteins expressed in media containing H_{10}- and D_{10}-Leu

Peptides[a]	M_r (cal)[b]	ΔM_r (cal)[b]	ΔM_r (obs)[c]	h_D/h_H[d] D:H = 1:3	ΔM_r (obs)[c]	h_D/h_H[d] D:H = 1:1	ΔM_r (obs)[c]	h_D/h_H[d] D:H = 3:1
TPI1_1	1096.3	10.0	9.3	0.35	9.3	1.04	9.4	3.13
TPI1_2	2519.8	20.0	18.2	0.36	18.1	1.11	18.3	3.10
TPI1_3	2763.1	20.0	18.3	0.38	18.0	1.08	18.4	2.89
HS26_1	814.0	30.0	27.1	0.26	27.2	0.83	27.5	3.42
HS26_2	1730.0	10.0	8.8	0.38	6.9	0.88	8.7	3.00
HS26_3	1806.0	10.0	8.6	0.37	8.4	1.03	8.9	2.87
HS26_4	2041.3	20.0	18.0	0.33	17.6	1.00	17.4	3.35
HS26_5	2428.7	20.0	16.5	0.27	17.4	1.28	21.4	3.12
ENO1_1	755.9	30.0	27.3	0.28	26.9	0.66	27.5	3.31
ENO1_2	1412.7	30.0	27.3	0.30	26.7	1.15	27.4	2.92
ENO1_3	1578.7	20.0	18.2	0.32	19.4	0.97	18.6	2.88
ENO1_4	2441.6	20.0	17.4	0.41	17.9	1.16	18.1	3.18
DCP1_1	726.8	10.0	9.2	0.26	8.9	0.93	9.2	2.68
DCP1_2	1596.8	10.0	8.6	0.44	8.6	1.11	10.6	2.58
DCP1_3	1977.4	10.0	9.1	0.35	8.5	1.06	9.4	2.60
DCP1_4	2388.7	30.0	27.9	0.30	27.3	1.32	28.3	3.25
DCP1_5	2743.2	40.0	37.0	0.32	36.6	0.91	36.8	3.12

[a] Tryptic peptides from proteins in spots labeled in Figure 6.2. TPI1-1, WVILGHSER; TPI1-2, ADVDGF LVGGASLKPEFVDIINSR; TPI1-3, DKADVDGFLVGGASLKPEFVDIINSR; HS26-1, LLGEGGLR; HS26-2, VITLPDYPGVDADNIK; HS26-3, EVARPNNYAGALYDPR; HS26-4, SVAVPVDILDHDNN YELK; HS26-5, NQILVSGEIPSTLNEESKDKVK; ENO-1, LNQLLR; ENO1-2, LGANAILGV SLAASR; ENO1-3, AVDDFLISLDGTANK; ENO1-4, IEEELGDNAVFAGENFHHGDKL; DCP1-1, YLFER; DCP1-2, YGGVYVGTLSKPEVK; DCP1-3, IRNATFPGVQMKFVLQK; DCP1-4, AQYNEIQGWDHLS LLPTFGAK; DCP1-5, TTYVTQRPVYLGLPANLVDLNVPAK.

[b] M_r (cal) is the average mass of the unlabeled (H_{10}-) peptides and ΔM_r (cal) the theoretical difference in average M_r values for the H_{10}- and D_{10}- peptides calculated using Iso Pro 3.0 software (http://www.i-mass.com).

[c] ΔM_r (obs) is the observed difference in average M_r between H_{10}- and D_{10}- peaks in the MALDI-ToF mass spectra of each peptide determined by the Data Explore 4.0 software (Applied Biosystems).

[d] H_D/H_H is the ratio of the peak-centroid-heights of D_{10}- and H_{10}- peptides determined by the Data Explore 4.0 software.

Table 6.2. Relative expression levels (REL)[a] of *S. cerevisiae* proteins grown on H_{10}- and D_{10}-Leu[b]

Protein	REL D:H=1:3	REL D:H=1:1	REL D:H=3:1	REL (Avg)[c]
TPI1	0.36±0.02	1.08±0.04	3.04±0.13	1.06
HS26	0.32±0.06	1.00±0.18	3.15±0.23	1.00
ENO1	0.33±0.06	0.99±0.23	3.07±0.21	1.00
DCP1	0.33±0.07	1.07±0.17	2.85±0.32	1.00

[a] RELs determined from H_D/H_H values given in Table 6.1.

[b] See footnotes to Table 6.1.

[c] Average value of RELs following normalization of mixtures to D:H = 1:1

Currently, several research groups are exploring methodologies for quantitative proteomics using different labeling and analytical techniques. A quantitative description of the protein expression and posttranslational modification (phosphorylation) in *S. cerevisiae* was obtained by analyzing strains grown on unlabeled and uniformly ^{15}N-labeled rich media (Cambridge Isotope Labs) by MALDI-ToF-MS and LC-ESI-MS-MS [248]. Comparative growth curves were not shown [248] so the results cannot be compared with those obtained here (Figure 6.1B). Another group used stable isotope depleted media (^{13}C-, ^{15}N- and ^{2}H- depleted) and Fourier transform ion cyclotron resonance MS (FTICR-MS) to compare the cadmium stress response in *E. coli* [237]. Furthermore, technology for quantifying proteomics based on isotope-coded affinity tags (ICAT) [249] has been marketed (Applied Biosystems). These three approaches provide quantitative information on protein expression levels although some disadvantages exist, such as high cost of labeling as well as low cell growth in the labeling media [246].

Our approach has several advantages compared to the others. First of all, it is easy to obtain high amounts of stable-isotope-labeled protein at very low cost ($0.05 *vs* $200

to label 100 μg protein with an ICAT) since the use of minimal D_{10}-Leu reduces the cost of labeling by a factor of five. Secondly, the mass shift can be predicted based on the protein sequence, and it provides an additional parameter for protein identification using relatively low cost linear MALDI-ToF instrumentation. Thirdly, the relative expression levels of low-abundance proteins can still be determined after any number of sample pre-fractionation steps. In addition, since special auxotrophic strains for labeling are readily available, the present approach should have broad application in quantitative proteomics involving different strains of *S. cerevisiae*, *E. coli* [250] or of any microorganisms with sequenced genomes [251]. In some cases, our current MS approach could also replace radioactive isotopic labeling methods for exploring the time-frame of proteome alteration in yeast and other organisms under challenging conditions, such as exposure to ultraviolet light or oxidative stress. We will investigate mitochondrial protein expression in wild-type *S. cerevisiae* and its *ccp1Δ* mutant using the approach outlined here.

6.6 Conclusions

S. cerevisiae strains grown on synthetic complete media with D_{10}-Leu yield high quantities of D_{10}-labeled proteins at low cost. Incorporation of D_{10}-Leu into yeast proteins was essentially stoichiometric with no metabolism of the label under our growth conditions. The label provided an effective internal mass calibrant for proteome comparisons using linear MALDI-ToF-MS. The relative abundance of each labeled protein, reflected in the intensities of its peptide peaks, corresponded closely to the amount of labeled culture used. The mass differences between peptides from yeast grown on H_{10}- and D_{10}-Leu indicate the number of Leu residues in the peptides and provide an additional parameter for identification.

6.7 Acknowledgement

I thank Macros Difalco, McGill University, Montreal, for technical assistance in carrying out the MALDI-ToF measurements. We are grateful to Dr. Farida Mohamed for her thoughtful discussions and help in preparing this manuscript.

Appendix 6.1. Preparation of yeast cell lysate for 2DE analysis

Cells harvested from 2 mL aliquots of yeast culture by centrifugation at 5000×g at 4°C for 2 min were washed with ice-cold phosphate buffered saline (pH 7.4) twice and resuspended in 300 μL of lysis solution [10 mM sodium fluoride (Fisher), 10 mM sodium chloride (Bioshop) and a complete protease inhibitor cocktail (yielding 1 mM EDTA, Roche Applied Science) in 20 mM Tris-HCl (pH 7.6, Fisher)]. The cells were mixed with an equal volume of acid-washed glass beads and vortexed vigorously for 4×30 s with 30-s intervals for cooling on ice between votexing. Cell debris was removed by centrifugation at 5000×g at 4°C for 2 min, the supernatant was transferred to a clear tube and mixed with 0.5 μL of Benzonase® nuclease (Novagen) to degrade DNA and RNA. The tubes were incubated on ice for 6 min, 225 μL of SDS solution [0.6% SDS in 0.1 M Tris-HCl (pH 8.0)] was added, and the samples were immediately heated at 100°C for 1 min before being cooled on ice and centrifuged at 13000×g at 4°C for 2 min. The supernatant was stored at –80°C after the protein concentration was determined using the Bio-Rad *DC* protein assay. The cell lysate was mixed with a 4× volume of ice-cold acetone and incubated at –20°C for 2 h to precipitate the proteins. The supernatant was removed following centrifugation at 13000×g for 30 min at 4°C, and the pellet was dissolved to a protein concentration of 2.5 mg/mL in isoelectric focusing (IEF) sample buffer (Section 5.3). After a 1-h incubation at 30°C, the proteins were separated by IEF (Section 5.3).

7 Evaluation of D_{10}-Leu metabolic labeling coupled with MALDI-MS analysis in studying the response of the yeast proteome to H_2O_2 challenge

7.1 Abstract

An efficient D_{10}-Leu metabolic-labeling method combined with isotope-ratio quantitation by MALDI-ToF MS was used to probe the response of the yeast proteome to H_2O_2. Control cultures correct for effects not associated with H_2O_2 challenge, and a stress-response index to H_2O_2 ($SRI_{H_2O_2}$) is defined. $SRI_{H_2O_2}$ values are reported for seven proteins at 45–225 min following exposure to 0.4 mM H_2O_2. The time course of protein accumulation in *unstressed* cells following the H_{10}- to D_{10}-SCD switch suggests that proteome responses at < 45 min could be monitored by addition of excess D_{10}-Leu to H_{10}-cultures.

7.2 Introduction

Metabolic labeling combined with mass spectrometry (MS) is frequently used for quantitative proteomics [252, 253]. We have developed a metabolic-labeling method for both qualitative and quantitative comparison of yeast proteomes in whole-cell lysates based on stoichiometric incorporation of perdeuterated leucine (D_{10}-Leu) into the organism's proteins [219]. A leucine auxotrophic yeast strain is grown on synthetic complete medium (SC) plus glucose (D) with either natural abundance leucine (H_{10}-Leu) or D_{10}-Leu, the cultures are mixed prior to protein separation by two-dimensional electrophoresis (2DE), and the proteomes are compared by isotope-ratio quantitation using matrix-assisted laser desorption ionization-time-of-flight (MALDI-ToF) MS [219]. The relative abundances of H_{10}- and D_{10}-proteins are determined from the intensities of their peptide peaks, and D_{10}-Leu labeling provides an effective internal calibrant for

quantitation by MS. The number of Leu residues per peptide yields an additional parameter for peptide and protein identification.

Changes in global protein expression have been examined in stressed yeast cells by a number of methods. A comparison of 2D gels was used to explore proteome responses to the mild physiological stress associated with the diauxic shift in *S. cerevisiae* [124]. Image analysis of the 2D gels from YPD cultures of early-exponential- and diauxic-phase yeast revealed 33 induced and 27 repressed proteins that were identified by peptide mass fingerprinting (PMF) using the Mascot search engine [129]. Responses to 15 metals were studied by differential in-gel electrophoresis (DIGE) by labeling control and metal-treated yeast protein extracts with two different fluorescent dyes, and the combined extracts were subjected to 2DE. Scanning the gels at different wavelengths identified over 50 proteins (out of ~400 protein spots) that exhibited significant changes in expressions in the treated and control cells [126]. Metabolic incorporation of ^{35}S-Met into proteins was used to probe proteome alteration at 30 min after exposure of *S. cerevisiae* to 0.2–0.8 mM H_2O_2 [125]. Both ^{35}S-labeled treated and control cultures were mixed with a ^{3}H-labeled culture prior to cell lysis to correct for variations in the 2DE analysis unrelated to H_2O_2-treatment. Comparisons of the $^{35}S/^{3}H$ ratios from the two gels revealed that 115 proteins were induced and 52 repressed by H_2O_2.

In the present work, we evaluate the use of our published D_{10}-Leu metabolic labeling/MS approach [219] to study the response of the yeast proteome to oxidative stress. Since proteins were stable-isotope-labeled, proteome alteration could be explored over an extended period of time following the challenge. Specifically, we examined proteome alteration in *S. cerevisiae* at 45–225 min following challenge with 0.4 mM

H_2O_2, and monitored protein accumulation in *unstressed* cells following a medium switch. The latter revealed methods to further optimize our D_{10}-Leu labeling approach.

7.3 Materials and methods

7.3.1 Materials

Regents were purchased from Sigma except where indicated. All reagents were used as supplied.

7.3.2 Cell growth and protein separation by 2DE

S. cerevisiae W303-1B cells (*MATα ade2*-1 *his3*-11,15 *leu2*-3,112 *ura3*-1 *trp1*-1 *can1*-100) [87], kindly provided by Dr. P. J. Hanic-Joyce (Concordia University), were grown to early-exponential phase (OD_{600} ~0.5) under high aeration in 100 mL of SC with 2% glucose and 80 mg/L H_{10}-Leu (H_{10}-SCD) in 500-mL flasks at 30°C while shaking at 225 rpm. Cells were washed twice with sterile 0.85% saline and transferred to 100 mL of SC with 2% glucose and 80 mg/L D_{10}-Leu [99.4% $(CD_3)_2CDCD_2CD(NH_2)COOH$, CDN Isotopes, Montreal] (D_{10}-SCD). The culture was divided into two portions: 100 µL of 200 mM H_2O_2 was added to one portion to give a final H_2O_2 concentration of 0.4 mM and 100 µL of 0.85% saline was added to the control. Incubation at 30°C with shaking at 225 rpm was continued and the consumption of H_2O_2 was determined by monitoring the HRP-catalyzed oxidation of ABTS (Roche Applied Science) at 405 nm [254] on a Beckman Coulter DU800 spectrophotometer. Aliquots (2 mL) were removed after 45, 90, 135, 180 and 225 min, and cell lysis and 2DE separation were performed as previously described [219]. To establish the effects on protein expression of washing the cells and replenishing the nutrients, growth in H_{10}-SCD was monitored under the same conditions with no medium switch.

7.3.3 In-gel digestion and MALDI-ToF MS analysis

Protein in-gel digestion was performed using the Montage In-Gel Digest$_{zp}$ Kit as per the manufacturer's instructions (Millipore). Multiple polyacrylamide slices were simultaneously digested and purified for MS analysis using the kit's disposable 96-well ZipPlate with C18 filters [255]. Samples were mixed with an equal volume of matrix solution [10 mg/mL α–cyano-4-hydroxycinnamic acid dissolved in 50% acetonitrile (Fisher) + 50% ethanol (Commercial Alcohol, Montreal)] and spotted on a stainless steel MALDI target plate (Waters Micromass). Tryptic peptides were analyzed using a Waters Micromass MALDI-ToF mass spectrometer (Model BAA037) in reflector mode. The ToF mass analyzer was found to have a mass accuracy of 50 ppm using the MH^+ ions of angiotensin I, renin and adrenocorticotropic hormone (18–39 clip) at m/z 1296.6853, 1758.9331 and 2465.1989, respectively, as external mass calibrants. Peptide mass maps were averaged over 100 laser shots, and isotopic clusters were collapsed to single peaks using the smoothing parameters (mean, smooth window ±20, number of smoothes 2) of the Masslynx 4.0 software. Between 5 and 11 peaks in the maps of the H_{10}-proteins were used in their identification by PMF using the *S. cerevisiae* database in NCBI and the Mascot search engine [129] (http://www.matrixscience.com/search_form_select.html). The number of missed cleavages was set as 2 and mass tolerance as 200 ppm.

Peak-centroid-heights output by the Masslynx software from the mass maps of the H_{10}-proteins (h_H) represent their expression levels before H_2O_2 exposure and the h_D values for the corresponding D_{10}-proteins indicate the incremental protein synthesis following the H_{10}- to D_{10}-SCD switch. Using data only from Leu-containing peptides that exhibited isolated MALDI peaks, the average h_D/h_H ratio (R) for a given protein was

calculated. A stress-response index (SRI) is defined for each protein using its R value from stressed and control cultures. Thus, $SRI_{H_2O_2}$ ($R_{H_2O_2}/Rc$) quantitatively measures the response of the cells to H_2O_2 exposure at the level of a given protein, and $SRI_{H_2O_2} > 1$ (< 1) indicates that expression of the specified protein is induced (repressed) by H_2O_2. The workflow is outlined in Figure 7.1.

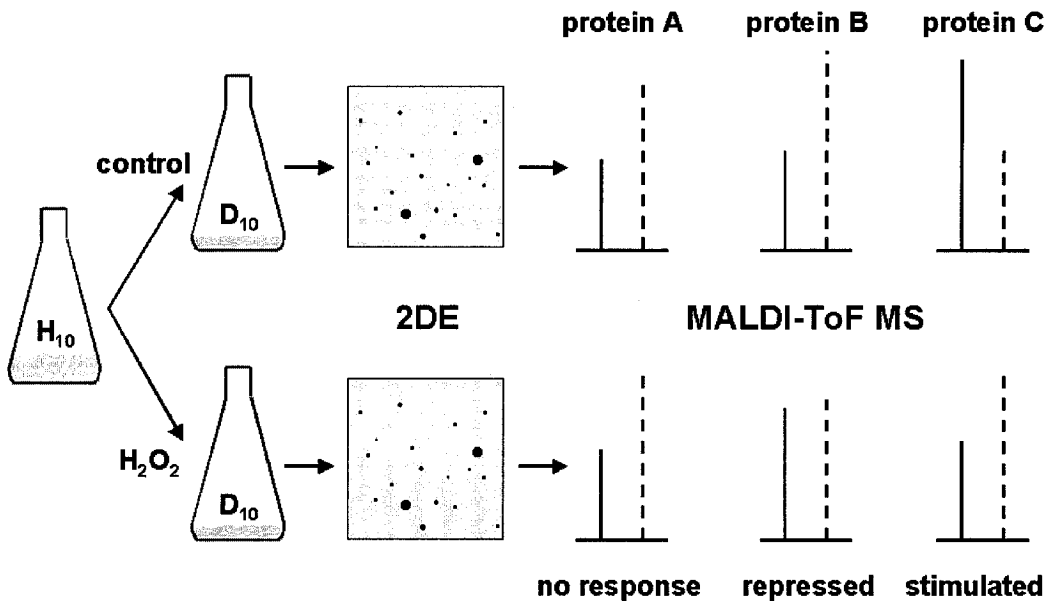

Figure 7.1. Workflow to quantify proteome response to H_2O_2. *S. cerevisiae* cells challenged with H_2O_2 following transfer from H_{10}- to D_{10}-SCD were harvested at different times, proteins were separated by 2DE and their tryptic digests analyzed by MALDI-ToF MS. Peak heights of the H_{10}-peptides (h_H, solid lines) and D_{10}-peptides (h_D, dashed lines) of Leu-containing peptides were measured, and the average value of h_D/h_H (R) revealed the incremental expression of a protein following the H_{10}- to D_{10}-SCD switch. The stress-response index to H_2O_2 ($SRI_{H_2O_2}$) obtained from $R_{H_2O_2}/Rc$, the R values of the challenged and control cells, respectively, gives a quantitative measure of the effect of H_2O_2 exposure on the expression of a given protein isolated in a single 2DE experiment.

7.4 Results

7.4.1 Yeast growth

Cells were transferred to fresh D_{10}-SCD at OD_{600} ~0.5 and challenged with 0.4 mM H_2O_2 at t = 0 min. The OD_{600} of the H_2O_2-exposed culture increased from 0.49 to

1.44 at t = 225 min while that of the control increased to 2.10 (Figure 7.2), which demonstrates the inhibitory effect of H_2O_2 on yeast growth. The H_2O_2 concentration decreased to 0.24 mM, 0.07 mM and 0.005 mM at t = 45, 90 and 135 min, respectively (Figure 7.2), revealing that the added H_2O_2 was essentially consumed after 135 min. The switch to fresh SCD at OD_{600} ~0.5 caused a similar stimulatory effect on cell growth (~10% at t = 225 min) in the presence and absence of H_2O_2 (Figure 7.2). Since we have shown previously that cells exhibit the same growth curves in H_{10}- and D_{10}-SCD [219], the growth spurt after the medium switch is attributed to the increased glucose content and optimal pH of fresh D_{10}-SCD.

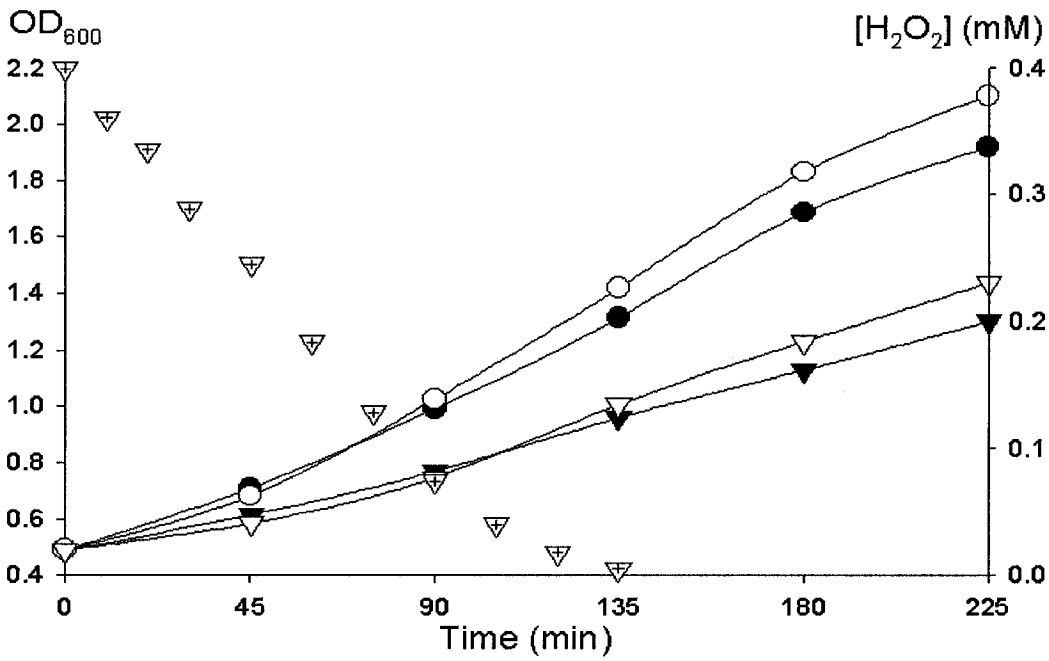

Figure 7.2. Effects of challenge with 0.4 mM H_2O_2 on cell growth. *S. cerevisiae* cells grown to early-exponential phase (OD_{600} ~0.5) in H_{10}-SCD at 30°C with shaking (225 rpm) were washed twice with sterile 0.85% saline and transferred to D_{10}-SCD. At t = 0 min, cells were challenged with 0.4 mM H_2O_2 and cell growth (left y-axis) monitored by measuring the OD_{600} of the H_2O_2-treated culture (open triangles) and of the untreated control culture (open circles). Growth in H_{10}-SCD without the transfer to fresh medium is also shown for 0.4 mM H_2O_2-treated (closed triangles) and untreated control cells (closed circles). The H_2O_2 concentration remaining in fresh SCD during growth (right y-axis, open triangles with +) was determined by monitoring the HRP-catalyzed oxidation of ABTS at 405 nm [254].

7.4.2 Protein separation and identification

Figure 7.3 compares the 2DE gels of control and stressed cells harvested at t = 180 min following exposure to 0.4 mM H_2O_2. Seven spots containing abundant proteins within mass and pI ranges of 26–62 kDa and 5.3–6.2 were selected for quantitation. The monoisotopic masses of 5–11 tryptic peptides from each of the selected H_{10}-proteins were used for protein identification. The labels on the spots are the Mascot search results of PMF [129] using the *S. cerevisiae* database in NCBI and the proteins are listed in Table 7.1.

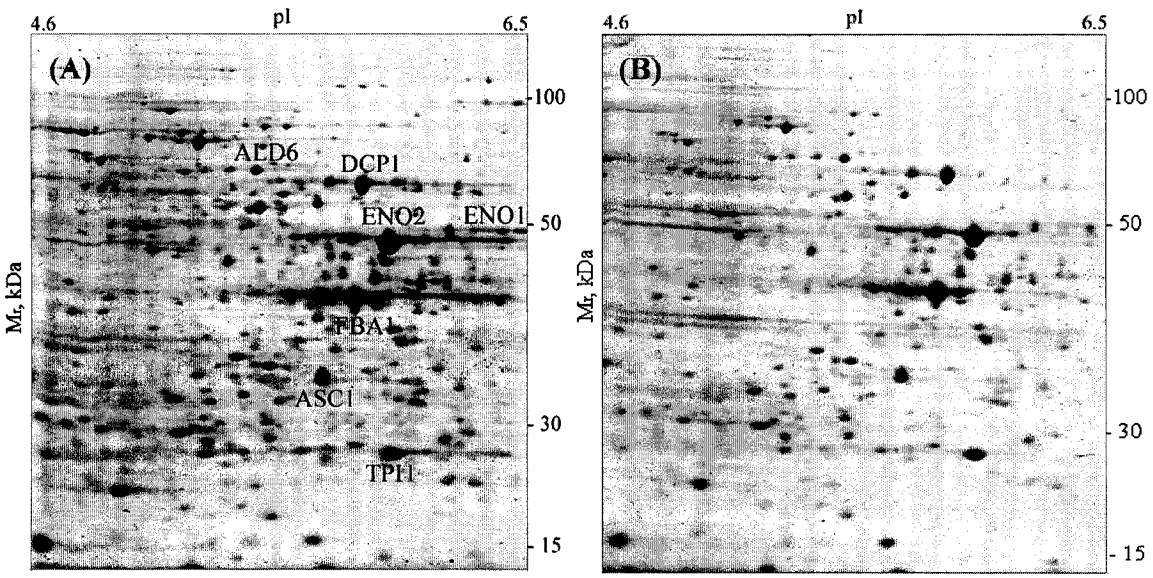

Figure 7.3. 2DE gels showing protein expression at t = 180 min after *S. cerevisiae* cells were switched to D_{10}-SCD (A) without and (B) with exposure to 0.4 mM H_2O_2. Proteins were separated on 10% polyacrylamide 7×10-cm gels in the first (horizontal) dimension by isoelectric focusing based on pI and in the second (vertical) dimension by SDS-PAGE based on mass. The labels on the spots are proteins identified by PMF using the *S. cerevisiae* database in NCBI with the Mascot search engine [129].

Table 7.1. Proteins selected from the 2DE gels for analysis[a]

Protein	M_r (kDa)	pI	% sequence coverage[b]	No. of peptides for quantitation[c]
ALD6 (aldehyde dehydrogenase)	54.4	5.31	33 (11)	2
DCP1 (pyruvate decarboxylase)	61.5	5.80	18 (7)	6
ENO1 (enolase 1)	46.8	6.16	36 (11)	4
ENO2 (enolase 2)	46.9	5.67	34 (11)	5
FBA1 (fructose-bisphosphate aldolase)	39.6	5.51	22 (5)	3
TPI1 (triosephosphate isomerase)	26.6	5.75	35 (7)	3
ASC1 (ribosomal protein)	34.8	5.80	24 (5)	4

[a] Proteins from the labeled spots in Figure 7.3 were identified by PMF using the *S. cerevisiae* database in NCBI with the Mascot search engine [129].

[b] Percentage of amino acid residues identified in the proteins and the number of matched peptides (in parenthesis) in the MALDI peptide mass maps of proteins from H_{10}-cultures.

[c] Number of Leu-containing tryptic peptides chosen for isotope-ratio quantitation (Table S7.4A).

7.4.3 Isotope-ratio quantitation by MALDI-ToF MS

Figure 7.4A shows the MALDI peaks of four H_{10}-TPI1 tryptic peptides with zero (TFFVGGNFK), one (WVI***L***GHSER) and two (ADVDGF***L***VGGAS***L***KPEFVDIINSR and DKADVDGF***L***VGGAS***L***KPEFVDI INSR) Leu (***L***) residues. Figures 7.4B and C show the same peptides from control and H_2O_2-stressed cells harvested at t = 180 min after the challenge. The peaks of the Leu-containing peptides appear as doublets with $\Delta M_r \sim n \times 9$ u rather than the expected $n \times 10$ u on D_{10}-Leu peptide labeling since H/D exchange occurs at the Leu α-carbon in the MALDI source [219, 243, 256]. Due to differential protein processing and modification, multiple spots can arise from a single gene and be detected on 2D gels [235]. Since we have observed that such spots (*e.g.*, the spots for ENO1 as well as those for ENO2, data not shown) exhibit the same R values, only a single spot from each protein was selected and quantitatively analyzed.

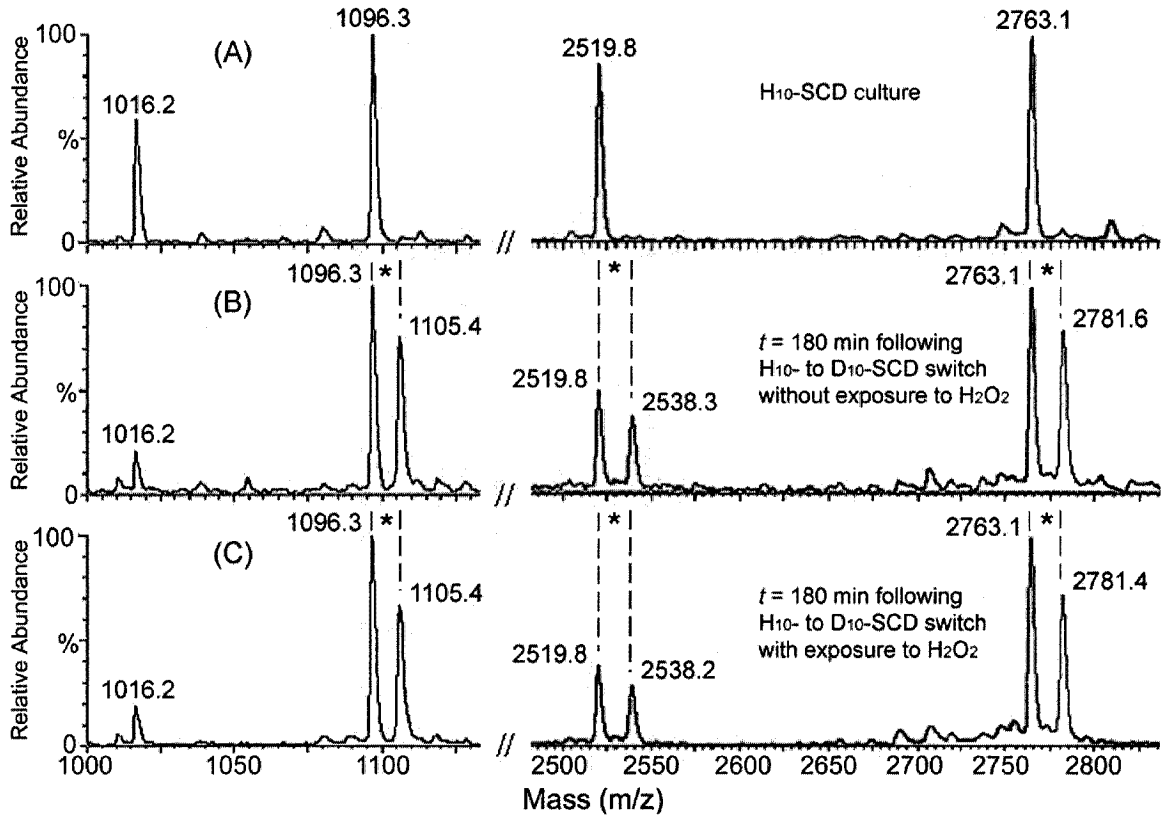

Figure 7.4. MALDI-ToF peptide mass maps of protein TPI1. (A) Map of TPI1 from the H_{10}-culture. (B) Map of TPI1 at 180 min following the H_{10}- to D_{10}-SCD switch without and (C) with exposure to 0.4 mM H_2O_2. Peptide mass maps were averaged over 100 laser shots and isotopic clusters were collapsed to single peaks using the smoothing parameters (mean, smooth window ±20, number of smoothes 2) of the Masslynx 4.0 software. D_{10}-Leu-labeled peptide peaks are mass shifted by $n \times 9$ u where n is the number of Leu residues in the peptide (see text) [219]. The peptides with theoretical average M_r values of 1016.2 u (TFFVGGNFK), 1096.3 u (WVI**L**GHSER), 2519.8 u (ADVDGF**L**VGGAS**L**KPEFVDIINSR) and 2763.1 u (DKADVDGF**L**VGGAS**L**KPEFVDIINSR) were identified by PMF using the *S. cerevisiae* database in NCBI with the Mascot search engine [129]. Paired peaks are indicated by an asterisk (*).

The h_D/h_H ratios and hence the R values increase with time (Table 7.2), reflecting the accumulation of D_{10}-TPI1 following the H_{10}- to D_{10}-SCD switch. Isolated peaks of 3 Leu-containing peptides were chosen for isotope-ratio quantitation of TPI1 and 2–6 peptides for the other proteins (Tables 7.1 and S7.4). Table 7.2 summarizes the R values

of the seven proteins obtained between 45–225 min for H_2O_2-challenged ($R_{H_2O_2}$) and control cells (Rc).

Table 7.2. Average %R values of six glycolytic enzymes and the ribosomal protein ASC1 at 45–225 min following challenge of *S. cerevisiae* with H_2O_2[a]

Protein and function[b]			%R[c]				
			45 min	90 min	135 min	180 min	225 min
ALD6	glycolysis	$R_{H_2O_2}$	13 ± 1.7	28 ± 5.4	69 ± 4.8	137 ± 0.4	185 ± 2.2
		Rc	18 ± 2.1	41 ± 3.3	67 ± 8.1	139 ± 8.1	186 ± 5.5
DCP1	glycolysis	$R_{H_2O_2}$	7.0 ± 1.3	17 ± 1.8	56 ± 3.3	123 ± 7.4	146 ± 6.6
		Rc	8.5 ± 1.1	19 ± 2.5	54 ± 4.7	127 ± 7.1	155 ± 9.6
ENO1	glycolysis	$R_{H_2O_2}$	7.9 ± 1.2	10 ± 0.8	13 ± 1.8	60 ± 4.0	98 ± 3.3
		Rc	6.2 ± 0.7	9.0 ± 1.1	15 ± 1.8	68 ± 8.9	110 ± 8.1
ENO2	glycolysis	$R_{H_2O_2}$	5.2 ± 1.0	9.6 ± 1.7	21 ± 2.3	40 ± 4.3	87 ± 6.4
		Rc	6.7 ± 0.9	11 ± 1.1	21 ± 2.0	41 ± 3.7	95 ± 10
FBA1	glycolysis	$R_{H_2O_2}$	9.7 ± 1.6	15 ± 1.4	36 ± 0.4	90 ± 6.2	156 ± 4.7
		Rc	15 ± 0.5	18 ± 3.0	38 ± 5.1	99 ± 1.4	150 ± 10
TPI1	glycolysis	$R_{H_2O_2}$	7.0 ± 1.4	13 ± 1.3	30 ± 3.8	72 ± 2.2	104 ± 6.0
		Rc	7.4 ± 1.2	14 ± 1.8	32 ± 1.5	78 ± 2.1	114 ± 2.1
ASC1	protein synthesis	$R_{H_2O_2}$	8.8 ± 1.3	27 ± 1.4	81 ± 7.1	146 ± 14	158 ± 9.1
		Rc	8.4 ± 1.2	28 ± 3.7	81 ± 6.6	146 ± 11	163 ± 13

[a] Early-exponential phase (OD_{600} ~0.5) cells (W303-1B strain) were challenged with 0.4 mM H_2O_2 at t = 0 min, cells were harvested at t = 45–225 min and their proteomes analyzed by 2DE and MALDI-ToF MS.

[b] Protein identities are given in Table 7.1 and their functional categories were obtained from the CYGD [41].

[c] %R = h_D/h_H ×100% averaged over 2–6 Leu-containing tryptic peptides (Footnote *c*, Tables 7.1 and S7.4) of the protein isolated in a single 2DE experiment; h_D (h_H) is the centroid-height of a D_{10}-peptide (H_{10}-peptide) peak in the MALDI mass map. $R_{H_2O_2}$ and Rc are the %R values for H_2O_2-challenged and control cells, respectively.

7.4.4 Effects of H_2O_2 challenge on glycolytic enzyme expression

The $SRI_{H_2O_2}$ of a protein is the ratio of its $R_{H_2O_2}$ and R_c values given in Table 7.2. The $SRI_{H_2O_2}$ values of the selected glycolytic enzymes and the ribosomal protein ASC1 [41] at t = 45–225 min after challenge with 0.4 mM H_2O_2 are summarized in Table 7.3. The published values [125] of the relative synthesis rates of the ^{35}S-Met- labeled proteins in challenged cells and the control at t = 30 min are given in Table 7.3 for comparison, and Figure 7.5 outlines the function of the six glycolytic enzymes examined here.

Table 7.3. $SRI_{H_2O_2}$ values of six glycolytic enzymes and the ribosomal protein ASC1 at 30–225 min following challenge of *S. cerevisiae* with H_2O_2

Protein[b]	$SRI_{H_2O_2}$[a]					
	30 min[c]	45 min[d]	90 min[d]	135 min[d]	180 min[d]	225 min[d]
ALD6	0.52	0.72 ± 0.13	0.68 ± 0.14	1.0 ± 0.14	0.99 ± 0.06	0.99 ± 0.03
DCP1	0.27	0.82 ± 0.19	0.89 ± 0.15	1.0 ± 0.11	0.97 ± 0.08	0.94 ± 0.07
ENO1	1.6	1.3 ± 0.24	1.1 ± 0.16	0.87 ± 0.16	0.88 ± 0.13	0.89 ± 0.07
ENO2	0.37	0.78 ± 0.18	0.87 ± 0.18	1.0 ± 0.15	0.98 ± 0.14	0.92 ± 0.12
FBA1	1.0	0.65 ± 0.11	0.83 ± 0.16	0.95 ± 0.13	0.91 ± 0.06	1.0 ± 0.08
TPI1	1.0	0.95 ± 0.24	0.93 ± 0.15	0.94 ± 0.13	0.92 ± 0.04	0.91 ± 0.06
ASC1	NR	1.0 ± 0.22	0.96 ± 0.14	1.0 ± 0.12	1.0 ± 0.12	0.97± 0.10

[a] Stress-response index to H_2O_2; $SRI_{H_2O_2} > 1$ (< 1) indicates that the protein is induced (repressed) by H_2O_2.

[b] See Footnote *a* of Table 7.1 for protein identification.

[c] Data from Ref. [125]. Early-exponential phase (OD_{600} ~0.3) *S. cerevisiae* (strain YPH98) cells were challenged with 0.2–0.8 mM H_2O_2 at t = 0 min. Proteins were pulsed-labeled with ^{35}S-Met at t = 15 min and separated by 2DE at t = 30 min. $SRI_{H_2O_2}$ values are the relative rates of instantaneous protein synthesis determined from 2DE protein gels from treated and control cultures. $SRI_{H_2O_2}$ values ≤ 1 were determined using cultures challenged with 0.4 mM H_2O_2, and the ENO1 $SRI_{H_2O_2}$ is the maximum value for cultures challenged with 0.2–0.8 mM H_2O_2 [125]. NR, not reported [125].

[d] $SRI_{H_2O_2}$ calculated from the $R_{H_2O_2}$/Rc values in Table 7.2. Experimental conditions are given in Footnote *a*, Table 7.2.

FBA1 catalyzes the cleavage of fructose 1,6-diphosphate to dihydroxyacetone phosphate and glyceraldehyde-3-phosphate while TPI1 catalyzes the interconversion of the two product triose phosphates. The FBA1 protein synthesis rate was unchanged 30 min after the H_2O_2 challenge [125], but we report $SRI_{H_2O_2}$ values of 0.65±0.11 at t = 45 min and 0.91±0.06 at t = 180 min (Table 7.3). The TPI1 synthesis rate at t = 30 min was also unaffected by H_2O_2 [125], and this protein exhibited $SRI_{H_2O_2}$ values of 0.91–0.95 at t = 45–225 min (Table 7.3). The ENO1 and ENO2 isozymes, which are involved in the metabolism of glyceraldehyde-3-phosphate to pyruvate (Figure 7.5), were differentially expressed during the oxidative-stress response. ENO1 translation was initially induced by 1.6-fold and ENO2 repressed by 2.7-fold at t = 30 min [125], and we found that ENO1 remained induced and ENO2 repressed over 90 min (Table 7.3). Reverse regulation of the enolase isozymes was also reported in respiring and non-respiring exponential-phase yeast cells: ENO1 protein levels were up-regulated by 2.4-fold and ENO2 down-regulated by 3.0-fold in SCE compared to SCD [236]. DCP1, which catalyzes the conversion of pyruvate to acetaldehyde, and ALD6, one of several yeast isoenzymes that catalyze acetaldehyde dehydrogenation to acetate (Figure 7.5), were both repressed by H_2O_2 at t = 30–90 min (Table 7.3).

The $SRI_{H_2O_2}$ values of the six glycolytic proteins approached unity at t = 135 min (Table 7.3). Thus, glycolysis likely returned to basal level at t ~2 h which, under the conditions described here, corresponds to the time required for H_2O_2 consumption (Figure 7.2). Interestingly, the $SRI_{H_2O_2}$ of ASC1, a ribosomal protein involved in protein synthesis, remained close to unity at t = 45–225 min (Table 7.3).

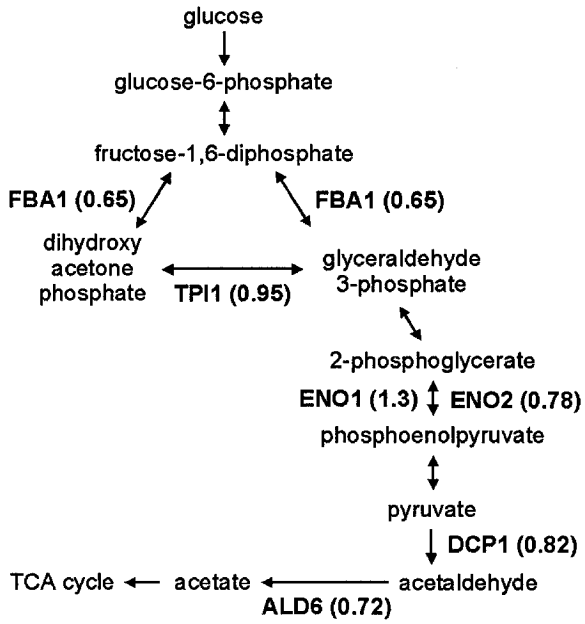

Figure 7.5. Glycolysis in yeast. Only pathways involving the enzymes studied here (bold font) are mapped. TCA, tricarboxylic acid. Protein $SRIH_2O_2$ values at 45 min following exposure to 0.4 mM H_2O_2 are given in parentheses.

7.4.5 Relative protein accumulation in unstressed cells

Variations in the accumulation of different proteins during cell growth in the absence of stressors can also be obtained from the R values. For example, the R value of ASC1, which is equal to the average h_D/h_H of four peptides, VFS***L***DPQY***L***VDD***L***RPEF AGYSK, GT***L***EGHNGWVTS***L***ATSAGQPN***LLL***SASR (Figure 7.6A), YW***L***AAATAT GIK and ***L***WDVATGETYQR (peaks not shown), increased from 0.28±0.04 at t = 90 min to 1.46±0.18 at t = 180 min (Figures 7.6B and C). Thus, 4-times less ASC1 accumulated in the 0–90-min interval compared to the 90–180-min interval after the H_{10}- to D_{10}-SCD switch.

Figure 7.7 summarizes the relative accumulation in early exponential-phase cells *vs* time of ASC1 plus the six glycolytic enzymes, ALD6, DCP1, ENO1, ENO2, FBA1 and TPI1. The relative accumulation of ALD6 (186%) at 225 min following H_{10}- to D_{10}-SCD switch was the highest while that of ENO2 (95%) was the lowest of the seven proteins examined. Since protein degradation was not detected in exponentially growing

yeast cells [236], either less ALD6 accumulated before the medium switch or more was newly synthesized after the switch compared to the other proteins. The data in Figure 7.7 also indicate that up-regulation during exponential growth of DCP1 and ALD6, which catalyze the two final steps of glycolysis (Figure 7.5), may possibly occur later than that of ENO2.

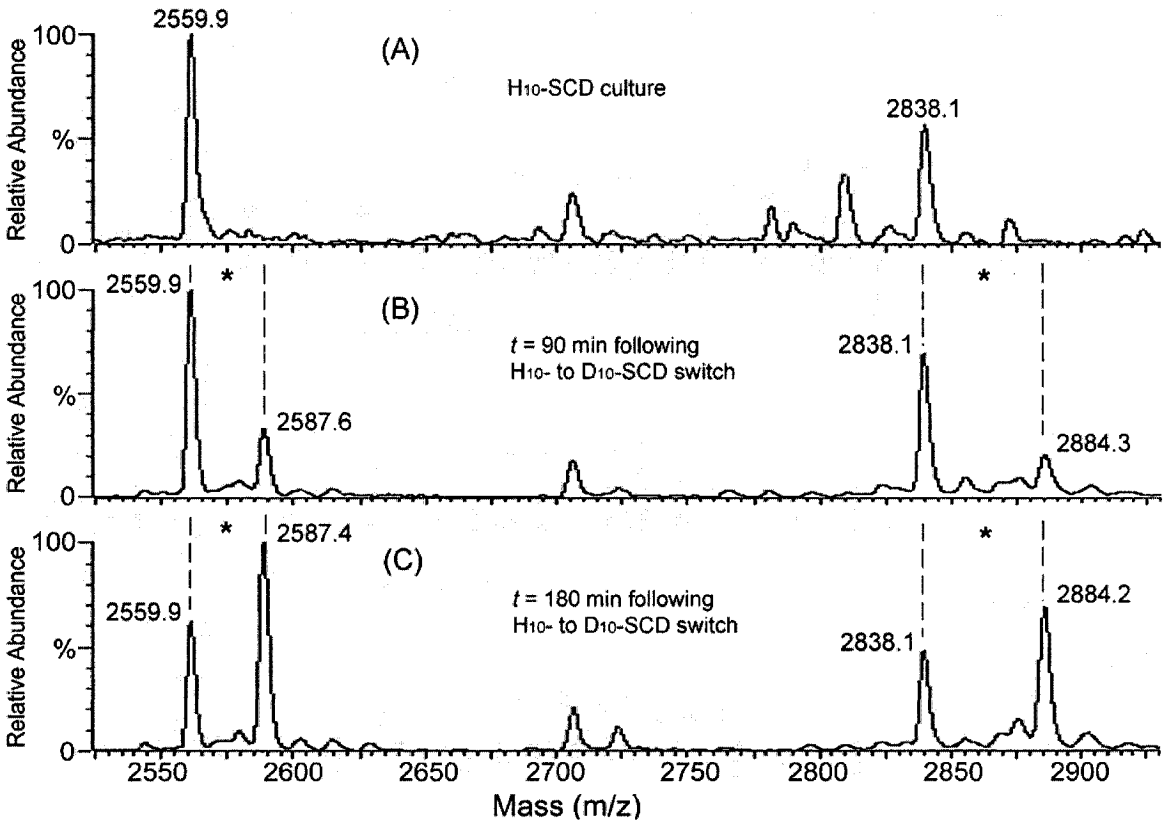

Figure 7.6. MALDI-ToF peptide mass maps of protein ASC1. (A) Map of ASC1 from the H_{10}-culture. (B) Map of ASC1 at 90 min and (C) at 180 min following the H_{10}- to D_{10}-SCD switch. Mass maps were recorded and the peptides with theoretical average M_r values of 2559.9 u (VFS***L***DPQY***L***VDD***L***RPEFAGY SK) and 2838.1 u (GT***L***EGHNGWVTS***L***ATSAGQPN***LLL***SASR) identified as described in the legend of Figure 7.4. Paired peaks are indicated by an asterisk (*).

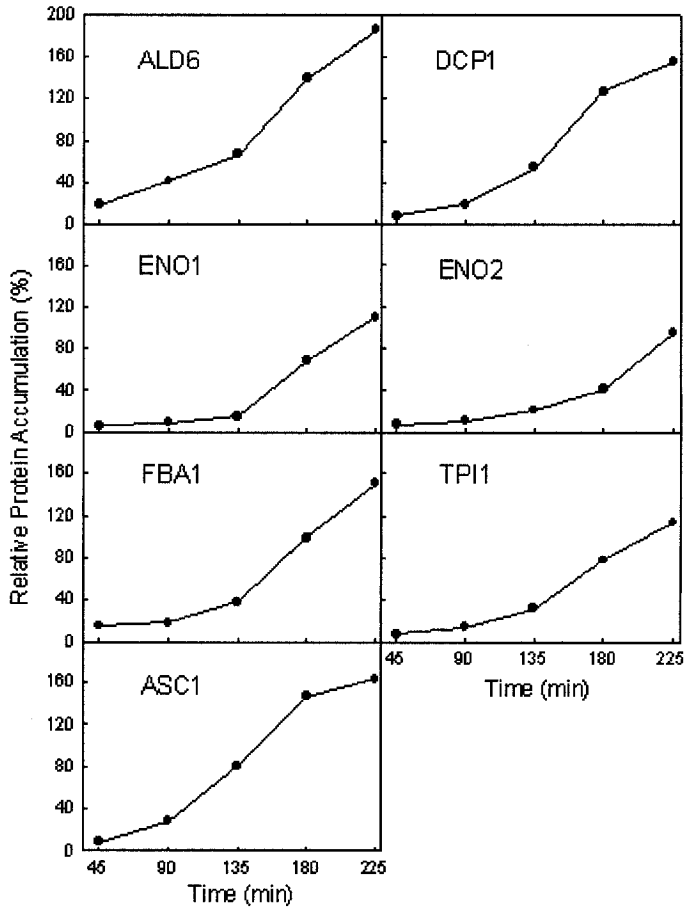

Figure 7.7. Relative protein accumulation in unstressed exponentially growing *S. cerevisiae* following medium change. Cells grown at 30°C to early-exponential phase (OD_{600} ~0.5) under high aeration with shaking at 225 rpm in H_{10}-SCD were transferred to D_{10}-SCD, harvested at t = 45, 90, 135, 180 and 225 min, and their proteins separated by 2DE. The H_{10}-peptide peak heights (h_H) in the MALDI mass maps were normalized to 100%. The relative accumulation at 45–225 min following the H_{10}- to D_{10}-SCD switch is given by the normalized h_D/h_H ratios of each protein averaged over 2–6 of its Leu-containing peptides (R values, see Footnote *c*, Table 7.2). A total of five 2DE gels were run to determine the R values given here (n =1).

7.5 Discussion

7.5.1 Use of stable *vs* radioisotopes in investigating a proteome's response to stress

Changes in protein expression have typically been measured using metabolic labeling with ^{3}H, ^{14}C and ^{35}S radioisotopes [26, 125, 127]. The latter, a β-emitter,

possesses higher energy than ^{3}H and a shorter half-life ($\tau_{1/2}$ = 87.4 days) than either ^{3}H or ^{14}C [257]. Since most proteins contain an N-terminal Met residue, ^{35}S-Met is commonly used to follow changes in protein expression following stress. However, due to the advances in biological mass spectrometry, stable-isotope labeling of biomolecules can now be followed by mass spectrometry obviating the use of radioisotopes [252].

The present metabolic labeling based on D_{10}-Leu incorporation into proteins [219] has several advantages over ^{35}S-Met labeling methods. First, it is easy to obtain large quantities of stable-isotope-labeled proteins at very low cost. Second, radioactive contamination during 2DE and MS analysis is avoided. Third, the ^{35}S β-emitting radioisotope causes severe injury to cells [258-260]. For example, metabolic labeling with 100 μCi/mL of ^{35}S-Met for 2 h was found to significantly inhibit cell-cycle progression and proliferation, induce apoptosis, and alter the morphology of mammalian cells [260]. The concentration of ^{35}S-Met commonly used for labeling yeast cells is 250–400 μCi/mL [125, 236, 261]. Fourth, ^{35}S-Met is chemically unstable during metabolic labeling since it can form volatile methyl mercaptan ($CH_3{}^{35}SH$) during incubation [262]. Fifth, ^{35}S-Met can be metabolically interconverted to ^{35}S-Cys [125, 261] whereas Leu is considered to be one of the most stable amino acids. For example, no label transfer from ^{14}C-Leu or ^{3}H-Leu to any other amino acids was detected after 5 h of metabolic labeling in exponentially growing yeast cells (OD_{600} ~0.3) [261]. Sixth Met is nonmetabolically incorporated into other proteins in the absence of cells [257]. Seventh, Leu is an abundant amino acid in proteins (9.0%) compared to Met (2.4%) [241], and 70% of tryptic peptides contain at least one Leu residue [263].

Because of its cytotoxicity, cells are pulse-labeled with ^{35}S-Met for 2–15 min to obtain instantaneous protein synthesis rates [125, 127, 236, 264]. Although this approach can be used to study proteome alteration at longer times following a challenge, changes in protein levels are more informative since protein synthesis rates vary considerably during stress [119]. The rate of protein degradation, which produces H_{10}-Leu to compete with D_{10}-Leu for incorporation into newly synthesized proteins, determines the upper time limit of our method. Contrary to a previous report that detected no protein degradation in exponentially growing yeast cells [236], a recent study using D_{10}-Leu metabolic labeling showed that 50 abundant proteins degraded at an average rate of 2.2% per hour in an aerobic yeast chemostat culture at steady state [265]. At this rate, <10% H_{10}-protein would be degraded in a four-hour period and would be corrected for by the control (R_c). Thus, the relative protein accumulation measured using our metabolic labeling/MS approach can provide accurate information on short- (45 min) and long term (4–5 h) proteome alteration. The latter is of interest since it took > 3 h to restore the basal rate of total protein synthesis in cells after 2 mM H_2O_2 was consumed [264].

Metabolic labeling with D_3-Leu was first used in 2002 to monitor proteome alterations during muscle differentiation in a mammalian cell line [266]. This was termed SILAC (stable isotope labeling with amino acids in cell culture) and in 2003, the same group introduced the use of $^{13}C_6$-Arg as a label [263]. Over 50% of peptides are labeled with $^{13}C_6$-Arg because trypsin specifically cleaves peptide bonds C-terminally of Arg and Lys residues. Proteins were fractionated by 1DE followed by trypsin digestion and isotope-ratio quantitation using LC-MS. $^{13}C_6$-Arg labeling can be combined with LC-MS analyses because $^{13}C_6$-Arg and $^{12}C_6$-Arg peptides coelute whereas D_3-Leu and H_3-Leu

peptides do not [263]. However, none of the commonly used laboratory yeast strains such as W303 [87], CEN.PK2 [70] and BY [267] are Arg auxotrophs, and the $^{13}C_6$-Arg label can scramble during metabolic labeling because of $^{13}C_6$-Arg interconversion to $^{13}C_5$-Pro [261, 263]. Furthermore, D_{10}-Leu labeling costs < 10% that of $^{13}C_6$-Arg labeling [263].

7.5.2 Metabolic *vs* chemical labeling of proteomes

A number of post-lysis chemical labeling methods for isotope-ratio quantitation of proteomes by LC-MS have recently been introduced [249, 268-270]. These include ICAT (isotope-coded affinity tags), AQUA (absolute quantification strategy), IDBEST (isotope-differentiated binding energy shift tags) and iTRAQ (isotope tags for relative and absolute quantification). All these methods required additional steps including chemical labeling and preconcentration of the labeled peptides by affinity columns, and the reagents used are very expensive.

Since image analysis of 2DE gels is widely used for low-cost, high-throughout proteomics, chemical labeling approaches have also been developed for quantitative gel-based proteomics. The DIGE technique, which allows up to three proteomes chemically labeled with different fluorescence dyes to be co-separated and visualized on one 2D gel [271], minimizes the effects of gel-to-gel variation in spot intensities associated with 2DE separation [245]. Additionally, the DIGE methodology provides a linear dynamic range over three orders of magnitude in protein concentration [271] *vs* the limited dynamic range of standard staining techniques (*e.g.*, silver staining offers a narrow range of 4–60 ng [244]). However, the DIGE approach highlights the problems frequently associated with chemical labeling. DIGE-labeled proteins exhibit altered solubility and migration in gels and may thus elude detection [242]. As a result, the number of spots detected in a

DIGE gel is about half that detected in a conventional silver-stained gel [272] despite the better detection sensitivity of the DIGE dyes [271]. Metabolic labeling overcomes the main limitations of DIGE and other chemical labeling methods because incorporation of isotopically labeled amino acids into a protein does not alter its migration or solubility [219].

7.5.3 Further optimization of D_{10}-Leu metabolic labeling for isotope-ratio quantitation

Since D_{10}-Leu metabolic labeling is inexpensive and the MALDI-ToF instrument is easy to maintain, optimization of the protocols described here is worth consideration. Linear correlations of MALDI-peak-intensity ratios with theoretical D/H ratios in mixtures of D_3-Leu labeled and unlabeled cells have been demonstrated up to 1:5 [273]. Since the %R values in Table 7.2 are < 20% at t = 45 min, it is desirable to increase the amount of labeled proteins at short times. Figure 7.7 shows that proteins are slowly synthesized in the 0–45-min interval after the H_{10}- to D_{10}-SCD switch; thus, cells could be grown for 1 h in the presence of D_{10}-Leu before challenged with H_2O_2. A total of 11 gels were run in this study to establish the proteome response to H_2O_2 at t = 45–225 min, and an additional control gel would be required to determine the amount of D_{10}-protein accumulated before exposure to H_2O_2. $SRI_{H_2O_2}$ would equal $(R_{H_2O_2} - R_0)/(R_c - R_0)$ where R_0 is calculated from h_D/h_H ratios of the stressed cells at t = 0 min.

It has been reported that transcription is depressed in yeast within 10 min of glucose withdrawal and immediately restored (≤ 2 min) upon re-addition of glucose [274]. Thus, washing exponentially growing yeast cells (OD_{600} ~0.5) with 0.85% saline prior to adding D_{10}-SCD appears to have inhibited protein synthesis for at least 45 min

(Figure 7.7), although no changes in cell growth were detected (Figure 7.2). To limit the inhibitory effects of glucose withdrawal on protein synthesis, a 2% glucose wash should be substituted for the saline wash. Another option would be to omit the medium switch altogether as is done in ^{35}S-Met metabolic labeling, which is carried out in yeast nitrogen base supplemented with 2% glucose and the nutrients essential for growth of the yeast auxotroph under study [125]. Newly synthesized proteins are efficiently pulse-labeled without a medium switch on addition of ^{35}S-Met allowing cells to avoid Met synthesis at large energetic expense [261]. Addition of excess H_{10}-Leu (*e.g.*, 300 mg/L) to cells grown in D_{10}-SCD containing minimal D_{10}-Leu (*e.g.*, 10–30 mg/L) would ensure 90–95% H_{10}-Leu incorporation into newly synthesized proteins, and would be only ~10% the cost of labeling cells grown in H_{10}-SCD with D_{10}-Leu. Since the cultures would be unperturbed except for H_{10}-Leu addition, protein accumulation in the 0–45-min interval should not be drastically reduced as seen after the saline wash (Figure 7.7).

Genome alteration in exponential-phase yeast (OD_{600} ~0.5) has been explored using a DNA microarray after cells were transferred from a fermentable (glucose) to a non-fermentable (glycerol) carbon source [275]. Our approach can be used to study global protein accumulation following a carbon-source shift. In outline, H_{10}-Leu (300 mg/L) plus glucose (20 g/L) or glycerol (30 mL/L) would be added to cells at OD_{600} ~0.5 in SC with minimal glucose (0.2%) and D_{10}-Leu (10–30 mg/L). Variations in protein expression due to the carbon-source shift would be quantifiable from the RG and RD values calculated from the h_H/h_D ratios measured at different times following the addition of H_{10}-Leu and glucose (D) or glycerol (G) to the cultures.

7.5.4 H_2O_2-induced inhibition of cell growth as viewed from a proteomics perspective

Yeast cells grow exponentially and produce ATP by glycolysis in the presence of glucose [192]. H_2O_2 can damage cells but it also participates in metabolic regulation [58, 71, 214, 276]. Down-regulating glycolysis would benefit H_2O_2-stressed cells by directing glucose-equivalents into the pentose phosphate pathway for the synthesis of NADPH [264], an electron donor to the glutaredoxin and thioredoxin systems crucial for antioxidant defense [209, 277]. Figure 7.2 reveals that although the 0.4 mM H_2O_2 added to a culture at OD_{600} ~0.5 was consumed within 135 min, the incremental growth between 135 and 180 min of stressed cells is ~75% that of unstressed cells. Thus, stressed cells likely use more of the ATP produced during glycolysis for antioxidant defense and repair compared to unstressed cells, which direct a larger fraction to cell multiplication.

Consistent with this view, stress genes including *CCP1*, *CTT1*, *SOD1*, *TSA1* and *TRX2* (encoding thioredoxin 2) remained 3–6-fold *induced* during a 160-min challenge of exponentially growing yeast with a constant amount (0.3 mM) of H_2O_2 [22]. In contrast, glycolytic genes such as *DCP1*, *ENO2*, *TPI1* and *TDH3* (encoding glyceraldehyde-3-phosphate dehydrogenase) were repressed for up to 120 min [22]. In a separate study, *TRX2* and *SAA1* (encoding a heat shock protein) remained 23- and 14-fold induced, respectively, 60 min following challenge of early-exponential phase (OD_{600} ~0.1) yeast with 0.4 mM H_2O_2 [26].

Rates of synthesis of antioxidant enzymes were found to be induced by 2–15-fold while glycolytic enzymes were up- or down-regulated by ~1–4-fold 30 min after 0.2–0.8 mM H_2O_2 exposure [125]. The data in Table 7.3 reveal that with the exception of ENO1,

expression of the glycolytic enzymes examined here was depressed by 0.4 mM H_2O_2 for $\geq$ 90 min. Also, enolase and other glycolytic enzymes including glyceraldehyde-3-phosphate dehydrogenase and alcohol dehydrogenase were found to be temporarily inactivated by *S*-thiolation following exposure of yeast cells to H_2O_2 [264]. Thus, H_2O_2-induced attenuation of glycolysis occurs by transcriptional, translational and post-translational mechanisms allowing the fine tuning of metabolism to benefit the stressed cells.

7.6 Conclusions

The D_{10}-Leu label provides an effective internal mass calibrant for isotope-ratio quantitation of proteomes by MALDI-ToF MS. The time frame of proteome alteration in yeast and other organisms following a challenge, such as exposure to oxidative stress or ultraviolet light, can be explored over extended time periods using our metabolic labeling/MS approach. For example, yeast glycolysis was found to be first inhibited and then restored within ~2 h after challenging cells with 0.4 mM H_2O_2. Although the controls can correct for effects not associated with H_2O_2 challenge, such as medium switch or protein degradation, the accuracy of our method at short times could be improved by adding excess H_{10}-Leu to D_{10}-SCD cultures instead of subjecting the cells to a medium switch, which perturbs protein synthesis. The current approach is proposed for studying the effects of carbon-source shifts on the yeast proteome over a wide range of time intervals.

7.7 Supporting Information Available:

Tryptic peptides chosen for quantitation are listed in Table S7.4A and %R values of the six glycolytic enzymes and the ribosomal protein ASC1 at 45-225 min following

challenge of *S. cerevisiae* with H_2O_2 are given in Table S7.4B. This material is available free at http://pubs.acs.org.

Table S7.4A. Tryptic peptides chosen for quantitation

Peptide	Theoretical average M_r (u)	Sequence	No. of Leu residues
ALD6_1	1872.2	IYVQEGIYDELLAAFK	2
ALD6_2	2233.6	ITLPNGLTYEQPTGLFINNK	3
DCP1_1	726.8	YLFER	1
DCP1_2	1596.8	YGGVYVGTLSKPEVK	1
DCP1_3	1998.1	WAGNANELNAAYAADGYAR	1
DCP1_4	2105.4	QLLLHHTLGNGDFTVFHR	4
DCP1_5	2388.7	AQYNEIQGWDHLSLLPTFGAK	3
DCP1_6	2743.2	TTYVTQRPVYLGLPANLVDLNVPAK	4
ENO1_1	1412.7	LGANAILGVSLAASR	3
ENO1_2	1578.7	AVDDFLISLDGTANK	2
ENO1_3	1822.0	SGETEDTFIADLVVGLR	2
ENO1_4	2441.6	IEEELGDNAVFAGENFHHGDKL	2
ENO2_1	755.9	LNQLLR	3
ENO2_2	1288.5	VNQIGTLSESIK	1
ENO2_3	1497.7	NVPLYQHLADLSK	3
ENO2_4	1557.7	AVYAGENFHHGDKL	1
ENO2_5	1578.7	AVDDFLLSLDGTANK	3
FBA1_1	1795.0	SPIILQTSNGGAAYFAGK	1
FBA1_2	1863.1	TGVIVGEDVHNLFTYAK	1
FBA1_3	2160.5	FAIPAINVTSSSTAVAALEAAR	1
TPI1_1	1096.3	WVILGHSER	1
TPI1_2	2519.8	ADVDGFLVGGASLKPEFVDIINSR	2
TPI1_3	2763.1	DKADVDGFLVGGASLKPEFVDIINSR	2
ASC1_1	1265.5	YWLAAATATGIK	1
ASC1_2	1438.6	LWDVATGETYQR	1
ASC1_3	2559.9	VFSLDPQYLVDDLRPEFAGYSK	3
ASC1_4	2838.1	GTLEGHNGWVTSLATSAGQPNLLLSASR	5

Table S7.4B. %R values of six glycolytic enzymes and the ribosomal protein ASC1 at 45-225 min following challenge of *S. cerevisiae* with H_2O_2

Peptides	%R									
	45 min		90 min		135 min		180 min		225 min	
	$R_{H_2O_2}$	R_c	$R_{H_2O_2}$	R_c	$R_{H_2O_2}$	R_c	$R_{H_2O_2}$	R_c	$R_{H_2O_2}$	R_c
ALD6_1	14.1	19.3	31.8	38.4	72.0	72.8	136.5	144.4	183.5	189.9
ALD6_2	11.7	16.3	24.1	43.1	65.2	61.3	137.1	133.0	186.6	182.1
DCP1_1	5.7	8.0	16.3	18.4	55.1	50.0	117.9	124.1	147.8	146.4
DCP1_2	7.3	10.2	18.3	20.8	58.6	59.2	127.2	136.7	145.3	164.5
DCP1_3	8.9	8.0	19.6	20.7	56.3	56.3	130.2	126.3	155.0	164.5
DCP1_4	6.9	9.0	18.6	16.7	53.4	49.8	110.5	125.1	136.0	142.4
DCP1_5	7.7	8.8	17.2	22.3	60.7	59.8	125.4	133.3	150.5	161.9
DCP1_6	5.6	6.9	14.6	16.2	51.9	50.4	126.6	116.6	142.1	152.7
ENO1_1	8.3	5.9	9.6	10.1	12.2	15.6	55.4	78.2	94.8	108.7
ENO1_2	9.3	5.8	11.0	9.2	15.1	16.5	58.9	63.7	100.1	115.8
ENO1_3	7.6	7.3	9.2	9.0	13.5	12.4	63.3	57.9	101.9	99.7
ENO1_4	6.5	5.9	10.1	7.5	10.8	15.9	64.0	71.3	96.4	117.4
ENO2_1	5.0	7.5	7.3	11.0	20.6	20.6	35.3	37.2	88.6	83.4
ENO2_2	6.5	7.1	11.7	10.6	23.1	19.6	42.4	40.1	78.1	99.8
ENO2_3	4.7	5.3	9.5	12.9	18.5	20.1	46.6	44.0	84.3	94.5
ENO2_4	5.8	6.3	8.8	9.9	24.2	24.5	38.5	38.6	91.7	109.7
ENO2_5	3.8	7.2	10.6	11.6	19.9	20.0	39.6	45.9	94.2	87.1
FBA1_1	9.1	15.0	14.9	21.3	35.9	36.9	84.3	100.4	157.4	143.9
FBA1_2	11.5	14.8	16.2	17.8	35.7	43.5	90.1	98.6	151.1	145.0
FBA1_3	8.4	15.7	13.5	15.4	36.4	33.4	96.7	97.6	160.3	162.4
TPI1_1	7.3	7.5	13.2	16.4	28.8	30.3	69.7	79.0	109.0	112.3
TPI1_2	5.5	6.1	14.6	13.3	26.8	32.8	73.1	75.9	106.6	113.3
TPI1_3	8.2	8.5	12.1	13.2	34.1	32.9	73.8	79.8	97.6	116.3
ASC1_1	10.1	9.8	25.8	24.1	76.2	78.6	135.6	160.4	147.3	168.4
ASC1_2	9.3	7.7	25.9	26.2	90.4	90.0	164.7	148.3	168.7	162.8
ASC1_3	8.8	9.1	28.7	32.5	75.1	80.5	147.8	142.5	160.8	176.4
ASC1_4	7.0	7.1	27.6	29.8	83.2	74.3	136.3	134.3	154.8	145.6

8 General conclusions and suggestions for future work

The goal of my research was to unravel the physiological roles of CCP in *S. cerevisiae* using genetic, biochemical and proteomics approaches. Yeast CCP was first isolated in 1940 and has been extensively examined *in vitro* over the last 60 years. However, the physiological function of CCP has not been clarified since only a few *in vivo* studies have been published on this protein.

8.1 Chapter 2

The diverse behavior of CCP and its W191F mutant upon H_2O_2 oxidation in the absence of donors is likely due to differences in the extent of polypeptide oxidation. This heme-mediated process appears to be more efficient in the wild-type protein than in the mutant. However, the rapid crosslinking of CCP^{W191F} on 1× H_2O_2 addition reveals that oxidizing equivalents are more efficiently translocated to yield protein surface-exposed radicals in the mutant than in the wild-type protein. Such radicals may signal oxidative stress *in vivo*. $TEMPO^{\bullet}$ inhibited H_2O_2-induced CCP crosslinking and could act as a donor to the heme on CCP oxidation.

8.2 Chapter 3

The mass spectral behavior of $TEMPO^{\bullet}$ was investigated in aqueous solutions to characterize its reaction with the H_2O_2-oxidized peroxidases. Quantum chemistry calculations supported the relative stabilities observed for the $TEMPO^{\bullet}$-derived ions. Use of sodium phosphate buffer as an MS solution should facilitate the ESI MS analysis of solution-based $TEMPO^{\bullet}$ scavenging and redox reactions by inhibiting redox turnover of the nitroxyl in the source and by removing $TEMPO^{\bullet}$-derived fragments from the mass spectra.

8.3 Chapter 4

The first systematic study of the effects of *CCP1* on cell survival and sensitivity to heat and oxidative stress in *S. cerevisiae* was carried out. Although the observed differences are not dramatic, in the aggregate the initial doubling time variation, the differential H_2O_2-sensitivity reflected in the indices of respiratory competence, the incremental growth and antioxidant enzyme activities of the three strains (wild-type, *ccp1Δ* and *ccp1Δ-ccp1*^{W191F}) support a regulatory function for CCP in H_2O_2 response independent of its antioxidant function in both exponential- and stationary-phase cells.

8.4 Chapters 5, 6 and 7

To obtain a global view of CCP's function in cellular redox control, a quantitative comparison of mitochondrial proteomes was initiated. An effort to map the mitochondrial proteomes of wild-type and *ccp1Δ* yeast was undertaken, but the quantitative reliability of 2DE image analysis on 7×10-cm gels was not acceptable for proteins with < 3-fold change in expression. Thus, an approach that combines efficient metabolic-labeling with D_{10}-Leu and isotope-ratio quantitation by MALDI-ToF MS was developed. A study on the response of the yeast proteome to H_2O_2-exposure was undertaken using this metabolic-labeling method. Glycolysis was initially inhibited and then restored within two hours after challenging exponentially growing yeast cells with 0.4 mM H_2O_2.

The D_{10}-Leu labeling method can be used to (i) quantitatively compare proteomes of wild-type and non-essential-gene-null-mutant yeast strains to discover gene function; (ii) explore the time frame of proteome alteration in yeast under challenging conditions; and (iii) monitor the amounts of protein accumulated on different media or during different growth stages.

8.5 Suggestions for further work

(1) Since TEMPO$^{\bullet}$ inhibits H_2O_2-induced crosslinking of CCP and accelerates the rate of oxyferryl heme reduction in the oxidized protein, absorption changes and crosslinking of oxidized CCP point mutants should be monitored in the absence and presence of TEMPO$^{\bullet}$. For example, Tyr39, Tyr153 and Tyr236, which might be involved in radical translocation [115, 117], should be changed to phenylalanine to explore the effects of TEMPO$^{\bullet}$ on the intramolecular electron-transfer pathways in CCP.

(2) Radical scavenging by TEMPO$^{\bullet}$ should be investigated using ESI MS to establish sites of radical formation in oxidized CCP. As described in Chapter 3, the efficiency of TEMPO$^{\bullet}$ as a donor to the heme could be monitored by measuring the relative abundance of the $TEMPO^{+}$ ion following TEMPO$^{\bullet}$ oxidation by oxyferryl CCP.

(3) TEMPO$^{\bullet}$ penetrates into mammalian cells and protects against H_2O_2-induced killing [170, 171]. Assuming that TEMPO$^{\bullet}$ can block the translocation of H_2O_2-induced radicals from CCP to other signaling molecules *in vivo*, growth and survival of yeast cells cultured in the presence of TEMPO$^{\bullet}$ should be investigated.

(4) Since *ccp1Δ* cells exhibit a short initial doubling time that might be related to altered Ca^{2+} and H_2O_2 levels [59, 212, 213], changes in intracellular free Ca^{2+} and H_2O_2 should be investigated in lag-phase cells grown in SCD and SCE.

(5) Using a CCP-GFP construct, it has been demonstrated in our lab that CCP is released from mitochondria as glucose is consumed (L. Zhang, personal communication). The localization of extramitochondrial CCP in yeast and

possible CCP protein complexes should be identified by confocal microscopy and immunoprecipitation to understand CCP's role in cell signaling.

(6) *S. cerevisiae* has proven to be a particularly suitable and relatively simple organism for exploring the molecular basis of cell aging related to oxidative stress [1]. Since *ccp1Δ* cells do not undergo the changes in mitochondrial morphology seen in wild-type cells on aging (L. Zhang, personal communication), a quantitative comparison of mitochondrial genomes and proteomes in exponential- and stationary-phase wild-type and *ccp1Δ* cells should be performed. The data will provide insight into aging and oxidative stress.

9 References

1 Dawes, W. I. (Ed.) **1999** The metabolism & molecular physiology of *Saccharomyces cerevisiae*, Taylor & Francis, London, Philadelphia

2 Plesset, J., Palm, C. and McLaughlin, C. S. **1982** Induction of heat shock proteins and thermotolerance by ethanol in *Saccharomyces cerevisiae*, *Biochem Biophys Res Commun* 108, 1340-5

3 Varela, J. C., van Beekvelt, C., Planta, R. J. and Mager, W. H. **1992** Osmostress-induced changes in yeast gene expression, *Mol Microbiol* 6, 2183-90

4 Trollmo, C. A., Lars; Blomberg, Anders; Adler, Lennart. **1988** Physiological overlap between osmotolerance and thermotolerance in *Saccharomyces cerevisiae*, *FEMS Microbiology Letters* 56, 321-5

5 Jamieson, D. J. **1992** *Saccharomyces cerevisiae* has distinct adaptive responses to both hydrogen peroxide and menadione, *J Bacteriol* 174, 6678-81

6 Flattery-O'Brien, J., Collinson, L. P. and Dawes, I. W. **1993** *Saccharomyces cerevisiae* has an inducible response to menadione which differs from that to hydrogen peroxide, *J Gen Microbiol* 139 (Pt 3), 501-7

7 Davidson, J. F., Whyte, B., Bissinger, P. H. and Schiestl, R. H. **1996** Oxidative stress is involved in heat-induced cell death in *Saccharomyces cerevisiae*, *Proc Natl Acad Sci U S A* 93, 5116-21

8 Kowaltowski, A. J. and Vercesi, A. E. **1999** Mitochondrial damage induced by conditions of oxidative stress, *Free Radic Biol Med* 26, 463-71

9 Gunstone, F. D. **1996** Fatty Acid and Lipid Chemistry, London Blackie Acdemic and Professional

10 Thannickal, V. J. and Fanburg, B. L. **2000** Reactive oxygen species in cell signaling, *Am J Physiol Lung Cell Mol Physiol* 279, L1005-28

11 Jamieson, D. J. **1998** Oxidative stress responses of the yeast *Saccharomyces cerevisiae*, *Yeast* 14, 1511-27

12 Ohtake, Y. and Yabuuchi, S. **1991** Molecular cloning of the gamma-glutamylcysteine synthetase gene of *Saccharomyces cerevisiae*, *Yeast* 7, 953-61

13 Inoue, Y., Sugiyama, K., Izawa, S. and Kimura, A. **1998** Molecular identification of glutathione synthetase (*GSH2*) gene from *Saccharomyces cerevisiae*, *Biochim Biophys Acta* 1395, 315-20

14 Wu, A. L. and Moye-Rowley, W. S. **1994** *GSH1*, which encodes gamma-glutamylcysteine synthetase, is a target gene for Yap1 transcriptional regulation, *Mol Cell Biol* 14, 5832-9

15 Lisowsky, T. **1993** A high copy number of yeast gamma-glutamylcysteine synthetase suppresses a nuclear mutation affecting mitochondrial translation, *Curr Genet* 23, 408-13

16 Stephen, D. W. and Jamieson, D. J. **1996** Glutathione is an important antioxidant molecule in the yeast *Saccharomyces cerevisiae*, *FEMS Microbiol Lett* 141, 207-12

17 Muller, E. G. **1996** A glutathione reductase mutant of yeast accumulates high levels of oxidized glutathione and requires thioredoxin for growth, *Mol Biol Cell* 7, 1805-13

18 Delaunay, A., Isnard, A. D. and Toledano, M. B. **2000** H_2O_2 sensing through oxidation of the Yap1 transcription factor, *Embo J* 19, 5157-66

19 Garrido, E. O. and Grant, C. M. **2002** Role of thioredoxins in the response of *Saccharomyces cerevisiae* to oxidative stress induced by hydroperoxides, *Mol Microbiol* 43, 993-1003

20 Petrova, V. Y., Drescher, D., Kujumdzieva, A. V. and Schmitt, M. J. **2004** Dual targeting of yeast catalase A to peroxisomes and mitochondria, *Biochem J* 380, 393-400

21 Marchler, G., Schuller, C., Adam, G. and Ruis, H. **1993** A *Saccharomyces cerevisiae* UAS element controlled by protein kinase A activates transcription in response to a variety of stress conditions, *Embo J* 12, 1997-2003

22 Gasch, A. P., Spellman, P. T., Kao, C. M., Carmel-Harel, O., Eisen, M. B., Storz, G., Botstein, D. and Brown, P. O. **2000** Genomic expression programs in the response of yeast cells to environmental changes, *Mol Biol Cell* 11, 4241-57

23 Lapinskas, P., Ruis, H. and Culotta, V. **1993** Regulation of *Saccharomyces cerevisiae* catalase gene expression by copper, *Curr Genet* 24, 388-93

24 Izawa, S., Inoue, Y. and Kimura, A. **1996** Importance of catalase in the adaptive response to hydrogen peroxide: analysis of acatalasaemic *Saccharomyces cerevisiae*, *Biochem J* 320 (Pt 1), 61-7

25 Gralla, E. B. and Valentine, J. S. **1991** Null mutants of *Saccharomyces cerevisiae* Cu,Zn superoxide dismutase: characterization and spontaneous mutation rates, *J Bacteriol* 173, 5918-20

26 Jamieson, D. J., Rivers, S. L. and Stephen, D. W. **1994** Analysis of *Saccharomyces cerevisiae* proteins induced by peroxide and superoxide stress, *Microbiology* 140 (Pt 12), 3277-83

27 Sturtz, L. A., Diekert, K., Jensen, L. T., Lill, R. and Culotta, V. C. **2001** A fraction of yeast Cu,Zn-superoxide dismutase and its metallochaperone, CCS, localize to the intermembrane space of mitochondria. A physiological role for *SOD1* in guarding against mitochondrial oxidative damage, *J Biol Chem* 276, 38084-9

28 Costa, V., Amorim, M. A., Reis, E., Quintanilha, A. and Moradas-Ferreira, P. **1997** Mitochondrial superoxide dismutase is essential for ethanol tolerance of *Saccharomyces cerevisiae* in the post-diauxic phase, *Microbiology* 143 (Pt 5), 1649-56

29 Guidot, D. M., McCord, J. M., Wright, R. M. and Repine, J. E. **1993** Absence of electron transport (*rho*^{0} state) restores growth of a manganese-superoxide dismutase-deficient *Saccharomyces cerevisiae* in hyperoxia. Evidence for electron transport as a major source of superoxide generation *in vivo*, *J Biol Chem* 268, 26699-703

30 Wallace, M. A., Bailey, S., Fukuto, J. M., Valentine, J. S. and Gralla, E. B. **2005** Induction of phenotypes resembling CuZn-superoxide dismutase deletion in wild-type yeast cells: an *in vivo* assay for the role of superoxide in the toxicity of redox-cycling compounds, *Chem Res Toxicol* 18, 1279-86

31 Inoue, Y., Matsuda, T., Sugiyama, K., Izawa, S. and Kimura, A. **1999** Genetic analysis of glutathione peroxidase in oxidative stress response of *Saccharomyces cerevisiae*, *J Biol Chem* 274, 27002-9

32 Avery, A. M. and Avery, S. V. **2001** *Saccharomyces cerevisiae* expresses three phospholipid hydroperoxide glutathione peroxidases, *J Biol Chem* 276, 33730-5

33 Huh, W. K., Falvo, J. V., Gerke, L. C., Carroll, A. S., Howson, R. W., Weissman, J. S. and O'Shea, E. K. **2003** Global analysis of protein localization in budding yeast, *Nature* 425, 686-91

34 Delaunay, A., Pflieger, D., Barrault, M. B., Vinh, J. and Toledano, M. B. **2002** A thiol peroxidase is an H_2O_2 receptor and redox-transducer in gene activation, *Cell* 111, 471-81

35 Inoue, Y., Tran, L. T., Kamakura, M., Izawa, S., Miki, T., Tsujimoto, Y. and Kimura, A. **1995** Oxidative stress response in yeast: glutathione peroxidase of *Hansenula mrakii* is bound to the membrane of both mitochondria and cytoplasm, *Biochim Biophys Acta* 1245, 325-30

36 Collinson, L. P. and Dawes, I. W. **1995** Isolation, characterization and overexpression of the yeast gene, *GLR1*, encoding glutathione reductase, *Gene* 156, 123-7

37 Grant, C. M., Collinson, L. P., Roe, J. H. and Dawes, I. W. **1996** Yeast glutathione reductase is required for protection against oxidative stress and is a target gene for Yap1 transcriptional regulation, *Mol Microbiol* 21, 171-9

38 Chae, H. Z., Chung, S. J. and Rhee, S. G. **1994** Thioredoxin-dependent peroxide reductase from yeast, *J Biol Chem* 269, 27670-8

39 Kwon, S. J., Park, J. W., Choi, W. K., Kim, I. H. and Kim, K. **1994** Inhibition of metal-catalyzed oxidation systems by a yeast protector protein in the presence of thioredoxin, *Biochem Biophys Res Commun* 201, 8-15

40 Kim, K., Kim, I. H., Lee, K. Y., Rhee, S. G. and Stadtman, E. R. **1988** The isolation and purification of a specific "protector" protein which inhibits enzyme inactivation by a thiol/Fe^{III}/O_2 mixed-function oxidation system, *J Biol Chem* 263, 4704-11

41 Comprehensive Yeast Genome Database (CYGD) at http://mips.gsf.de/genre/proj/yeast

42 Lee, S. M. and Park, J. W. **1998** Thermosensitive phenotype of yeast mutant lacking thioredoxin peroxidase, *Arch Biochem Biophys* 359, 99-106

43 Daum, G., Bohni, P. C. and Schatz, G. **1982** Import of proteins into mitochondria. Cytochrome *b2* and cytochrome *c* peroxidase are located in the intermembrane space of yeast mitochondria, *J Biol Chem* 257, 13028-33

44 Charizanis, C., Juhnke, H., Krems, B. and Entian, K. D. **1999** The oxidative stress response mediated via Pos9/Skn7 is negatively regulated by the Ras/PKA pathway in *Saccharomyces cerevisiae*, *Mol Gen Genet* 261, 740-52

45 Rhee, S. G. **1999** Redox signaling: hydrogen peroxide as intracellular messenger, *Exp Mol Med* 31, 53-9

46 Zhang, L. and Hach, A. **1999** Molecular mechanism of heme signaling in yeast: the transcriptional activator Hap1 serves as the key mediator, *Cell Mol Life Sci* 56, 415-26

47 Labbe-Rois, R., Labbe, P. **1990** Biosynthesis of Heme and Cholorophylls, Green, New York

48 Pfeifer, K., Arcangioli, B. and Guarente, L. **1987** Yeast HAP1 activator competes with the factor RC2 for binding to the upstream activation site UAS1 of the *CYC1* gene, *Cell* 49, 9-18

49 Pfeifer, K., Prezant, T. and Guarente, L. **1987** Yeast Hap1 activator binds to two upstream activation sites of different sequence, *Cell* 49, 19-27

50 Winkler, H., Adam, G., Mattes, E., Schanz, M., Hartig, A. and Ruis, H. **1988** Co-ordinate control of synthesis of mitochondrial and non-mitochondrial hemoproteins: a binding site for the Hap1 (Cyp1) protein in the UAS region of the yeast catalase T gene (*CTT1*), *Embo J* 7, 1799-804

51 Lowry, C. V. and Zitomer, R. S. **1988** *ROX1* encodes a heme-induced repression factor regulating *ANB1* and *CYC7* of *Saccharomyces cerevisiae*, *Mol Cell Biol* 8, 4651-8

52 Chance, B., Sies, H. and Boveris, A. **1979** Hydroperoxide metabolism in mammalian organs, *Physiol Rev* 59, 527-605

53 Seaver, L. C. and Imlay, J. A. **2001** Hydrogen peroxide fluxes and compartmentalization inside growing *Escherichia coli*, *J Bacteriol* 183, 7182-9

54 Branco, M. R., Marinho, H. S., Cyrne, L. and Antunes, F. **2004** Decrease of H_2O_2 plasma membrane permeability during adaptation to H_2O_2 in *Saccharomyces cerevisiae*, *J Biol Chem* 279, 6501-6

55 Antunes, F. and Cadenas, E. **2000** Estimation of H_2O_2 gradients across biomembranes, *FEBS Lett* 475, 121-6

56 Sousa-Lopes, A., Antunes, F., Cyrne, L. and Marinho, H. S. **2004** Decreased cellular permeability to H_2O_2 protects *Saccharomyces cerevisiae* cells in stationary phase against oxidative stress, *FEBS Lett* 578, 152-6

57 Gamaley, I. A. and Klyubin, I. V. **1999** Roles of reactive oxygen species: signaling and regulation of cellular functions, *Int Rev Cytol* 188, 203-55

58 Kamata, H. and Hirata, H. **1999** Redox regulation of cellular signalling, *Cell Signal* 11, 1-14

59 Suzuki, Y. J., Forman, H. J. and Sevanian, A. **1997** Oxidants as stimulators of signal transduction, *Free Radic Biol Med* 22, 269-85

60 Clapham, D. E. **1995** Calcium signaling, *Cell* 80, 259-68

61 Bootman, M. D. and Berridge, M. J. **1995** The elemental principles of calcium signaling, *Cell* 83, 675-8

62 Zheng, M., Aslund, F. and Storz, G. **1998** Activation of the OxyR transcription factor by reversible disulfide bond formation, *Science* 279, 1718-21

63 Lee, J., Godon, C., Lagniel, G., Spector, D., Garin, J., Labarre, J. and Toledano, M. B. **1999** Yap1 and Skn7 control two specialized oxidative stress response regulons in yeast, *J Biol Chem* 274, 16040-6

64 Wood, M. J., Andrade, E. C. and Storz, G. **2003** The redox domain of the Yap1 transcription factor contains two disulfide bonds, *Biochemistry* 42, 11982-91

65 Azevedo, D., Tacnet, F., Delaunay, A., Rodrigues-Pousada, C. and Toledano, M. B. **2003** Two redox centers within Yap1 for H_2O_2 and thiol-reactive chemicals signaling, *Free Radic Biol Med* 35, 889-900

66 Kuge, S., Jones, N. and Nomoto, A. **1997** Regulation of Yap1 nuclear localization in response to oxidative stress, *Embo J* 16, 1710-20

67 Krems, B., Charizanis, C. and Entian, K. D. **1996** The response regulator-like protein Pos9/Skn7 of *Saccharomyces cerevisiae* is involved in oxidative stress resistance, *Curr Genet* 29, 327-34

68 He, X. J. and Fassler, J. S. **2005** Identification of novel Yap1 and Skn7 binding sites involved in the oxidative stress response of *Saccharomyces cerevisiae*, *Mol Microbiol* 58, 1454-67

69 Juhnke, H., Charizanis, C., Latifi, F., Krems, B. and Entian, K. D. **2000** The essential protein Fap7 is involved in the oxidative stress response of *Saccharomyces cerevisiae*, *Mol Microbiol* 35, 936-48

70 Charizanis, C., Juhnke, H., Krems, B. and Entian, K. D. **1999** The mitochondrial cytochrome *c* peroxidase *CCP1* of *Saccharomyces cerevisiae* is involved in conveying an oxidative stress signal to the transcription factor Pos9 (Skn7), *Mol Gen Genet* 262, 437-47

71 Madeo, F., Frohlich, E., Ligr, M., Grey, M., Sigrist, S. J., Wolf, D. H. and Frohlich, K. U. **1999** Oxygen stress: a regulator of apoptosis in yeast, *J Cell Biol* 145, 757-67

72 Takeyama, N., Miki, S., Hirakawa, A. and Tanaka, T. **2002** Role of the mitochondrial permeability transition and cytochrome *c* release in hydrogen peroxide-induced apoptosis, *Exp Cell Res* 274, 16-24

73 Ludovico, P., Rodrigues, F., Almeida, A., Silva, M. T., Barrientos, A. and Corte-Real, M. **2002** Cytochrome *c* release and mitochondria involvement in programmed cell death induced by acetic acid in *Saccharomyces cerevisiae*, *Mol Biol Cell* 13, 2598-606

74 Pozniakovsky, A. I., Knorre, D. A., Markova, O. V., Hyman, A. A., Skulachev, V. P. and Severin, F. F. **2005** Role of mitochondria in the pheromone- and amiodarone-induced programmed death of yeast, *J Cell Biol* 168, 257-69

75 Zorov, D. B., Krasnikov, B. F., Kuzminova, A. E., Vysokikh, M. and Zorova, L. D. **1997** Mitochondria revisited. Alternative functions of mitochondria, *Biosci Rep* 17, 507-20

76 Newmeyer, D. D. and Ferguson-Miller, S. **2003** Mitochondria: releasing power for life and unleashing the machineries of death, *Cell* 112, 481-90

77 Netter, P., Petrochilo, E., Slonimski, P. P., Bolotin-Fukuhara, M., Coen, D., Deutsch, J. and Dujon, B. **1974** Mitochondrial genetics. VII. Allelism and mapping studies of ribosomal mutants resistant to chloramphenicol, erythromycin and spiramycin in *S. cerevisiae*, *Genetics* 78, 1063-100

78 Rickwood, D., Dujon, B. and Darley-Usmar, M. V. (Eds.) **1998** Yeast a practical approach, Oxford, England; Washington, D.C., IRL Press

79 de Zamaroczy, M. and Bernardi, G. **1985** Sequence organization of the mitochondrial genome of yeast--a review, *Gene* 37, 1-17

80 Dujon, B. **1983** In: Mitochondria 1983, Schweyen, R. J., Wolf, K. and Kaudewitz, F. (Ed.), W. de Gruyter, Berlin

81 Chandel, N. S. and Schumacker, P. T. **1999** Cells depleted of mitochondrial DNA (*rho*^{0}) yield insight into physiological mechanisms, *FEBS Lett* 454, 173-6

82 Petrova, V. Y. and Kujumdzieva, A. V. **2002** Catalase enzyme in mitochondria of *Saccharomyces cerevisiae*, *Electron. J. Biotechnol.* 5, 29-41

83 Boveris, A. C., E. **1982** Superoxide Dismutases, vol. 2

84 Han, D., Antunes, F., Daneri, F. and Cadenas, E. **2002** Mitochondrial superoxide anion production and release into intermembrane space, *Methods Enzymol* 349, 271-80

85 Boveris, A. **1976** Mitochondrial production of hydrogen peroxide in *Saccharomyces cerevisiae*, *Acta Physiol Lat Am* 26, 303-9

86 Batandier, C., Fontaine, E., Keriel, C. and Leverve, X. M. **2002** Determination of mitochondrial reactive oxygen species: methodological aspects, *J Cell Mol Med* 6, 175-87

87 Longo, V. D., Gralla, E. B. and Valentine, J. S. **1996** Superoxide dismutase activity is essential for stationary phase survival in *Saccharomyces cerevisiae*. Mitochondrial production of toxic oxygen species in vivo, *J Biol Chem* 271, 12275-80

88 Campos, E. G., Hermes-Lima, M., Smith, J. M. and Prichard, R. K. **1999** Characterisation of *Fasciola hepatica* cytochrome *c* peroxidase as an enzyme with potential antioxidant activity in vitro, *Int J Parasitol* 29, 655-62

89 Altschul, A. M., Abrams, R. and Hogness, T. R. **1940** Cytochrome *c* peroxiase, *J. Biol. Chem.* 136, 777-794

90 Kaput, J., Goltz, S. and Blobel, G. **1982** Nucleotide sequence of the yeast nuclear gene for cytochrome *c* peroxidase precursor. Functional implications of the pre sequence for protein transport into mitochondria, *J Biol Chem* 257, 15054-8

91 Goltz, S., Kaput, J. and Blobel, G. **1982** Isolation of the yeast nuclear gene encoding the mitochondrial protein, cytochrome *c* peroxidase, *J Biol Chem* 257, 11186-90

92 Dujon, B., Alexandraki, D., Andre, B., Ansorge, W., Baladron, V., Ballesta, J. P., Banrevi, A., Bolle, P. A., Bolotin-Fukuhara, M., Bossier, P. and et al. **1994** Complete DNA sequence of yeast chromosome XI, *Nature* 369, 371-8

93 The MIPS Yeast Genome Database (MYGD) in http://www.mips.biochem.mpg.de provided by Munich information center for protein sequences

94 Djavadi-Ohaniance, L., Rudin, Y. and Schatz, G. **1978** Identification of enzymically inactive apocytochrome *c* peroxidase in anaerobically grown *Saccharomyces cerevisiae*, *J Biol Chem* 253, 4402-7

95 Sels, A. A. and Cocriamont, C. **1968** Induced conversion of a protein precursor into cytochrome *c* peroxidase during adaptation of yeast to oxygen, *Biochem Biophys Res Commun* 32, 192-8

96 Zitomer, R. S. and Lowry, C. V. **1992** Regulation of gene expression by oxygen in *Saccharomyces cerevisiae*, *Microbiol Rev* 56, 1-11

97 Giles, S. S., Perfect, J. R. and Cox, G. M. **2005** Cytochrome *c* peroxidase contributes to the antioxidant defense of *Cryptococcus neoformans*, *Fungal Genet Biol* 42, 20-9

98 Erman, J. E. and Vitello, L. B. **2002** Yeast cytochrome *c* peroxidase: mechanistic studies *via* protein engineering, *Biochim Biophys Acta* 1597, 193-220

99 Loo, S., Erman, J. E. **1975** A kinetic study of the reaction between cytochrome *c* peroxidase and hydrogen peroxide. Dependence on pH and ionic strength, *Biochemistry* 14, 3467-70

100 Miller, M. A., Shaw, A. and Kraut, J. **1994** 2.2 Å structure of oxy-peroxidase as a model for the transient enzyme: peroxide complex, *Nat Struct Biol* 1, 524-31

101 Finzel, B. C., Poulos, T. L. and Kraut, J. **1984** Crystal structure of yeast cytochrome *c* peroxidase refined at 1.7- Å resolution, *J Biol Chem* 259, 13027-36

102 Pelletier, H. and Kraut, J. **1992** Crystal structure of a complex between electron transfer partners, cytochrome *c* peroxidase and cytochrome *c*, *Science* 258, 1748-55

103 Yonetani, T. **1967** Studies on cytochrome *c* peroxidase. X. Crystalline apo-and reconstituted holoenzymes, *J Biol Chem* 242, 5008-13

104 Ellfolk, N. **1967** Cytochrome *c* peroxidase. 1. Preparation of the crystalline enzyme from baker's yeast, *Acta Chem Scand* 21, 175-81

105 Ellfolk, N. and Sievers, G. **1969** Cytochrome *c* peroxidase. IV. Isoelectric focusing and analysis of the crystalline enzyme in an acidic pH gradient, *Acta Chem Scand* 23, 2550-1

106 Margoliash, E. and Schejter, A. **1966** Cytochrome *c*, *Adv Protein Chem* 21, 113-286

107 Erman, J. E. and Yonetani, T. **1975** The oxidation of cytochrome *c* peroxidase by hydrogen peroxide. Characterization of products, *Biochim Biophys Acta* 393, 343-9

108 Yonetani, T. and Ray, G. S. **1965** Studies on cytochrome *c* peroxidase. I. Purification and some properties, *J Biol Chem* 240, 4503-8

109 Yonetani, T. **1965** Studies on cytochrome *c* peroxidase. II. Stoichiometry between enzyme, H_2O_2, and ferrocytochrome *c* and enzymic determination of extinction coefficients of cytochrome *c*, *J Biol Chem* 240, 4509-14

110 Erman, J. E. and Yonetani, T. **1975** A kinetic study of the endogenous reduction of the oxidized sites in the primary cytochrome *c* peroxidase-hydrogen peroxide compound, *Biochim Biophys Acta* 393, 350-7

111 Fox, T., Tsaprailis, G. and English, A. M. **1994** Fluorescence investigation of yeast cytochrome *c* peroxidase oxidation by H_2O_2 and enzyme activities of the oxidized enzyme, *Biochemistry* 33, 186-91

112 Mauro, J. M., Fishel, L. A., Hazzard, J. T., Meyer, T. E., Tollin, G., Cusanovich, M. A. and Kraut, J. **1988** Tryptophan-191-phenylalanine, a proximal-side mutation in yeast cytochrome *c* peroxidase that strongly affects the kinetics of ferrocytochrome *c* oxidation, *Biochemistry* 27, 6243-56

113 Tsaprailis, G., English, A. M. **1996** Redox activity of tryptophan residues in recombinant cytochrome *c* peroxidase and its W51F and W191F mutants, *Can J Chem* 74, 2250-7

114 Wright, P. J. and English, A. M. **2003** Scavenging with TEMPO$^{\bullet}$ to identify peptide- and protein-based radicals by mass spectrometry: advantages of spin scavenging over spin trapping, *J Am Chem Soc* 125, 8655-65

115 Zhang, H., He, S. and Mauk, A. G. **2002** Radical formation at Tyr39 and Tyr153 following reaction of yeast cytochrome *c* peroxidase with hydrogen peroxide, *Biochemistry* 41, 13507-13

116 Pfister, T. D., Gengenbach, A. J., Syn, S. and Lu, Y. **2001** The role of redox-active amino acids on compound I stability, substrate oxidation, and protein cross-linking in yeast cytochrome *c* peroxidase, *Biochemistry* 40, 14942-51

117 Tsaprailis, G. and English, A. M. **2003** Different pathways of radical translocation in yeast cytochrome *c* peroxidase and its W191F mutant on reaction with H_2O_2 suggest an antioxidant role, *J Biol Inorg Chem* 8, 248-55

118 Wasinger, V. C., Cordwell, S. J., Cerpa-Poljak, A., Yan, J. X., Gooley, A. A., Wilkins, M. R., Duncan, M. W., Harris, R., Williams, K. L. and Humphery-Smith, I. **1995** Progress with gene-product mapping of the Mollicutes: *Mycoplasma genitalium*, *Electrophoresis* 16, 1090-4

119 Godovac-Zimmermann, J. and Brown, L. R. **2001** Perspectives for mass spectrometry and functional proteomics, *Mass Spectrom Rev* 20, 1-57

120 Smith, R. D. **2000** Probing proteomes--seeing the whole picture?, *Nat Biotechnol* 18, 1041-2

121 Goffeau, A., Barrell, B. G., Bussey, H., Davis, R. W., Dujon, B., Feldmann, H., Galibert, F., Hoheisel, J. D., Jacq, C., Johnston, M., Louis, E. J., Mewes, H. W., Murakami, Y., Philippsen, P., Tettelin, H. and Oliver, S. G. **1996** Life with 6000 genes, *Science* 274, 546, 563-7

122 Gavin, A. C., Bosche, M., Krause, R., Grandi, P., Marzioch, M., Bauer, A., Schultz, J., Rick, J. M., Michon, A. M., Cruciat, C. M., Remor, M., Hofert, C., Schelder, M., Brajenovic, M., Ruffner, H., Merino, A., Klein, K., Hudak, M., Dickson, D., Rudi, T., Gnau, V., Bauch, A., Bastuck, S., Huhse, B., Leutwein, C., Heurtier, M. A., Copley, R. R., Edelmann, A., Querfurth, E., Rybin, V., Drewes, G., Raida, M., Bouwmeester, T., Bork, P., Seraphin, B., Kuster, B., Neubauer, G. and Superti-Furga, G. **2002** Functional organization of the yeast proteome by systematic analysis of protein complexes, *Nature* 415, 141-7

123 Ghaemmaghami, S., Huh, W. K., Bower, K., Howson, R. W., Belle, A., Dephoure, N., O'Shea, E. K. and Weissman, J. S. **2003** Global analysis of protein expression in yeast, *Nature* 425, 737-41

124 Trabalzini, L., Paffetti, A., Scaloni, A., Talamo, F., Ferro, E., Coratza, G., Bovalini, L., Lusini, P., Martelli, P. and Santucci, A. **2003** Proteomic response to physiological fermentation stresses in a wild-type wine strain of *Saccharomyces cerevisiae*, *Biochem J* 370, 35-46

125 Godon, C., Lagniel, G., Lee, J., Buhler, J. M., Kieffer, S., Perrot, M., Boucherie, H., Toledano, M. B. and Labarre, J. **1998** The H_2O_2 stimulon in *Saccharomyces cerevisiae*, *J Biol Chem* 273, 22480-9

126 Hu, Y., Wang, G., Chen, G. Y., Fu, X. and Yao, S. Q. **2003** Proteome analysis of *Saccharomyces cerevisiae* under metal stress by two-dimensional differential gel electrophoresis, *Electrophoresis* 24, 1458-70

127 Vido, K., Spector, D., Lagniel, G., Lopez, S., Toledano, M. B. and Labarre, J. **2001** A proteome analysis of the cadmium response in *Saccharomyces cerevisiae*, *J Biol Chem* 276, 8469-74

128 Rogowska-Wrzesinska, A., Larsen, M. P., Blomberg, A., Gorg, A., Roepstorff, P., Norbeck, J. and Fey, J. S. **2001** Comparison of the proteomes of three yeast wild type strains: CEN.PK2, FY1679 and W303, *Comp Funct Genom* 2, 207-225

129 Perkins, D. N., Pappin, D. J., Creasy, D. M. and Cottrell, J. S. **1999** Probability-based protein identification by searching sequence databases using mass spectrometry data, *Electrophoresis* 20, 3551-67

130 O'Farrell, P. H. **1975** High resolution two-dimensional electrophoresis of proteins, *J Biol Chem* 250, 4007-21

131 Perrot, M., Sagliocco, F., Mini, T., Monribot, C., Schneider, U., Shevchenko, A., Mann, M., Jeno, P. and Boucherie, H. **1999** Two-dimensional gel protein database of *Saccharomyces cerevisiae* (update 1999), *Electrophoresis* 20, 2280-98

132 Futcher, B. **1999** Cell cycle synchronization, *Methods Cell Sci* 21, 79-86

133 Gygi, S. P., Rochon, Y., Franza, B. R. and Aebersold, R. **1999** Correlation between protein and mRNA abundance in yeast, *Mol Cell Biol* 19, 1720-30

134 Henzel, W. J., Billeci, T. M., Stults, J. T., Wong, S. C., Grimley, C. and Watanabe, C. **1993** Identifying proteins from two-dimensional gels by molecular mass searching of peptide fragments in protein sequence databases, *Proc Natl Acad Sci U S A* 90, 5011-5

135 Prokisch, H., Scharfe, C., Camp, D. G., 2nd, Xiao, W., David, L., Andreoli, C., Monroe, M. E., Moore, R. J., Gritsenko, M. A., Kozany, C., Hixson, K. K., Mottaz, H. M., Zischka, H., Ueffing, M., Herman, Z. S., Davis, R. W., Meitinger, T., Oefner, P. J., Smith, R. D. and Steinmetz, L. M. **2004** Integrative analysis of the mitochondrial proteome in yeast, *PLoS Biol* 2, e160

136 Link, A. J., Eng, J., Schieltz, D. M., Carmack, E., Mize, G. J., Morris, D. R., Garvik, B. M. and Yates, J. R., 3rd. **1999** Direct analysis of protein complexes using mass spectrometry, *Nat Biotechnol* 17, 676-82

137 Arnold, R. J. and Reilly, J. P. **1999** Observation of *Escherichia coli* ribosomal proteins and their posttranslational modifications by mass spectrometry, *Anal Biochem* 269, 105-12

138 Sickmann, A., Reinders, J., Wagner, Y., Joppich, C., Zahedi, R., Meyer, H. E., Schonfisch, B., Perschil, I., Chacinska, A., Guiard, B., Rehling, P., Pfanner, N. and Meisinger, C. **2003** The proteome of *Saccharomyces cerevisiae* mitochondria, *Proc Natl Acad Sci U S A* 100, 13207-12

139 Andreoli, C., Prokisch, H., Hortnagel, K., Mueller, J. C., Munsterkotter, M., Scharfe, C. and Meitinger, T. **2004** MitoP2, an integrated database on mitochondrial proteins in yeast and man, *Nucleic Acids Res* 32, D459-62

140 Miller, M. A., Vitello, L. and Erman, J. E. **1995** Regulation of interprotein electron transfer by Trp 191 of cytochrome *c* peroxidase, *Biochemistry* 34, 12048-58

141 Erman, J. E., Vitello, L. B., Miller, M. A. and Kraut, J. **1992** Active-site mutations in cytochrome *c* peroxidase: a critical role for histidine-52 in the rate of formation of compound I, *J. Am. Chem. Soc.* 114, 6592-6593

142 Erman, J. E., Vitello, L. B., Mauro, J. M. and Kraut, J. **1989** Detection of an oxyferryl porphyrin pi-cation-radical intermediate in the reaction between hydrogen peroxide and a mutant yeast cytochrome *c* peroxidase. Evidence for tryptophan-191 involvement in the radical site of compound I, *Biochemistry* 28, 7992-5

143 Coulson, A. F. and Yonetani, T. **1972** Oxidation of cytochrome *c* peroxidase with hydrogen peroxide: identification of the "endogenous donor", *Biochem Biophys Res Commun* 49, 391-8

144 Lenaz, G. **1998** Role of mitochondria in oxidative stress and ageing, *Biochim Biophys Acta* 1366, 53-67

145 Fishel, L. A., Villafranca, J. E., Mauro, J. M. and Kraut, J. **1987** Yeast cytochrome *c* peroxidase: mutagenesis and expression in *Escherichia coli* show tryptophan-51 is not the radical site in compound I, *Biochemistry* 26, 351-60

146 Margoliash, E. and Frohwirt, N. **1959** Spectrum of horse-heart cytochrome *c*, *Biochem J* 71, 570-2

147 Vitello, L. B., Huang, M. and Erman, J. E. **1990** pH-dependent spectral and kinetic properties of cytochrome *c* peroxidase: comparison of freshly isolated and stored enzyme, *Biochemistry* 29, 4283-8

148 Yonetani, T. and Anni, H. **1987** Yeast cytochrome *c* peroxidase. Coordination and spin states of heme prosthetic group, *J Biol Chem* 262, 9547-54

149 Roggenkamp, R., Sahm, H. and Wagner, F. **1974** Microbial assimilation of methanol induction and function of catalase in *Candida boidinii*, *FEBS Lett* 41, 283-6

150 Briere, R., Lemaire, H. and Rassat, A. **1965** Synthese et Etude de Radicaux Libres Stables Piperidiniques et Pyrrolidinique, *Bull Soc Chim Fr* 11, 3273-83

151 Sherman, F., Stewart, J. W. and Tsunasawa, S. **1985** Methionine or not methionine at the beginning of a protein, *Bioessays* 3, 27-31

152 Hsu, M. C. and Woody, R. W. **1971** The origin of the heme Cotton effects in myoglobin and hemoglobin, *J Am Chem Soc* 93, 3515-25

153 Garber, E. A. and Margoliash, E. **1994** Circular dichroism studies of the binding of mammalian and non-mammalian cytochromes *c* to cytochrome *c* oxidase, cytochrome *c* peroxidase, and polyanions, *Biochim Biophys Acta* 1187, 289-95

154 Erman, J. E. and Vitello, L. B. **1980** The binding of cytochrome *c* peroxidase and ferricytochrome *c*. A spectrophotometric determination of the equilibrium association constant as a function of ionic strength, *J Biol Chem* 255, 6224-7

155 Jiang, B., Drouet, E., Milas, M. and Rinaudo, M. **2000** Study on TEMPO$^{\bullet}$-mediated selective oxidation of hyaluronan and the effects of salt on the reaction kinetics, *Carbohydr Res* 327, 455-61

156 Filosa, A. and English, A. M. **2001** Mass spectral analysis of protein-based radicals using DBNBS. Nonradical adduct formation versus spin trapping, *J Biol Chem* 276, 21022-7

157 Rychnovsky, S. D., Vaidyanathan, R., Beauchamp, T., Lin, R. and Farmer, P. J. **1999** AM1-SM2 Calculations Model the Redox Potential of Nitroxyl Radicals Such as TEMPO$^{\bullet}$, *J Org Chem* 64, 6745-6749

158 Traber, R., Kramer, H. E. A. and Hemmerich, P. **1982** Mechanism of Light-Induced Reduction of Biological Redox Centers by Amino Acids. A Flash Photolysis Study of Flavin Photoreduction by Ethylenediaminetetraacetate and Nitrilotriacetatet, *Biochemistry* 21, 1687-93

159 Bhattacharyya, D. K., Bandyopadhyay, U. and Banerjee, R. K. **1996** EDTA inhibits lactoperoxidase-catalyzed iodide oxidation by acting as an electron-donor and interacting near the iodide binding site, *Mol Cell Biochem* 162, 105-11

160 Sakai, H., Masada, Y., Onuma, H., Takeoka, S. and Tsuchida, E. **2004** Reduction of methemoglobin via electron transfer from photoreduced flavin: restoration of O_2-binding of concentrated hemoglobin solution coencapsulated in phospholipid vesicles, *Bioconjug Chem* 15, 1037-45

161 Kaplan, P., Babusikova, E., Lehotsky, J. and Dobrota, D. **2003** Free radical-induced protein modification and inhibition of Ca^{2+}-ATPase of cardiac sarcoplasmic reticulum, *Mol Cell Biochem* 248, 41-7

162 Welch, K. D., Davis, T. Z., Van Eden, M. E. and Aust, S. D. **2002** Deleterious iron-mediated oxidation of biomolecules, *Free Radic Biol Med* 32, 577-83

163 Schafer, F. Q., Qian, S. Y. and Buettner, G. R. **2000** Iron and free radical oxidations in cell membranes, *Cell Mol Biol (Noisy-le-grand)* 46, 657-62

164 Qian, S. Y. and Buettner, G. R. **1999** Iron and dioxygen chemistry is an important route to initiation of biological free radical oxidations: an electron paramagnetic resonance spin trapping study, *Free Radic Biol Med* 26, 1447-56

165 Bolm, C., Magnus, A. S. and Hildebrand, J. P. **2000** Catalytic synthesis of aldehydes and ketones under mild conditions using TEMPO$^{\bullet}$/Oxone, *Org Lett* 2, 1173-5

166 Miller, R. A. and Hoerrner, R. S. **2003** Iodine as a chemoselective reoxidant of TEMPO$^{\bullet}$: application to the oxidation of alcohols to aldehydes and ketones, *Org Lett* 5, 285-7

167 Jiang, N. and Ragauskas, A. J. **2005** Copper^{II}-catalyzed aerobic oxidation of primary alcohols to aldehydes in ionic liquid [bmpy]PF6, *Org Lett* 7, 3689-92

168 Sheldon, R. A., Arends, I. W., Ten Brink, G. J. and Dijksman, A. **2002** Green, catalytic oxidations of alcohols, *Acc Chem Res* 35, 774-81

169 Mitchell, J. B., Xavier, S., DeLuca, A. M., Sowers, A. L., Cook, J. A., Krishna, M. C., Hahn, S. M. and Russo, A. **2003** A low molecular weight antioxidant decreases weight and lowers tumor incidence, *Free Radic Biol Med* 34, 93-102

170 Gelvan, D., Moreno, V., Clopton, D. A., Chen, Q. and Saltman, P. **1995** Sites and mechanisms of low-level oxidative stress in cultured cells, *Biochem Biophys Res Commun* 206, 421-8

171 Samuni, A. M., DeGraff, W., Krishna, M. C. and Mitchell, J. B. **2001** Cellular sites of H_2O_2-induced damage and their protection by nitroxides, *Biochim Biophys Acta* 1525, 70-6

172 Krause, E., Wenschuh, H. and Jungblut, P. R. **1999** The dominance of arginine-containing peptides in MALDI-derived tryptic mass fingerprints of proteins, *Anal Chem* 71, 4160-5

173 Stapels, M. D. and Barofsky, D. F. **2004** Complementary use of MALDI and ESI for the HPLC-MS/MS analysis of DNA-binding proteins, *Anal Chem* 76, 5423-30

174 Bodnar, W. M., Blackburn, R. K., Krise, J. M. and Moseley, M. A. **2003** Exploiting the complementary nature of LC/MALDI/MS/MS and LC/ESI/MS/MS for increased proteome coverage, *J Am Soc Mass Spectrom* 14, 971-9

175 Wright, P. J. **2003** PhD. Thesis, Analysis of TEMPO•-adducts of protein-based radicals by mass spectrometry, Department of Chemistry and Biochemistry, Concordia University, Montreal

176 Metzger, J. O. and Griep-Raming, J. **1999** Electrospray ionization and atmospheric pressure ionization mass spectrometry of stable organic radicals, *Eur J Mass Spectrom* 5, 157-63

177 Marjasvaara, A., Torvinen, M. and Vainiotalo, P. **2004** Laccase-catalyzed mediated oxidation of benzyl alcohol: the role of TEMPO• and formation of products including benzonitrile studied by nanoelectrospray ionization Fourier transform ion cyclotron resonance mass spectrometry, *J Mass Spectrom* 39, 1139-46

178 Koch, W. and Holthausen, M. C. **2001** A Chemist's Guide to Density Functional Theory

179 Becke, A. D. **1993** Density-functional thermochemistry. III. The role of exact exchange, *J Chem Phys* 98, 5648-52

180 Lee, C., Yang, W. and Parr, R. G. **1988** Development of the Colle-Salvetti correlation-energy formula into a functional of the electron density, *Physical Review B. Condensed Matter* 37, 785-9

181 Smith, C. D., Bartley, J. P., Bottle, S. E., Micallef, A. S. and Reid, D. A. **2000** Electrospray ionization mass spectrometry of stable nitroxide free radicals and two isoindoline nitroxide dimers, *J Mass Spectrom* 35, 607-11

182 Chen, G., Kasthurikrishnan, N. and Cooks, R. G. **1995** Proton affinity of the stable free radical 2,2,6,6-tetramethyl-l-piperidinyloxy measured by the kinetic method, *Inter J Mass Spec and Ion Proc* 151, 69-75

183 Bader, R. F. W. **1990** Atoms in Molecules: A Quantum Theory, Oxford University Press, Oxford

184 Hunter, E. P. and Lias, S. G. **1998** Evaluated Gas Phase Basicities and Proton Affinities of Molecules: An Update, *J Phys Chem* 27, 413-656

185 Amicangelo, J. C. and Armentrout, P. B. **2001** Relative and absolute bond dissociation energies of sodium cation complexes determined using competitive collision-induced dissociation experiments, *Int J Mass Spectrom* 212, 301-25

186 Bordeaux, D., Lajzerowicz-Bonneteau, J., Briere, R., Lemaire, H. and Rassat, A. **1973** Détermination des Axes Propres et des Valeurs Principales du Tenseur dans

deux Radicaux Libres Nitroxydes par Étude de Monocristaux, *Org Mag Res* 5, 47-52

187 Anelli, P. L., Biffi, C., Montanari, F. and Quici, S. **1987** Fast and selective oxidation of primary alcohols to aldehydes or to carboxylic acids and of secondary alcohols to ketones mediated by oxoammonium salts under two-phase conditions, *J Org Chem* 52, 2559-62

188 Anelli, P. L., Banfi, S., Montanari, F. and Quici, S. **1989** Oxidation of diols with alkali hypochlorites catalyzed by oxammonium salts under two-phase conditions, *J Org Chem* 54, 2970-2

189 Fish, J. R., Swarts, S. G., Sevilla, M. D. and Malinski, T. **1988** Electrochemistry and spectroelectrochemistry of nitroxyl free radicals, *J Phys Chem* 92, 3745-51

190 Lee, J. K., Ross, R. T., Thampi, S. and Burganst, S. **1992** Resolution of the Properties of Hydrogen-Bonded Tyroslne Using a Trilinear Model of Fluorescence, *J Phys Chem* 96, 9158-62

191 Taylor, D. E., Ghio, A. J. and Piantadosi, C. A. **1995** Reactive oxygen species produced by liver mitochondria of rats in sepsis, *Arch Biochem Biophys* 316, 70-6

192 Campbell, I. D., Duffus, J. H. **1998** Yeast a practical approach, IRL Press, Oxford, Washington DC

193 Spangler, B. D. and Erman, J. E. **1986** Cytochrome *c* peroxidase compound I: formation of covalent protein crosslinks during the endogenous reduction of the active site, *Biochim Biophys Acta* 872, 155-7

194 Giulivi, C. and Davies, K. J. **1993** Dityrosine and tyrosine oxidation products are endogenous markers for the selective proteolysis of oxidatively modified red blood cell hemoglobin by (the 19 S) proteasome, *J Biol Chem* 268, 8752-9

195 Longo, V. D., Liou, L. L., Valentine, J. S. and Gralla, E. B. **1999** Mitochondrial superoxide decreases yeast survival in stationary phase, *Arch Biochem Biophys* 365, 131-42

196 Wach, A., Brachat, A., Pohlmann, R. and Philippsen, P. **1994** New heterologous modules for classical or PCR-based gene disruptions in *Saccharomyces cerevisiae*, *Yeast* 10, 1793-808

197 Johnston, J. R. **1994** Molecular genetics of yeast-a practical approach, Oxford University Press, Oxford

198 Gietz, R. D. and Sugino, A. **1988** New yeast-*Escherichia coli* shuttle vectors constructed with in vitro mutagenized yeast genes lacking six-base pair restriction sites, *Gene* 74, 527-34

199 Borzani, W. and Vairo, M. L. **1958** Quantitative adsorption of methylene blue by dead yeast cells, *J Bacteriol* 76, 251-5

200 McCord, J. M. and Fridovich, I. **1969** Superoxide dismutase. An enzymic function for erythrocuprein (hemocuprein), *J Biol Chem* 244, 6049-55

201 Di Ilio, C., Polidoro, G., Arduini, A., Muccini, A. and Federici, G. **1983** Glutathione peroxidase, glutathione reductase, glutathione S-transferase, and gamma-glutamyltranspeptidase activities in the human early pregnancy placenta, *Biochem Med* 29, 143-8

202 Hassan, H. M. and Fridovich, I. **1979** Intracellular production of superoxide radical and of hydrogen peroxide by redox active compounds, *Arch Biochem Biophys* 196, 385-95

203 Grant, C. M., Maciver, F. H. and Dawes, I. W. **1996** Stationary-phase induction of *GLR1* expression is mediated by the Yap1 transcriptional regulatory protein in the yeast *Saccharomyces cerevisiae*, *Mol Microbiol* 22, 739-46

204 DeRisi, J. L., Iyer, V. R. and Brown, P. O. **1997** Exploring the metabolic and genetic control of gene expression on a genomic scale, *Science* 278, 680-6

205 Cyrne, L., Martins, L., Fernandes, L. and Marinho, H. S. **2003** Regulation of antioxidant enzymes gene expression in the yeast *Saccharomyces cerevisiae* during stationary phase, *Free Radic Biol Med* 34, 385-93

206 Yonetani, T. **1970** Cytochrome *c* peroxidase, *Adv Enzymol Relat Areas Mol Biol* 33, 309-35

207 Pigeolet, E., Corbisier, P., Houbion, A., Lambert, D., Michiels, C., Raes, M., Zachary, M. D. and Remacle, J. **1990** Glutathione peroxidase, superoxide dismutase, and catalase inactivation by peroxides and oxygen derived free radicals, *Mech Ageing Dev* 51, 283-97

208 Kwon, M., Chong, S., Han, S. and Kim, K. **2003** Oxidative stresses elevate the expression of cytochrome *c* peroxidase in *Saccharomyces cerevisiae*, *Biochim Biophys Acta* 1623, 1-5

209 Minard, K. I. and McAlister-Henn, L. **2001** Antioxidant function of cytosolic sources of NADPH in yeast, *Free Radic Biol Med* 31, 832-43

210 Brejning, J., Jespersen, L. and Arneborg, N. **2003** Genome-wide transcriptional changes during the lag phase of *Saccharomyces cerevisiae*, *Arch Microbiol* 179, 278-94

211 Brejning, J. and Jespersen, L. **2002** Protein expression during lag phase and growth initiation in *Saccharomyces cerevisiae*, *Int J Food Microbiol* 75, 27-38

212 Richter, C., Gogvadze, V., Laffranchi, R., Schlapbach, R., Schweizer, M., Suter, M., Walter, P. and Yaffee, M. **1995** Oxidants in mitochondria: from physiology to diseases, *Biochim Biophys Acta* 1271, 67-74

213 Friis, J., Szablewski, L., Christensen, S. T., Schousboe, P. and Rasmussen, L. **1994** Physiological studies on the effect of Ca^{2+} on the duration of the lag phase of *Saccharomyces cerevisiae*, *FEMS Microbiol Lett* 123, 33-6

214 Boveris, A. and Cadenas, E. **2000** Mitochondrial production of hydrogen peroxide regulation by nitric oxide and the role of ubisemiquinone, *IUBMB Life* 50, 245-50

215 Shephard, T. **1999** MSc. Thesis, The effects of elevated mitochondrial hydrogen peroxide in *Saccharomyces cerevisiae*: a physiological role of cytochrome *c* peroxidase, Department of Chemistry and Biochemistry, Concordia University, Montreal

216 Chang, E. C., Crawford, B. F., Hong, Z., Bilinski, T. and Kosman, D. J. **1991** Genetic and biochemical characterization of Cu,Zn superoxide dismutase mutants in *Saccharomyces cerevisiae*, *J Biol Chem* 266, 4417-24

217 Higgins, V. J., Alic, N., Thorpe, G. W., Breitenbach, M., Larsson, V. and Dawes, I. W. **2002** Phenotypic analysis of gene deletant strains for sensitivity to oxidative stress, *Yeast* 19, 203-14

218 Longo, V. D., Ellerby, L. M., Bredesen, D. E., Valentine, J. S. and Gralla, E. B. **1997** Human Bcl-2 reverses survival defects in yeast lacking superoxide dismutase and delays death of wild-type yeast, *J Cell Biol* 137, 1581-8

219 Jiang, H. and English, A. M. **2002** Quantitative analysis of the yeast proteome by incorporation of isotopically labeled leucine, *J Proteome Res* 1, 345-50

220 Pope, B. and Kent, H. M. **1996** High efficiency 5 min transformation of *Escherichia coli*, *Nucleic Acids Res* 24, 536-7

221 Bullock, W. O., Fernandez, J. M. and Short, J. M. **1987** XL1-Blue: A high efficiency plasmid transforming recA *Escherichia coli* strain with beta-galactosidase selection., *Biotechniques* 5, 376-9

222 Gietz, R. D. and Woods, R. A. **2002** Transformation of yeast by lithium acetate/single-stranded carrier DNA/polyethylene glycol method, *Methods Enzymol* 350, 87-96

223 Lopez, M. F., Kristal, B. S., Chernokalskaya, E., Lazarev, A., Shestopalov, A. I., Bogdanova, A. and Robinson, M. **2000** High-throughput profiling of the mitochondrial proteome using affinity fractionation and automation, *Electrophoresis* 21, 3427-40

224 Rabilloud, T., Kieffer, S., Procaccio, V., Louwagie, M., Courchesne, P. L., Patterson, S. D., Martinez, P., Garin, J. and Lunardi, J. **1998** Two-dimensional electrophoresis of human placental mitochondria and protein identification by mass spectrometry: toward a human mitochondrial proteome, *Electrophoresis* 19, 1006-14

225 Hanson, B. J., Schulenberg, B., Patton, W. F. and Capaldi, R. A. **2001** A novel subfractionation approach for mitochondrial proteins: a three-dimensional mitochondrial proteome map, *Electrophoresis* 22, 950-9

226 Ohlmeier, S., Kastaniotis, A. J., Hiltunen, J. K. and Bergmann, U. **2004** The yeast mitochondrial proteome, a study of fermentative and respiratory growth, *J Biol Chem* 279, 3956-79

227 DiMauro, S. and Schon, E. A. **1998** Nuclear power and mitochondrial disease, *Nat Genet* 19, 214-5

228 Kumar, A., Agarwal, S., Heyman, J. A., Matson, S., Heidtman, M., Piccirillo, S., Umansky, L., Drawid, A., Jansen, R., Liu, Y., Cheung, K. H., Miller, P., Gerstein, M., Roeder, G. S. and Snyder, M. **2002** Subcellular localization of the yeast proteome, *Genes Dev* 16, 707-19

229 Li, Z. B., Flint, P. W. and Boluyt, M. O. **2005** Evaluation of several two-dimensional gel electrophoresis techniques in cardiac proteomics, *Electrophoresis* 26, 3572-85

230 Molloy, M. P., Herbert, B. R., Walsh, B. J., Tyler, M. I., Traini, M., Sanchez, J. C., Hochstrasser, D. F., Williams, K. L. and Gooley, A. A. **1998** Extraction of membrane proteins by differential solubilization for separation using two-dimensional gel electrophoresis, *Electrophoresis* 19, 837-44

231 Diekert, K., de Kroon, A. I., Kispal, G. and Lill, R. **2001** Isolation and subfractionation of mitochondria from the yeast *Saccharomyces cerevisiae*, *Methods Cell Biol* 65, 37-51

232 Rizzuto, R., Pinton, P., Carrington, W., Fay, F. S., Fogarty, K. E., Lifshitz, L. M., Tuft, R. A. and Pozzan, T. **1998** Close contacts with the endoplasmic reticulum as determinants of mitochondrial Ca^{2+} responses, *Science* 280, 1763-6

233 Klose, J. and Kobalz, U. **1995** Two-dimensional electrophoresis of proteins: an updated protocol and implications for a functional analysis of the genome, *Electrophoresis* 16, 1034-59

234 Voss, T. and Haberl, P. **2000** Observations on the reproducibility and matching efficiency of two-dimensional electrophoresis gels: consequences for comprehensive data analysis, *Electrophoresis* 21, 3345-50

235 Gygi, S. P., Corthals, G. L., Zhang, Y., Rochon, Y. and Aebersold, R. **2000** Evaluation of two-dimensional gel electrophoresis-based proteome analysis technology, *Proc Natl Acad Sci U S A* 97, 9390-5

236 Futcher, B., Latter, G. I., Monardo, P., McLaughlin, C. S. and Garrels, J. I. **1999** A sampling of the yeast proteome, *Mol Cell Biol* 19, 7357-68

237 Pasa-Tolic, L. J., P. K.; Anderson, G. A.; Lipton, M. S.; Peden, K. K.; Martinovic, S.; Tolic, N.; Bruce, J. E.; Smith, R. D. **1999** High Throughput Proteome-wide Precision Measurements of Protein Expression Using Mass Spectrometry, *J. Am. Chem. Soc.* 121, 7949-7950

238 Veenstra, T. D., Martinovic, S., Anderson, G. A., Pasa-Tolic, L. and Smith, R. D. **2000** Proteome analysis using selective incorporation of isotopically labeled amino acids, *J Am Soc Mass Spectrom* 11, 78-82

239 Schieltz, D. M. **1999** Preparing 2-D protein extracts from yeast, *Methods Mol Biol* 112, 31-4

240 Berkelman, T. S., T. **1998** Amersham Pharmacia Biotech Inc.

241 McCaldon, P. and Argos, P. **1988** Oligopeptide biases in protein sequences and their use in predicting protein coding regions in nucleotide sequences, *Proteins* 4, 99-122

242 Unlu, M., Morgan, M. E. and Minden, J. S. **1997** Difference gel electrophoresis: a single gel method for detecting changes in protein extracts, *Electrophoresis* 18, 2071-7

243 Hirayama, K. Y., Reiko; Yamada, Naoyuki; Noguchi, Kazuyoshi; Yamaguchi, Yoshiki; Enokizono, Junichi; Kato, Koichi; Arata, Yoji; Shimada, Ichio. **1998** Convenient peptide mapping of immunoglobulin G2b and differentiation between leucine and isoleucine residues by mass spectrometry using ^{2}H-labeled leucine., *J. Mass Spectrom. Soc. Jap.* 46, 83-89

244 Berggren, K., Chernokalskaya, E., Steinberg, T. H., Kemper, C., Lopez, M. F., Diwu, Z., Haugland, R. P. and Patton, W. F. **2000** Background-free, high sensitivity staining of proteins in one- and two-dimensional sodium dodecyl sulfate-polyacrylamide gels using a luminescent ruthenium complex, *Electrophoresis* 21, 2509-21

245 Haynes, P. A. and Yates, J. R., 3rd. **2000** Proteome profiling-pitfalls and progress, *Yeast* 17, 81-7

246 Gygi, S. P., Rist, B. and Aebersold, R. **2000** Measuring gene expression by quantitative proteome analysis, *Curr Opin Biotechnol* 11, 396-401

247 Ji, J., Chakraborty, A., Geng, M., Zhang, X., Amini, A., Bina, M. and Regnier, F. **2000** Strategy for qualitative and quantitative analysis in proteomics based on signature peptides, *J Chromatogr B Biomed Sci Appl* 745, 197-210

248 Oda, Y., Huang, K., Cross, F. R., Cowburn, D. and Chait, B. T. **1999** Accurate quantitation of protein expression and site-specific phosphorylation, *Proc Natl Acad Sci U S A* 96, 6591-6

249 Gygi, S. P., Rist, B., Gerber, S. A., Turecek, F., Gelb, M. H. and Aebersold, R. **1999** Quantitative analysis of complex protein mixtures using isotope-coded affinity tags, *Nat Biotechnol* 17, 994-9

250 Blattner, F. R., Plunkett, G., 3rd, Bloch, C. A., Perna, N. T., Burland, V., Riley, M., Collado-Vides, J., Glasner, J. D., Rode, C. K., Mayhew, G. F., Gregor, J., Davis, N. W., Kirkpatrick, H. A., Goeden, M. A., Rose, D. J., Mau, B. and Shao, Y. **1997** The complete genome sequence of *Escherichia coli* K-12, *Science* 277, 1453-74

251 Kunst, F., Ogasawara, N., Moszer, I., Albertini, A. M., Alloni, G., Azevedo, V., Bertero, M. G., Bessieres, P., Bolotin, A., Borchert, S., Borriss, R., Boursier, L., Brans, A., Braun, M., Brignell, S. C., Bron, S., Brouillet, S., Bruschi, C. V., Caldwell, B., Capuano, V., Carter, N. M., Choi, S. K., Codani, J. J., Connerton, I. F., Danchin, A. and et al. **1997** The complete genome sequence of the gram-positive bacterium *Bacillus subtilis*, *Nature* 390, 249-56

252 Goshe, M. B. and Smith, R. D. **2003** Stable isotope-coded proteomic mass spectrometry, *Curr Opin Biotechnol* 14, 101-9

253 Beynon, R. J. and Pratt, J. M. **2005** Metabolic labeling of proteins for proteomics, *Mol Cell Proteomics* 4, 857-72

254 Pütter, J. and Becker, R. **1983** Methods of Enzymatic Analysis, vol. 3, Verlug Chemie, Deerfield Beach

255 Pluskal, M. G., Bogdanova, A., Lopez, M., Gutierrez, S. and Pitt, A. M. **2002** Multiwell in-gel protein digestion and microscale sample preparation for protein identification by mass spectrometry, *Proteomics* 2, 145-50

256 Pratt, J. M., Robertson, D. H., Gaskell, S. J., Riba-Garcia, I., Hubbard, S. J., Sidhu, K., Oliver, S. G., Butler, P., Hayes, A., Petty, J. and Beynon, R. J. **2002** Stable isotope labelling in vivo as an aid to protein identification in peptide mass fingerprinting, *Proteomics* 2, 157-63

257 Chen, L. C. and Casadevall, A. **1999** Labeling of proteins with ^{35}S-methionine and/or [^{35}S]cysteine in the absence of cells, *Anal Biochem* 269, 179-88

258 Minor, R. R. **1982** Cytotoxic effects of low levels of ^{3}H-, ^{14}C-, and ^{35}S-labeled amino acids, *J Biol Chem* 257, 10400-13

259 Yeargin, J. and Haas, M. **1995** Elevated levels of wild-type p53 induced by radiolabeling of cells leads to apoptosis or sustained growth arrest, *Curr Biol* 5, 423-31

260 Hu, V. W. and Heikka, D. S. **2000** Radiolabeling revisited: metabolic labeling with ^{35}S-methionine inhibits cell cycle progression, proliferation, and survival, *Faseb J* 14, 448-54

261 Maillet, I., Lagniel, G., Perrot, M., Boucherie, H. and Labarre, J. **1996** Rapid identification of yeast proteins on two-dimensional gels, *J Biol Chem* 271, 10263-70

262 Meisenhelder, J. and Hunter, T. **1988** Radioactive protein-labelling techniques, *Nature* 335, 120

263 Ong, S. E., Kratchmarova, I. and Mann, M. **2003** Properties of ^{13}C-substituted arginine in stable isotope labeling by amino acids in cell culture (SILAC), *J Proteome Res* 2, 173-81

264 Shenton, D. and Grant, C. M. **2003** Protein S-thiolation targets glycolysis and protein synthesis in response to oxidative stress in the yeast *Saccharomyces cerevisiae*, *Biochem J* 374, 513-9

265 Pratt, J. M., Petty, J., Riba-Garcia, I., Robertson, D. H., Gaskell, S. J., Oliver, S. G. and Beynon, R. J. **2002** Dynamics of protein turnover, a missing dimension in proteomics, *Mol Cell Proteomics* 1, 579-91

266 Ong, S. E., Blagoev, B., Kratchmarova, I., Kristensen, D. B., Steen, H., Pandey, A. and Mann, M. **2002** Stable isotope labeling by amino acids in cell culture, SILAC, as a simple and accurate approach to expression proteomics, *Mol Cell Proteomics* 1, 376-86

267 Brachmann, C. B., Davies, A., Cost, G. J., Caputo, E., Li, J., Hieter, P. and Boeke, J. D. **1998** Designer deletion strains derived from *Saccharomyces cerevisiae* S288C: a useful set of strains and plasmids for PCR-mediated gene disruption and other applications, *Yeast* 14, 115-32

268 Gerber, S. A., Rush, J., Stemman, O., Kirschner, M. W. and Gygi, S. P. **2003** Absolute quantification of proteins and phosphoproteins from cell lysates by tandem MS, *Proc Natl Acad Sci U S A* 100, 6940-5

269 Hall, M. P. and Schneider, L. V. **2004** Isotope-differentiated binding energy shift tags (IDBEST) for improved targeted biomarker discovery and validation, *Expert Rev Proteomics* 1, 421-31

270 Schneider, L. V. and Hall, M. P. **2005** Stable isotope methods for high-precision proteomics, *Drug Discov Today* 10, 353-63

271 Marouga, R., David, S. and Hawkins, E. **2005** The development of the DIGE system: 2D fluorescence difference gel analysis technology, *Anal Bioanal Chem* 382, 669-78

272 Tonge, R., Shaw, J., Middleton, B., Rowlinson, R., Rayner, S., Young, J., Pognan, F., Hawkins, E., Currie, I. and Davison, M. **2001** Validation and development of fluorescence two-dimensional differential gel electrophoresis proteomics technology, *Proteomics* 1, 377-96

273 Zhu, H., Pan, S., Gu, S., Bradbury, E. M. and Chen, X. **2002** Amino acid residue specific stable isotope labeling for quantitative proteomics, *Rapid Commun Mass Spectrom* 16, 2115-23

274 Ashe, M. P., De Long, S. K. and Sachs, A. B. **2000** Glucose depletion rapidly inhibits translation initiation in yeast, *Mol Biol Cell* 11, 833-48

275 Kuhn, K. M., DeRisi, J. L., Brown, P. O. and Sarnow, P. **2001** Global and specific translational regulation in the genomic response of *Saccharomyces cerevisiae* to a rapid transfer from a fermentable to a nonfermentable carbon source, *Mol Cell Biol* 21, 916-27

276 Finkel, T. **2003** Oxidant signals and oxidative stress, *Curr Opin Cell Biol* 15, 247-54

277 Holmgren, A. **1989** Thioredoxin and glutaredoxin systems, *J Biol Chem* 264, 13963-6